

**Functional analysis of the  
CNS-specific F-box protein FBXO41  
in cerebellar development**

**Ph.D. Thesis**

in partial fulfillment of the requirements  
for the degree “Doctor rerum naturalium (Dr. rer.nat.)”

in the Neuroscience Program  
at the Georg-August-Universität Göttingen,

Faculty of Biology

submitted by

**Chaitali Mukherjee**

Born in Patna, India

**Göttingen 2015**



**Thesis Committee Members:**

**Dr. Judith Stegmüller** (*Reviewer*)

Laboratory of Cellular and Molecular Neurobiology,

Max Planck Institute for Experimental Medicine

**Prof. Dr. Mikael Simons** (*Reviewer*)

Laboratory of Cellular Neuroscience,

Max Planck Institute for Experimental Medicine

**Prof. Dr. Michael Hörner**

Dept. of Cellular Neurobiology

Johann-Friedrich-Blumenbach-Institute for Zoology and Anthropology

**Date of thesis submission:** 30<sup>th</sup> April 2015

**Date of the oral examination:** 8<sup>th</sup> June 2015

I hereby declare that this Ph.D. thesis

„Functional analysis of the  
CNS-specific Fbox protein FBXO41 in cerebellar development“

has been written independently with no other aids or sources than quoted.

Göttingen, April 2015

Chaitali Mukherjee

# Table of Contents

<b>ACKNOWLEDGEMENTS</b> .....	<b>1</b>
<b>ABSTRACT</b> .....	<b>3</b>
<b>ABBREVIATIONS</b> .....	<b>4</b>
<b>1 INTRODUCTION</b> .....	<b>12</b>
<b>1.1 THE CEREBELLUM</b> .....	12
<b>1.2 CEREBELLAR ARCHITECTURE AND COMPOSITION</b> .....	12
<b>1.3 CEREBELLAR CIRCUITRY</b> .....	14
<b>1.4 CEREBELLAR DEVELOPMENT</b> .....	16
1.4.1 Granule neuron migration during cerebellar development .....	17
<i>1.4.1.1 Molecular regulation of granule neuron migration in the cerebellum</i> .....	19
1.4.2 Parallel fiber formation and axon growth regulation in cerebellar granule neurons.....	20
<i>1.4.2.1 Molecular regulation of axon growth in CGNs</i> .....	22
1.4.3 Neuronal number and cell integrity within the cerebellum.....	23
<b>1.5 UBIQUITINATION AS A MEANS OF CELL-INTRINSIC REGULATION OF CEREBELLAR DEVELOPMENT</b> .....	24
1.5.1 The ubiquitnation cascade .....	25
1.5.2 E3 ligases and their role in proper cerebellar development .....	27
1.5.3 SCF complexes and their contribution in neurodevelopment and disease .....	30
<b>1.6 AIM AND SCOPE OF THE STUDY</b> .....	32
<b>2 MATERIALS AND METHODS</b> .....	<b>33</b>
<b>2.1 LAB EQUIPMENT</b> .....	33
<b>2.2 CHEMICAL REAGENTS AND COMMERCIAL KITS</b> .....	33
<b>2.3 COMMON LAB REAGENTS AND KITS</b> .....	33
<b>2.4 ANTIBODIES</b> .....	34
<b>2.5 ENZYMES</b> .....	36
<b>2.6 BUFFERS AND STOCK SOLUTIONS</b> .....	37
<b>2.7 PLASMIDS CONSTRUCTS AND PRIMERS</b> .....	40
<b>2.8 MOLECULAR CLONING</b> .....	41
<b>2.9 RNA INTERFERENCE</b> .....	43
2.9.1 Generation of vector-based RNAi constructs.....	43

2.9.2 Annealing of primers.....	43
2.9.3 Phosphorylation of oligos.....	44
2.9.4 Preparation of the U6/pBS vector and ligation .....	44
2.9.5 Screening for positive ligation clones .....	44
<b>2.10 SITE-DIRECTED MUTAGENESIS .....</b>	<b>45</b>
<b>2.11 FUSION PCR FOR GENERATING DELETION MUTANTS.....</b>	<b>45</b>
<b>2.12 CELL CULTURE.....</b>	<b>46</b>
2.12.1 HEK293T cell culture .....	46
2.12.2 Primary neuronal culture .....	47
<b>2.13 TRANSFECTION OF PRIMARY NEURONS AND HEK293T CELLS.....</b>	<b>47</b>
2.13.1 HEK293T cell transfection.....	47
2.13.2 Primary neuron transfection .....	48
<b>2.14 IMMUNOCYTOCHEMISTRY .....</b>	<b>48</b>
<b>2.15 MORPHOLOGICAL ANALYSES OF NEURONS.....</b>	<b>49</b>
<b>2.16 SURVIVAL ASSAY IN NEURONS .....</b>	<b>49</b>
<b>2.17 BIOCHEMICAL TECHNIQUES .....</b>	<b>50</b>
2.17.1 Tissue lysate preparation.....	50
2.17.2 Cell lysate preparation.....	50
2.17.3 Bradfords assay for protein concentration measurement .....	51
2.17.4 Co-immunoprecipitation (CoIP) .....	51
2.17.5 Centrosomal purification.....	51
2.17.6 Ubiquitination assay .....	52
2.17.7 SDS-PAGE and western blot .....	52
2.17.8 Densitometric quantifications .....	54
2.17.9 Reverse transcription PCR (RT-PCR).....	54
2.17.9.1 mRNA isolation .....	54
2.17.9.2 cDNA synthesis and PCR .....	54
2.17.9.3 qRT-PCR .....	55
<b>2.18 IN VIVO ELECTROPORATION .....</b>	<b>56</b>
<b>2.19 GENERATION OF THE FBXO41-/- KNOCKOUT MOUSE LINE .....</b>	<b>56</b>
<b>2.20 HISTOLOGICAL ANALYSIS.....</b>	<b>58</b>
2.20.1 Perfusion and fixation of mouse tissue .....	58
2.20.2 Immunohistochemistry of frozen sections .....	58
2.20.3 $\beta$ -galactosidase staining.....	59
2.20.4 Post-fixation and paraffin embedding of tissue samples.....	59

2.20.5 Immunohistochemistry of paraffin embedded samples .....	60
2.20.5.1 <i>Haematoxylin and Eosin staining</i> .....	61
2.20.5.2 <i>Immunostaining using the LSAB2 detection system</i> .....	61
2.20.5.3 <i>Analyses and quantification of chromogenically stained sections</i> .....	63
<b>2.21 MOUSE BEHAVIOR</b> .....	68
2.21.1 Mouse behavior at P16 .....	68
2.21.1.1 <i>The Clasping test</i> .....	68
2.21.1.2 <i>Ledge test</i> .....	69
2.21.1.3 <i>Gait analysis</i> .....	69
2.21.1.4 <i>Rotarod</i> .....	69
2.21.2 Adult mouse behavior .....	69
2.21.2.1 <i>Elevated plus maze</i> .....	70
2.21.2.2 <i>Open Field</i> .....	70
2.21.2.3 <i>Clasping test</i> .....	70
2.21.2.4 <i>Rotarod: motor learning paradigm</i> .....	70
2.21.2.4 <i>Pole test</i> .....	71
2.21.2.5 <i>Balance beam</i> .....	71
2.21.2.6 <i>Olfaction</i> .....	71
<b>3 RESULTS</b> .....	<b>73</b>
<b>3.1 IN VIVO CHARACTERIZATION OF FBXO41 FUNCTION</b> .....	73
3.1.1 FBXO41 expression is restricted to the CNS.....	73
3.1.2 FBXO41 has a dual localization at the cytoplasm and the centrosome .....	77
3.1.3 Loss of FBXO41 results in retarded growth and severe motor deficits .....	78
3.1.4 P16 FBXO41 <sup>-/-</sup> mice do not show signs of neurodegeneration.....	79
3.1.5 FBXO41 <sup>-/-</sup> mice show abnormal cerebellar morphology.....	82
3.1.6 Loss of FBXO41 results in delayed neuronal migration.....	84
3.1.7 Cytoplasmic FBXO41 regulates proper neuronal migration.....	90
3.1.8 FBXO41 is essential for neuronal survival .....	93
3.1.9 FBXO41 <sup>-/-</sup> mice show impaired axon growth.....	96
<b>3.2 MOLECULAR MECHANISM OF FBXO41-MEDIATED AXON GROWTH REGULATION</b> .....	100
3.2.1 FBXO41 together with Skp1 and cullin7 forms an atypical SCF-like E3 ligase.....	100
3.2.2 Cytoplasmic FBXO41 promotes axon growth in an E3 ligase activity-dependent manner.....	104
3.2.3 The cytoskeletal protein neurofilament medium polypeptide (NFM) interacts with FBXO41 .....	105

3.2.4 NFM is a substrate of FBXO41-Cul7 .....	107
3.2.5 Loss of FBXO41-Cul7 leads to destabilization of NFM.....	108
3.2.6 Dysregulation of NFM levels leads to uncontrolled axon out growth .....	111
3.2.7 NFM acts downstream of FBXO41 to promote axon growth.....	116
<b>3.3 BEHAVIORAL ANALYSIS OF THE ADULT FBXO41+/- MICE.....</b>	<b>121</b>
3.3.1 FBXO41+/- mice show no abnormal appearance and body weight.....	121
3.3.2 Adult FBXO41+/- mice show no signs of abnormal locomotion and anxiety	121
3.3.3 Absence of hind limb clasping in adult FBXO41+/- mice.....	123
3.3.4 Intact olfaction in adult FBXO41+/- mice .....	125
3.3.5 Adult FBXO41 +/- display intact motor function and coordination .....	125
<b>4 DISCUSSION .....</b>	<b>128</b>
<b>4.1 LOSS OF THE CNS-SPECIFIC F-BOX PROTEIN FBXO41 RESULTS IN AN ATAXIA-LIKE PHENOTYPE IN MICE ALONG WITH IMPAIRED NEURONAL MIGRATION AND NEURODEGENERATION IN THE DEVELOPING CEREBELLUM .....</b>	<b>128</b>
<b>4.2 MOLECULAR MECHANISMS GUIDING FBXO41-MEDIATED AXON GROWTH.....</b>	<b>132</b>
4.2.1 FBXO41-Cul7 is a CNS-specific neuronal E3 ligase .....	132
4.2.2 The FBXO41-Cul7–NFM pathway of axon growth control.....	134
<b>4.3 FBXO41+/- MICE DO NOT SHOW ANY SIGNS OF LATE ONSET MOTOR PHENOTYPE</b>	<b>139</b>
<b>4.4 OPEN QUESTIONS AND SCOPE FOR FURTHER RESEARCH .....</b>	<b>141</b>
<b>4.5 CONCLUSION .....</b>	<b>142</b>
<b>5 REFERENCES .....</b>	<b>146</b>
<b>APPENDIX 1 .....</b>	<b>167</b>
<b>APPENDIX 2 .....</b>	<b>169</b>
<b>6 CURRICULUM VITAE .....</b>	<b>172</b>

## List of Figures

- Figure 1.1. Cellular composition of the cerebellum 14
- Figure 1.2. Circuitry of the cerebellum 16
- Figure 1.3. CGN migration in the developing cerebellum 19
- Figure 1.4. Polarization and neurite extension in CGNs in culture 22
- Figure 1.5. Overview of the ubiquitin proteasome system 26
- Figure 1.6. Different types of ubiquitination on substrates 27
- Figure 1.7. HECT and RING E3 ligases 28
- Figure 1.8. SCF complexes are multi-subunit RING ligases 30
- Figure 3.1 FBXO41 is exclusively expressed in the CNS 73
- Figure 3.2 Genotyping of FBXO41<sup>-/-</sup> mice 74
- Figure 3.3 FBXO41 expression within the CNS 75
- Figure 3.4 FBXO41 localizes to the centrosome 77
- Figure 3.5 Loss of FBXO41 results in diminished body and brain weights 78
- Figure 3.6 FBXO41<sup>-/-</sup> mice display severe motor deficits 79
- Figure 3.7 FBXO41<sup>-/-</sup> mice display no signs of apoptosis or neurodegeneration at P16 80
- Figure 3.8 FBXO41<sup>-/-</sup> mouse brains show no signs of inflammation at P16 81
- Figure 3.9 FBXO41<sup>-/-</sup> mice show reduced cerebellar size and abnormal cerebellar foliation 83
- Figure 3.10 FBXO41<sup>-/-</sup> mice show impaired neuronal migration in the cerebellum 85
- Figure 3.11 FBXO41<sup>-/-</sup> mice show delayed neuronal migration in the cerebellum 87
- Figure 3.12 FBXO41<sup>-/-</sup> mice display a residual EGL at P16 88
- Figure 3.13 Loss of FBXO41 does not affect Purkinje cell layer 89
- Figure 3.14 FBXO41 harbors a centrosomal targeting region 90
- Figure 3.15 Cytoplasmic FBXO41 promotes neuronal migration 91
- Figure 3.16 P30 FBXO41<sup>-/-</sup> displays persistent motor impairment 94
- Figure 3.17 P30 FBXO41<sup>-/-</sup> mice show increased apoptosis in the cerebellum 95
- Figure 3.18 FBXO41 is essential for neuronal survival 96
- Figure 3.19 FBXO41<sup>-/-</sup> mice display thinner parallel fiber bundles in the cerebellum 97
- Figure 3.20 FBXO41<sup>-/-</sup> mice show reduced white matter tracts within the cerebellum 98
- Figure 3.21 FBXO41 interacts with Skp1 but not cullin1 101
- Figure 3.22 FBXO41 interacts with cullin7 102



Figure 3.23 FBXO41 interacts with cullin7 independent of its F-box domain 103

Figure 3.24 FBXO41-Cul7 is a functional E3 ligase 104

Figure 3.25 FBXO41 regulates axon growth in a ligase-activity dependent manner 105

Figure 3.26 FBXO41 interacts with NFM 106

Figure 3.27 NFM associates with cullin7 in the presence of FBXO41 107

Figure 3.28 FBXO41 ubiquitinates NFM via K63-linked polyubiquitination 108

Figure 3.29 FBXO41<sup>-/-</sup> mice show diminished NFM levels 109

Figure 3.30 NFM mRNA levels in the P16 FBXO41<sup>+/+</sup> and FBXO41<sup>-/-</sup> mice 110

Figure 3.31 Loss of FBXO41-Cul7 leads to destabilization of NFM 110

Figure 3.32 NFM is expressed in the developing cerebellum of mice 111

Figure 3.33 NFM promotes axon growth 112

Figure 3.34 Knockdown of NFM 113

Figure 3.35 Loss of NFM leads to uncontrolled axon growth 114

Figure 3.36 NFM knockdown also promotes axon growth 115

Figure 3.37 The NFM / FBXO41 pathway of axon growth regulation 117

Figure 3.38 Loss of NFM has no effect on FBXO41 localization 119

Figure 3.39 Loss of FBXO41 leads to defasciculated NFM in axons 120

Figure 3.40 FBXO41<sup>+/-</sup> do not show abnormal body weight at 10 months 121

Figure 3.41 FBXO41<sup>+/-</sup> mice do not show elevated anxiety levels in the elevated plus maze paradigm 122

Figure 3.42 FBXO41<sup>+/-</sup> mice display comparable locomotor activity in the open field arena 123

Figure 3.43 FBXO41<sup>+/-</sup> mice display no hind limb clasping 124

Figure 3.44 FBXO41<sup>+/-</sup> mice do not show loss of olfaction 125

Figure 3.45 FBXO41<sup>+/-</sup> mice don't display any observable motor deficits 126

Figure 4.1 Current working model of the F-box protein FBXO41 144  
in cerebellar development

## **List of Tables**

- Table 2.1 List of all cell culture reagents used in the study 33
- Table 2.2 List of the commercially available kits used in the study 34
- Table 2.3 List of all the primary antibodies used in this study 35
- Table 2.4 List of all the secondary antibodies used in this study 36
- Table 2.5 List of various enzymes used in the study 36
- Table 2.6 Recipe for general PCR reaction 41
- Table 2.7 PCR program for general molecular cloning 41
- Table 2.8 Recipe of the ligation reaction 42
- Table 2.9 List of the shRNA-targeting sequences of FBXO41 and NFM RNAs 43
- Table 2.10: Annealing of primers 44
- Table 2.11: Site-directed mutagenesis PCR 45
- Table 2.12 PCR recipe for N-and C- terminal fragments 46
- Table 2.13 PCR recipe for fusion PCR 46
- Table 2.14 Recipe of SDS-PAGE gels of containing varying percentages of acrylamide 53
- Table 2.15 Recipe of reagents used for the PCR reaction for amplification of a gene from cDNA 55
- Table 2.16 Genotyping PCR recipe of reagents 57
- Table 2.17 Genotyping PCR thermocycler program 57
- Table 2.18 List showing the automated paraffin embedding program used by the HMP 110, MICROM embedding machine. 60
- Table 2.19 List showing the deparaffinization steps the 5  $\mu$ m thick paraffin sections were subjected to prior to staining. 60

---

## Acknowledgements

*“A leader is one that knows the way, goes the way and shows the way”- John C Maxwell.* I deeply appreciate my supervisor Dr. Judith Stegmüller for living up to each of these qualities of a leader and even more. Her vision, optimism and drive are just some of the many qualities in her that I look up to. I am incredibly thankful to her for taking me under her wing and showing me the ropes of molecular biology. She is an excellent teacher and pushes you to do your best. I am deeply indebted to her for all that she has thought me and for the encouragement, guidance and support she provided in the lab for the past four and half years.

Furthermore, I would like to thank my thesis committee members Prof. Dr. Mikael Simons and Prof. Dr. Michael Hörner for their guidance and valuable suggestions during every committee meeting. A special heartfelt thank you to the IMPRS Neuroscience program and its coordinators, Michael, Sandra and Mirja for making our journey in Göttingen as smooth as possible.

I would take this opportunity to also thank the Stegmüller lab - Alina, Annika, Mayur, Ghergana, Siv and Sabitha for being the most amazing colleagues, who were not only supportive and helpful but also made work so much fun that it felt like play. A special thank you to Madhu for her invaluable advice, as well as showing me the tips and tricks to working efficiently and effectively. I would also like to give a special thank you to Shih-Ju, who has been my lab sister from day one and for introducing me to the new and fascinating things from Taiwan! I have extremely fond memories of working with her, having very productive brain storming sessions together and sharing the office with her. I also thank Nicola for all the professional and personal help and advice she provided during these four years. I will miss our coffee breaks! The list would not be complete without thanking my project partner Anna. She has been a true team player, extremely supportive and a very valuable member of the FBXO41 team. I am very grateful to her for taking me under her wing and letting me work alongside her on this project. An excellent teammate and a great friend, I could not have asked for a better project partner. Thank you so much Anna! It has truly been a pleasure working together with you to take a crack at FBXO41. I would additionally like to thank the Simons and Ehrenreich groups for providing a friendly working atmosphere.

I would have not made it this far if it wasn't for all the love, support and cheer provided by my friends. Aki, Veens and Zams, you guys have been like a family for me in since I am here in Goettingen. Ash, Jigs, Prat, Swe and Tinu you guys are my soul sisters. Bekir and Diana, you guys have been a pillar of support in times of crisis and source of joy and laughter on stormy days. I a deep heartfelt thank you to all of you! I truly cherish all the happiness, joy, sorrows, tears, laughter and the incredible ride I have shared with all of you so far. A special thank you to Gabi for being a second mother to me during the time of my PhD! Furthermore, I would like to thank David Brockelt for proof reading my thesis and his continuous support throughout my PhD.

Last but by far not the least! I would like to thank my mother and father for being the ultimate support system, fulfilling all my needs and demands, guiding me and providing me with the right advice, picking me up each time I have fallen, for being the most understanding parents, loving me so unconditionally and teaching me never to give up. I am deeply, deeply grateful and indebted to you both for everything I am today. I may not say it often, but I love you both tremendously and you are always in my thoughts.

---

## Abstract

Neurodevelopment is a highly dynamic process governed by the tight orchestration of events such as neurogenesis, neuronal migration, morphogenesis and synaptogenesis that ultimately shape the brain. These neurodevelopmental events are tightly regulated by the interplay of cell-extrinsic and intrinsic mechanisms. Over the past decades, the ubiquitin proteasome system has emerged as an intrinsic regulator of neurodevelopment as well as disease. In this study, I explored the function of the CNS-specific F-box protein FBXO41 *in vivo* and established it as a key regulator of cerebellar development. I found that loss of FBXO41 results in a severely ataxic and uncoordinated gait in mice, along with impaired granule neuron migration, neurodegeneration and axon growth defects in the cerebellum. In addition, I identified FBXO41 as the second F-box protein to form an SCF-like E3 ligase complex with cullin7. Furthermore, I discovered that FBXO41-Cul7 non-proteolytically ubiquitinates the cytoskeletal protein neurofilament medium polypeptide (NFM), thereby stabilizing it. Last but not the least, I uncovered that FBXO41-Cul7 operates upstream of NFM in the pathway of axon growth regulation. Collectively, my study has uncovered the function of FBXO41 in cerebellar development and has identified FBXO41-Cul7 as a novel E3 ligase providing the first insights into its ligase activity and axon growth regulation.

---

## Abbreviations

<b>Aa</b>	Amino acid
<b>ANOVA</b>	Analysis of variance
<b>APC</b>	Anaphase-promoting complex
<b>APC2</b>	Adenomatous Polyposis Coli 2
<b>aPKC</b>	Atypical protein kinase C
<b>APP</b>	Amyloid precursor protein
<b>ATP</b>	Adenosine triphosphate
<b>Ahi1</b>	Abelson Helper Integration Site 1
<b>AraC</b>	$\beta$ -D-arabinofuranoside
<b>Arp2/3</b>	Actin-Related Proteins 2/3
<b>Atoh1</b>	Atonal homolog 1
<b><math>\beta</math>-Gal</b>	$\beta$ -Galactosidase
<b><math>\beta</math>-TRCP</b>	Beta-transducin repeat containing
<b>BCL-xl</b>	B-cell lymphoma-extra large
<b>BDNF</b>	Brain-derived neurotrophic factor
<b>bp</b>	Basepairs
<b>BME</b>	Basal Medium Eagle
<b>BSA</b>	Bovine serum albumin
<b>CA1, CA2, CA3</b>	Cornu ammonis 1, 2, 3
<b>CB</b>	Cerebellum
<b>CC</b>	Corpus callosum
<b>cDNA</b>	complementary DNA
<b>CDC42</b>	Cell division control protein 42
<b>Cdk</b>	Cyclin-dependent kinase
<b>CGN</b>	Cerebellar granule neuron
<b>CIP</b>	Calf intestine phosphatase
<b>CMV</b>	Cytomegalovirus
<b>CNPase</b>	2',3'-Cyclic-nucleotide 3'-phosphodiesterase
<b>CRMP2</b>	Collapsing-response mediator protein2

<b>CS</b>	Calf serum
<b>Cul7</b>	Cullin7
<b>CTR</b>	Centrosomal targeting region
<b>CoIP</b>	Co-Immunoprecipitation
<b>Ctx</b>	Cortex
<b>Cul1</b>	Cullin1
<b>cm</b>	centimeter
<b>DAB</b>	Diaminobenzidine
<b>DAPI</b>	4'6-diamidino-2-phenylindole
<b>DCN</b>	Deep cerebellar nuclei
<b>ddH<sub>2</sub>O</b>	Double-distilled water
<b>DISC1</b>	Disrupted in schizophrenia 1
<b>DIV</b>	Day <i>in vitro</i>
<b>DMEM</b>	Dulbecco's modified eagle's medium
<b>DMSO</b>	Dimethylsulfoxide
<b>DNA</b>	Deoxyribonucleic acid
<b>dNTP</b>	Nucleoside triphosphate
<b>DTT</b>	Dithiothreitol
<b>E</b>	Embryonic day
<b>E1</b>	Ubiquitin-activating enzyme
<b>E2</b>	Ubiquitin-conjugating enzyme
<b>E3</b>	Ubiquitin ligase enzyme
<b>ECL</b>	Enhanced chemiluminescence
<b>EDTA</b>	Ethylenediaminetetraacetic acid
<b>EGL</b>	External granular layer
<b>En1, 2</b>	Engrailed homeobox 2
<b>EPSP</b>	Excitatory postsynaptic potential
<b>ES</b>	Embryonic stem cells
<b>ErbB4</b>	Receptor tyrosine-protein kinase erbB-4
<b>ERK</b>	Extracellular signal-regulated kinases
<b>FBS</b>	Fetal bovine serum
<b>FBXL</b>	F-box protein with leucine-rich repeats
<b>FBXO</b>	F-box protein with other domain motifs

<b>FBXW</b>	F-box protein with WD40 domains
<b>Fgf8</b>	Fibroblast growth factor 8
<b>Fo</b>	Fornix
<b>g</b>	gram
<b>GABA</b>	$\gamma$ -Aminobutyric acid
<b>GAPDH</b>	Glyceraldehyde 3-phosphate dehydrogenase
<b>GFAP</b>	Glial fibrillary acidic protein
<b>GFP</b>	Green fluorescent protein
<b>GIRD2</b>	glutamate receptor, ionotropic, delta 2
<b>Gli1</b>	GLI family zinc finger 1
<b>GS</b>	Goat serum
<b>GSK-3B</b>	Glycogen synthase kinase 3
<b>GTP</b>	Guanosine-5'-triphosphate
<b>H&amp;E</b>	Haematoxylin and Eosin
<b>HA</b>	Hemagglutinin
<b>HBSS</b>	Hank's Balanced Salt Solution
<b>HECT</b>	Homologous to E6-AP carboxy terminal
<b>HEK</b>	Human Embryonic Kidney
<b>HEPES</b>	4-(2-hydroxyethyl)-1-piperazineethanesulfonic acid
<b>HRP</b>	Horseradish peroxidase
<b>HS</b>	Horse serum
<b>HTh</b>	Hypothalamus
<b>Hpc</b>	Hippocampus
<b>IB</b>	Immunoblot
<b>IBA1</b>	Ionized calcium-binding adapter molecule 1
<b>ICC</b>	Immunocytochemistry
<b>Id2</b>	Inhibitor of DNA binding 2
<b>IGL</b>	Internal granular layer
<b>IHC</b>	Immunohistochemistry
<b>IO</b>	Inferior olive
<b>IP</b>	Immunoprecipitation
<b>Ic</b>	Inferior colliculus
<b>IgG</b>	Immunoglobulin G



<b>JNK</b>	c-Jun N-terminal kinase
<b>kb</b>	kilobase
<b>kDa</b>	Kilodalton
<b>KOMP</b>	Knockout Mouse Project
<b>LSAB2</b>	Labelled Streptavidin-Biotin2 System
<b>LTD</b>	Long term depression
<b>Lis1</b>	Lissencephaly 1
<b>M</b>	Medulla oblongata
<b>MAP1B</b>	Microtubule-associated protein 1B
<b>MB</b>	Midbrain
<b>mg</b>	Milligram
<b>ml</b>	Milliliter
<b>ML</b>	Molecular layer
<b>Mm2</b>	Square millimeter
<b>mRNA</b>	Messenger RNA
<b>µg</b>	Microgram
<b>µl</b>	Microliter
<b>µM</b>	Micromolar
<b>µm</b>	Micrometer
<b>mM</b>	Milimolar
<b>mm</b>	millimeter
<b>N-WASP</b>	Neuronal Wiskott–Aldrich Syndrome protein
<b>NB2a/d1</b>	Neuroblastoma cell line
<b>NDEL1</b>	Nuclear distribution protein nudE-like 1
<b>NEM</b>	N-ethylmaleimide
<b>NFH</b>	Neurofilament heavy
<b>NFM</b>	Neurofilament medium
<b>NFL</b>	Neurofilament light
<b>NFkb</b>	Nuclear factor kappa B
<b>NGF</b>	Nerve growth factor
<b>NGS</b>	Normal goat serum
<b>nm</b>	Nanometer
<b>Notch2</b>	Neurogenic locus notch homolog protein 2

<b>NT-3</b>	Neurotrophin-3
<b>NeuN</b>	Neuronal nuclear antigen
<b>Olf</b>	Olfactory bulb
<b>P</b>	Postnatal day
<b>p27Kip1</b>	Cyclin-dependent kinase inhibitor 1B
<b>PAM</b>	Protein associated with Myc
<b>Pax2, 5</b>	Paired box 2, 5
<b>PBS</b>	Phosphate-buffered saline
<b>PBST</b>	Phosphate-buffered saline with Triton-X
<b>PCL</b>	Purkinje cell layer
<b>PCNA</b>	Proliferating cell nuclear antigen
<b>PCR</b>	Polymerase chain reaction
<b>PFA</b>	Paraformaldehyde
<b>PMSF</b>	Phenylmethanesulfonylfluoride
<b>PNK</b>	Polynucleotide kinase 3'-phosphatase
<b>PNS</b>	Peripheral nervous system
<b>PTM</b>	Posttranslational modification
<b>Rac1</b>	Ras-related C3 botulinum toxin substrate 1
<b>Rbx1</b>	RING-box protein 1
<b>REST</b>	RE1-Silencing Transcription factor
<b>RhoA</b>	Ras homolog family member A
<b>RING</b>	Really Interesting New Gene
<b>RIPA</b>	Radioimmunoprecipitation assay buffer
<b>RNA</b>	Ribonucleic acid
<b>RNAi</b>	RNA interference
<b>RNF157</b>	Ring finger protein 157
<b>rpm</b>	Revolutions per minute
<b>RT</b>	Room temperature
<b>RT-PCR</b>	Reverse transcription PCR
<b>s.e.m.</b>	Standard error of the mean
<b>Sc</b>	Superior colliculus
<b>SCA1</b>	Spinocerebellar ataxia type 1
<b>SCF</b>	Skp, Cullin, F-box-containing complex

<b>SDS</b>	Sodium dodecyl sulfate
<b>SDS-PAGE</b>	SDS-Polyacrylamide gel electrophoresis
<b>Shh</b>	Sonic hedgehog
<b>shRNA</b>	Short hairpin RNA
<b>Skp1</b>	S-phase kinase-associated protein 1
<b>SnoN</b>	Ski-related novel protein N
<b>SNP</b>	Single nucleotide polymorphism
<b>Snr</b>	Substantia nigra pars reticulata
<b>SpC</b>	Spinal canal
<b>Str</b>	Striatum
<b>TAE</b>	Tris base, Acetic acid and EDTA
<b>TEMED</b>	Tetramethylethylenediamine
<b>TRCP3</b>	Transient receptor potential cation channel, subfamily C, member 3
<b>TUNEL</b>	TdT-mediated dUTP Nick-End Labeling
<b>TdT</b>	Terminal deoxynucleotidyl transferase
<b>UPS</b>	Ubiquitin proteasome system
<b>WAVE1</b>	WAS protein family, member 1
<b>WB</b>	Western blot
<b>WM</b>	White matter
<b>Wnt1</b>	Wingless-type MMTV integration site family, member 1
<b>WT</b>	Wildtype
<b>Zic1,2</b>	zinc finger protein in cerebellum 1, 2

<b>Nucleotide</b>	<b>Single-letter code</b>
Adenosine	A
Cytosine	C
Guanine	G
Thymine	T

<b>Amino acid</b>	<b>3-letter code</b>	<b>Single-letter code</b>
Alanine	Ala	A
Arginine	Arg	R
Asparagine	Asn	N
Aspartic acid	Asp	D
Cysteine	Cys	C
Glutamic acid	Glu	E
Glutamine	Gln	Q
Glycine	Gly	G
Histidine	His	H
Isoleucine	Ile	I
Leucine	Leu	L
Lysine	Lys	K
Methionine	Met	M
Phenylalanine	Phe	F

## Abbreviations

Proline	Pro	P
Serine	Ser	S
Threonine	Thr	T
Tryptophan	Trp	W
Tyrosine	Tyr	Y
Valine	Val	V

---

# 1 Introduction

## 1.1 The cerebellum: *It is all about timing!*

The cerebellum also known as the little brain is indispensable for proper motor control and coordination. Although the cerebellum itself does not initiate movement, it serves as an integration system, receiving inputs from the sensory system, spinal cord and various cortical regions thereby calibrating the precision and timing of any given movement (*Glickstein and Doron, 2008; Mauk et al., 2000; Middleton and Strick, 1998*). This is further illustrated by the fact that various malformations or atrophy affecting the cellular composition and architecture of the cerebellum consistently lead to motor deficits (*Chizhikov and Millen, 2003; Millen and Gleeson, 2008*). Typical symptoms of cerebellar dysfunction include ataxic gait, postural instability, dysmetria, nysthagmus, dysarthria, improper reflexes and dysdiadochokinesia (*Assadi et al., 2008; Millen and Gleeson, 2008; Trouillas et al., 1997*). Recent studies have also implicated the cerebellum in reflex control, motor learning, cognition, language and emotion (*Boyden et al., 2004; Ferrucci et al., 2012; Leggio et al., 2000; Marien et al., 2001; Middleton and Strick, 1998; Rapoport et al., 2000; Stoodley, 2012; Strata et al., 2011; Strick et al., 2009*). In order to fully appreciate the role of the cerebellum in motor coordination and higher cognitive functions, we must first understand its architecture and composition.

## 1.2 Cerebellar architecture and composition: *Simplicity is the ultimate sophistication- Leonardo da Vinci*

The cerebellum is a distinct structure from the cerebrum, having its own characteristic morphological and cellular architecture. At a morphological level, it is defined by two cerebellar hemispheres that are fused at the midline by the protruding vermis. The surface of the cerebellum has fissures that give it a foliated morphology. The foliation of the cerebellum is thought to increase its surface area to accommodate the diverse and functionally complex circuits that can be highly organized within specific micro-domains in certain folias (*Cerminara et al., 2015; Goldowitz and Hamre, 1998; Sillitoe and Joyner, 2007; Sotelo, 2004; Voogd and Glickstein, 1998b*). At a cellular level, the cerebellum is composed of eight

types of neurons including the Purkinje cells, cerebellar granule neurons (CGNs), stellate cells, basket cells, Golgi cells, Lugaro cells, the recently identified unipolar bush cells and candelabrum cells (*Cerminara et al., 2015; Goldowitz and Hamre, 1998; Sotelo, 2004; Voogd and Glickstein, 1998a; White and Sillitoe, 2013*) (**Figure 1.1**). Except for CGNs and unipolar bush cells that use glutamate as their neurotransmitter, the other neuronal types are GABAergic (*Goldowitz and Hamre, 1998; Sotelo, 2004; Voogd and Glickstein, 1998a; White and Sillitoe, 2013*). Most of the cerebellar cell types are evenly distributed across all the folia to give rise to a uniform architecture consisting of three major layers, namely the molecular layer (ML), Purkinje cell layer (PCL) and the internal granule cell layer (IGL) (*Altman and Bayer, 1978*). The ML is the site of extensive synaptic exchange housing the dendritic arbors of the Purkinje neurons and the parallel fibers (axons) of the CGNs. With the exception of small interneurons, the stellate and basket cells, the ML is devoid of cell bodies. At the border of the ML and IGL reside the Purkinje cells. They possess large somas and are arranged in a “string of pearls”-like fashion forming the PCL. Their elaborate dendritic branches span the entire ML. Additionally the GABAergic candelabrum interneurons are also distributed within the PCL. Below the PCL lie the densely packed CGNs that form the IGL. An average adult (human) cerebellum consists of ~50 billion CGNs that are densely packed in the IGL, making them the most numerous cell-type in the entire brain (*Altman and Bayer, 1978; White and Sillitoe, 2013*). CGNs have a small soma, with the nucleus occupying most of the space. They have 3-4 short dendrites harboring claw-shaped tips and bifurcating axons that reside in the ML forming the parallel fibers. The IGL also houses the GABAergic Lugaro and Golgi interneurons.

The three layers, namely the ML, PCL and the IGL together form the cerebellar cortex. Below the cerebellar cortex is the white matter of the cerebellum consisting of the major efferent tracts of the cerebellum. Within the white matter lies a small cluster of grey matter called the deep cerebellar nuclei (DCN), representing the final output and checkpoint of the cerebellum (*Altman and Bayer, 1978; Glickstein and Doron, 2008; Goldowitz and Hamre, 1998; Sotelo, 2004; White and Sillitoe, 2013*).

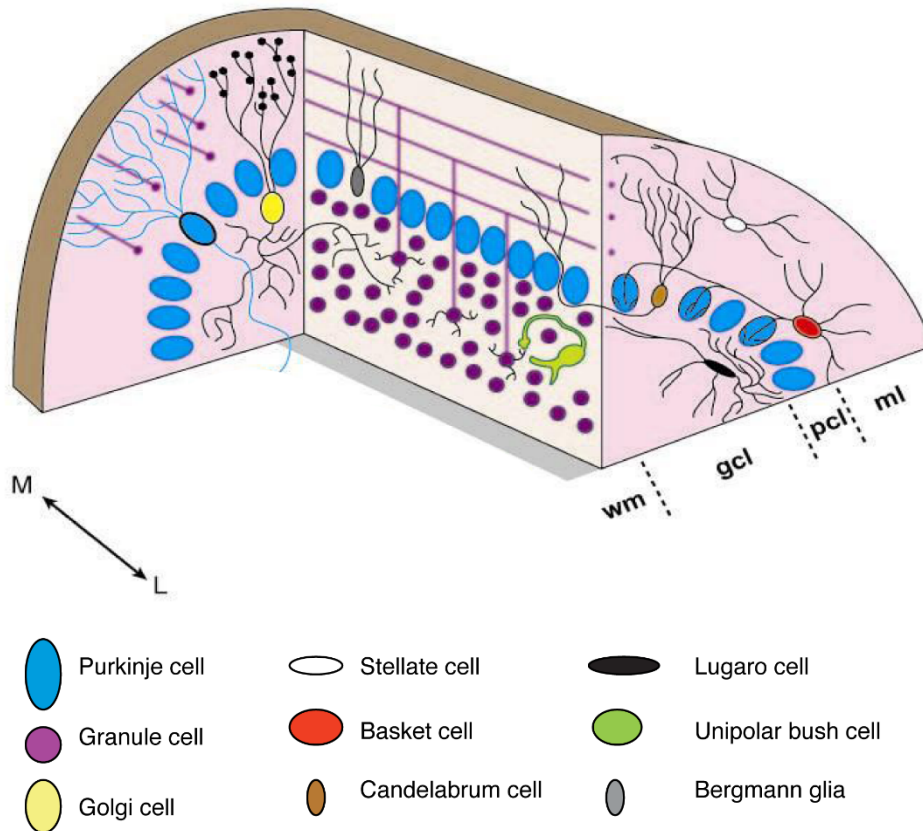


**Figure 1.1. Cellular composition of the cerebellum:** Schematic depicts the various layers of the cerebellar cortex and their cellular composition. Abbreviations: wm= white matter, gcl= granule cell layer, pc= Purkinje cell layer, ml= molecular layer. (*modified from Sillitoe and Joyner, 2007*).

### 1.3 Cerebellar circuitry: *Don't get all your wires crossed just yet!*

The different neurons of the cerebellum are connected via a well-defined circuitry. The cerebellar cortex receives afferent inputs from the climbing fibers, mossy fibers, diffused mono-aminergic and cholinergic fibers while the Purkinje cell axons serve as the sole efferent output of the cerebellar cortex that project onto the DCN (*Sotelo, 2004; Voogd and Glickstein, 1998b*).

The climbing fibers arise from the inferior olive (IO), which in turn relays afferent inputs coming from the certain cortical areas, brain stem and the spinal cord. While each climbing fiber from the IO synapses onto the dendritic arbors of exactly one Purkinje neuron, it synapses multiple times along the dendrites of the same cell (*Cerminara et al., 2015; Sotelo, 2004; Voogd and Glickstein, 1998b; White and Sillitoe, 2013*). The Climbing fibers use



glutamate as their neurotransmitter and generate strong EPSPs on the recipient Purkinje neuron (*Ito, 2006; Sillitoe and Joyner, 2007; Sotelo, 2004; Voogd and Glickstein, 1998b; White and Sillitoe, 2013*). The mossy fibers arising from the pontine nuclei, vestibular nuclei and the spinal cord also use glutamate as their neurotransmitter (*Cerminara et al., 2015; Ito, 2006; Sillitoe and Joyner, 2007; White and Sillitoe, 2013*). Each mossy fiber forms an enlarged rosette in the IGL that synapses onto dendritic claws from ~20 different CGNs (*R R Llinas, 2004*). This synaptic cluster is ensheathed by glia and in turn receives inhibitory inputs from the Golgi interneurons. While climbing fibers and Purkinje cells maintain a one to one ratio, each mossy fiber can send out collaterals to several cerebellar folias resulting in 20-30 rosettes thus synapsing on ~400-600 CGNs at a time (*Mark F Bear, 2006; R R Llinas, 2004*). The CGN axonal tracts reside in the ML where they bifurcate into T shaped unmyelinated parallel fibers that run bidirectionally, synapsing on the Purkinje cell dendrites, which are flattened and oriented perpendicular to the direction of the parallel fibers (*Sotelo, 2004; Voogd and Glickstein, 1998b*). While each parallel fiber synapses only once onto each Purkinje cell, it synapses onto several Purkinje cells along its path. Correspondingly, each Purkinje cell can receive excitatory inputs from several parallel fibers (*Eccles et al., 1966a, b, c; Mark F Bear, 2006; R R Llinas, 2004*). Taken together a single Purkinje cell receives inputs from a single climbing fiber, but several parallel fibers. These synapses are further regulated by the inhibitory synapses from the stellate and basket cells, which result in a feed forward inhibition of the Purkinje cells (*Eccles et al., 1966a, b, c; Voogd and Glickstein, 1998a*). The climbing fiber inputs are often regarded as a “teaching” signal, since the strong excitatory post synaptic potentials (EPSPs) produced by them are known to modulate the synapses between Purkinje cells and parallel fibers by long term depression (LTD), which is thought to contribute to motor learning (*Ito, 2006; (Albus., 1989)*). The GABAergic efferents of the Purkinje cell finally synapse onto the DCN neurons, which send excitatory efferents out of the cerebellum onto effector regions. The DCN serves as the final output center of the cerebellum, which apart from the inhibitory Purkinje efferents, also receives excitatory inputs from the IO and the pontine nucleus (*Ito, 2006*) (**Figure 1.2**). A small subset of GABAergic neurons in the DCN are also known to form a feed back loop by synapsing on the IO (*Middleton and Strick, 1998*). The inhibitory Purkinje efferents are thought to be the regulatory signal that modulates the output of the cerebellum at the DCN, thus contributing significantly in precision and central timing of movements (*Cerminara et al., 2015; Ito, 2002a; Middleton and Strick, 1998; Sotelo, 2004*).

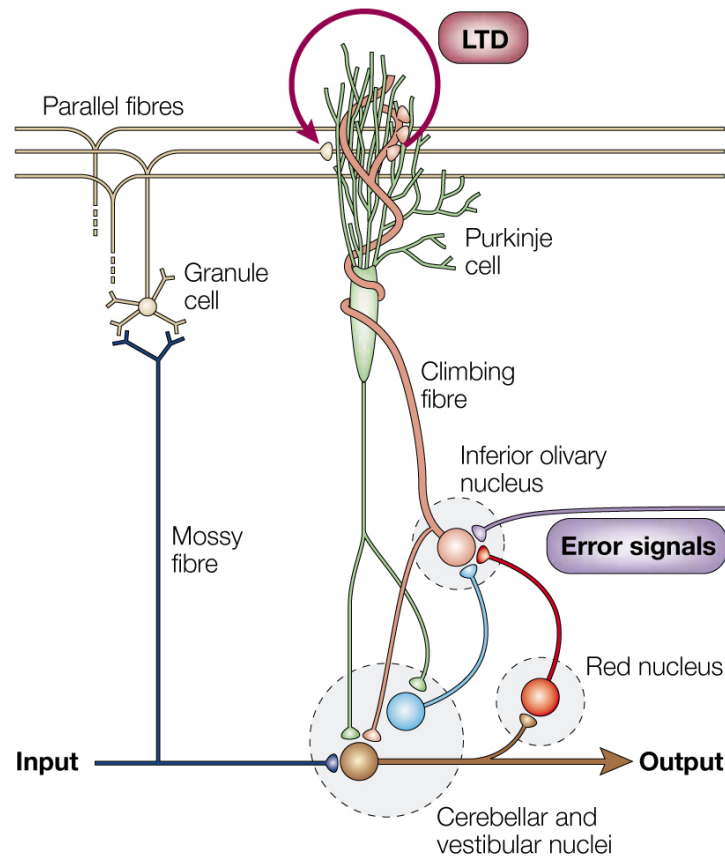


**Figure 1.2. Circuitry of the cerebellum:** Schematic depicts the circuitry of the cerebellum, demonstrating the efferent and afferent connections. Abbreviations: LTD= long term depression. (with permission from Ito, 2002b). *Nature publishing group license number 3614321463665.*

#### 1.4 Cerebellar development: *You can't play a symphony alone; it takes an orchestra to play it.* - Navjoth Singh Siddhu

The cerebellum develops from the constriction at the border of the mesencephalon and metencephalon called the isthmus organizer, a derivative of the hindbrain rhombomere 1. The isthmus organizer expresses a number of growth and transcription factors such as Wnt1, En1 and En2, Pax2, Pax5 and Fgf8, all of which are shown to be crucial for the induction of the cerebellar primordium. The cerebellar primordium spans from the caudal third of the mesencephalic vesicle up until the anterior part of rhombomere 2 (Sgaier *et al.*, 2005; Sotelo, 2004; Wingate, 2001). After the induction of the cerebellar fate, several neurodevelopmental events such as progenitor proliferation, neuronal differentiation, neuronal migration, axon outgrowth and synaptogenesis have to be precisely timed, so that proper lamination and circuitry of the cerebellum can be achieved (Komuro and Yacubova, 2003; Sillitoe and Joyner, 2007; Sotelo, 2004). Deficits in these developmental events are often associated with

various disorders, such as Dandy-Walker Malformations, Jouberts syndrome and Cayman type ataxia (*Chizhikov and Millen, 2003; Itoh et al., 2011; Millen and Gleeson, 2008*). In the following sections, I will focus on key neurodevelopmental events namely, neuronal migration, axon growth and apoptosis in the developing cerebellum, with an emphasis on CGN development.

#### **1.4.1 Granule neuron migration during cerebellar development:**

Neuronal migration is a highly dynamic event, defined by neuronal precursor cells and newborn neurons travelling large distances across the brain to reach their destined locations to give rise to mature neurons. These neurons in turn form the appropriate synaptic connections that eventually compose the fully functional brain (*Ghashghaei et al., 2007; Hatten, 1999*). Disturbances in neuronal migration often result in improper lamination of the brain leading to several neurological conditions including, schizophrenias, autism spectrum disorders and ataxias, depending on the region affected (*Gleeson and Walsh, 2000; Nadarajah and Parnavelas, 2002*).

Radial and tangential migrations are two of the most well characterized types of neuronal migration. Radial migration occurs radially inward or outward via the support of radial glial scaffolds, also referred to as gliophilic migration. Tangential migration on the other hand occurs tangentially via the help of neuronal processes and cell bodies. Tangential migration is thus also referred to as neurophilic migration. While radial migration is mostly observed in newborn neurons, tangential migration is observed in neuronal precursor cells that must reach their destined location, where they divide further or differentiate (*Ghashghaei et al., 2007; Hatten, 1999; Nadarajah and Parnavelas, 2002*). Both radial and tangential migration occur extensively during cerebellar development (*Hatten, 1999; Sotelo, 2004*).

Cells of the developing cerebellum originate from two different germinal centers, the subventricular zone of the fourth ventricle as well as from the rhombic lip (interface between the dorsal roof plate and dorsal neuroepithelium of the alar plate) of rhombomere 1. While the Purkinje cells and Golgi cells originate from the former, the CGN precursors originate from the latter (*Hatten and Heintz, 1995; Sgaier et al., 2005; Sotelo, 2004*). Newborn Purkinje and Golgi neurons migrate embryonically from the subventricular zone of the fourth ventricle to the cerebellar cortex, while the interneurons of the ML, namely the basket and

stellate cells, originate from neuronal precursor cells within the white matter of the cerebellum, proliferate further by interstitial proliferation and migrate to the ML (*Sotelo, 2004*). Unlike the other cerebellar cell types, the CGN precursors migrate dorsolaterally from the rhombic lip to the cerebellar primordium (E10-E15), where they form a second proliferative region called the external granule layer (EGL). The EGL spans the entire surface of the cerebellar primordium and initially consists of a single layer of CGN precursor cells (*Alder et al., 1996; Sgaier et al., 2005; Sotelo, 2004*). Postnatally (E16-P10), these precursor cells undergo several rounds of cell division, resulting in a 6-7-fold expansion of the thickness of this layer (*Altman and Bayer, 1985; Hatten and Heintz, 1995; Sillitoe and Joyner, 2007; Sotelo, 2004*). By P7, the EGL consists of two distinctive regions, the upper EGL consisting of neuronal precursors that are proliferative, and the lower EGL consisting of newly differentiated neurons (*Altman, 1972b; Chedotal, 2010; Sillitoe and Joyner, 2007*). The neuronal precursors of the EGL differentiate to give rise to the CGNs, which then migrate tangentially to reach their destined folia before migrating radially inward to the IGL by gliophilic migration. During the process of tangential migration, the newborn CGNs extend two processes, a longer leading process and a shorter trailing process (*Chedotal, 2010; Komuro and Yacubova, 2003; Komuro et al., 2001; Sotelo, 2004*). The leading and trailing processes go through repetitive cycles of contraction and extension. The leading process constantly extends and retracts leading to a net elongation, consequently the cell soma is dragged into the leading process, followed by a contraction of the trailing leading to cellular movement (*Edmondson and Hatten, 1987; Komuro and Yacubova, 2003*). Upon completion of tangential migration, the CGNs from the lower EGL migrate across the ML into the IGL with the help of astrocytic radial glial scaffolds that span the entire ML from the pia to the IGL (*Chedotal, 2010; Goldowitz and Hamre, 1998; Hatten and Heintz, 1995; Sotelo, 2004; Wang and Zoghbi, 2001*) (**Figure 1.3**). The migration of CGNs is a long-lasting process that continues up until the third postnatal week. As neuronal migration proceeds, the EGL becomes thinner and disappears by P15 or P16 (*Altman, 1972b; Chedotal, 2010; Sgaier et al., 2005; Sotelo, 2004*). Once neuronal migration is complete the astrocytic radial glia lose their radial glia properties and mature into Bergmann glia spanning the entire ML in the adult cerebellum (*Sotelo, 2004*). Proper neuronal migration in the cerebellum is indispensable as it ensures the correct lamination of the cerebellum (*Millen and Gleeson, 2008*). The majorly neonatal proliferation and migration of CGNs of the cerebellum in rodents also makes it an

attractive model system to study neuronal migration and development (*Alder et al., 1996; Hatten and Heintz, 1995*).

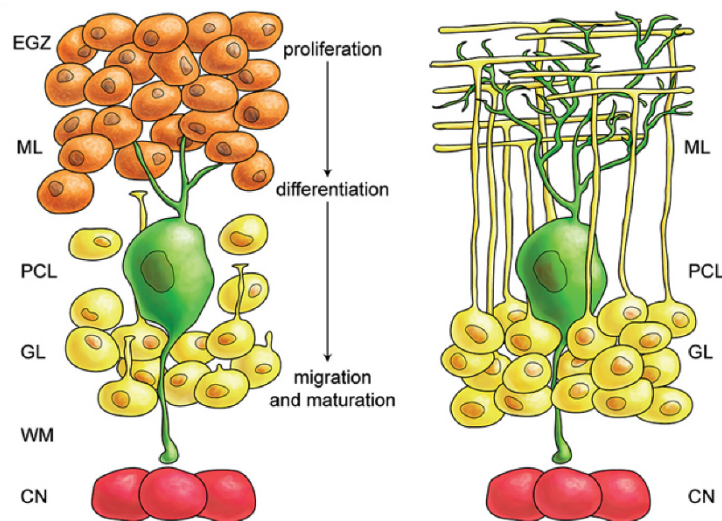


**Figure 1.3. CGN migration in the developing cerebellum:** Schematic demonstrates the migration of CGN from the EGL to the IGL, highlighting their expansive proliferation in the EGL and subsequent differentiation and migration across the ML and PCL to the IGL. Abbreviations: EGZ= external germinal layer (zone), ML= molecular layer, PCL= Purkinje cell layer, GL= granule cell layer, WM= white matter, CN=cerebellar nuclei. (*modified from Marzban et al., 2014*). Licensed by Creative Commons (CC BY 4.0) <http://creativecommons.org/licenses/by/4.0/>

#### 1.4.1.1 Molecular regulation of granule neuron migration in the cerebellum:

Neuronal migration in the cerebellum is governed by the interplay of various cell-extrinsic and intrinsic factors. Extrinsic secretory molecules, such as the semaphorins, netrins and slits comprise a large family of guidance cues that are well characterized in neuronal migration (*Casazza et al., 2007; Lai Wing Sun et al., 2011; Marin et al., 2003*). These molecules act as chemo-attractants or repellents eliciting intracellular signaling cascades that control the cytoskeletal dynamics of the migrating neuron thereby guiding the newborn neurons to their correct destination (*Ghashghaei et al., 2007; Komuro and Yacubova, 2003; Yacubova and Komuro, 2003*). Studies in the past decades have further highlighted the role of these extrinsic guidance molecules in the context of cerebellar development. Sema6A and its interaction to the receptor plexin A2 was found to be crucial for centrosome-mediated nucleokinesis of the granule cell soma and the initiation of radial migration of postmitotic CGNs in the cerebellum (*Kerjan et al., 2005*). Netrin1 was found to act as a chemo-attractant for neurons migrating

from the lower rhombic lip, however, it also functions as a chemo-repellent by steering the migrating CGNs away from the EGL towards the ML (*Alcantara et al., 2000; Marin and Rubenstein, 2001*). Studies have also demonstrated that the brain derived growth factor (BDNF) and its receptor TrkB are crucial for proper radial neuronal migration in the cerebellum as loss of BDNF in *BDNF*<sup>-/-</sup> mice leads to impaired migration of CGNs (*Borghesani et al., 2002; Komuro and Yacubova, 2003*). Moreover, neuregulin and its receptor ErbB4 have been implicated in proper adhesion and migration of CGNs along radial glia (*Komuro and Yacubova, 2003; Rio et al., 1997*).

Apart from the various extrinsic factors, the migrating neuron itself has an array of intrinsic molecular cascades that can be modulated to shape the cytoskeleton thereby influencing its migration. Examples include regulation at the transcriptional level or posttranslational modification (PTM) of key regulator proteins thereby changing the activity state of their respective pathways (*Coskun and Luskin, 2002; Frank and Tsai, 2009; Govek et al., 2011*). As such, cyclin-dependent kinase 5 (Cdk5) was recently found to be crucial for CGN migration in the cerebellum. Oshima and colleagues demonstrated that loss of CDK5 in the *cdk5*<sup>-/-</sup> chimeric cerebellum lead to stalled CGNs in the ML of the adult mice cerebella (*Komuro and Yacubova, 2003; Ohshima et al., 1999*). PTM of cytoskeletal regulators of actin and microtubules directly influences cell motility and neuronal migration (*da Silva and Dotti, 2002; Kuijpers and Hoogenraad, 2011*). A recent study demonstrated that ubiquitination and proteolytic degradation of the RhoGTPase RhoA by the E3 ligase Smurf1 lead to impaired axon growth and neuronal migration in the developing rat cerebellum (*Kannan et al., 2012b*).

#### **1.4.2 Parallel fiber formation and axon growth regulation in cerebellar granule neurons:**

Neurite extension and axon growth are fundamental events of neurodevelopment that ensure the proper connectivity of the adult brain. Neurite outgrowth and axon specification *in vivo* are strongly related to neuronal migration. Upon completion of neuronal migration, the leading process of the migrating cell gives rise to dendrites whereas the trailing process gives rise to the axon (*Lewis et al., 2013; Rakic, 1971, 1972; Shoukimas and Hinds, 1978*).

The postnatal differentiation and maturation of CGNs in rodents makes them a suitable model to study axon growth and guidance *in vivo* as well as *in vitro* (Hatten and Heintz, 1995). During cerebellar development, the newborn CGNs adopt a bipolar shape by extending two processes, the leading and trailing processes, prior to radial migration. These processes grow in parallel to the pial surface and aid in tangential migration of the CGN across the EGL of the cerebellar cortex. Upon completion of tangential migration, these neurons migrate radially inward towards the IGL by extension of a third process perpendicular to the two previously formed processes. This third process now assumes the role of the new leading process that translocates the nucleus inward (nucleokinesis) to the IGL along the radial glia. The inward migration of the CGN cell body causes the two initially created processes to fuse, resulting in T-shaped axons that are connected to the migrating soma of the CGN. The T-shaped axonal processes of the CGNs are restricted to the ML and are oriented in parallel to the EGL. They grow and elongate bidirectionally to give rise to the fasciculated, unmyelinated axonal bundles of the parallel fibers in the ML in the developed cerebellum (Altman, 1972a, b; Kawaji et al., 2004). Dissociated CGN cultures have been long used to study axon specification and growth *in vitro* (Bilimoria and Bonni, 2008; Hatten, 1985; Holubowska et al., 2014; Segal et al., 1995; Stegmuller et al., 2006). They recapitulate well-defined phases from being unpolarized to polarized with specified processes, similar to other *in vitro* neuronal model systems such as hippocampal or cortical neurons (Arimura and Kaibuchi, 2007; Polleux and Snider, 2010) (Figure 1.4).

During neurodevelopment, axons are guided to their final destination by the growth cone, a highly dynamic structure at the tip of the axon that is receptive and reactive to stimuli from its environment. The growth cone comprises the peripheral P-domain and the central C-domain that are different in their structure and molecular identity. The P-domain is highly dynamic consisting of the flattened lamellipodia and its finger-like protrusions, the filopodia. It is rich in actin and is invaded by single dynamic microtubules. On the other hand, the C-domain is less dynamic and mainly characterized by intense polymerization of microtubules and organelle transport (Dent and Gertler, 2003; Lowery and Van Vactor, 2009).

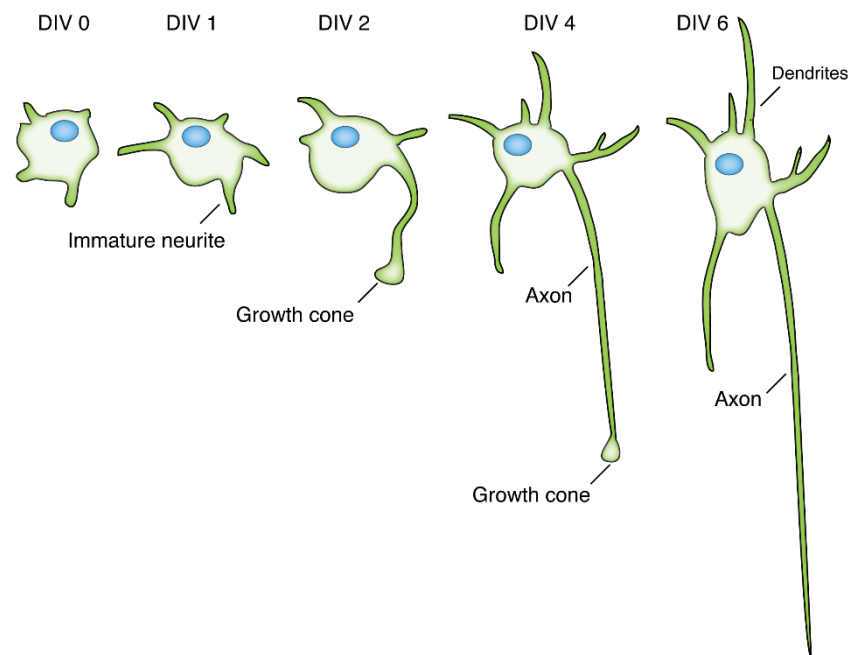


**Figure 1.4. Polarization and neurite extension in CGNs in culture:** Schematic recapitulates the different stages of maturation and neurite outgrowth in cultured CGNs from DIV 0 until DIV 6. The cells at DIV 1 start slowly sprouting neurites and become polarized by DIV2. By DIV 4 axon growth is ongoing, leading to a mature axon by DIV6-8 (*adapted from Arimura and Kaibuchi, 2007*).

Axon growth and elongation is compartmentalized into three steps: i) Protrusion: lamellipodia and filopodia are formed as a result of actin polymerization. ii) Engorgement: vesicles and organelle transport is directed to the growth cone. iii) Consolidation: the proximal part of the axon forms the extension of the axon and bidirectional movement of vesicles and organelles is established (*Dent and Gertler, 2003; Lowery and Van Vactor, 2009*).

#### 1.4.2.1 Molecular regulation of axon growth in CGNs:

Cytoskeletal dynamics are the major driving force behind axon growth and elongation in developing neurons. While actin polymerization and depolymerization at the growth cone mainly influences axon guidance, microtubule polymerization regulates axon growth. Factors that affect the cytoskeletal dynamics directly influence axon extension and pathfinding (*Dent and Gertler, 2003; Dent et al., 2011; Kalil and Dent, 2005*). Much like neuronal migration, axon growth is also guided by various extracellular cues, such as semaphorins, netrins and ephrins as well as growth factors such as NGF (nerve growth factor), BDNF and NT-3



(neurotrophin 3) that act at the growth cone by binding to their receptors and eliciting intracellular signaling cascades (*Bixby and Harris, 1991; Kennedy, 2000; Kullander and Klein, 2002; Pasterkamp and Kolodkin, 2003; Segal et al., 1995; Zhou and Snider, 2006*). Apart from the cell-extrinsic factors, a number of cell intrinsic regulators have been identified to play a direct role in axon growth and elongation. Cytoskeletal regulators such as CDC42 and Rac1 have been reported to stimulate actin protein 2/3 (Arp2/3) activity by binding to their effectors neuronal Wiskott-Aldrich syndrome protein (N-WASP) and WAVE1 respectively, leading neurite extension (*Goley et al., 2006; Goley and Welch, 2006; Pak et al., 2008*). Microtubule-associated protein 1B (MAP1B) levels at the growth cone also influence neurite extension (*Gonzalez-Billault et al., 2004*). Several transcriptional regulators, such as SnoN and Id2, have been shown to promote axon growth in CGNs (*Lasorella et al., 2006; Stegmuller et al., 2006*). On the other hand, posttranslational modifications, such as phosphorylation of collapsing-response mediator protein2 (CRMP2) by GSK-3 $\beta$  prevents it from stabilizing microtubules resulting in a negative regulatory effect on axon growth (*Yoshimura et al., 2005*). C-Jun N-terminal kinase (JNK) and Cdk5 have been implicated in axon growth regulation (*Connell-Crowley et al., 2000; Hirai et al., 2006*). Recent evidences also implicate the UPS components and E3 ligases in axon growth regulation. FBXO31-SCF reportedly ubiquitinates and degrades its substrate Par6 resulting in axon growth (*Vadhvani et al., 2013*). Similarly, the E3 ligase Smurf-1 was identified to ubiquitinate and degrade the RhoGTPase RhoA in order to promote axon growth in CGNs (*Kannan et al., 2012b*). The interplay of signaling cascades regulated by the various cell-extrinsic and -intrinsic factors ultimately exert their effect on the growing axon by dynamically remodeling its cytoskeleton. As a result, the continual assembly and disassembly of the actin cytoskeleton together with the ongoing polymerization of microtubules regulate axon growth and guidance to ensure proper wiring (*Bixby and Harris, 1991; Dent and Gertler, 2003; Dent et al., 2011; Kalil and Dent, 2005; Polleux and Snider, 2010*).

### **1.4.3 Neuronal number and cell integrity within the cerebellum:**

The cerebellum is a highly organized structure with a defined number of all of its cell types. During cerebellar development the proper number of cells is maintained on one hand by the tight regulation of progenitor proliferation and differentiation and on the other hand by influencing the neuronal survival of differentiated cells. During neurodevelopment, not all

progenitors differentiate into neurons that get integrated into functional circuits resulting in apoptosis of these excess cells. Thus, regulating the neuronal progenitor pool is crucial to ensure the right number of cells in the developing cerebellum (*Chizhikov and Millen, 2003*). Previously, studies have identified several mechanisms that regulate progenitor proliferation. Cell-extrinsic events such as Purkinje cell and CGN progenitor interactions mediated by Shh signaling, or notch2-mediated signal transduction in the EGL have been found to positively influence cell numbers within the EGL (*Chizhikov and Millen, 2003; Goldowitz and Hamre, 1998; Solecki et al., 2001*). Cell-intrinsic pathways governed by transcription factors such as Zfp1, Zic1 (zinc finger protein in cerebellum 1) and Zic2 (zinc finger protein in cerebellum 2) have been implicated in keeping a check on CGN progenitor population in the developing cerebellum (*Aruga et al., 1998; Chizhikov and Millen, 2003; Goldowitz and Hamre, 1998; Yang et al., 1999*). Moreover, several cell cycle regulators including cyclin D2, p27 Kip1 and N-myc were also found to regulate the CGN progenitor pool in the EGL (*Huard et al., 1999; Knoepfler et al., 2002; Miyazawa et al., 2000*). Following neuronal differentiation, it is important to maintain proper cellular health for maintenance of cell number and structural integrity of the cerebellum. Examination of mouse models with a hypoplastic cerebellum and neurodegenerative phenotypes such as *lurcher*, *tottering* and *weaver* have helped to identify several genes which encode for ion channel subunits, thus highlighting the role of ionic homeostasis in survival of CGNs and Purkinje cells in the developing cerebellum (*Heintz and Zoghbi, 2000; Lalonde and Strazielle, 2001*). The transcription factor NeuroD for example was found to be crucial for survival of postmitotic CGNs, as loss of NeuroD resulted in large-scale apoptosis of CGNs (*Chizhikov and Millen, 2003; Miyata et al., 1999*). Recent studies have also implicated E3 ligases such as E6-AP and RNF 157 as critical regulators of neuronal survival in the developing cerebellum (*Cummings et al., 1999; Matz et al., 2015*).

### **1.5 Ubiquitination as a means of cell-intrinsic regulation of cerebellar development: *To be or not to be?* – William Shakespeare**

As previously introduced, various neurodevelopmental events rely heavily on both cell-extrinsic and cell-autonomous mechanisms. While cell-extrinsic mechanisms have been extensively studied, the contribution of cell-intrinsic regulators still remains poorly understood. Advances in recent decades have not only shed light on the role of transcriptional regulation in neurodevelopment, but have also identified the posttranslational modification of

proteins as a major contributor of intrinsic regulation of neurodevelopment (*Kawabe and Brose, 2011; Lancaster et al., 2011b; Moore and Goldberg, 2011; Trakhtenberg and Goldberg, 2012*). Following synthesis, a protein can be modified by the addition of functional groups such as phosphates, carbohydrates, lipids, acetates or nitrates. Similarly, the covalent addition of the small, 76 aa protein ubiquitin onto substrates is another type of posttranslational modification referred to as ubiquitination. Protein ubiquitination occurs in all cells of the eukaryotic organism regulating protein activity as well as spatial and temporal expression (*Chen et al., 2001; Hochstrasser, 1996; Welchman et al., 2005*). Several studies have previously implicated ubiquitination as a major cell-intrinsic regulator of neurodevelopment (*Kawabe and Brose, 2011*).

### **1.5.1 The ubiquitination cascade:**

Ubiquitination occurs via a 3-step enzymatic cascade that was first characterized by Avram Hershko, Aron Ciechanover and Irwin Rose in the 1980s, for which they were awarded the Nobel Prize in chemistry in 2004. The cascade is initiated by the E1 ubiquitin-activating enzyme (E1) that catalyzes the activation of ubiquitin in an ATP-dependent manner, resulting in the formation of a thioester bond between the C-terminus of ubiquitin and the catalytic cysteine of the E1. Subsequently, the E2 ubiquitin-conjugating enzyme (E2) mediates the transfer of the activated ubiquitin onto itself by thioesterification. In the final step the E3 ubiquitin ligase enzyme (E3) recruits the E2-ubiquitin as well as a specific protein substrate, thus mediating the transfer of ubiquitin from E2 onto a lysine residue of the substrate. Ubiquitination of the substrate occurs by the formation of an amide-isopeptide bond between Gly 76 of the ubiquitin-ATP conjugate and a lysine residue on the substrate protein (*Hershko and Ciechanover, 1998; Hochstrasser, 1996*) (**Figure 1.5**).

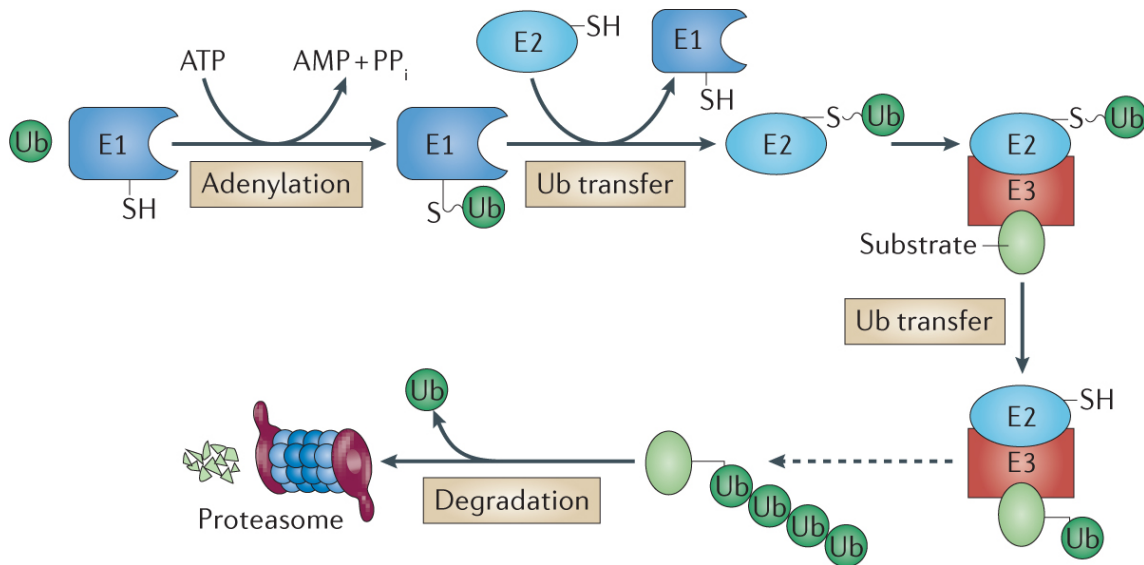


**Figure 1.5. Overview of the ubiquitin proteasome system:** Schematic displays the mechanism of protein ubiquitination by the E1 ubiquitin-activating enzyme, the E2 ubiquitin-conjugating enzyme and the E3 ubiquitin ligase. The E1 brings about the catalytic activation of ubiquitin in an ATP-dependent manner, resulting in the formation of a thioester E1-ubiquitin intermediate. Subsequently, the E2 transfers the ubiquitin onto itself, forming an E2 thioester intermediate. In the final step, the E3 recruits specific substrates and mediates the transfer of ubiquitin from the E2 onto the substrate. The ubiquitinated substrate can then be turned over by the proteasome. Abbreviations: Ub= ubiquitin, E1= ubiquitin activating enzyme, E2= E2 ubiquitin conjugating enzyme, E3= E3 ubiquitin ligase. (*With permission from Maupin-Furlow, 2012*). Nature publishing group license number 3614400042383.

Ubiquitination may have very different consequences on the protein's fate. Studies have previously implicated mono- or multi-monoubiquitination in influencing protein interactions, localization and substrate activity (**Figure 1.6 a**). However, the outcome of polyubiquitination can vary from proteolytic protein degradation to regulation of signaling cascades, depending on the ubiquitin chain type. Polyubiquitination occurs by the addition of another ubiquitin onto the lysine of an existing ubiquitin on the substrate. Different chain types of polyubiquitination can be formed based on the ubiquitin lysine (K) residue at which further chain extension occurs, including K6, K11, K27, K29, K33, K48 and K63. Depending on the type of lysine linkage and the structure of the polyubiquitin chain, the ubiquitinated protein can have very different fates. Non-linear chains with closed conformations, as observed in K11- or K48- mediated polyubiquitination are readily recognized by the 26S proteasome and lead to proteolytic degradation of the substrate. In contrast, linear chains with open conformations, as seen in K63-mediated polyubiquitination are implicated in regulation of signal transduction pathways. K63 polyubiquitination was for instance found to regulate

NF- $\kappa$ B activation, DNA repair pair, protein stability as well as lysosomal degradation of certain substrates (**Figure 1.6 b**). The outcome of K6-, K27-, K29- and K33-linked polyubiquitination however still is poorly understood (*Bocquet et al., 2009; Komander and Rape, 2012*).

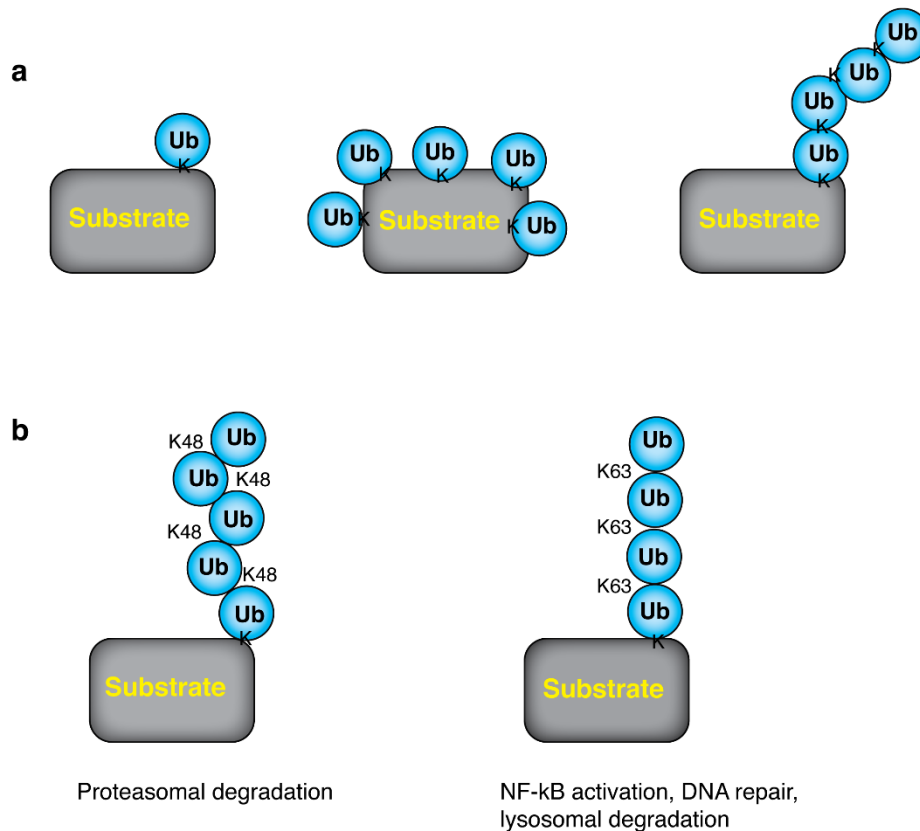


**Figure 1.6. Different types of ubiquitination on substrates:** **a.** Schematic depicts the different topologies of ubiquitination that can occur on protein substrates, ranging from mono or multi mono ubiquitination, to polyubiquitination. **b.** The kind of ubiquitination determines the fate of the ubiquitinated protein. While K48-linked polyubiquitination leads to proteasomal degradation, K63-linked linear chains serve as non-proteolytic modifications. K= lysine, Ub= ubiquitin. (*Adapted from Komander and Rape, 2012*).

### 1.5.2 E3 ligases and their role in proper cerebellar development:

E3 ligases are responsible for identifying and recruiting specific protein substrates for ubiquitination. While there are only 2 E1s and ~30 E2s identified in the mammalian genome, it is predicted to contain more than 600 E3s (*Artinian et al., 2008*). Since the total number of ubiquitinated proteins clearly outnumbers the amount of E3 ligases that can subject them for

ubiquitination, it is not surprising that several studies have reported E3 ligases having multiple protein ubiquitination substrates (*Peters, 2006*). One of the well-known E3 ligases exemplifying the aforementioned is Cdh1-APC (*Peters, 2006*). It ubiquitinates several substrates, including the transcription factors SnoN and Id2, the E3 ligase Smurf1 as well as the Rho GTPase activator p250GAP for proteolytic degradation in order to regulate axon growth and migration in the developing cerebellum (*Kannan et al., 2012a; Kannan et al., 2012b; Lasorella et al., 2006; Stegmuller et al., 2006*). Another example is the SCF E3 ligase Skp2, that ubiquitinates several targets such as p21, p27, p57 as well as cyclin A/D1 and E, in order to regulate cell cycle progression (*Bornstein et al., 2003; Carrano et al., 1999; Frescas and Pagano, 2008; Nakayama et al., 2004; Pateras et al., 2006*). In this section, I will elaborate on the two major classes of E3 ligases and highlight a few notable members from each class that have been implicated in regulating cerebellar development.

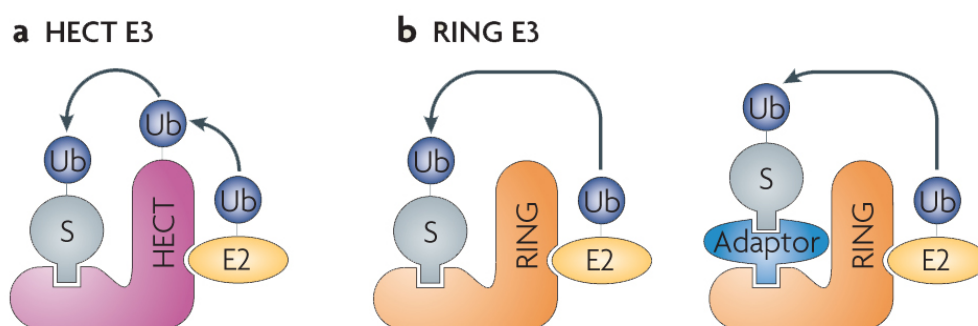


**Figure 1.7. HECT and RING E3 ligases:** Schematic displays the mechanism of protein ubiquitination by two different classes of E3 ubiquitin ligases. **a.** HECT E3 ligases harbor a HECT domain, which recruits the E2, while the substrate is recruited via its other domains. The HECT ligases mediate the transfer of ubiquitin from the E2 onto itself, forming an E3-ubiquitin conjugate. Subsequently, it transfers the ubiquitin onto the substrate. **b.** RING ligases recruit E2s at their RING domain, and they bring the substrate and E2-ubiquitin conjugate in very close proximity, thereby mediating the direct transfer of ubiquitin from the E2 onto the substrate. While HECT ligases are single subunit E3 ligases, RING ligases can be either single or multisubunit in nature. Abbreviations: Ub= ubiquitin, S= substrate, E2= E2 ubiquitin conjugating enzyme. (*With permission from Rotin and Kumar, 2009*). *Nature publishing group license number 3614410726001*.

The sheer number of E3 ligases and their multiple substrates makes them one of the most diverse and versatile members of the ubiquitin cascade. Most E3 ligases can be classified into two major classes - the HECT type and the RING type ligases (**Figure 1.7 a, b**). The HECT type ligases share the homologous to E6-AP carboxy terminal (HECT) domain. They bind to the E2 enzyme and covalently bind the ubiquitin with their catalytic cysteine, forming an E3-

thioester intermediate. Subsequently, it transfers the ubiquitin onto a lysine of the recruited protein substrate (*Rotin and Kumar, 2009*). Several HECT ligases have been implicated in proper cerebellar development. For instance, the E3 ligase Huwe1 is found to be critical for proper cerebellar development as it regulates the CGN progenitor pool by ubiquitinating and degrading its substrates N-myc and Atoh1 (*Forget et al., 2014; Zhao et al., 2008*). It is also crucial for Bergmann glial differentiation and proper migration of CGNs across the ML to the IGL (*D'Arca et al., 2010*). The HECT ligase Itch was recently implicated in ubiquitination and degradation of the Shh transcription factor Gli1, thus suppressing the Shh signaling in the developing cerebellum. By ubiquitinating Gli1, Itch keeps a check on CGN progenitor proliferation and promotes neuronal differentiation (*Di Marcotullio et al., 2006*). Other studies have also reported that the HECT ligase Smurf1 regulates axon growth and neuronal migration in the developing cerebellum by targeting the Rho GTPase RhoA for degradation (*Kannan et al., 2012b*).

The RING ligases comprise the largest family of E3 ligases, sharing a common, really interesting new gene (RING) domain. The RING E3 ligases bind to the E2 enzyme using their RING domain and mediate the direct transfer of ubiquitin from the E2 onto the recruited substrate. They act like a scaffold that brings the E2 and the substrate in very close proximity to facilitate the ubiquitin transfer. RING ligases can be classified into single subunit or multi-subunit RING ligases (*Deshaies and Joazeiro, 2009; Pickart, 2001; Pickart and Eddins, 2004*). The anaphase-promoting complex (APC) and the Skp1-Cullin1-Fbox protein (SCF) complexes among other cullin-RING ligases comprise the largest groups and are the most well characterized subfamilies of the multi-subunit RING E3 ligases (*Deshaies and Joazeiro, 2009; Peters, 1998, 2006; Pickart, 2001*). The SCF complexes and the other cullin-RING ligases will be discussed in greater depth under section 1.5.3. A number of studies have implicated RING ligases in the regulation of cerebellar development. As previously mentioned, the E3 ligase Cdh1-APC has been implicated in control of axon growth in CGNs (*Konishi et al., 2004*). Similarly, the related cell cycle regulator Cdc20-APC, too, has been found to influence dendritogenesis, having no effect on axons in the developing cerebellum (*Kim et al., 2009*). Interestingly, it was also implicated in presynaptic differentiation of CGNs by targeting the transcription factor NeuroD2 for degradation (*Fang et al., 2009; Yang and Bonni, 2010*). Several other studies have also identified SCF-complexes and cullin-based RING ligases crucial for cerebellar development that will be discussed in the next section.

### 1.5.3 SCF complexes and their contribution in neurodevelopment and disease:

The SCF complex type E3 ligases were first identified in yeast (*Feldman et al., 1997; Skowrya et al., 1997*). They are one of the largest and most studied subfamilies of the multi-subunit RING ligases. The SCF complex comprises of four components: Skp1 (S-phase-kinase-associated protein1), Cull1 (cullin1), F-box protein and the small RING finger protein RBX1 or RBX2 (RING-box protein1 or 2) (**Figure 1.8. a**). F-box proteins serve as the interchangeable protein adaptors that recruit specific substrates to the E3 complex for ubiquitination (*Zheng et al., 2002*). All members of the F-box protein family share the common, approximately 40 amino acid long F-box domain. Based on the additional motifs or domains present on the protein apart from its F-box domain, the members of the F-box family can be classified into three categories: The FBXLs, FBXWs and FBXOs. The FBXWs harbor WD40 domains, the FBXLs harbor leucine-rich repeats and the FBXOs (F-box other) may or may not harbor other domains. While these additional domains are speculated to be responsible for substrate binding, the F-box domain is known to be indispensable for mediating the interaction of the F-box protein with Skp1 and cullin1 and thus maintaining the integrity of the complex (*Deshaies, 1999; Jin et al., 2004; Kipreos and Pagano, 2000*). Apart from the cullin1-based SCF complex, several other cullin-based RING ligases have been reported that use different cullins and substrate-recruiting adaptors (*Skaar et al., 2013*). Besides cullin1, the only other cullin identified to interact with both Skp1 and F-box proteins to form a multi-subunit E3 SCF-like complex is cullin7. To date, the only cullin7-based atypical SCF-like complex reported is formed together with the F-box protein FBXW8 (*Sarikas et al., 2008*) (**Figure 1.8. b**).

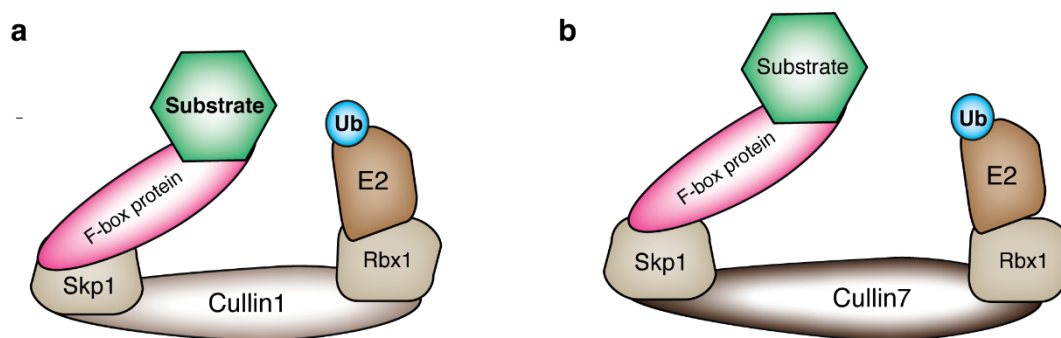


**Figure 1.8. SCF complexes are multi-subunit RING ligases: a.** Schematic shows the



components of the canonical SCF complex E3 ligases, namely the RING protein Rbx1 that recruits the E2-ubiquitin thioester to the complex, the scaffold protein cullin1, the adaptor protein Skp1 and the substrate recruiting F-box protein. **b.** Schematic of the atypical cullin7-based SCF complex, with the components Rbx1, cullin7, Skp1 and the substrate-recruiting F-box protein. Ub= ubiquitin.

Although 68 F-box proteins have been identified in the mammalian genome so far, only a few of them have been well characterized. A majority of the F-box protein SCF complexes including FBXW7-SCF,  $\beta$ -TrCP-SCF and Skp2-SCF have been studied in the context of cell cycle and cancer (*Skaar et al., 2013*). Recent studies have also identified a role for many of them in neurodevelopment and disease. For instance  $\beta$ -TrCP-SCF ensures the proper differentiation of neuronal progenitors during neurogenesis by mediating the degradation of its substrate REST (RE1-silencing transcription factor) (*Westbrook et al., 2008*). FBXO45 regulates proper axonal pathfinding in the cortex, as loss of FBXO45 in mice resulted in defects in cortical axon tracts and improper innervation of the diaphragm (*Saiga et al., 2009*). FBXW7 on the other hand regulates proliferation of CGN precursors in the developing cerebellum, prevents premature migration of CGNs and additionally regulates Purkinje cell number and axonal arborization. It is speculated that FBXW7 exerts its function in the developing cerebellum by regulating the levels of its substrates including notch, N-myc and c-Jun (*Jandke et al., 2011*). Recent studies also identified FBXW8 and FBXO31 as important players of cerebellar development. While FBXW8 was found to regulate dendrite growth (*Litterman et al., 2011*), FBXO31 was identified as a key player in the control of axon growth and neuronal migration (*Vadhvani et al., 2013*). Interestingly, a recent study reported a truncated form of FBXO31-SCF that caused non-syndromic autosomal recessive intellectual disability in a Pakistani family (*Mir et al., 2014*). FBXO31 and FBXO21 have additionally also been linked to other neurodevelopment disorders including schizophrenia (*Chen et al., 2008; Narayan et al., 2008*).

Apart from neurodevelopment, recent studies also implicate several F-box proteins in neurodegenerative diseases. For example, FBXO2 has previously been shown to regulate the processing of APP by targeting the APP-cleaving  $\beta$ -secretase for degradation (*Gong et al., 2010*). A recent study has identified APP itself as a target of FBXO2 thus presenting FBXO2 as a potential therapeutic target of Alzheimer's disease (*Atkin et al., 2014*). Numerous research papers have also identified specific autosomal-recessive mutations on the FBXO7

gene to be responsible for early-onset Juvenile Parkinsonism in certain Iranian, Dutch, Turkish, Italian and Pakistani families (*Di Fonzo et al., 2009; Paisan-Ruiz et al., 2010*).

### **1.6 Aim and scope of the study:**

As previously discussed, F-box proteins have been thoroughly studied in the control of cell cycle in cancer, but have only recently emerged as important players in neurodevelopment and disease. Of the ~70 mammalian F-box proteins identified so far several are highly expressed in the nervous system. However, only a handful has been investigated regarding their function in the brain and the underlying implications in neurological diseases. It is thus essential to characterize the functions of the several understudied F-box proteins and identify the underlying pathways regulated by them. The F-box protein FBXO41 has been previously proposed as a genetic marker for multiple system atrophy (*Langerveld et al., 2007*), and certain SNPs in the *Fbxo41* gene are speculated as risk factors for Parkinson's disease in the Chinese Han population (*Liang et al., 2013*). A previous study from our lab has presented the initial characterization of FBXO41 in the nervous system. It has identified FBXO41 as brain-dominant cytoplasmic neuronal F-box protein, harboring a C2H2 zinc finger domain at its N-terminus and the F-box domain at its C-terminus. The study also reported a potential role of FBXO41 in regulation of axon growth and neuronal migration in the developing rat cerebellum (*Holubowska, 2013*).

As a first aim of the study, I investigated the implications of loss of FBXO41 *in vivo* using an FBXO41 knockout mouse model. Behavioral and histological analysis of the FBXO41 knockout mice further led to better understanding of some of the neurodevelopmental events governed by FBXO41 in the developing cerebellum. As a second aim, I complemented my *in vivo* findings with *in vitro* cell culture, imaging and supporting biochemical techniques to establish FBXO41 as a novel E3 ligase and to identify putative molecular players that may act in the same pathway as FBXO41. Combining mouse genetics and molecular techniques, this study establishes FBXO41 as a crucial cell-intrinsic regulator of cerebellar development.

---

## 2 Materials and methods

### 2.1 Lab equipment:

The following equipments were used to carry out experiments: pipettes (Gilson, USA), plastic ware (Eppendorf, Germany, Sarstedt AG, Germany and Greiner Bio-One, Germany), centrifuges (Eppendorf), rocker and shaker (Heidolph, Germany), thermocycler (Biometra, Germany), heater block (Grant Instruments, UK), spectrophotometer (GE, UK), fluorescent microscope (Eclipse Ti), inverted light microscope (Eclipse TS100), dissection microscope (SMZ645) (Nikon, Japan), brightfield light microscope (Zeiss Axiophot), Fluorescent microscope (Zeiss observer Z.1), confocal microscope (Leica SP5), rotarod (Ugo Basile, Comerio, Varese, Italy), open field area (custom made ), elevated plus maze (custom made), 12mm and 6mm beams used in balance beam tests (custom made), pole test (custom made).

### 2.2 Chemical reagents and commercial kits:

All the chemicals used during the study were purchased from Merck (Darmstadt, Germany), Sigma-Aldrich (Munich, Germany), Roth (Karlsruhe, Germany), Applichem (Darmstadt, Germany), Biomol (Hamburg, Germany), Serva Electrophoresis (Heidelberg, Germany), Invitrogen (Darmstadt, Germany), Becton Dickinson and Company (USA) and Worthington (UK) unless mentioned otherwise.

### 2.3 Common lab reagents and kits:

All the cell culture mediums, supplements and reagents used are listed in table 2.1.

**Table 2.1** List of all cell culture reagents used in the study

Reagent	Manufacturer
Dulbecco's modified eagle's medium (DMEM)	GIBCO®, Life Technologies™ (Darmstadt)

Hank's Balanced Salt Solution (HBSS)	GIBCO®, Life Technologies™ (Darmstadt)
Basal Medium Eagle (BME)	GIBCO®, Life Technologies™ (Darmstadt)
Trypsin	Worthington
Fetal bovine serum (FBS)	Biochrom, Germany
Calf serum (CS)	Hyclone, Germany
Horse serum (HS)	PAA, Coelbe Germany
Goat serum (GS)	Sigma Aldrich
Poly-L-ornithine hydrobromide	Sigma Aldrich

The DNA and protein ladders used were also obtained from Fermentas. N -Ethylmaleimide (NEM) and the ECL western blotting detection kit from Thermo Fischer Scientific. Protein A-Sepharose beads and Flag-sepharose beads from GE Healthcare and Sigma Alrich respectively.

The commercially available kits used in the study are listed in table 2.2 and were used as per manufacturer's instructions:

**Table 2.2** List of the commercially available kits used in the study.

<b>Kit</b>	<b>Manufacturer</b>
Nucleobond® Xtra Midi EF kit	Macherey-Nagel (Dueren, Germany).
NucleoSpin® Plasmid QuickPure kits	Macherey-Nagel (Dueren, Germany).
NucleoSpin® Gel and PCR Clean-up kit	Macherey-Nagel (Dueren, Germany).
QuickChange II Site-Directed Mutagenesis Kits	Agilent Technologies (USA)
SuperScript® III First strand synthesis kit	Invitrogen

## 2.4 Antibodies:

All primary and secondary antibodies used in the study are listed in table 2.3 and 2.4 below.

**Table 2.3** List of all the primary antibodies used in this study

Primary Antibody	Host	Application	Dilution	Source
$\alpha$ FBXO41	rabbit	WB	1:250	Eurogentec (custom made)
$\alpha$ pan-14-3-3	mouse	WB	1:10000	Santa Cruz Biotechnology
$\alpha$ $\gamma$ -Tubulin	mouse	WB	1:10000	Sigma-Aldrich
$\alpha$ myc	mouse	WB	1:1000	Santa Cruz Biotechnology
$\alpha$ Flag	mouse	WB	1:1000	Sigma-Aldrich
$\alpha$ GFP	mouse	WB	1:1000	Santa Cruz Biotechnology
$\alpha$ GFP	rabbit	WB ICC	1:1000 1:1000	Invitrogen
$\alpha$ Cullin1	mouse	WB	1:1000	Santa Cruz Biotechnology
$\alpha$ Cullin7	mouse	WB	1:1000	Sigma-Aldrich
$\alpha$ SnoN	rabbit	WB	1:500	Santa Cruz Biotechnology
$\alpha$ HA	mouse	WB	1:500	Santa Cruz Biotechnology
$\alpha$ NFM	mouse	WB ICC	1:500 1:200	Santa Cruz Biotechnology
$\alpha$ Pericentrin 2	mouse	ICC	1:500	Abcam
$\alpha$ $\beta$ -galactosidase	mouse	ICC	1:100	Santa Cruz Biotechnology
$\alpha$ cleaved caspase-3	rabbit	ICC	1:200/ 1:100	Cell signalling
$\alpha$ Calbindin	rabbit	IHC (DAB)	1:100	Sigma-Aldrich
$\alpha$ GFAP	mouse	IHC (DAB)	1:200	Nova Castra
$\alpha$ Iba1	mouse	IHC (DAB)	1:1000	WAKO
$\alpha$ Tau	rabbit	IHC (FL)	1:2000	DAKO
$\alpha$ PCNA	rabbit	IHC (DAB)	1:1000	Abcam
$\alpha$ NeuN	mouse	IHC (DAB)	1:400	EMD Milipore

$\alpha$ Parvalbumin	rabbit	IHC (FL)	1:100	Gift from Prof. K.A. Nave, MPI of Experimental Medicine, Göttingen
----------------------	--------	----------	-------	--

**Table 2.4** List of all the secondary antibodies used in this study

Secondary Antibody	Host	Conjugated substrate / dye	Application	Dilution	Source
$\alpha$ mouse IgG	Goat	HRP	WB	1:10000	Dianova
$\alpha$ rabbit IgG	Goat	HRP	WB	1:10000	Dianova
$\alpha$ mouse IgG	Goat	Cy2/ Alexa 488	ICC	1:1000	Dianova
$\alpha$ rabbit IgG	Goat	Cy2/ Alexa488	ICC	1:1000	Dianova
$\alpha$ mouse IgG	Goat	Cy3/ Alexa555	ICC	1:1000	Dianova
$\alpha$ rabbit IgG	Goat	Cy3/ Alexa555	ICC	1:1000	Dianova

**2.5 Enzymes:**

The detailed sources of various enzymes used in this study are listed in table 2.5 below

**Table 2.5** List of various enzymes used in the study

Enzymes	Source
Restriction enzymes	New England Biolabs
GoTaq® DNA polymerase	Promega

Pfu DNA polymerase	Thermo Scientific
Alkaline calf intestinal phosphatase	New England Biolabs
T4 DNA ligase	Fermentas
T4 polynucleotide kinase	New England Biolabs
T4 DNA polymerase	Fermentas

## 2.6 Buffers and Stock solutions:

Listed below are all the solutions and buffers used during the course of this study:

### Buffers and media for primary neuron culture:

HHGN: 1x HBSS, 2.5 mM HEPES pH 7.5, 35 mM glucose, 4 mM NaHCO<sub>3</sub>

Cbc: BME [+] Earle's salts [-] L-Glutamine, 10% calf serum (heat inactivated), 1% PSG, 25 mM KCl

DnB: 500 µl DNase (2ug/ul), 10ml BME [+] Earle's salts [-] L-Glutamine

TDn: 250 µl DNase (2ug/ul), 5ml HHGN, 50 mg Trypsin

### Media for HEK293T cell culture:

HEK293T medium: DMEM [+] 4.5 g/l glucose [-] glutamine [-] pyruvate, 10% FBS, 1% GlutaMAX®

### Buffers for HEK293T cell and neuronal transfection

2X HBSS: 50 mM HEPES pH 7.05-7.11, 10 mM KCl, 280 mM NaCl, 15 mM glucose, 1.5 mM Na<sub>2</sub>HPO<sub>4</sub>

2.5 M CaCl<sub>2</sub>

Nucleofection plating media: DMEM [+] 4.5 g/l glucose [-] glutamine [-] pyruvate, 10% FCS (Hyclone)

Buffers and medium used for molecular cloning:

Annealing buffer: 100 mM CH<sub>3</sub>COOK, 30 mM HEPES-KOH, 2mM (CH<sub>3</sub>COO)<sub>2</sub>Mg

2X TAE pH 8.5: 80 mM Tris-acetate, 2 mM EDTA

2X YT (1000 ml): 16 g tryptone, 10 g yeast extract, 5 g NaCl

Buffers and reagents used for biochemical techniques:

Triton® X-100 lysis buffer: 150 mM NaCl, 50 mM Tris-HCl, 1 mM EDTA, 1% Triton® X-100

Co-IP buffer: 150 mM NaCl, 20 mM Tris-HCl pH 7.4, 1mM EDTA, 1% Nonidet P-40, 10% glycerol

Mild Co-IP buffer: 150 mM NaCl, 20 mM Tris-HCl pH 7.4, 1mM EDTA, 0.5% Nonidet P-40, 10% glycerol

RIPA buffer: 150 mM NaCl, 50 mM Tris-HCl pH 8.0, 0.5% sodium deoxycholate, 1% Nonidet P-40, 5 mM EDTA (0.1% SDS optional)

SDS-sample buffer: 300 mM Tris-HCl pH 6.8, 10% SDS, 50% glycerol, 25% β-mercaptoethanol, and 0.05% bromophenol blue

Centrosomal purification buffer: 1 mM HEPES pH 7.2, 0.5% NP40, 0.5 mM MgCl<sub>2</sub>, 0.1% β-mercaptoethanol, cytochalasin D (1 μg/ml), nocodazole (0.2 μM)

Lysis buffer for ubiquitination assay (denaturing protocol): 50 mM HEPES pH 7.5, 150 mM NaCl, 10% glycerol, 1.5 mM MgCl<sub>2</sub>, 1% TritonX100, (10 mM NEM, 1 mM NaVO<sub>3</sub>, 0.5 mM NaF) \*

NaVO<sub>3</sub> 1000 mM: 180 mg of NaVO<sub>3</sub> in 1ml of H<sub>2</sub>O

NaF 500 mM: 21 mg of NaF in 1ml of H<sub>2</sub>O



HNTG buffer: 20 mM HEPES pH 7.5, 150 mM NaCl, 0.1% TritonX100, 10% glycerol

\* = Added fresh before use

Buffers used for SDS-PAGE

Lower buffer: 1.5 M Tris pH 8.8, 0.4% SDS

Upper buffer: 0.5 M Tris pH 6.8, 0.4% SDS

Running buffer: 125 mM Tris, 1.25 M glycine, 0.5% SDS

Transfer buffer: 20 mM Tris, 153 mM glycine, 20% methanol

10X PBS pH 7.4: 1.37 M NaCl, 14.7 mM KCl, 78.1 mM Na<sub>2</sub>HPO<sub>4</sub>, 26.8 mM KH<sub>2</sub>PO<sub>4</sub>

PBST: 1x PBS, 0.1% Tween-20

Buffers used for genotyping:

Tail lysis buffer: 200 mM NaCl, 10 mM Tris pH 8.0, 10 mM EDTA, 0.5 % SDS

Proteinase K\*

\* = Added fresh before use

Buffers and reagents used for immunocytochemistry:

BME + 10% Horse serum: BME + 10% heat inactivated horse serum

8% PFA: 375 ml sterile H<sub>2</sub>O at 60°C, 40 g PFA, 50 ml 10% PBS, 40 g sucrose, set pH to 7.4  
fill up with sterile H<sub>2</sub>O to 500 ml

4% PFA: 50% [v/v] 8% PFA and 50% [v/v] PBS

0.4% TX-100 lysis buffer: 0.4% [v/v] TX-100 in PBS

Buffers and reagents for immunohistochemistry

*X-gal staining*

X-gal: 0.5 mg/ml X-gal, in PBS

X-gal buffer: 2 mM MgCl<sub>2</sub>, 0.02% NP40, 0.01% sodium deoxycholate, 5 mM potassium ferrocyanide, 5 mM potassium ferricyanide

0.2M phosphate buffer (fixation buffer): 0.36% [w/v] NaH<sub>2</sub>PO<sub>4</sub>, 3.1% [w/v] Na<sub>2</sub>HPO<sub>4</sub>, 1% [w/v] NaCl

4% [w/v] PFA for immunohistochemistry (paraffin embedding): 4% [w/v] PFA, 0.1M phosphate buffer (fixation buffer)

#### *Haematoxylin and Eosin staining:*

Hamatoxylin: ready to use mayer's haematoxylin from Merck

Eosin: 0.1% eosin dissolved in dd H<sub>2</sub>O and 12 drops of CH<sub>3</sub>COOH

HCL-alcohol: 0.09% [v/v] HCL, 70% [v/v] ethanol

Scott's reagent: ready to use Scotts reagent from Thermo Scientific

#### *DAB staining:*

Citrate buffer for IHC: 1.8 mM C<sub>6</sub>H<sub>8</sub>O<sub>7</sub>xH<sub>2</sub>O, 8.2 mM C<sub>6</sub>H<sub>5</sub>Na<sub>3</sub>O<sub>7</sub>x2H<sub>2</sub>O (pH 6.0, always freshly prepared from stock solutions)

Tris buffer for IHC: 0.9% [w/v] NaCl, 50 mM Tris-HCl pH 7.6, pH 7.6

Tris buffer+ 2% Milk powder: 2% [w/v] Milk powder (Ferma) dissolved in Tris buffer for IHC

Blocking buffer: 20% goat serum [v/v] dissolved in BSA/PBS

BSA/PBS: 0.04M NaH<sub>2</sub>PO<sub>4</sub>, 0.16M Na<sub>2</sub>HPO<sub>4</sub>, 1.8%[w/v], NaCl, 1% [w/v] BSA

#### *Immunoflourescence staining of cryo-sections:*

Blocking buffer (IHC): 10% NGS, 3% BSA, 0.5% TX-100 in PBS

#### *Mounting media*

Mowiol mounting media: 6 g glycerol AR, 2.4 g Mowiol 4-88 (Calbiochem), 6 ml H<sub>2</sub>O, 12 ml 0.2 M Tris-HCl pH 8.5

Eukitt (Kindler, Freiburg, Germany)

Aqua-poly/mount (Merck)

### Anesthetics

**Ketamine/xylazine:** 10% ketamine [v/v] (10% Ketamine, Medistar, Arzneimittelvertrieb GMBH®), 5% xylazine (2% xylazine, CP Pharma®)

## 2.7 Plasmids constructs and primers:

All details concerning the various plasmids constructs and primers used in this study can be found listed in Appendices 1 and 2.

## 2.8 Molecular cloning:

In order to clone the desired cDNA sequence into a plasmid, the PCR recipe and program used are listed in table 2.6 and 2.7. The annealing temperature for the primers were set 5°C below the primer melting temperatures. For the amplification, the elongation time was set at 72°C depending on the length of the template (1 min/500 bp of template).

**Table 2.6** Recipe for general PCR reaction

Reagent	Volume
Template DNA (10 ng/μl)	1 μl
Forward primer (10 pmol/μl)	1 μl
Reverse primer (10 pmol/μl)	1 μl
dNTPs (25 mM)	0.4 μl
Pfu DNA polymerase (2.5 units/ μl)	0.5 μl
10X reaction buffer (+MgSO <sub>4</sub> )	5 μl

H <sub>2</sub> O	41.1 µl
------------------	---------

**Table 2.7** PCR program for general molecular cloning

Temperature	Cycles	
Denaturation 95°C	3 min	
Denaturation 95°C	30 sec	30 cycles
Annealing X°C	30 sec	
Elongation 72°C	X min	
Final elongation 72°C	5 min	

In order to determine the size and quality of the PCR product, the product was subjected to gel electrophoresis in a 1% agarose gel. DNA fragments of the expected size were excised from the gel, extracted using NucleoSpin® Gel and PCR Clean-up kit and eluted in 40 µl H<sub>2</sub>O.

The purified PCR product (insert) and the desired expression plasmid (2 µg) were digested using corresponding restriction enzymes for 1-2 hours at 37°C in a 50 µl reaction volume. Immediately after digestion, the insert was purified by the NucleoSpin® Gel and PCR clean-up kit and eluted in 20 µl H<sub>2</sub>O. 5-7 µl of the linearized insert was used for ligation along with 1 µg of the linearized vector. The recipe of the ligation mix is listed below in table 2.8

**Table 2.8** Recipe of the ligation reaction

Reagent	Volume
Insert	5-7 µl
Vector	1 µl
ATP (10 mM)	1 µl

10X T4 ligation buffer	1 $\mu$ l
T4 DNA ligase	1 $\mu$ l
Overnight in icy water (10°C)	

On the following day, the entire ligation reaction was used to transform 100  $\mu$ l of chemically competent DH5 alpha E. coli cells. The bacteria were incubated on ice for 20 min, followed by a heat shock at 37°C for 2 minutes and subsequent cool down on ice for 1 minute. Afterwards, 500  $\mu$ l 2X YT media without antibiotics was added to the bacterial cells and then incubated for 30 minutes at 37°C by shaking. Next, the bacteria were centrifuged at 4000 rpm for 5 minutes and plated onto pre-warmed 2X YT agar plates with suitable antibiotics as per the resistance gene encoded in the vector. The plates were kept at 37°C overnight.

To account for successful ligation, colonies from the plates were cultured overnight at 37°C in 2X YT media, supplemented with the corresponding antibiotic. On the next day, the plasmid DNA from each culture was extracted using the NucleoSpin<sup>®</sup> Plasmid Quick Pure kit. The plasmids were then digested with the appropriate enzymes to identify positive clones, which had been successfully transformed with the plasmid carrying the insert. The positive clones were sequenced by the AGCT lab (Central facility at the Max Planck Institute of Experimental Medicine, Goettingen, Germany).

## 2.9 RNA interference:

### 2.9.1 Generation of vector-based RNAi constructs:

The shRNA targeting regions of FBXO41 and NFM are listed in Table 2.9. The constructs were generated by cloning an inverted repeat into the pBlueScript/U6 vector at the ApaI restriction enzyme site. Each 40-nucleotide-long inverted repeat, separated by a 9-nucleotide loop containing HindIII restriction site was inserted after the U6 promoter. An EcoRI restriction site was inserted downstream of antisense strand providing a blunt end for ligation with the vector while the ApaI restriction site provided the sticky end. The sense strand of the hairpin was homologous to a 20-nucleotide region in the FBXO41 or NFM mRNA target. Primers 16104/16105 were used to clone the FBXO41 RNAi #5 and primers 20268/20269 for FBXO41 RNAi#8. Primers 24562/24563 were used to generate the NFM RNAi#5 and

primers 24560/24561 for NFM RNAi#3 respectively.

**Table 2.9** List of the shRNA-targeting sequences of FBXO41 and NFM RNAs

shRNA	Nucleotide sequence	Species specificity
FBXO41 RNAi#5	5'-GGGTGCCGGCATCGAGAAGGT-3'	Human, mouse, rat
FBXO41 RNAi#8	5'-AGCTGCTACTGCCGTGCCCT-3'	Human, mouse, rat
NFM RNAi#5	5'-GGAAATGGCTCGTCATTTGC-3'	Human, mouse, rat
NFM RNAi#3	5'-GAAGAGTGGTTCAAATGCCGC-3'	Human, mouse, rat

### 2.9.2 Annealing of primers:

Annealing of the sense and antisense primer pairs (2  $\mu$ l each) was carried out by first, diluting the primers (2  $\mu$ l each of 50 pmol/  $\mu$ l) in 46  $\mu$ l of annealing buffer. The annealing of primer pairs was carried out using a Biometra thermo cycler as per the indicated program shown in Table 2.10.

**Table 2.10:** Annealing of primers

Temperature	Time
95°C	4 minutes
16°C	10 minutes, slow cool 0.1°C/sec

### 2.9.3 Phosphorylation of oligos:

20  $\mu$ l of the annealed oligos were mixed with 5  $\mu$ l of 10X PNK buffer, 10 U of polynucleotide kinase (PNK) and ATP to a final concentration of 1 mM in a 50  $\mu$ l kinase reaction and subsequently incubated at 37°C for 30 minutes. 10  $\mu$ l of phosphorylated oligos were used for ligation.

### 2.9.4 Preparation of the U6/pBS vector and ligation:

3  $\mu$ g of pBS/U6 vector were digested with *Apa*I for 1 hour at 37°C and the linearized vector was purified using the gel extraction columns (Macherey Nagel kit). For generating blunt ends, the linearized plasmid was then incubated with T4 DNA polymerase at 12°C for 15

minutes. The vector was then digested with EcoRI at 37°C for 1 hour followed by addition of calf intestinal phosphatase (CIP) for 1 hour to remove 5'-phosphate groups. The vector was purified using column and eluted in 50 µl sterile water. Lastly, a 20 µl ligation reaction was set up using 10 µl phosphorylated oligos, 1 µl digested vector, 2 µl 10X ligase buffer and 1 µl T4 DNA ligase. The reaction was incubated at 16°C overnight.

### **2.9.5 Screening for positive ligation clones:**

The E.coli DH5 alpha cells were transformed by adding the entire ligation mix to the bacteria and first incubating the cells for 30 minutes on ice. Next the cells were subjected to a brief 2-minute heat shock at 37°C, followed by 10 minutes incubation on ice. The bacteria were then resuspended in 500 µl of 2X YT media without antibiotics and grown for 30 minutes at 37°C. Lastly the bacterial cells were briefly centrifuged at 4000 rpm and the excess medium was removed. The bacterial pellet was subsequently resuspended in 100 µl of 2X YT medium and plated onto 2X YT plate with ampicillin and incubated at 37°C overnight. The next day, the bacterial colonies were selected and cultured overnight in liquid 2X YT media (supplemented with ampicillin). On the following day, plasmid DNA was isolated from each inoculate and digested with HpaI enzyme to screen for positive clones. Upon digestion with HpaI, the clones with ligated shRNA insert gave a linear band of approximately 3 kbp while the non-ligated clones remained uncut. The plasmid DNA from positive clones was submitted to the AGCT lab for sequencing.

### **2.10 Site-directed mutagenesis:**

In order to generate “rescue” constructs that are resistant to degradation by RNAi, site-directed mutagenesis was performed. Primers harboring 4-6 silent nucleotide mutations in the RNAi targeting region were designed as per the instructions provided in the Quick Change site-directed mutagenesis manual. The PCR reaction was set up with 10 ng of plasmid DNA, 10 pmol forward primer, 10 pmol reverse primer, 10X Pfu DNA polymerase buffer, 1 µl Pfu DNA polymerase and 25 mM dNTP in a 50 µl total volume reaction. The PCR reaction timings were set as shown in table Table 2.11. Following PCR, the samples were incubated on ice for 2 minutes followed by addition of DpnI and incubation for 1 hour at 37°C. 1-2 µl of reaction mix was used to transform E.coli DH5 alpha competent cells that were plated on 2xYT-agar plate and incubated overnight at 37°C. The clones were sequenced to confirm the mutations in the vector.

**Table 2.11:** Site-directed mutagenesis PCR

Temperature	Time	
95°C	3 minutes	
95°C	30 seconds	20 cycles
X°C	30 seconds	
72°C	- 20 cycles 500 bp/minute	
72°C	5 minutes	

**2.11 Fusion PCR for generating deletion mutants:**

Deletion mutants lacking specific domains of the protein of interest were generated by first performing two separate PCR reactions that amplify fragments from the start codon until right before the deletion domain and from right after the deletion domain until the stop codon. As a second step, a “fusion PCR” was performed using specific primers that fuse the two fragments, resulting in a protein lacking the desired domain. The reaction setup used to generate the N- and C-terminal fragments and the fusion PCR recipes are listed in tables 2.12 and 2.13.

**Table 2.12** PCR recipe for N- and C- terminal fragments

Reagent	Volume
Forward primer (10 pmol/ $\mu$ l)	1 $\mu$ l
Reverse primer (10 pmol/ $\mu$ l)	1 $\mu$ l
Template DNA	100 ng
10X reaction buffer (+) Mg	5 $\mu$ l
dNTPs	0.6 $\mu$ l
Pfu DNA polymerase (2.5 units/ $\mu$ l)	0.5 $\mu$ l
H <sub>2</sub> O	40.9 $\mu$ l

**Table 2.13** PCR recipe for fusion PCR

Reagent	Volume
Forward primer (10 pmol/ $\mu$ l)	1 $\mu$ l



Reverse primer (10 pmol/ $\mu$ l)	1 $\mu$ l
N-terminal fragment	1 $\mu$ l
C-terminal fragment	1 $\mu$ l
10X reaction buffer (+) Mg	5 $\mu$ l
dNTPs	0.6 $\mu$ l
Pfu DNA polymerase (2.5 units/ $\mu$ l)	0.5 $\mu$ l
H <sub>2</sub> O	40.9 $\mu$ l

## 2.12 Cell culture:

All cell culture work was carried out inside a biological safety cabinet (HERAsafe®, Thermo Scientific) under sterile conditions.

### 2.12.1 HEK293T cell culture:

HEK293T cells were cultured in DMEM (GIBCO®, Life Technologies™, Catalog no. 11960) supplemented with 10% FBS and 1 % GlutaMAX® at 37°C with 5% CO<sub>2</sub> in an incubator (HERAsafe®, Thermo Scientific, Bonn). Once the cells achieved a confluency of > 90%, they were regularly passaged onto 10 cm dishes or 6 well plates. When passaging, the cells were first rinsed briefly in sterile PBS, followed by incubation with 1 ml of trypsin-EDTA at 37°C for 5 minutes. Cold DMEM supplemented with serum was added in order to stop the enzymatic reaction. HEK293T cells were then detached from their culture surface by means of gentle mechanical agitation as a result of pipetting up and down slowly. Cells in suspension were collected and centrifuged at 4°C 800 rpm for 5 minutes. The supernatant was discarded and the cell pellet was resuspended in fresh media. The cell suspension was subsequently plated onto either 10 cm plates for maintenance of the cell line or onto 6-well plates designed for biochemical experiments.

### 2.12.2 Primary neuronal culture:

Cerebellar granule neurons (CGNs) were cultured from isolated cerebella of postnatal day 6 (P6) Wistar rat pups as previously described (*Bilimoria and Bonni, 2008*). Cerebella were isolated using fine forceps and the meninges and the surrounding tissues were removed. The dissected cerebella were briefly washed thrice in HBSS and incubated in 5 ml of TDn for 10 minutes at 37°C and 10 minutes at RT. Next, the cerebella were washed thrice in HBSS and

subsequently triturated in 4 ml of DnB until a homogenous suspension of cells was achieved. The suspension was centrifuged at 800 rpm at 4°C, the supernatant discarded and the pellet was resuspended in 20 ml of Cbc medium. The number of cells was determined using a haemocytometer. Neurons were cultured either onto polyornithine-coated glass coverslips or directly into the culture plates. The cultures were maintained in Cbc medium. The CGNs were cultured at the following densities: 50 million cells per 6 well plate, 20 million cells per 24 well plate and 100 million cells per 10 cm petridish. For survival assays 24 million cells per 24 well plate were plated. In order to prevent non-neuronal cells from proliferating, the CGNs were treated at *day in vitro* (DIV) 1 with 10 µM of the mitotic inhibitor cytosine β-D-arabino-furanoside (AraC). At DIV 3, 25 mM glucose was additionally supplemented into the conditioned medium to replenish the carbon source.

## **2.13 Transfection of primary neurons and HEK293T cells:**

### **2.13.1 HEK293T cell transfection:**

The HEK293T cells used for biochemical experiments were transfected using the modified calcium phosphate method as previously described by Konishi et al 2004. One day prior to transfection, the HEK293T cells were split into 6 well plates to be used for biochemical assays. Once the cells reached 70-80% confluency, the cells were transfected. For each well of the 6 well plates 10 ng-2 µg of DNA was diluted in sterile H<sub>2</sub>O. 10 µl of 2.5 M CaCl<sub>2</sub> followed by 100 µl of 2XHBSS were then added to the diluted DNA. The mixture was gently pipetted up and down to ensure proper mixing of the constituents followed by a 5-minute incubation at RT. This DNA mixture was then added drop-wise onto the cells.

### **2.13.2 Primary neuron transfection:**

Rat CGNs cultured in 24 well plates were transfected at DIV 1 (for morphological analyses) or DIV2 (for survival assay) with the indicated plasmids using the modified calcium phosphate method. First, the conditioned medium in which the neurons were cultured was collected in a separate falcon and kept aside at 37°C. Cells were then gently washed twice with DMEM and followed by starvation in 500 µl of DMEM for 45-50 minutes at 37°C. In the meantime the to be transfected plasmid DNA was diluted in sterile H<sub>2</sub>O to achieve a final volume of 18 µl per well of the 24 well plate. The diluted DNA was then thoroughly mixed

with 2  $\mu$ l of 2.5M CaCl<sub>2</sub> and 20  $\mu$ l of 2XHBSS. The mixture was then allowed to incubate for at least 5 minutes at RT, following which it was added gently drop wise onto the starved neurons. The neurons were then incubated at 37°C for 15 minutes. Subsequently, the starvation media was aspirated off, cells were washed twice in DMEM and the previously collected conditioned medium returned.

For nucleofection, 8 million rat CGNs were resuspended in 100  $\mu$ l of DMEM. 10  $\mu$ g of the indicated plasmid together with the anti-apoptotic plasmid Bcl-x<sub>L</sub> were added to the suspension, following which the neurons in suspension were electrically pulsed using the O-005 program on the nucleofector (Amaxa, Lonza). The freshly pulsed neurons were then incubated in 1 ml of pre-warmed DMEM for 5 minutes at RT. Subsequently, the neurons were plated onto 6 well plates with pre-warmed DMEM supplemented with 10% FCS. 4 hours after plating the medium was replaced by warm Cbc (neuron growth medium) medium. The nucleofected neurons were kept in culture for 4 days following which they were subjected to biochemical assays.

#### **2.14 Immunocytochemistry:**

CGNs, which were subjected to morphological assays, were washed twice with PBS and then fixed in 4% PFA for 10 minutes at RT, while the CGNs used for survival assay were directly fixed by adding equal volume of 8% PFA to the medium in which they were maintained. The cells were then washed twice in PBS and permeabilized using 0.04% Triton X-100 in PBS for 10 minutes at RT. Following two more washes in PBS the cells were blocked using BME supplemented with 10% horse serum (blocking buffer) for 30 minutes to 1 hour at RT. After blocking, the primary antibody diluted in blocking buffer was added to the cells and incubated for either 1 hour at RT or overnight at 4°C. Following incubation with the primary antibody, cells were washed with the blocking buffer and then incubated with the secondary antibody diluted in the blocking buffer for 30 minutes at RT. Subsequently, the cells were washed in PBS and incubated with a DNA dye (bisbenzimidazole Hoechst 33258 or 4',6-diamidino-2-phenylindole (DAPI)) for 10 minutes at RT. The coverslips were rinsed in PBS and then mounted onto glass slides (Marienfeld) using the anti-fade mounting medium Mowiol and stored at 4°C until analysis.

### 2.15 Morphological analyses of neurons:

For all morphological analyses, the cultured CGNs prepared as mentioned in sections (culture and transfection) were transfected at DIV1 with 0.2  $\mu\text{g}$  of GFP, which served as a transfection marker, together with the plasmids of interest. In order to rule out any effects on the cellular morphology as a result of compromised cell health, 0.2  $\mu\text{g}$  of the anti-apoptotic Bcl-x<sub>L</sub> plasmid was co-transfected. At DIV5 the neurons were subjected to immunocytochemistry using the GFP antibody and the previously mentioned DNA dyes. Neurons were imaged using a fluorescent microscope and axonal lengths as well as dendrite lengths, when necessary, of transfected neurons were measured using the free imageJ (NIH) software as previously described (*Holubowska et al., 2014; Kannan et al., 2012b; Konishi et al., 2004; Vadhvani et al., 2013*). Image acquisition and analyses was done in a blinded manner using the Nikon Ti eclipse fluorescent microscope and the NIS-Elements Basic research software. The length of the longest process was measured as the axon using Image NIH (*Holubowska et al., 2014*). At least 40-60 neurons were included in the analyses per condition per experiment. GraphPad Prism 5.0 was used to perform statistical analysis using ANOVA (Bonferroni post hoc) test or the Student's t test (unpaired t test), depending on the experimental design.

### 2.16 Survival assay in neurons:

The survival assay was performed as previously described (*Matz et al., 2015*). In summary, CGNs were cultured and transfected as previously mentioned in sections 2.12.2 and 2.13.2. At DIV2 the neurons were transfected with the indicated plasmids and 0.3  $\mu\text{g}$  of  $\beta$ -galactosidase ( $\beta$ -gal), which served as a transfection marker. At DIV6 the cultured neurons were subjected to immunocytochemistry using  $\beta$ -gal and cleaved caspase-3 specific antibodies as well as the aforementioned DNA dyes. The  $\beta$ -gal-positive neurons were examined for neuronal survival and death based on the integrity of the neurites, nuclear morphology and presence or absence of the apoptotic marker cleaved caspase-3. Cells were analyzed in a blinded manner under the Nikon Ti eclipse fluorescent microscope and the NIS-Elements Basic research software. Approximately 100-150 cells were analyzed per condition

per experiment. GraphPad Prism 5.0 was used to perform statistical analysis using ANOVA (Bonferroni post hoc) test.

## **2.17 Biochemical techniques:**

### **2.17.1 Tissue lysate preparation:**

Mice or rats were sacrificed either by CO<sub>2</sub> inhalation or decapitation (for pups only). The isolated tissues were immediately placed in ice-cold TX-100 lysis buffer with freshly added cocktail of protease inhibitors (1 mM DTT, 3 µg /ml aprotinin, 1 µg / µl leupeptin and 1 µg / µl pepstatin). The tissue-lysis buffer mix was then homogenized using a 2 ml dounce. Obtained lysates were incubated on ice for 30 minutes, followed by centrifugation at 10000 rpm for 10 minutes at 4°C. The supernatant was collected in a fresh tube, and the pellet discarded. When not immediately using the lysates, the samples were snap frozen using liquid nitrogen and stored at -80°C.

### **2.17.2 Cell lysate preparation:**

Lysates from HEK293T cells or primary neurons were harvested by first aspirating off the cultured medium and giving the cells a brief rinse in PBS. The PBS was aspirated off followed by addition of TX-100 lysis buffer freshly supplemented with protease inhibitors (1 mM DTT, 3 µg /ml aprotinin, 1 µg / µl leupeptin and 1 µg / µl pepstatin). Adherent cells were scraped off the 6-well plate surface using a cell scraper, and lysates were collected in fresh tubes. Following 30 minutes incubation on ice, the samples were centrifuged at 10000 rpm for 10 minutes at 4°C. The supernatants were transferred into fresh tubes and stored on ice for further biochemical experiments or immediately snapfrozen in liquid nitrogen and stored at -80°C for later use.

### **2.17.3 Bradford's assay for protein concentration measurement:**

The Bradford reagent (Bio-Rad<sup>®</sup>) was used for determination of protein concentration. The reagent was diluted 1:5 in PBS. 2, 4, 6, 8 and 10 µg of bovine serum albumin (BSA) diluted in 1 ml of the Bio-Rad<sup>®</sup>/PBS solution was used to make a standard curve. 2 µl of the lysate of interest was added into 1 ml of the Bio-Rad<sup>®</sup>/PBS solution. The shift in absorbance as a result of protein binding to Coomassie Brilliant Blue G-250 was determined by a spectrophotometer

(Amersham Biosciences, Ultra spec 3100 pro) at a wavelength of 595 nm. Finally, the protein concentration was determined using the BSA standard curve.

#### **2.17.4 Co-immunoprecipitation (CoIP):**

P9 cortices or cerebellum from mice or transfected HEK293T cells were briefly rinsed in PBS and lysed in ice-cold CoIP buffer freshly supplemented with protease inhibitors (1 mM DTT, 3 µg/ml aprotinin, 1 µg/µl leupeptin and 1 µg/µl pepstatin) on ice. Following 30 minutes incubation on ice the samples were centrifuged at 4°C at 10000 rpm for 10 minutes. The supernatants were collected in fresh tubes and the protein concentration determined using the Bradford's assay. While 50 µg of each sample were set aside as input controls, 1 mg of tissue/cell lysate was incubated with the primary antibody, under constant rotation for at least 3 hours at 4°C. Subsequently 30 µl of Protein A-sepharose beads (Protein A-Sepharose<sup>TM</sup> Fast Flow, GE Healthcare), previously washed and stored in CoIP buffer, were added to the samples and the samples were further incubated for 40-60 minutes at 4°C on the rotator. Next, the samples were centrifuged at 10000 rpm for 1 minute and the supernatant was discarded. The beads were washed 3 times with the TX-100 lysis buffer and once with PBS. Finally, the beads were boiled for 5 minutes at 95°C in 30 µl of SDS-sample buffer. The boiled samples and the input controls were either subsequently subjected to SDS-PAGE and western blot analyses or stored at -20°C until later use.

#### **2.17.5 Centrosomal purification:**

Centrosomal purification was performed as previously described (*Vadhvani et al., 2013*). Cultured CGNs were treated with cytochalasin D (1 µg/ml) and nocodazole (0.2 µM) for 1 hour prior to lysis (1 mM HEPES pH 7.2, 0.5% NP40, 0.5 mM MgCl<sub>2</sub>, 0.1% β-mercaptoethanol supplemented with protease inhibitors 1 µg/ml pepstatin, 1 µg/ml aprotinin, 1 µg/ml leupeptin and 1 mM PMSF). After lysis the lysates were subjected to a gradient centrifugation (60% sucrose, 10000g, 30 min, 4°C). The resulting centrosomal fractions were then purified using a discontinuous sucrose density gradient centrifugation (40%/50%/70% sucrose, 34000g, 1 hour, 4°C). The supernatant fractions were subjected to immunoprecipitation by FBXO41 antibody followed by immunoblotting analysis using the FBXO41 and γ-Tubulin antibodies.

#### **2.17.6 Ubiquitination assay:**

The cell-based ubiquitination assays were performed under denaturing conditions as per the protocol from Vadhvani et al, (*Vadhvani et al., 2013*) with a few modifications, in order to avoid detection of unspecific ubiquitin smears. In brief, transfected HEK293T cells were lysed in RIPA buffer (50 mM Tris-HCl pH 8, 150 mM NaCl, 1% NP40, 0.5% sodium deoxycholate, 5 mM EDTA) with freshly added protease inhibitors (1 µg/ml pepstatin, 3 µg/ml aprotinin and 1 µg/ml leupeptin), 10 mM N-ethylmaleimide (NEM) and phosphatase inhibitors (0.5 mM NaVO<sub>3</sub> and 1 mM NaF). 50 µg of protein per sample was collected separately as input control. 1 mg protein was incubated with 1% SDS on a shaker for 5 minutes followed by boiling at 95°C for 15 minutes. The sample was further diluted to 0.1% SDS with lysis buffer (50 mM HEPES pH 7.5, 150 mM NaCl, 10% Glycerol, 1.5 mM MgCl<sub>2</sub>, 1% TritonX-100) and incubated with either a primary antibody or with antibody-conjugated beads for immunoprecipitation overnight at 4°C on the rotator. Following immunoprecipitation, for non-conjugated antibodies, the samples were additionally incubated for 40 minutes with Protein A-Sepharose. The precipitated proteins bound to the beads were then washed twice with lysis buffer, twice with HNTG buffer (20 mM HEPES pH 7.5, 150 mM NaCl, 0.1% Triton-X100, 10% Glycerol) and eluted from the beads into 30 µl of SDS-sample buffer by boiling at 95°C for 5 minutes. Boiled samples and input controls were then analyzed by SDS-PAGE and western blotting.

#### 2.17.7 SDS-PAGE and western blot:

The SDS-PAGE gels were cast in the gel casting system (Mini-PROTEAN Tetra Electrophoresis System, Bio-Rad®). A gel used for standard SDS-PAGE consists of two layers, the lower separating gel (contains 7-15% acrylamide depending on the experiment) and the upper stacking gel (contains 3.9% acrylamide). During the course of this study 7.5%, 8%, 10% and 12% gel were used as per the experimental design. The reagents needed along with the recipe for make these gels are listed below in table 2.14.

**Table 2.14** Recipe of SDS-PAGE gels of containing varying percentages of acrylamide.

	Separating gel				Stacking gel
% Acrylamide	7.5%	8%	10%	12%	3.9%
30%Acrylamide	1.875	2	2.5	3	0.65

(ml)					
<b>Lower buffer (ml)</b>	1.875	1.875	1.875	1.875	1.25 ml <b>Upper buffer</b>
H <sub>2</sub> O ml	3.75	3.625	3.125	2.625	3.05
10% APS (μl)	30				25
TEMED (μl)	3				2.5

The reagents of the separating gel were mixed and loaded onto the gel casting chambers and covered by a thin film of isopropanol. Gels were allowed to polymerize for 45-60 minutes, following which the isopropanol was rinsed out with H<sub>2</sub>O. The stacking gel was then added on top by inserting a 10-well comb. The upper gel was allowed to polymerize for 40 minutes.

The lysates boiled in SDS sample buffer were loaded onto the gels along with a protein ladder and the proteins separated at 25 mA per gel. Following electrophoresis the proteins on the gel were transferred onto a nitrocellulose membrane using a Mini-Trans-Blot<sup>®</sup> cell (Bio-Rad<sup>®</sup>) at 250 mA for 100 minutes. After transferring the proteins, the nitrocellulose membrane was blocked using PBST supplemented with 4% milk, for 30 minutes at RT. Following three 10 minute PBST washes, the membrane was incubated in the appropriate primary antibody diluted either in 3% BSA or 4% milk (in PBST) supplemented with 0.02% NaN<sub>3</sub>, for 1 hour at RT or overnight at 4°C. Subsequently, the membranes were again washed thrice for 10 minutes in PBST and incubated in secondary antibody (1:10000) diluted in 4% milk (in PBST) for 30 minutes at RT. The secondary antibodies used were coupled with horseradish peroxidase (HRP). After the last three 10 minutes PBST washes the membrane was incubated shortly in enhanced chemiluminescent (ECL) horseradish peroxidase substrates (Thermo Fischer Scientific). A photographic film was exposed onto the membrane and developed using an automatic film processor (Kodak imaging station).

#### **2.17.8 Densitometric quantifications:**

The developed films from western blot analysis were subjected to densitometric analyses using the ImageJ Gel Analyzer plug-in, which measures the intensity of each band of interest. The intensity of each sample and that of their respective loading controls were always



measured. In order to rule out differences due to loading, relative intensities for each sample were calculated by dividing the relative intensity of each sample by the relative intensity of its loading control. The obtained relative intensities were then compared using statistical analyses. GraphPad Prism was used to perform statistical analysis using ANOVA (Bonferroni post hoc) test or the Student's t test (paired t test) as per experimental design.

### **2.17.9 Reverse transcription PCR (RT-PCR):**

#### **2.17.9.1 mRNA isolation:**

P20 male mice were sacrificed by CO<sub>2</sub> inhalation, the organs of interest extracted and collected into clean autoclaved RNase-free tubes. To the tissues extracted, 1 ml of trizol was added followed by gentle pipetting for homogenizing the tissue. Subsequently, 200 µl of chloroform was added gently and vortexed well. The samples were then incubated on ice for 15 minutes and then subjected to centrifugation at 14000 rpm for 15 minutes at 4°C. At this point the sample has separated into 2 phases. The top phase was transferred into a fresh tube without disturbing the interphase. To the collected top phase an equal volume of isopropanol was added and mixed. The samples were then incubated on ice for 15 minutes followed by centrifugation at 14000 rpm for 15 minutes at 4°C. The supernatant was carefully discarded and the pellet was washed in 1 ml 70% ethanol by centrifugation at 10000 rpm for 10 minutes at 4°C. The supernatant was discarded and the excess liquid was allowed to air dry followed by resuspension of the pellet in H<sub>2</sub>O. The concentration of RNA in each sample was determined by using a spectrophotometer (Amersham Biosciences, Ultraspec 3100 pro) at a wavelength of 260/280 nm.

#### **2.17.9.2 cDNA synthesis and PCR:**

2-3 µg of the isolated mRNA was used to synthesize the cDNA using the SuperScript<sup>TM</sup> III First-Strand Synthesis System for RT-PCR from Invitrogen life technologies, as per the manufacturer's instructions.

50 ng of the isolated cDNA was then used as template to amplify the gene of interest using specific forward and reverse primers and subjecting this mixture to 20-30 PCR cycles. The recipe for the PCR reaction used most often for this technique is provided in table 2.15 below.

**Table 2.15** Recipe of reagents used for the PCR reaction for amplification of a gene from cDNA

Reagent	Volume
10X PCR buffer (200 mM Tris-HCl pH 8.4, 500 mM KCl)	5 $\mu$ l
50 mM MgCl <sub>2</sub>	1.5 $\mu$ l
10 mM dNTP Mix	1 $\mu$ l
Sense primer (10 $\mu$ M)	1 $\mu$ l
Antisense primer (10 $\mu$ M)	1 $\mu$ l
Taq polymerase (5 U/ $\mu$ l)	0.4 $\mu$ l
cDNA (from first strand reaction)	2 $\mu$ l
Sterile H <sub>2</sub> O	50 $\mu$ l

The amplified samples were visualized using agarose gel electrophoresis, wherein the samples were loaded onto 1% agarose gel containing the DNA staining gel-red and run in a chamber bathed in 2X TAE buffer. The gel was run at 50 V for 50 minutes. The amplified DNA in the gels could be visualized under UV light using a gel documentation system (INTAS).

### 2.17.9.3 qRT-PCR:

qRT-PCR was performed using the Roche Light cycler to evaluate the mRNA levels of NFM in P16 FBXO41<sup>+/+</sup> and FBXO41<sup>-/-</sup> mice litter pairs. NFM- and GAPDH-specific primer pairs 32180/32181-2 and 4876/4877-2 were used for the qRT-PCR. mRNA isolation and cDNA synthesis was performed as mentioned in section 2.16.9.1 and 2.16.9.2. The NFM levels were normalized to GAPDH and represented relative to the cerebellar values for each age group.

### 2.18 *In vivo* electroporation:

*In vivo* electroporation was performed as previously described (*Holubowska et al., 2014; Kannan et al., 2012a; Kannan et al., 2012b; Konishi et al., 2004; Stegmuller et al., 2006; Vadhvani et al., 2013*). Briefly, the plasmid DNA was diluted in sterile PBS together with 0.03% Fast Green. Using a Hamilton syringe with a 30-gauge needle, the plasmid DNA (3-4  $\mu$ l / animal) was injected into the cerebellar cortex of P4 Wistar rat pups. U6/cmv-EGFP or FBXO41 RNAi#5-cmv-EGFP together with myc-CMV, FBXO41-Res  $\Delta$ CTR or FBXO41-Res plasmids, at a concentration of 8  $\mu$ g/ $\mu$ l were injected together with 1  $\mu$ g/ $\mu$ l of Bcl-X<sub>L</sub> expression plasmid. After injecting the DNA, the animals were given five short electric pulses (160-170 V for 50 msec with intervals of 950 msec). The pups were allowed to recover under an infrared lamp and then returned to the dam. 5 days later, the electroporated pups were sacrificed, the cerebella isolated and screened for presence of GFP, which served as means to determine the transfection efficiency.

The transfected cerebella were fixed in 4% PFA overnight at 4°C with gentle shaking and on the following day briefly washed with PBS and placed in 30% sucrose (in PBS) solution for 4-5 hours, as a measure of cryoprotection. The cerebella were then mounted in OCT (Tissue TEK™) and sectioned (40  $\mu$ m) using a Leica cryostat. The coronal cerebellar sections were subjected to immunohistochemistry using the GFP antibody (Santa Cruz Biotechnology). GraphPad Prism was used to perform statistical analysis of neuronal migration and distribution using Two-way ANOVA (Bonferroni correction) test. Sections were imaged using the Leica SP5 confocal microscope.

### **2.19 Generation of the FBXO41<sup>-/-</sup> knockout mouse line:**

The embryonic stem (ES) cells for the FBXO41 knockout mouse line were purchased from the KOMP repository ([www.KOMP.org](http://www.KOMP.org)). In the ES cells, the entire *Fbxo41* gene was replaced by a  $\beta$ -galactosidase reporter cassette and a neomycin resistance gene under the human ubiquitin C promoter. ES cells were injected into a blastocyst from a C57/BL6 mouse. The blastocyst in turn was implanted into a foster mother mouse, and the resulting chimeras were then crossed to wild type C57/BL6 mice to achieve germline transmission.

Tail probes from the mice were used to isolate DNA for genotyping. The tail samples were digested in 200  $\mu$ l of “tail lysis “ buffer supplemented with proteinase K at 55°C for 5-6

hours. The samples were centrifuged and the supernatant transferred into a fresh tube. 100% ethanol was used to precipitate the DNA from the supernatant. The samples were centrifuged for 10 minutes at RT, the supernatant discarded and the pellet washed twice in 70% ethanol. The supernatant was discarded, the pellet was air dried and dissolved in 100  $\mu$ l of water. The DNA concentration of each sample was determined using a spectrophotometer (Amersham Biosciences, Ultraspec 3100 pro) at 295/296 nm.

The genotyping of the DNA isolated from the mice tail probes were carried out using specific primers 2322/2323 (WT forward/reverse) and 2322/23560 (KO forward/reverse) as per the protocol listed below in table 2.16 and 2.17.

**Table 2.16** Genotyping PCR recipe of reagents

Reagent	Volume
Forward primer (10 pmol/ $\mu$ l)	1 $\mu$ l
Reverse primer (10 pmol/ $\mu$ l)	1 $\mu$ l
5X GoTaq® buffer	5 $\mu$ l
2.5 mM dNTPs	2.1 $\mu$ l
GoTaq® DNA polymerase	0.1 $\mu$ l
DMSO	2 $\mu$ l
H <sub>2</sub> O	8.3 $\mu$ l
DNA	100 ng (0.5 $\mu$ l)

**Table 2.17** Genotyping PCR thermocycler program

Temperature	Time
95°C	5 minutes
95°C	30 seconds

95°C	30 seconds	20 cycles
55°C	1 minute	
68°C		
72°C	10 minutes	
16°C	Stop	

## 2.20 Histological analysis:

### 2.20.1 Perfusion and fixation of mouse tissue:

Mice were anesthetized by injecting a ketamine/xylazine mixture (10% ketamine [v/v], 5% xylazine [v/v]) intraperitoneally. The successful anesthesia of the mice was determined by testing for inter digital pinching reflex of the hind limbs, following which the animals were stabilized with their ventral side facing upwards. Using dissection scissors and forceps, the abdomen was opened and the diaphragm removed so as to expose the heart. A small butterfly canula (Venoflix®, Braun) attached to a peristaltic pump was inserted into the left ventricle, simultaneously making an incision on the right atrium, thus creating a small opening. The blood was flushed out using PBS, following which 15-20 ml 4% PFA was to fix the tissue. Upon fixation, the tissues and organs of interest were harvested from the mice and placed in 4% PFA overnight in 4°C for further fixation. Depending on the aim of the experiment, the tissues were further processed in different post fixation solutions.

### 2.20.2 Immunohistochemistry of frozen sections:

Tissues of interest extracted from mice or rats of indicated ages were post fixed overnight in 4% PFA with gentle agitation. On the following day, tissues were placed in a 30% sucrose solution for cryoprotection for 4-5 hours at 4°C. Subsequently the tissues were embedded in OCT (Tissue TEK™) and frozen and stored at -80°C. The tissue samples were either cut into 12 µm thick sagittal sections or 30 µm thick coronal sections as per experimental design, using a cryostat (Leica, Wetzlar, Germany) and mounted onto glass slides. The cryosections

were thoroughly rinsed in PBS to remove OCT (Tissue TEK™). Then they were blocked in blocking buffer (10% NGS, 3% BSA, 0.5% TX-100 in PBS), followed by incubation with the appropriate primary antibody, which was diluted in the blocking buffer (without TX-100) overnight at 4°C. On the following day the sections were washed 3 times in PBS and incubated with the fluorophore coupled secondary antibody diluted in blocking buffer (without TX-100) for 2 hours at RT. Next the slides were briefly washed in PBS and incubated with the DNA dye DAPI (1:8000) for 10 minutes at RT. Finally the slides were rinsed twice in PBS and mounted using the antifade mounting medium Mowiol. The sections were imaged using the Leica SP5 confocal microscope.

### **2.20.3 $\beta$ -galactosidase staining:**

For the  $\beta$ -galactosidase staining, P30 FBXO41<sup>+/-</sup> mice and their FBXO41<sup>+/+</sup> littermates were subjected to transcardial perfusion under deep anesthesia (Ketamine/Xylazine). Subsequent to perfusion with PBS (pH 7.4), the tissues were perfused and fixed *in situ* with 4% (w/v) PFA in PBS. The brains and spinal cords were extracted and post-fixed in the same fixative for 3-4 hours. Following a brief rinse in PBS, the tissues were transferred to 30% sucrose in PBS for cryoprotection (overnight). The brains were stored in PBS at 4°C. 40  $\mu$ m thick sagittal brain and cerebellar sections and 40  $\mu$ m thick cross sections of the spinal cord were obtained using a Leica VT1000s vibratome (Nussloch, Germany) and collected in PBS. The free-floating sections were incubated in the following solution: 2 mM MgCl<sub>2</sub>, 0.02% NP40, 0.01% sodium deoxycholate, 5 mM potassium ferrocyanide, 5 mM potassium ferricyanide, and 0.5 mg/ml X-gal, in PBS overnight at 37°C in the dark. The sections were washed in PBS and mounted onto glass slides, air-dried and coverslipped with 50% glycerol. The sections were imaged using the Zeiss Axio Z1 brightfield microscope with the Zen 2011 software (Zeiss, Oberkochen, Germany).

### **2.20.4 Post-fixation and paraffin embedding of tissue samples:**

Mice were transcardially perfused using 4% (w/v) PFA and their brains extracted and postfixed overnight in the same fixative. For achieving thin sectioning, brains were embedded in paraffin (Paraplast, Leica, Wetzlar, Germany), using an automated program listed in table 2.18 in the embedding machine (HMP 110, MICROM).

**Table 2.18** List showing the automated paraffin embedding program used by the HMP 110,

MICROM embedding machine.

Procedure	Time
50%[v/v] Ethanol	1 hour
70%[v/v] Ethanol	2 x 2 hours
96%[v/v] Ethanol	2 x 2 hours
100%[v/v] Ethanol	2 x 2 hours
Isopropanol	1 hour
Xylol	2 x 2 hours
Paraffin	2 x 2 hours

Subsequently, the brains were placed in metal moulds and casted into blocks using 60°C warm paraffin. The blocks were labeled and allowed to solidify by cooling, subsequently being stored at RT. 5 µm thick sections were cut from the tissues embedded in the paraffin blocks using the microtome (HM 430 Thermo Scientific) and dried at RT.

#### 2.20.5 Immunohistochemistry of paraffin embedded samples:

5 µm thick sagittal brain sections from paraffin embedded samples were subjected to several deparaffinization steps listed in table 2.19 before subjecting them to immunohistochemistry.

**Table 2.19** List showing the deparaffinization steps the 5 µm thick paraffin sections were subjected to prior to staining.

Procedure	Time
60°C	10 minutes
Xylol	2 x 10 minutes
Xylol/Isopropanol (1:2)	10 minutes

100%[v/v] Ethanol	5 minutes
90%[v/v] Ethanol	5 minutes
70%[v/v] Ethanol	5 minutes
50%[v/v] Ethanol	5 minutes
dd H <sub>2</sub> O	5 minutes

#### **2.20.5.1 Haematoxylin and Eosin staining:**

For Haematoxylin and Eosin (H&E) staining after the deparaffinization steps the 5 µm thick sections were stained in haematoxylin (Merck) for 5 minutes, which stained the nuclei. Following a rinse in ddH<sub>2</sub>O, the sections were briefly differentiated in HCl/alcohol mixture and then rinsed again in ddH<sub>2</sub>O. Then the sections were incubated in Scott's solution (Thermo Scientific) for 5 minutes. Scott's solution is a bluing agent, which makes the haematoxylin dye bluer in color. After this the sections were again rinsed well in ddH<sub>2</sub>O and counterstained with 0.1% eosin [w/v] for 2-4 minutes. Eosin stained the cytoplasm pink. The sections were rinsed well in ddH<sub>2</sub>O to remove excess eosin, and were subjected to subsequent dehydration by immersing the sections in a gradient of alcohol (50%[v/v], 70% [v/v], 90% [v/v] and 100% [v/v] ethanol, 15 seconds each) and finally in isopropanol/xylol (1:2) for 3 minutes, and 2 times in xylol for 3 minutes each. The sections were eventually coverslipped-using Eukit (Kindler) mounting medium.

#### **2.20.5.2 Immunostaining using the LSAB2 detection system:**

For the purpose of immunostaining with either IBA1, GFAP, NeuN or PCNA antibodies, the paraffin embedded 5 µm thick sagittal brain sections from the FBXO41<sup>+/+</sup> and FBXO41<sup>-/-</sup> mice were firstly deparaffinized as in table 2.19, following which they were incubated in citrate buffer for 5 minutes. The tissue sections were then permeabilized in cooking them in boiling citrate buffer for 10 minutes (in a microwave oven at 650 watts). The sections were allowed to cool down at room temperature for 20-30 minutes. Subsequently, slides were rinsed briefly in Tris-buffer containing 2% [w/v] milk powder and placed into Shandon coverplates (Thermo Scientific, Cheshire, UK), specially designed for even distribution of



solutions across the slide. Once placed inside the coverplates, the slides were rinsed again in Tris buffer-containing 2% milk [w/v] powder. For visualization of the staining, HRP-conjugated secondary antibodies were used, hence it was necessary to ensure inhibition of endogenous peroxidase activity, for which the sections were treated with 3% H<sub>2</sub>O<sub>2</sub> for 5 minutes and subsequently washed with Tris buffer with 2% milk [w/v] powder. The sections were blocked in blocking buffer (20% goat serum in BSA/PBS) for 10 minutes at room temperature. The slides were then incubated with the primary antibody diluted in PBS/BSA overnight at 4°C. Next day the sections were washed in Tris buffer with 2% milk [w/v] powder and the LSAB<sub>2</sub> kit was used to detect the protein of interest bound to the primary antibodies. The slides were incubated with a biotinylated secondary antibody for 10 minutes at RT. Following a rinse with Tris-buffer with 2% milk [w/v] powder, a second HRP complex coupled secondary antibody was added onto the slides and incubated for 10 minutes at RT. The coverplates were dismantled and the slides washed in Tris-buffer without milk. The HRP substrate Diaminobenzidine (DAB) was applied onto the slides using the DAB kit (DAKO) and incubated for 5-10 minutes. Appearance of brown labeling indicated the recognition of target proteins by the specific antibodies. After being rinsed several times in ddH<sub>2</sub>O, the sections were incubated in 0.1% Haematoxylin [w/v] for 30 seconds. Subsequently the sections were rinsed in water to remove excess unbound dye and briefly dipped in HCl-alcohol solution to achieve better differentiation. Next the slides were again briefly rinsed in water and incubated in Scotts solution for 5 minutes at RT to achieve a desirable bluing of the nuclei stained by the Haematoxylin. The slides were again rinsed briefly in water and subjected to a gradient of alcohol steps (50% [v/v], 70% [v/v], 90% [v/v] and 100% [v/v] ethanol, 3 minutes each) to achieve dehydration. Then, the tissue samples were incubated in isopropanol/xylol and twice in xylol for 7 minutes each. Finally, the slides were coverslipped using the xylol-based mounting medium Eukit (Kindler).

The DeadEnd™ Colorimetric TUNEL System kit from Promega was used as per the instructions from the manufacturer for specifically labeling apoptotic cells. The kit labels the fragmented DNA of apoptotic cells using TUNEL (TdT-mediated dUTP Nick-End Labeling) assay. Biotinylated nucleotides are incorporated at the 3'-OH of DNA ends by the Terminal Deoxynucleotidyl Transferase (TdT) enzyme. Horseradish-peroxidase-labeled streptavidin (Streptavidin HRP) then binds to these biotinylated nucleotides, which are detected using the peroxidase substrate, hydrogen peroxide, and the stable chromogen, diaminobenzidine

(DAB). Using this procedure, dark brown stained apoptotic nuclei level can be detected at the single cell. The stained slides were coverslipped using Aqual-Poly/Mount (Merk) mounting medium.

All the images for H&E and DAB based chromogenic stains were acquired using the Zeiss Axio Z1 brightfield microscope and the Zen 2011 software from Zeiss (Zeiss, Oberkochen, Germany).

### **2.20.5.3 Analyses and quantification of chromogenically stained sections:**

For the samples stained for H&E and DAB staining (TUNEL, IBA1, NeuN and PCNA), 3 anatomically matched sections per animal brain per genotype were included in the analyses. 3 FBXO41<sup>-/-</sup> animals and corresponding wild type littermates of the indicated ages were analyzed manually in a blinded manner.

The number of Haematoxylin-positive nuclei within the molecular layer of the sagittal cerebellar sections was quantified using a custom designed macro for ImageJ. Dr. Miso Mitkovski designed the macro. The script of the macro is mentioned below:

```
//Getting ready

setBackground(0,0,0);

setForegroundColor(255,255,255);

run("Select None");

roiManager("Deselect");

//Image processing

run("Split Channels");

close();close();

run("Invert");

run("32-bit");

run("Gaussian Blur...", "sigma=4");
```

```
resetMinAndMax();

//ROI manager removes non-molecular layer portion

n = roiManager("count");

for (i=0; i<n; i++) {

    roiManager("select", i);

    run("Clear Outside");

}

//Close ROI-Manager

if (isOpen("ROI Manager")) {

    selectWindow("ROI Manager");

    run("Close");

}

//Thresholding and mask generation

setAutoThreshold("Yen");

setOption("BlackBackground", false);

run("Convert to Mask");

run("Options...", "iterations=1 count=1 edm=Overwrite do=Close");

run("Make Binary");

run("Watershed");

//Analyze particles

run("Analyze Particles...", "size=60-1800 circularity=0.5-1 exclude clear add");

//Set measurement types
```

```

run("Set Measurements...", "area shape redirect=None decimal=3");

//Tell ROI-Manager to measure all ROIs

n = roiManager("count");

for (i=0; i<n; i++) {

    roiManager("select", i);

    roiManager("Measure");

}

beep(); showMessage("Feedback", "Counting finished!");

```

The area measurement tool in ImageJ was used to measure the thickness of the EGL. For the distribution of TUNEL-positive nuclei and of IBA1-positive cells, the counting was manually performed in a blinded manner.

For the area distribution of DAB-positive signal of GFAP, another custom designed imageJ macro was used, which converted the picture into a black and white image, with the black representing the DAB signal. Then it measured the percentage of the area occupied the DAB signal relative to the total area of the region on interest. The macro was designed by Dr. Miso Mitkovski and the detailed script is below:

```

run("Close All");

roiManager("reset")

run("Clear Results");

open("");

run("Set Scale...", "distance=0 known=0 pixel=1 unit=pixel");

setTool("polygon");

beep();

```

```
waitForUser("Hi there", "Select the region of interest and click OK");

run("Add to Manager");

////

// Color Thresholder 1.45k

// Autogenerated macro, single images only!

min=newArray(3);

max=newArray(3);

filter=newArray(3);

a=getTitle();

run("HSB Stack");

run("Convert Stack to Images");

selectWindow("Hue");

rename("0");

selectWindow("Saturation");

rename("1");

selectWindow("Brightness");

rename("2");

min[0]=0;

max[0]=50;

filter[0]="pass";

min[1]=54;

max[1]=255;
```

```

filter[1]="pass";

min[2]=0;

max[2]=163;

filter[2]="pass";

for (i=0;i<3;i++){

    selectWindow(""+i);

    setThreshold(min[i], max[i]);

    run("Convert to Mask");

    if (filter[i]=="stop") run("Invert");

}

imageCalculator("AND create", "0","1");

imageCalculator("AND create", "Result of 0","2");

for (i=0;i<3;i++){

    selectWindow(""+i);

    close();

}

selectWindow("Result of 0");

close();

selectWindow("Result of Result of 0");

rename(a);

// Colour Thresholding-----

/////

```

```

run("Set Measurements...", "area redirect=None decimal=3");

roiManager("Select", 0);

roiManager("Measure");

run("32-bit");

setThreshold(200.0000, 255.0000);

run("NaN Background");

roiManager("Select", 0);

roiManager("Measure");

setMinAndMax(200, 255);

```

For determining the density of cellular distribution for H&E and DAB stained pictures, the following formula was used:

$$\text{Cell distribution (cells/mm}^2\text{)} = \frac{\text{N (number of cells counted in region)}}{\text{Area of the region of interest (mm}^2\text{)}}$$

All statistical analyses were performed using Graphpad Prizm 5.0 Student's t-test (Paired t - test) or Two-way ANOVA.

## 2.21 Mouse behavior:

All experiments that involved live animals were conducted in agreement with the animal protocols approved by the Verbraucherschutz und Lebensmittelsicherheit of Lower Saxony, Germany.

### 2.21.1 Mouse behavior at P16:

At least 10 P16 animals per genotype (FBXO41+/+, FBXO41+/- and FBXO41-/-) and 3 P30 animals per genotype (FBXO41+/+ and FBXO41-/-) were subjected to an ataxia scoring protocol adapted from the previously described paper from Guyenet and colleagues (*Guyenet et al., 2010*). To evaluate their basic motor functions such as balance and coordination, P16

(FBXO41<sup>+/+</sup>, FBXO41<sup>+/-</sup> or FBXO41<sup>-/-</sup>) mice were subjected to four basic tests by a blinded investigator.

#### **2.21.1.1 The Clasping test:**

For the clasping test mice were suspended by their tails for 10 seconds and evaluated whether they clasped their fore and hind limbs close to their bodies or if they spread their limbs when suspended by their tail. The extent of clasping was scored on a scale of 0 to 3, where 0 represented no clasping and 3 represented severe clasping of the limbs. Each mouse was subjected to the clasping test three times and an average of all three trials was considered as the final score. The presence of clasping is often regarded as a sign of disease progression and neurological deficits in several neurodegenerative diseases (*Guyenet et al., 2010*).

#### **2.21.1.2 Ledge test:**

The ledge test was performed as previously described (*Guyenet et al., 2010*). The mice were placed on a 5 mm wide and 30 cm long ledge of a Plexiglas box. The mice were encouraged to walk across from one end of the ledge to the other. The coordination and grace with which they crossed the ledge was scored from 0 to 3. 0 represented no phenotype and the ability to cross the ledge gracefully in a coordinated manner with no limb dragging, while 3 represented the most severe phenotype, with inability to cross the ledge.

#### **2.21.1.3 Gait analysis:**

The mice were subjected to a gait analysis test as previously demonstrated (*Guyenet et al., 2010*). The test was performed in order to evaluate coordination and muscle function. The mice were placed on a flat surface with their heads facing away from the investigator. The mice were scored on how well they supported their body weight and moved on all four limbs. For the above test the mice were scored between 0 and 3 (0 was for best performance and 3 for worst). Each mouse was subjected to the gait analyses test three times and an average of all three trials was considered as the final score.

#### **2.21.1.4 Rotarod:**

The rotarod test has been previously described (*Radyushkin et al., 2009*) and was used to assess the balance and motor coordination of P16 mice. Briefly, the rotarod is a rotating drum (Ugo Basile, Comerio, Varese, Italy), which accelerated from 4 to 40 rpm at a rate of 0.1



rpm/sec. The mice were placed one by one on the rotarod, under a non-accelerating speed of 12 rpm, and their latency to fall off was recorded using a stopwatch. The mice were kept on the rotarod for a maximum of 240 seconds during acceleration. Each mouse had three trials on the rotarod and an average of all three trials was considered as the final score.

### **2.21.2 Adult mouse behavior:**

10-month-old adult FBXO41<sup>+/+</sup> and FBXO41<sup>+/-</sup> mice were subjected to a battery of behavior tests. A total of 40 animals from 2 independent cohorts were analyzed. During the period of behavioral testing the animals were housed in groups of 4-6 along with their littermates in standard plastic cages (26.5 x 20 x 14cm) under standard 12-hour light/dark cycle with food and water being provided *ad libitum*. The temperature of the behavior room was maintained at 21 $\pm$  2°C and all the experiments were conducted in a blinded manner during the light phase of the day. The experiments were conducted in the following order: Elevated plus maze, open field, clasping test, rotarod, balance beam, pole test, olfaction.

#### **2.21.2.1 Elevated plus maze:**

To evaluate anxiety in the mice, they were subjected to the elevated plus maze. The maze is made up of grey perspex having a 5 x 5 cm central platform and 2 open and 2 closed arms (30 x 15 x 15 cm). The elevated plus maze was placed in a light room with 110 lx. Each mouse was placed in the central quadrant facing one of the open arms of the elevated plus maze. The exploratory behavior of the mice was monitored using an overhead video recorder, which was connected to the computer, using the “Viewer 2” software (Biobserve GmbH, Bonn Germany). Each animal was allowed to explore the elevated plus maze for 10 minutes and their behavior recorded and analyzed for the time spent in open or closed arms. Excessive time spent in open arms is readout for reduced anxiety.

#### **2.21.2.2 Open Field:**

The open field test was used to assess the general locomotor activity of the mice. The mice were placed at the center of an open circular grey perspex arena (120 cm in diameter, 25 cm high), in a room with a light intensity of 110 lx. The mice were allowed to explore the arena for 10 minutes. The behavior was recorded using the overhead camera connected to the computer equipped with the “Viewer 2” software. The velocity, distance travelled and the time spent in central, intermediate and peripheral zones of the arena were analyzed.

### **2.21.2.3 Clasping test:**

The clasping test for the 10-month-old FBXO41<sup>+/+</sup> and FBXO41<sup>+/-</sup> mice was performed as per section 2.21.1.1.

### **2.21.2.4 Rotarod: motor learning paradigm:**

To assess the motor coordination and balance in the mice, the 10-month-old FBXO41<sup>+/+</sup> and FBXO41<sup>+/-</sup> mice were subjected to the rotarod test. Each animal was placed on the rotating drum of the rotarod and its latency to fall off was noted. The time and speed that each animal can withstand on a rotarod accelerating at 4-40rpm was determined. To check if the animals show motor learning, the animals were subjected to the rotarod test at 3 hours after the first trial and after 24 hours. In cases where motor learning had occurred, the animals performed better with time. Each animal was allowed for a maximum of 5 minutes per trial on the rotarod.

### **2.21.2.4 Pole test:**

The pole test has been previously demonstrated as a reliable measure to assess basal ganglia related motor function (*Matsuura et al., 1997*). Each animal was placed on top of a pole (50 cm tall) with its head up. The base of the pole was placed inside the home cage of the animal. A healthy animal when placed on top of the pole head up orients itself downward and descends into the cage. Prior to testing each animal was trained on the previous day to descend into its home cage when placed onto the pole. On the test day each animal was allowed five trials. The time taken to orient itself downward and descend into the cage was measured. The best of five trials per animal was included in the analyses.

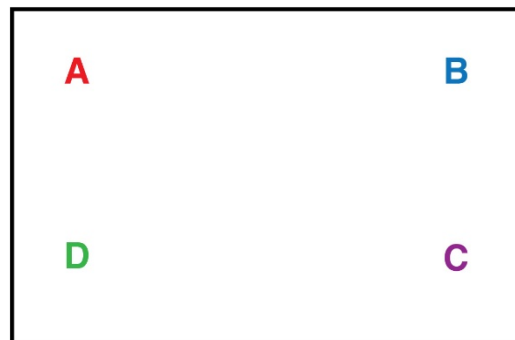
### **2.21.2.5 Balance beam:**

The balance beam test was performed as previously described by (*Luong et al., 2011*). Two wooden beams of 80 cm length and 12 mm and 6 mm thickness each were used to gauge the motor coordination and balance of the mice. The beams were placed onto a wooden stand with the end of the wooden beam leading into the home cage of the mouse. Each animal was trained to walk across the length of the beam from the start point to the end and into its home cage. All the animals were trained to walk across both the 12 mm and 6 mm beam for 2 days prior to the test day. On the test day the time taken by the animal to cross each of the two

beams (12 mm and 6 mm) was measured. The animals were additionally scored from 0-7 on their motor coordination while walking on the beams. 7 represented normalcy and 0 represented dragging of both hind and fore limbs and complete inability to cross the beam. Each animal was given 3 trials per beam. The average time and score of all three trials was analyzed per animal.

#### 2.21.2.6 Olfaction:

Two days prior to habituation, 2 pieces of chocolate chips per animals were placed into the cages. For habituation of the testing environment, each animal was placed into the testing cage (29.5 x 18.5 x 13 cm) with a piece of chocolate chip visibly placed on the surface of the bedding inside the cage per trial. The chocolate chip was randomly placed at any of the four positions A, B, C or D as indicated in the illustration below.



In every trial, the animal was released in the center of the cage and allowed to explore for 10 minutes. Each mouse was subjected to 4 trials per day with an inter-trial interval of 50 minutes per trial. The animals were habituated for 2 days, following which they were food deprived overnight, although the water was available *ad libitum*. 2 pieces of chocolate chip were placed into the home cage.

On day 5 the animals were tested. Each mouse was placed into the test cage with a chocolate chip hidden randomly at positions A, B, C or D 1cm below the standard bedding. Each mouse was given five minutes to explore and find the chocolate chip. Each animal was tested twice with an inter-trial interval of 100 minutes. The time taken by the animal to find the hidden chip of chocolate from the time it was released into the cage was measured. The average of both the trials was analyzed and represented the measure of the integrity of the olfactory

system. In order to account for other sensory and motor or motivational factors that might influence the latency to finding the chocolate chip, the test was performed a third time as described previously, but this time the chocolate chip was placed clearly visible on top of the bedding. For all the animals and all the trials fresh cages and bedding were used.

---

## 3 Results

### 3.1 *In vivo* characterization of FBXO41 function:

Increasing evidence points to the important function of F-box proteins during neurodevelopment and progression of disease in various neurological disorders (*Gong et al., 2010; Jandke et al., 2011; Litterman et al., 2011; Liu et al., 2011; Saiga et al., 2009; Westbrook et al., 2008*). However, of the ~70 known mammalian F-box proteins only a few have been extensively studied. Hence, it is crucial to further identify and dissect the various unknown or understudied molecular pathways governed by these F-box proteins, orchestrating brain development and disease. Previous results from the lab identified FBXO41 as a brain-abundant F-box protein, with a possible role in axon growth and neuronal migration. As the first aim of my study, I shed further light on the role of FBXO41 function *in vivo* using the FBXO41 knockout mouse.

#### 3.1.1 FBXO41 expression is restricted to the CNS:

A previous study from our lab reported FBXO41 to have a brain-specific expression, which was highly upregulated during pre- and postnatal neurodevelopment having a constant expression throughout adulthood in mice (*Holubowska, 2013*). In order to characterize the spatial distribution of FBXO41 within the nervous system, I performed an RT-PCR analysis using cerebellar, splenic, spinal cord and sciatic nerve cDNA isolated from P20 male mice (**Figure 3.1 A**). As previously reported, I observed that FBXO41 mRNA was detectable in the cerebellum but not in spleen. However, I observed an additional expression of FBXO41 mRNA in the spinal cord, which was completely absent from sciatic nerve (exemplar for peripheral nervous system (PNS) tissue). I further validated the finding at the protein level, by using the previously validated custom-made FBXO41 specific antibody (**Figure 3.1 B**).

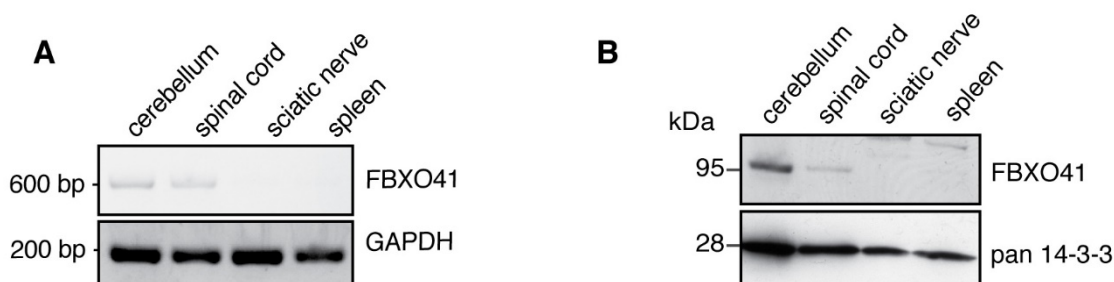


**Figure 3.1 FBXO41 is exclusively expressed in the CNS:** (A) RT-PCR analysis was performed from mRNA isolated from cerebellar, spinal cord, sciatic nerve and splenic tissues from P20 male mice. GAPDH served as loading control. (B) 50  $\mu$ g of cerebellar, spinal cord, sciatic nerve and splenic lysates from P20 male mice were subjected to immunoblotting with the FBXO41-specific antibody. The pan 14-3-3 antibody served as loading control.

The lab has previously generated an FBXO41 conventional knockout mouse line, where the entire *Fbxo41* gene has been excised after its promoter region and replaced by a  $\beta$ -galactosidase reporter cassette and neomycin selection cassette (Figure 3.2 A). The  $\beta$ -neo cassette thus results in the expression of  $\beta$ -galactosidase ( $\beta$ -gal) driven by the endogenous FBXO41 promoter. We were able to identify and distinguish the homozygous and heterozygotes from the wild types by genotyping using specific primers, which recognize either wild type or mutant alleles (Figure 3.2 B).

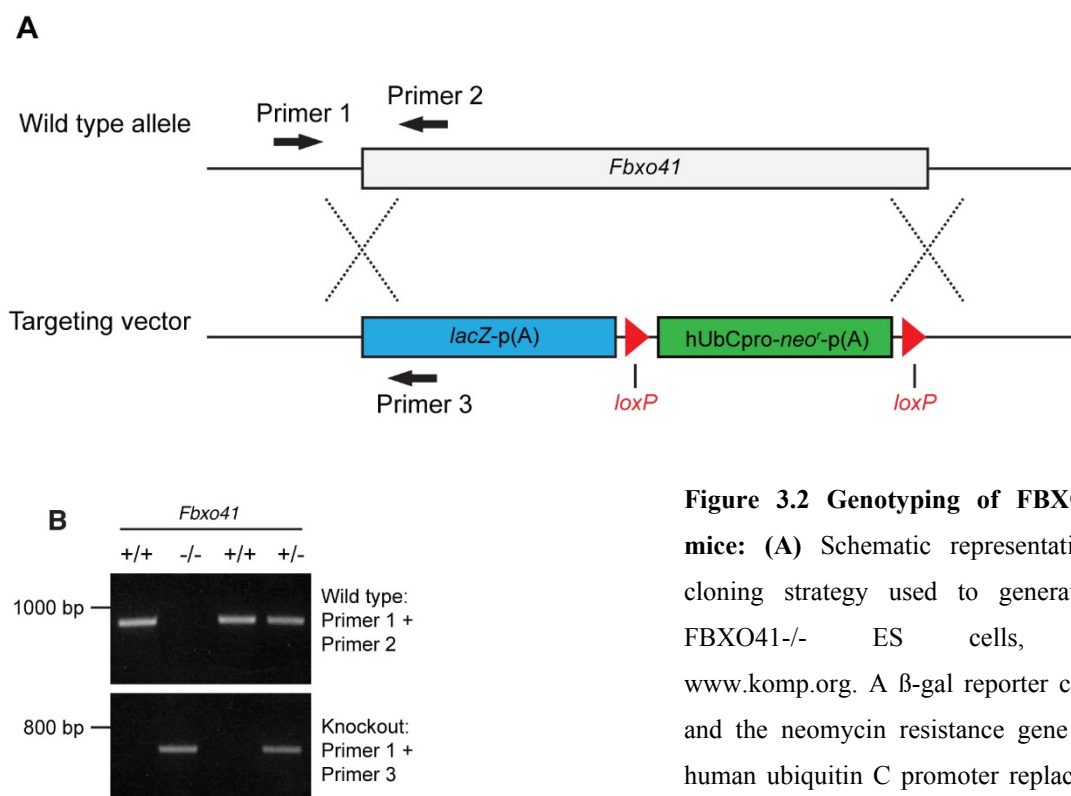


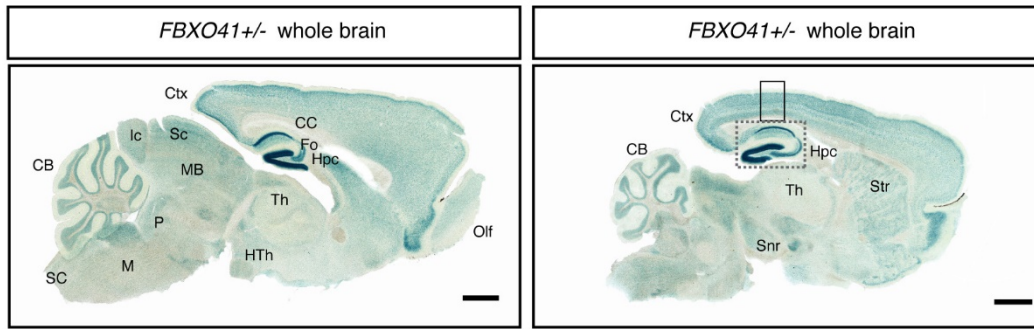
**Figure 3.2 Genotyping of FBXO41<sup>-/-</sup> mice:** (A) Schematic representation of cloning strategy used to generate the FBXO41<sup>-/-</sup> ES cells, from [www.komp.org](http://www.komp.org). A  $\beta$ -gal reporter cassette and the neomycin resistance gene under human ubiquitin C promoter replaced the entire *Fbxo41* gene. (B) Representative genotyping PCR of the mice after germline transmission was achieved. Arrows in A represent the location of the primers 1, 2 and 3 used for genotyping.

In addition to the biochemical validation of the expression of FBXO41, I further went on to explore the spatial distribution of FBXO41 *in vivo* within the various CNS compartments. I

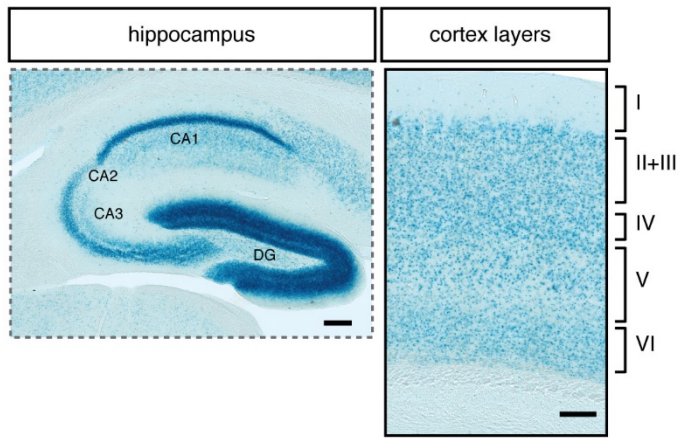
subjected sagittal brain sections from P30 FBXO41 +/- (heterozygous) mice and their wild type littermates to X-gal staining. I observed intense  $\beta$ -gal enzymatic activity throughout the brain of the FBXO41 +/- mice and to a weaker extent in the spinal cord (**Figure 3.3 A, C**). Apart from the striatum and the midbrain, I also found robust  $\beta$ -gal activity in the cortex hippocampus and cerebellum (**Figure 3.3 A**). Higher magnification panels of the cortex, hippocampus and cerebellum revealed that FBXO41 has a neuron-specific expression, as the  $\beta$ -gal enzymatic activity was absent from white matter regions in the brain as well as the spinal cord (**Figure 3.3 B, D**).

Interestingly, a closer look at the various cerebellar layers revealed that FBXO41 expression was restricted only to the cerebellar granule neurons (CGNs) and the deep cerebellar nuclei (DCN). The Purkinje cell layer (PCL), molecular layer (ML) and white matter were completely devoid of  $\beta$ -gal activity (**Figure 3.3 D inset**). Additionally, I observed no  $\beta$ -gal activity in the 40 $\mu$ m sagittal brain section from P30 FBXO41+/+ mice, when stained for X-gal, serving as a negative control (**Figure 3.3 E**). Collectively, these results establish FBXO41 as a CNS-specific F-box protein with a neuronal expression.

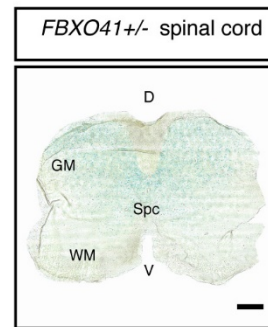
**A**



**B**



**C**





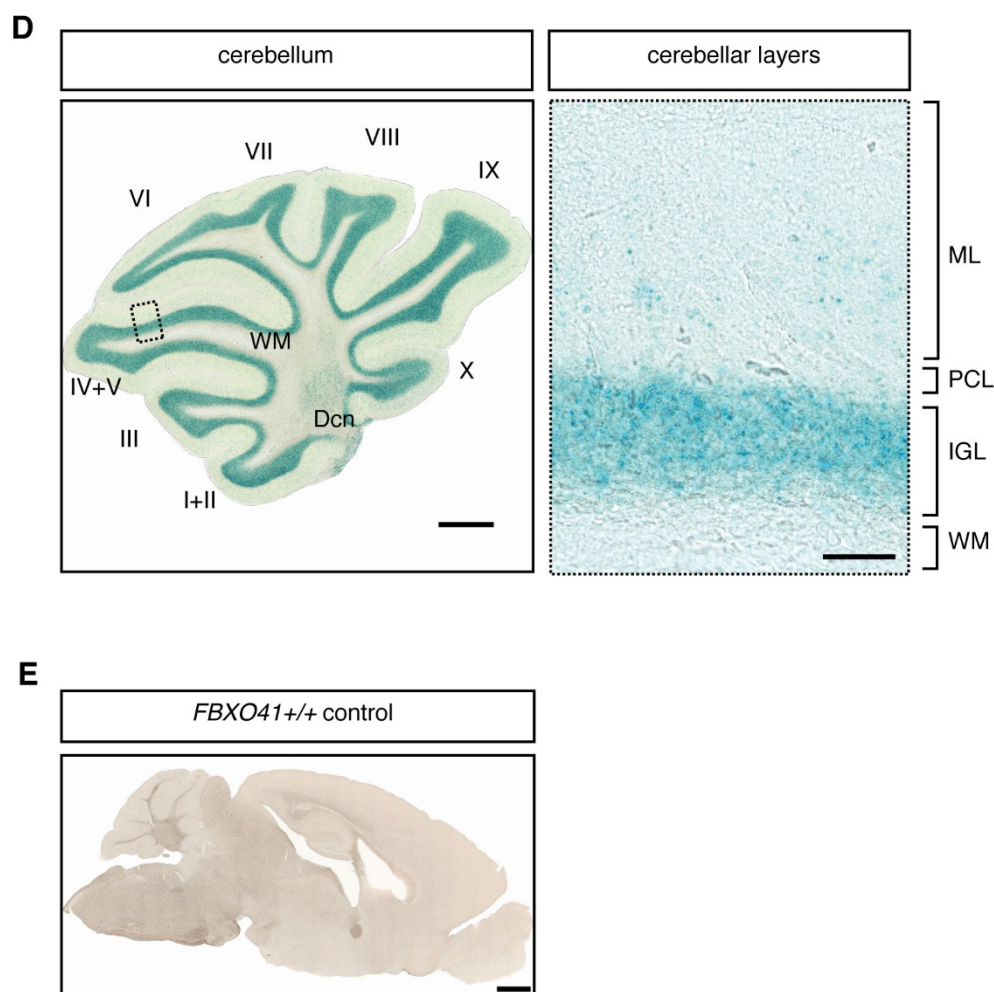


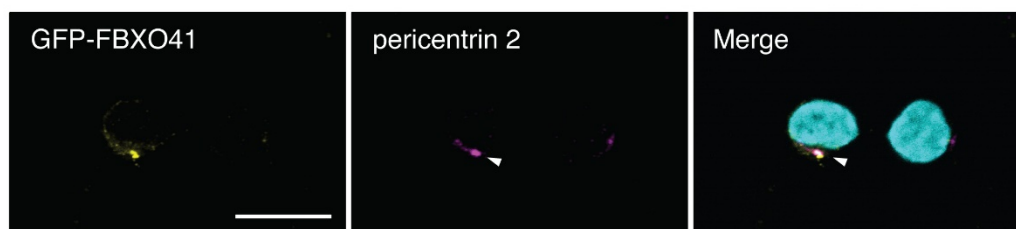
**Figure 3.3 FBXO41 expression within the CNS:** (A) 40  $\mu$ m thick sagittal sections of P30 *FBXO41*<sup>+/-</sup> mouse brain were subjected to X-gal staining. Ctx= cortex, CB= cerebellum, CC= corpus callosum, Fo= fornix, Hpc= hippocampus, Th= thalamus, HTh= hypothalamus, Str= striatum, Snr= substantia nigra, Olf= olfactory bulb, MB= midbrain, Sc= superior colliculus, Ic= inferior colliculus, P= pons, M= medulla oblongata, SC= spinal cord. Scale bars equal 1000  $\mu$ m. (B) Insets marked in A depict higher magnification images of the hippocampus and the various cortical layers in B. CA1= cornu ammonis 1, CA2= cornu ammonis 2, CA3= cornu ammonis 3 and DG= dentate gyrus. The roman numerals represent the various cortical layers. Scale bars equal 200  $\mu$ m and 100  $\mu$ m respectively. (C) 40  $\mu$ m cross section of the P30 *FBXO41*<sup>+/-</sup> mouse spinal cord was subjected to X-gal staining. SC= spinal cord, GM= grey matter, WM= white matter, SpC= spinal canal, D= dorsal, V= ventral. Scale bar equals 200  $\mu$ m. (D) 40  $\mu$ m thick sagittal section of the P30 *FBXO41*<sup>+/-</sup> mouse cerebellum was subjected to X-gal staining. The roman numerals I-X represent the various cerebellar folia. Inset depicts higher magnification of the cerebellar layers. WM= white matter, Dcn= deep cerebellar nuclei, ML= molecular layer, PCL= Purkinje cell layer, IGL= internal granule layer. Scale bars equal 500  $\mu$ m for the panel depicting the cerebellum and 50  $\mu$ m for the inset representing higher magnification. (E) 40  $\mu$ m thick sagittal section of the P30 *FBXO41*<sup>+/+</sup> brain when subjected to X-gal staining shows no  $\beta$ -gal reactivity, thus serving as negative

control. Scale bar equals 1000  $\mu\text{m}$ .

### 3.1.2 FBXO41 has a dual localization at the cytoplasm and the centrosome:

Having established the neuronal CNS-specific expression of FBXO41, we went on to study the subcellular localization of FBXO41. We resorted to transfection of cultured CGNs with GFP-tagged FBXO41 expression plasmids. Subsequently, these cultured neurons were subjected to immunocytochemistry with the GFP antibody. Previous findings from the lab reported a predominantly cytoplasmic localization of FBXO41, which was absent from the nucleus, localizing along both the axons as well as dendrites. Additionally, we verified and confirmed its dual localization at the centrosome, as we observed that GFP-FBXO41 also colocalized with the centrosomal protein pericentrin 2 (performed by Dr. A. Holubowska) (**Figure 3.4 A**). Centrosomal enrichment experiments performed by N. Schwedhelm-Domeyer further validated the dual localization of FBXO41, as endogenous FBXO41 could be detected in the cytosolic as well as the enriched centrosomal fractions using the FBXO41-specific antibody (**Figure 3.4 B**).

**A**



**B**

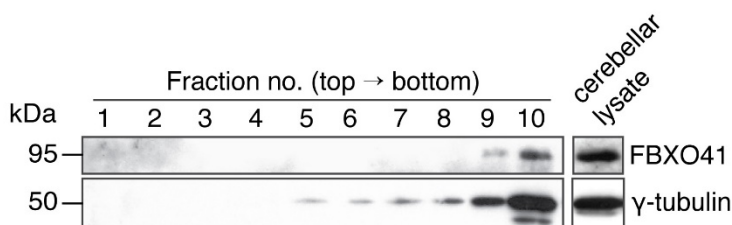


**Figure 3.4 FBXO41 localizes to the centrosome:** (A) Confocal images of cultured CGNs, transfected with a plasmid expressing GFP-FBXO41 followed by immunocytochemistry using the GFP and pericentrin 2 antibodies with the DNA binding dye DAPI. Arrowheads indicate the centrosomal marker pericentrin 2 and its colocalization with GFP-FBXO41. Scale bar equals 10  $\mu\text{m}$ . *Experiment was*

performed by Dr. A. Holubowska **(B)** Lysates harvested from cultured CGNs at DIV8 were subjected to a centrosomal purification protocol using a sucrose gradient, followed by immunoblotting with the FBXO41 antibody.  $\gamma$ -tubulin served as marker for centrosomal enrichment in the bottom fractions. Cerebellar lysates from P16 wild type mice served as positive control. *Experiment was performed by N.Schwedhelm-Domeyer.*

### 3.1.3 Loss of FBXO41 results in retarded growth and severe motor deficits:

Owing to its CNS-specific neuronal expression, an FBXO41 conventional knockout mouse line was generated to study the effects of loss of FBXO41 *in vivo*. The FBXO41<sup>-/-</sup> mice have been previously reported to have an extremely high mortality rate, with only 20% of all knockout mice born making it past the second postnatal week. Apart from the high mortality rate, a decreased body weight was also observed at P5 (*Holubowska, 2013*). Due to the limited availability of the knockout mice past P18, as a result of high mortality rate, I restricted my behavioral analysis to the age of P16. The most striking phenotype at P16 was the dramatically reduced body size of the FBXO41<sup>-/-</sup> animals in contrast to the FBXO41<sup>+/+</sup> and FBXO41<sup>+/-</sup> littermates (**Figure 3.5 A**). This was accompanied with significantly reduced body and brain weights (**Figure 3.5 B, C**).

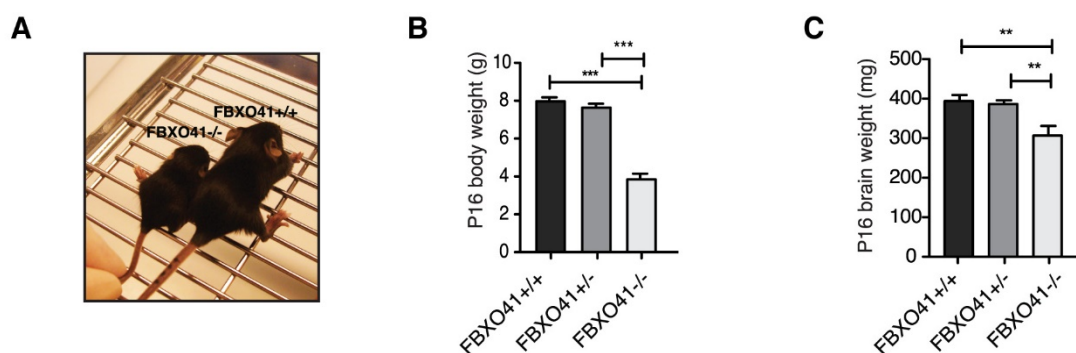


**Figure 3.5 Loss of FBXO41 results in diminished body and brain weights:** (A) Representative image of the P16 FBXO41<sup>+/+</sup> and FBXO41<sup>-/-</sup> littermates. (B, C). Average body and brain weights of the FBXO41<sup>+/+</sup>, FBXO41<sup>+/-</sup> and FBXO41<sup>-/-</sup> mice at P16, respectively. A total of 86 P16 mice were analyzed (ANOVA, \*\*p<0.01, \*\*\*p<0.001, mean +s.e.m.).

Apart from the diminished body size, the FBXO41<sup>-/-</sup> also displayed an abnormal ataxic gait and severe motor deficits when analyzed for motor coordination and function. In order to assess the extent of the ataxic phenotype observed in the FBXO41<sup>-/-</sup> mice, I subjected the animals to an ataxia scoring protocol previously described by (*Guyenet et al., 2010*). It involves a battery of simple motor tests, namely gait analysis, ledge test, hind limb clasp

and rotarod. While gait analysis is often used to assess motor coordination and muscle function, the ledge test and rotarod measure coordination. Hind limb clasp is a marker of disease progression and hints to neurological deficits (*Guyenet et al., 2010*). The performance of each animal was scored from 0 to 3, where 0 represented no phenotype and 3 being the worst manifestation of the phenotype. The results showed that while the healthy FBXO41<sup>+/+</sup> and FBXO41<sup>+/-</sup> littermates were indistinguishable at P16 with no signs of hind limb clasp, the FBXO41<sup>-/-</sup> mice consistently performed worse in all the tests and adopted a severe hind limb clasp posture when suspended by their tails (**Figure 3.6 A, B, C, D, E**). Collectively, these results demonstrate that the CNS-specific expression of FBXO41 is crucial for proper growth and motor function in mice.

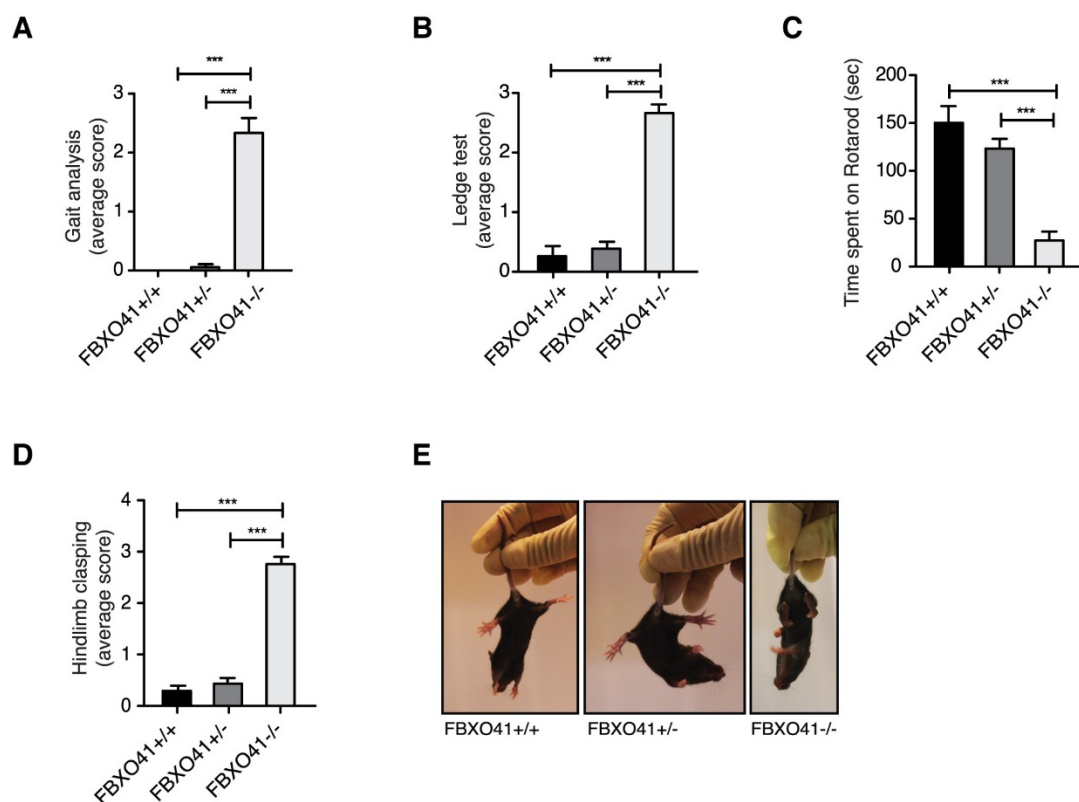


**Figure 3.6 FBXO41<sup>-/-</sup> mice display severe motor deficits:** (A) P16 FBXO41<sup>+/+</sup>, FBXO41<sup>+/-</sup> and FBXO41<sup>-/-</sup> littermates were subjected to gait analysis. 0= normal phenotype, 3= worst manifestation of phenotype. (B) P16 FBXO41<sup>+/+</sup>, FBXO41<sup>+/-</sup> and FBXO41<sup>-/-</sup> littermates were subjected to the ledge test. 0= normal phenotype, 3= worst manifestation of phenotype. (C) P16 FBXO41<sup>+/+</sup>, FBXO41<sup>+/-</sup> and FBXO41<sup>-/-</sup> littermates were tested for time spent on rotarod at a speed of 12 rpm, with 240 seconds being the cut-off time. (D) P16 FBXO41<sup>+/+</sup>, FBXO41<sup>+/-</sup> and FBXO41<sup>-/-</sup> littermates were tested for hind limb clasp. 0= normal phenotype, 3= worst manifestation of phenotype. (E) Representative images of P16 FBXO41<sup>+/+</sup>, FBXO41<sup>+/-</sup> and FBXO41<sup>-/-</sup> littermates when tested for hind limb clasp. (A-D) For all the

behavioral tests, the observations and analyses were recorded in a blinded manner with at least 10 animals of each genotype being included in the analysis (ANOVA, \*\*\* $p < 0.001$ , mean + s.e.m.).

### 3.1.4 P16 FBXO41<sup>-/-</sup> mice do not show signs of neurodegeneration:

The brain-dominant neuronal expression of FBXO41 prompted me to verify whether the reduced brain weights observed in the FBXO41<sup>-/-</sup> mice at P16 were a consequence of increased cell death and neurodegeneration. To address this, I analyzed 5  $\mu\text{m}$  thick sagittal paraffin sections from P16 FBXO41<sup>+/+</sup> and FBXO41<sup>-/-</sup> mice brains for apoptosis using the TUNEL assay (**Figure 3.7 A, B, C, D**).

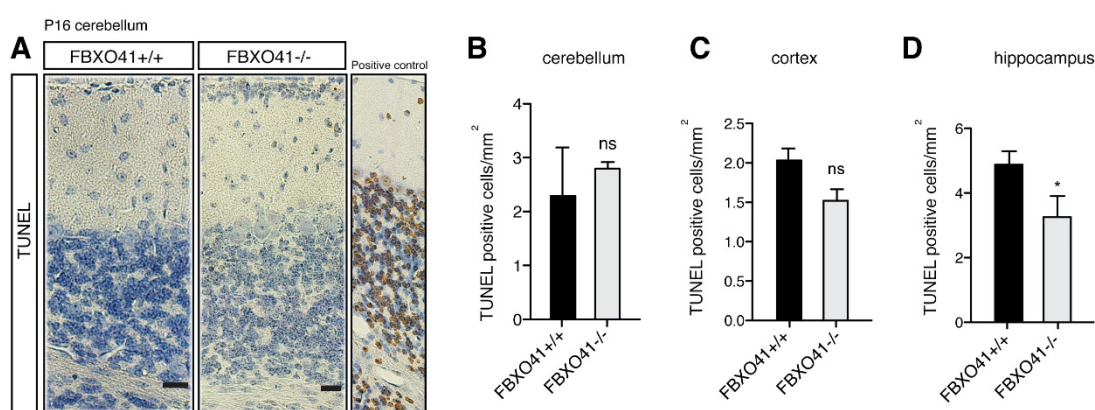


**Figure 3.7 FBXO41<sup>-/-</sup> mice display no signs of apoptosis or neurodegeneration at P16:** (A) Representative images of the cerebellar region from 5  $\mu\text{m}$  thick paraffin embedded sagittal brain sections of P16 FBXO41<sup>+/+</sup> and FBXO41<sup>-/-</sup> mice. These sections were subjected to immunohistochemistry using a TUNEL detection kit, detecting apoptotic cells. The DNase-treated cerebellar tissue served as positive control. Scale bar equals 20  $\mu\text{m}$ . (B, C, D) Quantification (cells/mm<sup>2</sup>) of the distribution of TUNEL-positive cells within the cerebellar, cortical and hippocampal regions of FBXO41<sup>+/+</sup> and FBXO41<sup>-/-</sup> mice from A. Quantifications were done manually, in a blinded manner. At least three different anatomically matched sections per animal were quantified, and at least three independent littermates per genotype were included in the analyses (Students's t-test, \* $p < 0.05$ , ns=non significant, mean+s.e.m). *I performed sample collection, sectioning, imaging quantification and analysis, while Dr. A. Matz carried out histochemical procedures.*

Additionally, we also checked for signs of inflammation, namely microglia and astrogliosis, using the markers IBA1 and GFAP, respectively (**Figure 3.8 A-F**)

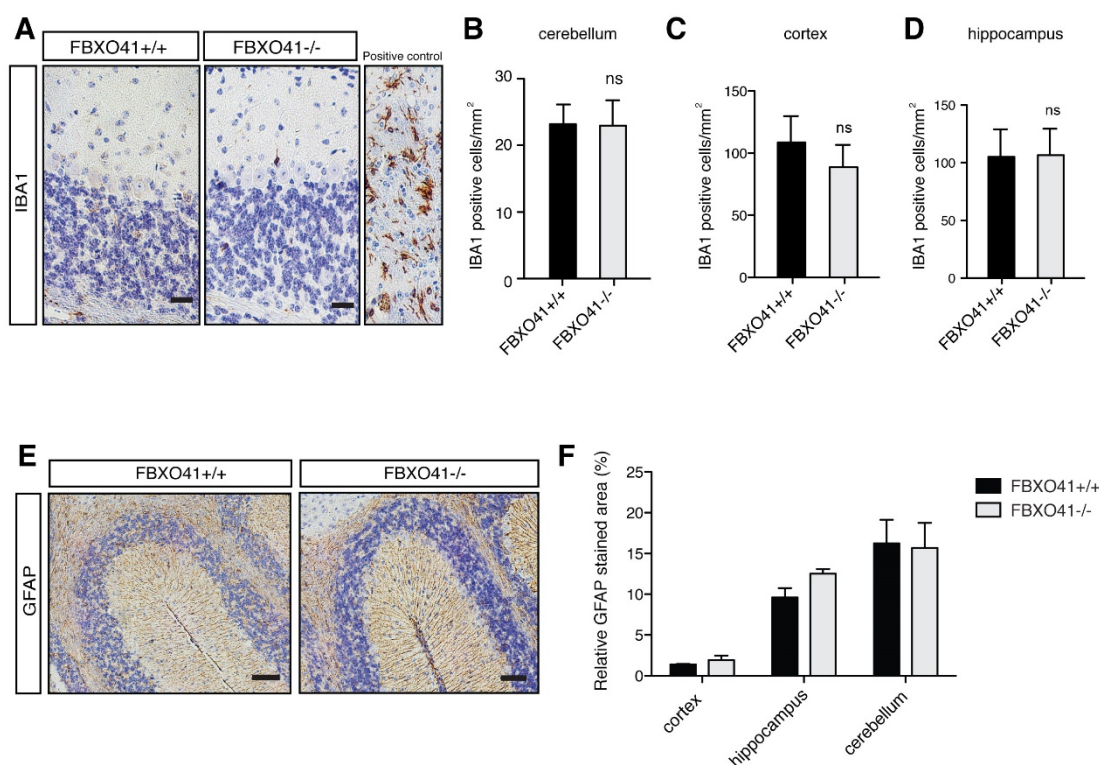


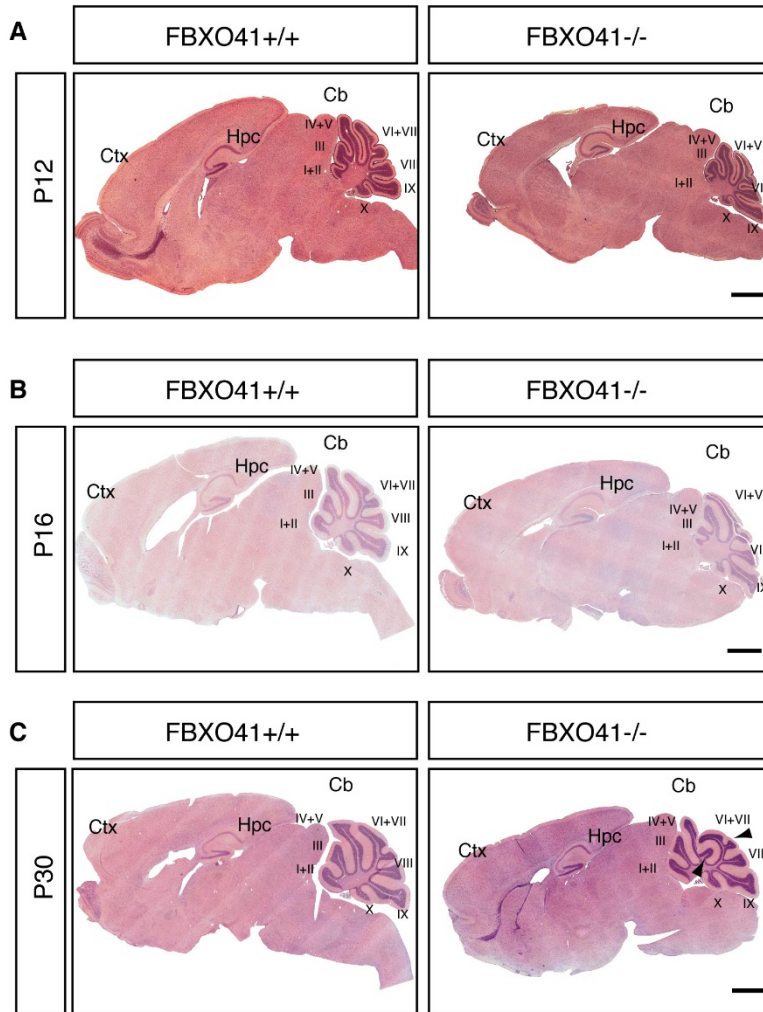
**Figure 3.8** **FBXO41<sup>-/-</sup> mouse brains show no signs of inflammation at P16:** (A, E) Representative images of the cerebellar region of 5  $\mu$ m thick paraffin embedded sagittal brain sections obtained from P16 FBXO41<sup>+/+</sup> and FBXO41<sup>-/-</sup> mice. Sections were subjected to immunohistochemistry using either the IBA1-specific antibody that binds to microglia, with tissue from CNPase<sup>Cre/Cre</sup> mouse serving as a positive control (Lappe-Siefke et al., 2003) (A), or the GFAP antibody to identify astrocytes (E). Scale bars equal 20  $\mu$ m and 50  $\mu$ m for A, E respectively. (B, C, D) Quantification (cells/mm<sup>2</sup>) of IBA1-positive cells in the cerebellar, cortical and hippocampal regions of P16 FBXO41<sup>+/+</sup> and FBXO41<sup>-/-</sup> mice from A. Quantifications were done manually, in a blinded manner. Three different anatomically matched sections per animal were quantified, and at least three independent littermates per genotype were included in the analyses (Student's t-test, ns=non significant, mean +s.e.m.). (F) Quantification (percentage of stained area/mm<sup>2</sup>) of GFAP-positive regions in the cortex, hippocampus and cerebellum of P16 FBXO41<sup>+/+</sup> and FBXO41<sup>-/-</sup> mice in E. Three different anatomically matched sections per animal were quantified, and at least three independent littermates per genotype were included in the analyses. The quantification and analyses were carried out in a blinded manner using a custom-designed macro. (Two-Way, ANOVA, mean =s.e.m.). A-F, I performed the sample collection, sectioning, imaging, quantification and analysis, and Dr. A. Matz carried out histochemical procedure.

At P16 the quantification of relative distribution of TUNEL-positive apoptotic cells, DAB-positive IBA1 cells or relative area stained by GFAP showed no signs of ongoing apoptosis, inflammation or astrogliosis in the cortex, hippocampus and the cerebellum. These results

suggested that the diminished sizes of the knockout mice brains are a result of developmental deficits rather than neurodegeneration.

### **3.1.5 FBXO41<sup>-/-</sup> mice show abnormal cerebellar morphology:**

Apart from the severe motor deficits, I wanted to gain further insights on the consequence of loss of FBXO41 on brain morphology and architecture. I thus went on to analyze the wild type and knockout mice at three different time points, namely P12, P16 and P30. In order to assess if loss of FBXO41 results in any gross morphological alterations in the brain, I first subjected 5 $\mu$ m thick sagittal sections from FBXO41 <sup>+/+</sup> and knockout animals at the indicated ages to H&E staining (**Figure 3.9 A, B, C**). While the overall brain sizes were reduced, there were no noticeable deformities in the cortical area and only a slight but not significant reduction of the P30 hippocampal area (**Figure 3.9 D, E**). However, the cerebellum seemed to shrink in size in P30 FBXO41<sup>-/-</sup> mice when compared to its healthy wild type littermates, especially adopting an abnormal morphology with intralobular outfoldings visible at lobule IV/V and a shrunken lobe VI and VII (**Figure 3.9 C, F**).





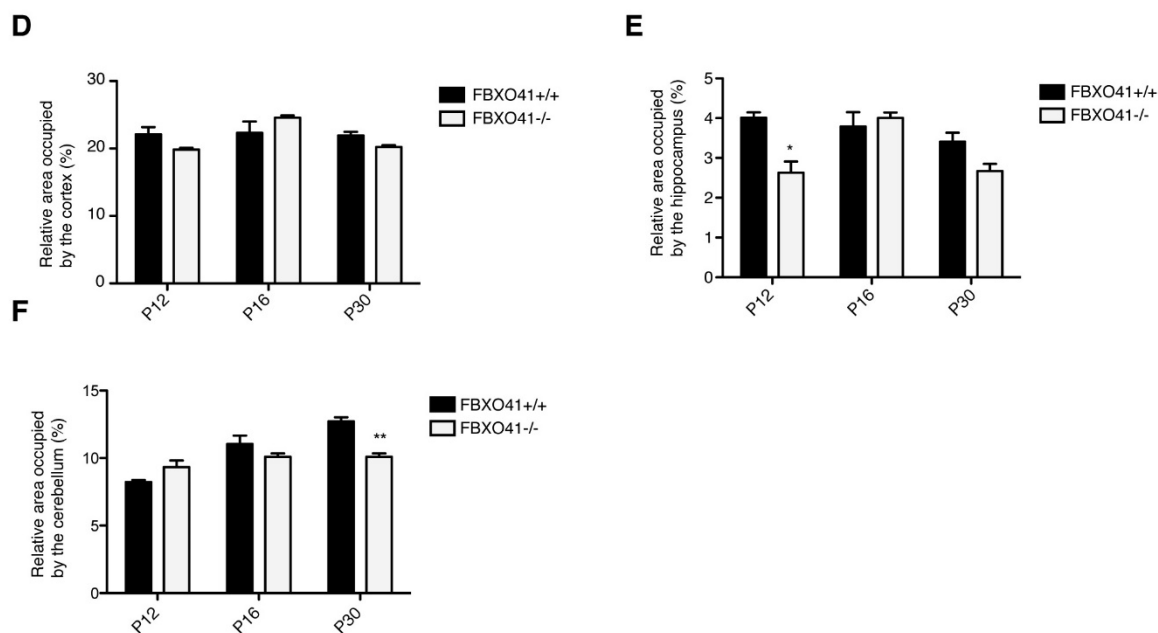


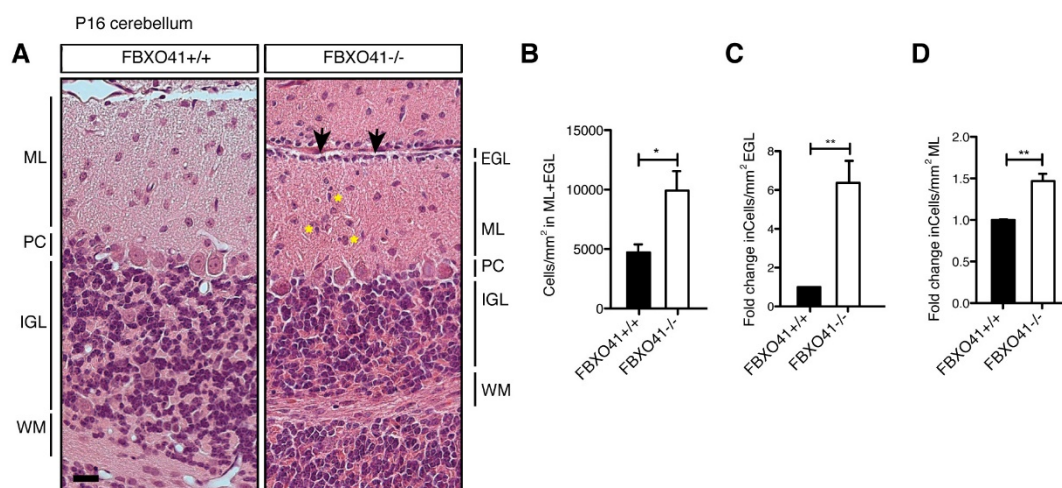
**Figure 3.9 FBXO41<sup>-/-</sup> mice show reduced cerebellar size and abnormal cerebellar foliation: (A, B, C)**

Panels depict 5 μm sagittal brain sections of FBXO41<sup>+/+</sup> and FBXO41<sup>-/-</sup> mice at P12, P16 and P30 that were subjected to H&E staining. Scale bars equal 1000 μm. (D, E, F) Quantifications of the relative area occupied by the cortex, hippocampus and the cerebellum, respectively, as observed in the FBXO41<sup>+/+</sup> and FBXO41<sup>-/-</sup> mice at the indicated ages (P12, P16 and P30). All quantifications were performed in a blinded manner. Areas are represented as percentages. At least 3 animals per genotype were analyzed (Two-way ANOVA, \*\*p<0.01, \*p<0.05, mean + s.e.m.).

### 3.1.6 Loss of FBXO41 results in delayed neuronal migration:

The observations indicating the absence of neurodegeneration and inflammatory processes in the P16 FBXO41<sup>-/-</sup> brain, suggested that the motor deficits and the accompanying morphological defects in the cerebella of these mice are a consequence of disruption of neurodevelopmental events. Prior results from the lab indicated a role for FBXO41 in neuronal migration, by means of the *in vivo* electroporation technique. Using the cerebellum as a model system (Holubowska, 2013) the study demonstrated that over-expression of FBXO41 resulted in enhanced neuronal migration in the cerebellum while knockdown of FBXO41 on the other hand resulted in delayed migration (Dr. A. Holubowska PhD thesis). This prompted me to examine, if loss of FBXO41 also results in migrational deficits in the

developing cerebellum of the FBXO41 knockout mice. The newborn CGNs undergo radial migration, migrating from the pial external granule layer (EGL) to the internal granule layer (IGL). Since FBXO41<sup>-/-</sup> mice displayed a striking ataxic gait at P16, I first analyzed the cerebellar lamination of FBXO41<sup>+/+</sup> and FBXO41<sup>-/-</sup> mice at P16, when migratory events subside (*Altman, 1972b*). Therefore, I subjected 5  $\mu\text{m}$  thick paraffin sagittal cerebellar sections from P16 FBXO41<sup>+/+</sup> and FBXO41<sup>-/-</sup> mice to H&E staining. Interestingly, at P16 in the FBXO41<sup>+/+</sup> cerebella, the EGL ceased to exist as a result of cells migrating through molecular layer (ML) and into the IGL, in contrast to the FBXO41<sup>-/-</sup> cerebella, where I could still observe a residual EGL together with a marked increase in the number of cells in the ML (**Figure 3.10 A, B, C, D**). To monitor the progression of this impaired migration at P16, I additionally analyzed the FBXO41<sup>+/+</sup> and FBXO41<sup>-/-</sup> cerebella at P12, when there is active ongoing neuronal migration and at P30, when the neuronal migration is completed. At P12, I not only observed a thicker EGL in the FBXO41<sup>-/-</sup> mice (**Figure 3.10 E, F**), but also a higher number of cells in the molecular layer (**Figure 3.10 G**). In contrast at P30, however, both FBXO41<sup>+/+</sup> and FBXO41<sup>-/-</sup> cerebella both no longer possessed an EGL. Interestingly, the FBXO41<sup>-/-</sup> mice still showed a significantly higher cell number in the ML of the cerebellum in contrast to their FBXO41<sup>+/+</sup> littermates (**Figure 3.10 H, I, J**).



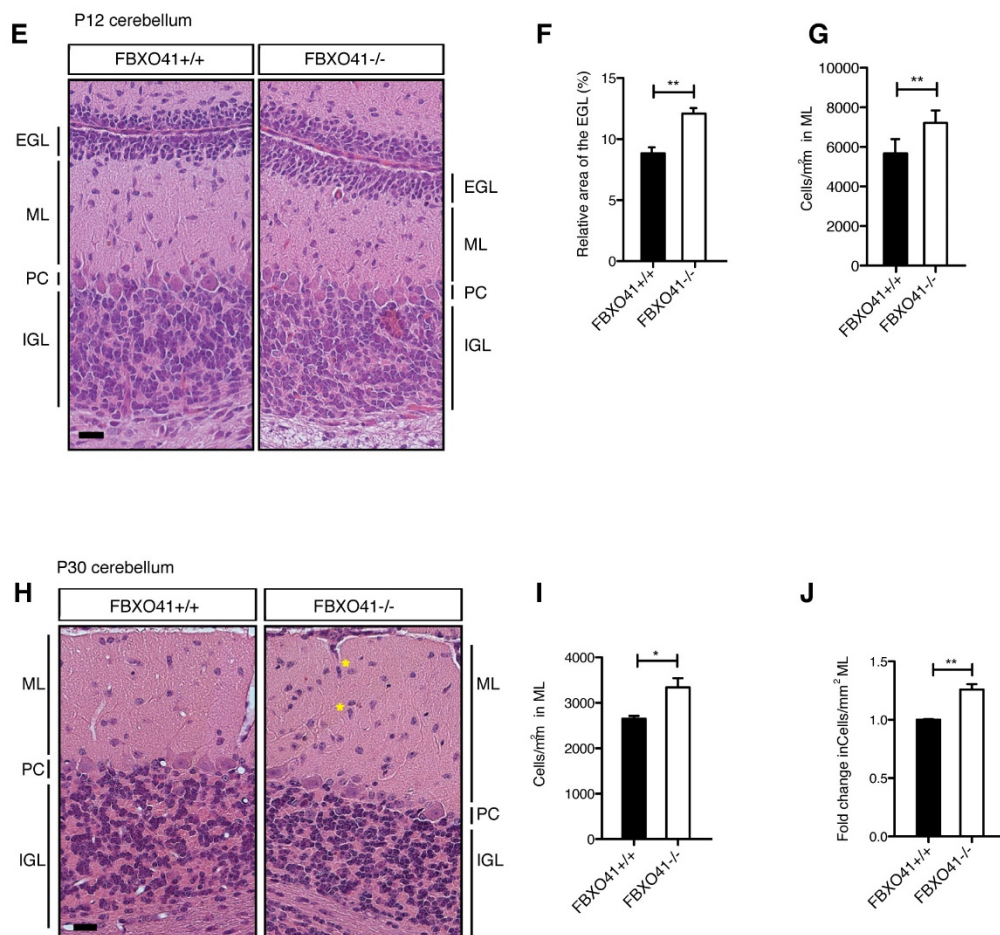


**Figure 3.10 FBXO41<sup>-/-</sup> mice show impaired neuronal migration in the cerebellum: (A, E, H)** Representative images of 5  $\mu$ m thick sections from P16, P12, P30 FBXO41<sup>+/+</sup> and FBXO41<sup>-/-</sup> cerebella, respectively that were subjected to H&E staining. Arrows and yellow asterisks in **A** and **H** indicate the residual EGL and migrating cells in the ML, respectively, in the FBXO41<sup>-/-</sup> cerebella at P16 and P30. EGL= external granular layer, ML= molecular layer, PC= Purkinje cell layer, IGL= internal granular layer. Scale bars equal 20  $\mu$ m. **(B)** Quantification of the cell density (cells/mm<sup>2</sup>) in the EGL+ML of the cerebella of FBXO41<sup>+/+</sup> and FBXO41<sup>-/-</sup> mice at P16. **(C, D)** Graphs represent the resulting fold change of cell number (cells/mm<sup>2</sup>) in EGL or ML **(C and D)** at P16 in the FBXO41<sup>+/+</sup> and FBXO41<sup>-/-</sup> cerebellum. **(F, G)** Quantification of and the relative thickness of the EGL and the cell density (cells/mm<sup>2</sup>) in ML at P12 in the FBXO41<sup>+/+</sup> and FBXO41<sup>-/-</sup> cerebella. **(I, J)** Graphs represent the quantification of the cell density (cells/mm<sup>2</sup>) in ML and resulting fold change of cell number (cells/mm<sup>2</sup>) in ML at P30 in the FBXO41<sup>+/+</sup> and FBXO41<sup>-/-</sup> cerebella. **(B, C, D, F, G, I, J)** Quantifications were done in a blinded manner using a custom designed macro. Three different anatomically matched sections per animal were quantified and at least three independent FBXO41<sup>+/+</sup> and FBXO41<sup>-/-</sup> littermates were included in the analyses for all the three ages (P12, P16, P30) (Student's t-test, \*\*p<0.01 and \*p<0.05, mean + s.e.m.).

In order to determine if the super numerous cells observed in FBXO41<sup>-/-</sup> cerebella were indeed migrating CGNs, I additionally subjected 5  $\mu$ m thick sagittal cerebellar sections from FBXO41<sup>+/+</sup> and FBXO41<sup>-/-</sup> mice to DAB staining using a NeuN-specific antibody at P12, P16 and P30 (**Figure 3.11 A**). NeuN is predominantly expressed by the CGNs in the cerebellum and is completely absent from, for example, the Purkinje cells. While in P12 cerebella, within the EGL, NeuN expression was restricted to the lower EGL at P16 most of the cells of the residual EGL were NeuN-positive (**Figure 3.11 A**). Upon quantifying the density of NeuN-positive cells of wild type and knockout cerebella, I observed that at all three ages P12, P16 and P30, FBXO41<sup>-/-</sup> mice had significantly higher number of NeuN-expressing cells in the ML (**Figure 3.11 B**). Taken together these results identify the super numerous cells observed in the ML of the FBXO41<sup>-/-</sup> as CGNs.

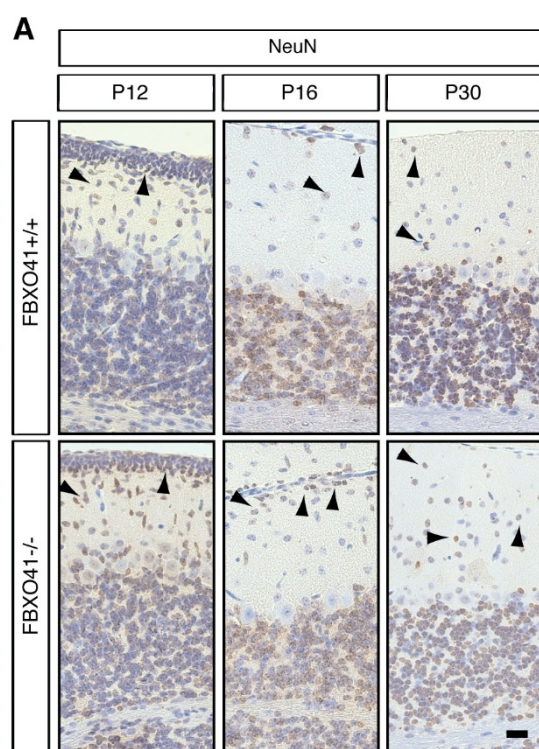
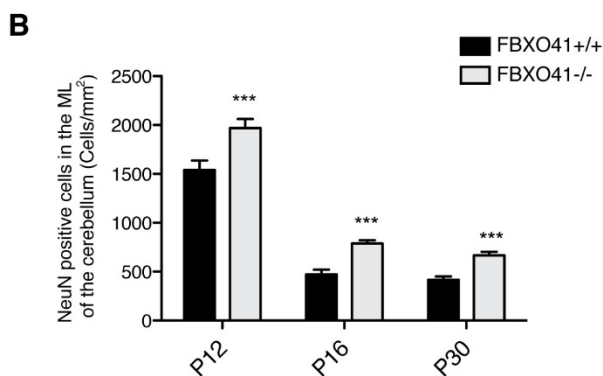


**Figure 3.11 FBXO41<sup>-/-</sup> mice show delayed neuronal migration in the cerebellum:** (A) Representative images of the 5  $\mu$ m thick sections of P12, P16, P30 FBXO41<sup>+/+</sup> and FBXO41<sup>-/-</sup> cerebella subjected to immunohistochemistry using the NeuN antibody. Arrowheads indicate NeuN-positive cells. Scale bar equals 20  $\mu$ m. (B) Graph represents the quantification of the density of NeuN-positive cells (cells/mm<sup>2</sup>) in the ML at P12, P16 and P30. All the quantifications were carried out manually, in a blinded manner. Three different anatomically matched sections per animal were quantified and three independent FBXO41<sup>+/+</sup> and FBXO41<sup>-/-</sup> littermates for all the indicated ages (P12, P16, P30) were included in the analyses (Two-way ANOVA, \*\*\*p<0.001, mean + s.e.m).



In addition to the NeuN staining, I also subjected 5  $\mu$ m thick paraffin sections from P12, P16 and P30 FBXO41<sup>+/+</sup> and FBXO41<sup>-/-</sup> cerebella to DAB staining using the PCNA-specific antibody. PCNA is a nuclear transcription factor, which is exclusively expressed in mitotic cells and in the developing cerebellum for example in the neuronal progenitors (*Dietrich, 1993*). Interestingly, while the PCNA staining was purely restricted to the upper EGL of P12 FBXO41<sup>+/+</sup> and FBXO41<sup>-/-</sup> mice (**Figure 3.12 A**), at P16, the residual EGL of the FBXO41<sup>-/-</sup> mice still had several cells that were PCNA-positive (**Figure 3.12 A**). This indicated that while most of the cells of the residual EGL at P16 had attained a neuronal fate, a significant number of cells still trailed behind in migration and possessed the neural progenitor characteristics (**Figure 3.12 B**). Expectedly at P30, both the FBXO41<sup>+/+</sup> and the FBXO41<sup>-/-</sup> cerebella were PCNA-negative within the ML (**Figure 3.12 A**). These results further identify the nature of the cells residing in the residual EGL of the FBXO41<sup>-/-</sup> mice at P16 as also neuronal progenitors.

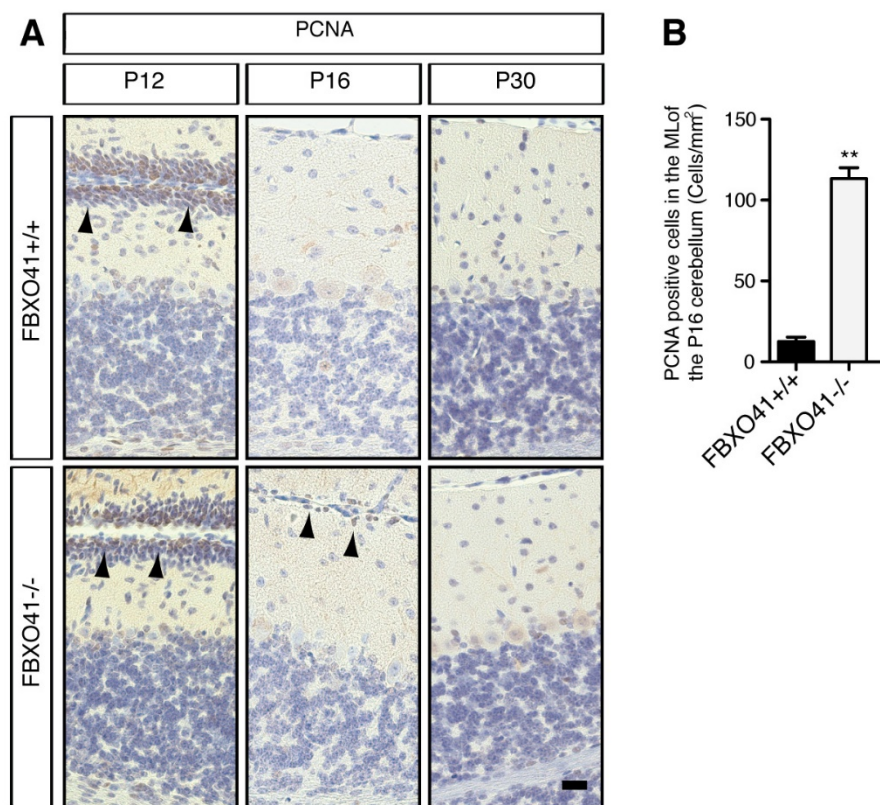


**Figure 3.12 FBXO41<sup>-/-</sup> mice display a residual EGL at P16:** (A) Representative images of 5  $\mu$ m thick sagittal cerebellar sections from FBXO41<sup>+/+</sup> and FBXO41<sup>-/-</sup> cerebella at P12, P16 and P30 subjected to immunohistochemistry using a PCNA-specific antibody. Arrowheads indicate PCNA-positive cells. Scale bar equals 20  $\mu$ m. (B) Graph represents the quantification of the distribution of PCNA-positive cells (cells/mm<sup>2</sup>) in the ML at P16. All the quantifications were carried out manually, in a blinded manner. Three different anatomically matched sections per animal were quantified and three independent P16 FBXO41<sup>+/+</sup> and FBXO41<sup>-/-</sup> littermates were included in the analyses (Student's t-test, \*\* $p < 0.01$ , mean + s.e.m).

After establishing the identity of the cells residing in the residual EGL of the P16 FBXO41<sup>-/-</sup> mice, I went on to check if the Purkinje cell layer was also affected due to these migrational deficiencies. I subjected sagittal sections from P16 FBXO41<sup>+/+</sup> and FBXO41<sup>-/-</sup> mice to both calbindin and parvalbumin staining, which stain Purkinje cells as well as the interneurons of the ML in the cerebellum (Figure 3.13 A, B). I observed no differences in the Purkinje cell layer between the two genotypes; further suggesting the abnormal neuronal migration was CGN-specific. Interestingly, however, I observed that the dendritic arbors of the Purkinje cells spanning the ML were pushed back in the FBXO41<sup>-/-</sup> cerebella as a result of the cells in the residual EGL, when compared to the FBXO41<sup>+/+</sup> cerebella, where the dendrites spanned the entire ML up until the pial surface (Figure 3.13 B).

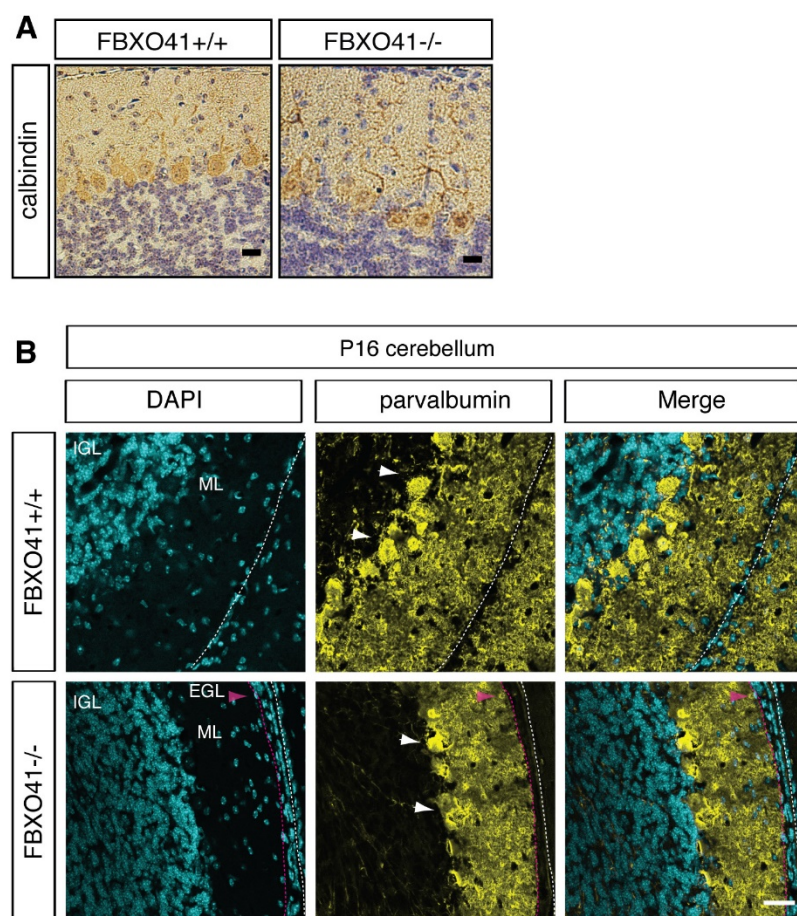


**Figure 3.13 Loss of FBXO41 does not affect the Purkinje cell layer:** (A) Representative images of 5  $\mu\text{m}$  thick paraffin sagittal cerebellar sections from P16 FBXO41<sup>+/+</sup> and FBXO41<sup>-/-</sup> mouse stained for the Purkinje cell marker calbindin. Scale bar equal 20  $\mu\text{m}$ . (B) Representative confocal images of 12  $\mu\text{m}$  sagittal cryosections from P16 FBXO41<sup>+/+</sup> and FBXO41<sup>-/-</sup> cerebella that were subjected to immunofluorescence staining using the parvalbumin antibody for visualization of Purkinje cells. Scale bar equals 100  $\mu\text{m}$ . White arrowheads indicate Purkinje cell bodies; red arrowhead indicates residual EGL in the P16 FBXO41<sup>-/-</sup> cerebella. IGL= internal granule layer, ML= molecular layer, EGL= external granule layer.

Taken together, these results demonstrate that loss of FBXO41 results in delayed migration speed, as the P30 FBXO41<sup>-/-</sup> cerebella almost catches up in migration. It additionally unveils the identity of the supernumerous cells within the EGL and ML of the FBXO41<sup>-/-</sup> mice cerebellum as CGNs and residual neural progenitors. Moreover, it also demonstrates that while CGN migration is impaired, loss of FBXO41 has no effect on the Purkinje cell layer.

### 3.1.7 Cytoplasmic FBXO41 regulates proper neuronal migration:

Since FBXO41 displays a dual cytoplasmic and centrosomal localization within the cell, I determined if either or both the cytoplasmic and the centrosomal FBXO41 contributes to its role in neuronal migration. Previously, the lab has identified the region on FBXO41 (amino acids 179-354) responsible for its targeting to the centrosome, the so-called “centrosomal targeting region” (CTR). Consequently, while FBXO41 WT localizes to both the centrosome and the cytoplasm, the FBXO41  $\Delta$ CTR mutant failed to localize to the centrosome, localizing purely to the cytoplasm (Holubowska, 2013) (**Figure 3.14**).

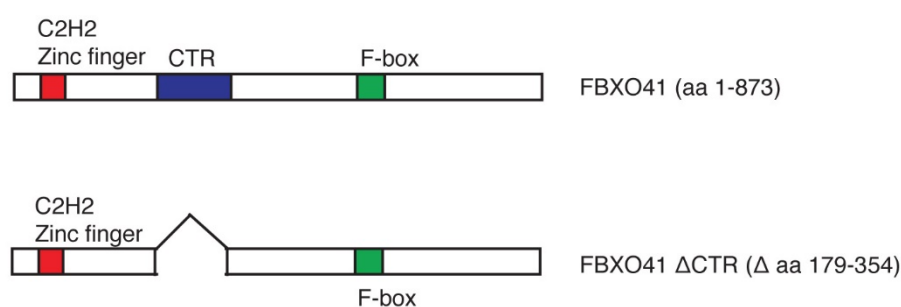
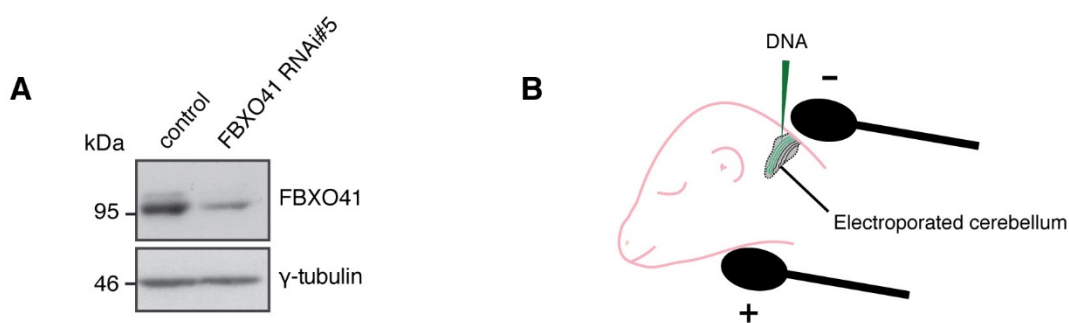


**Figure 3.14 FBXO41 harbors a centrosomal targeting region:** Schematic representation of the FBXO41 full-length and the deletion mutant FBXO41  $\Delta$ CTR that lacks aa 179-354 (the centrosomal targeting region).

In order to assess whether centrosomal or cytoplasmic FBXO41 contributes to neuronal migration, I first validated the efficiency of the previously generated functional FBXO41 RNAi#5 in cultured CGNs. I therefore nucleofected neurons with either control U6 or the FBXO41 RNAi#5. Four days following nucleofection, I analyzed the neuronal lysates with immunoblotting using the custom made FBXO41-specific antibody (**Figure 3.15 A**). Subsequently, I used the validated FBXO41 RNAi#5, to carry out *in vivo* electroporation (Materials and methods section 2.18), wherein I electroporated P4 rat cerebella with either control U6 empty or FBXO41 RNAi#5 together with control vector, FBXO41-Res or FBXO41-Res  $\Delta$ CTR plasmid (**Figure 3.15 B**). Both the FBXO41-Res and FBXO41-Res  $\Delta$ CTR plasmids are resistant to knockdown by the FBXO41 RNAi#5 as they harbor silent mutations in the RNAi-targeting region. The electroporated cerebella were isolated from the rat pups at P9, and coronal sections of the cerebella were subjected to immunohistochemistry using the GFP antibody. The distribution of GFP-positive neurons was determined across the different cerebellar layers, namely the EGL, ML and the IGL. The IGL of the cerebella was further divided into three equal parts- the Outer IGL, Middle (Mid) IGL and the Inner (In)



IGL. I observed that while FBXO41 RNAi#5 led to stalled neuronal migration, with most cells being stranded in the EGL, ML and outer IGL, the neurons in the control condition had migrated away from the EGL into the IGL, with most cells residing in the deeper regions of the IGL, namely the Mid and In IGL. The FBXO41-Res and FBXO41-Res  $\Delta$ CTR were able to “rescue” this phenotype as most of the transfected neurons had migrated away from the EGL and ML. While the FBXO41-Res displayed only a partial rescue as most of the cells resided in the Outer IGL and Mid IGL, the FBXO41-Res  $\Delta$ CTR on the other had could restore neuronal migration back to control levels, with most of the GFP-positive cells residing in the Mid and In IGL (**Figure 3.15 C, D**). These results recapitulate the impaired neuronal migration phenotype observed in FBXO41<sup>-/-</sup> mice, supporting the notion that FBXO41 promotes neuronal migration. Lastly, it also indicates that FBXO41-regulated neuronal migration is independent of its centrosomal localization.



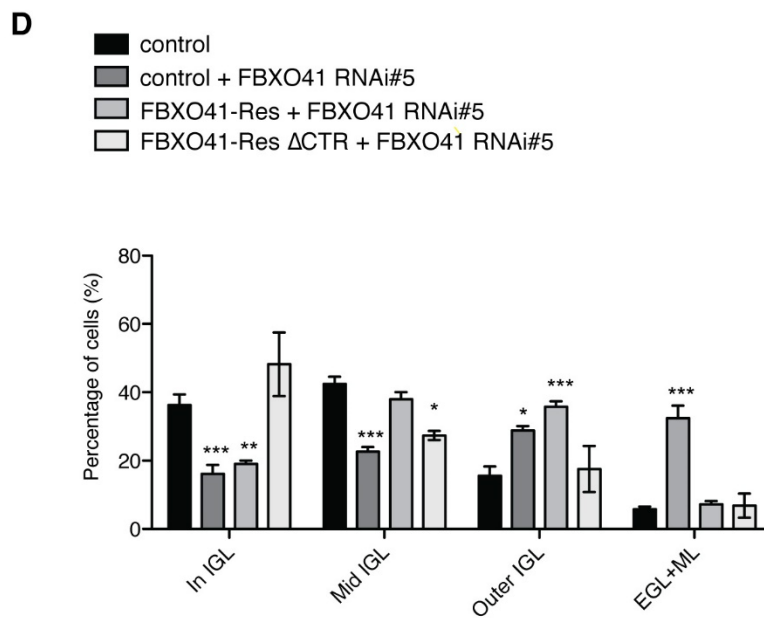
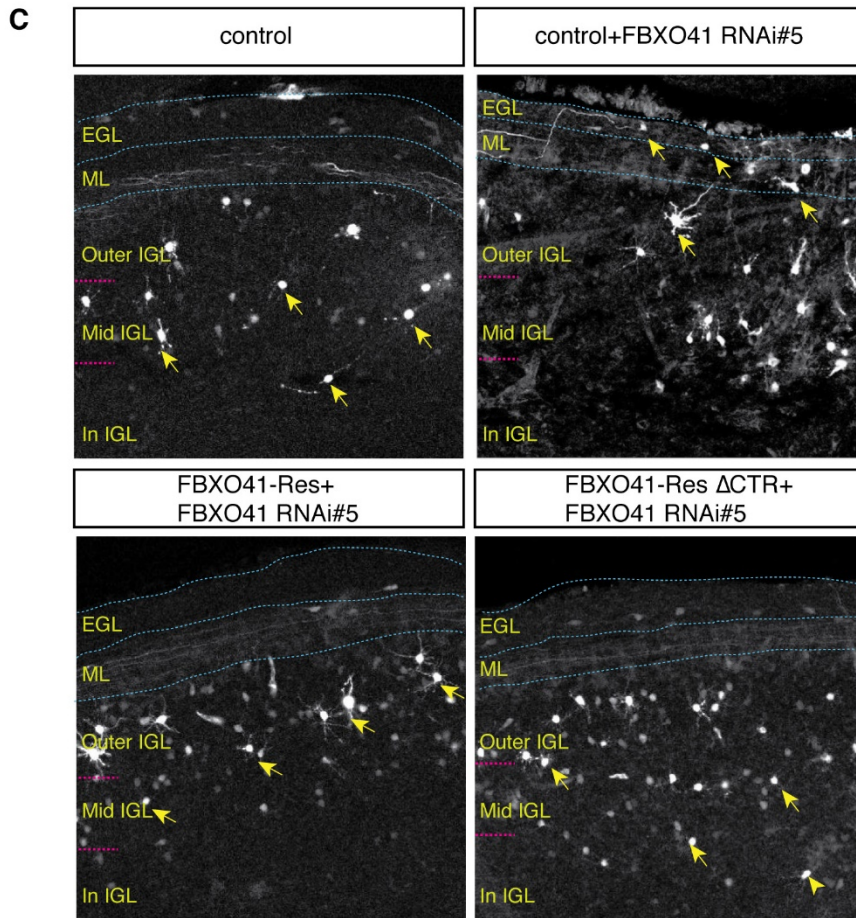


**Figure 3.15 Cytoplasmic FBXO41 promotes neuronal migration: (A)** CGNs in suspension were mixed

with either U6 control vector or the FBXO41RNAi#5 plasmid, and were electroporated with the Amaxa nucleofector. These electroporated neurons were then cultured for 5 days. Neuronal lysates were immunoblotted with the FBXO41 and the  $\gamma$ -tubulin antibodies, where the latter served as loading control. **(B)** Schematic of *in vivo* electroporation of P4 rat pup cerebella, redrawn from (Holubowska et al., 2014; Konishi et al., 2004). **(C)** Representative confocal images of cerebella of P4 rat pups were subjected to *in vivo* electroporation with bicistronic control vector (U6/cmv-GFP) or the bicistronic FBXO41 RNAi#5-cmv-GFP plasmid, together with control, FBXO41-Res or FBXO41-Res  $\Delta$ CTR. Five days later at P9, coronal cerebellar sections were subjected to immunohistochemistry with the GFP antibody and the distribution of GFP-positive neurons were analyzed, within each of the cerebellar layers (EGL, ML and IGL). The internal granule layer was further divided into 3 equal parts, namely the outer IGL, middle IGL (Mid IGL) and the inner IGL (In IGL) for the analysis. Dotted lines demarcate layers. Arrows indicate electroporated neurons and scale bar equals 50  $\mu$ m. **(D)** Graph represents quantification of **C**, wherein the distribution of GFP-positive neurons in each of the indicated layers are represented as percentages. Analysis was carried out in a blinded manner with a total of 5515 neurons from 5 control, 5 FBXO41 RNAi#5, 5 FBXO41-Res and 5 FBXO41-Res  $\Delta$ CTR cerebella being included in the analysis (Two-Way ANOVA, \*\*\* $p$ < 0.001, \*\* $p$ <0.01 and \* $p$ <0.05, mean + s.e.m.). *The electroporations were performed in assistance with Dr. J. Stegmüller, the cryosectioning and immunohistochemistry was performed by Dr. S. J. Lee and the electroporation in part, screening of GFP-positive cerebella, imaging, quantification and analyses was performed by me.*

### 3.1.8 FBXO41 is essential for neuronal survival:

Since neuronal migration appeared to be slowly catching up in the P30 FBXO41<sup>-/-</sup> cerebella, I performed behavioral analysis on P30 knockout animals to assess if their ataxic motor symptoms had improved. Due to the high mortality rate of >80% the P30 FBXO41<sup>-/-</sup> mice are extremely rare. Hence, I restricted the behavioral analysis to 4 pairs of wild type and knockout littermates. I noticed that, while the FBXO41<sup>-/-</sup> mice gain weight over time, they were always significantly lighter than their healthy FBXO41<sup>+/+</sup> littermates (**Figure 3.16 A**). The knockout mice were still motor impaired and too weak to reach the top of the cage for food or water. Thus, they required a special supply of food and water inside the cage. In order to gauge the extent of motor impairment, I subjected P30 FBXO41<sup>+/+</sup> and FBXO41<sup>-/-</sup> littermates to the previously described hind limb clasping test, ledge test and gait analyses. P30 FBXO41<sup>-/-</sup> mice performed consistently and significantly worse than their healthy wild type littermates in all the three tests (**Figure 3.16 B, C, D**). Taken together these results demonstrate that the motor symptoms observed in the P16 still persist in P30 FBXO41<sup>-/-</sup> mice.

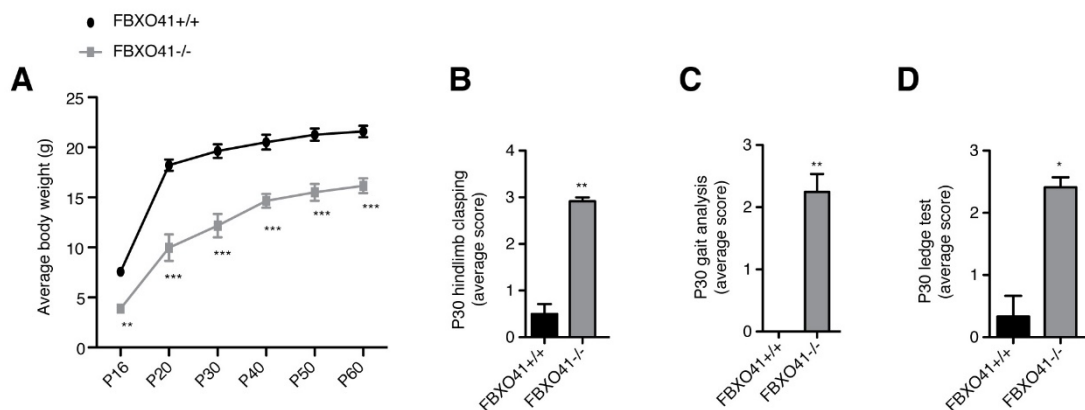


**Figure 3.16 P30 FBXO41<sup>-/-</sup> display persistent motor impairment:** (A) Graph depicts the weight curve of FBXO41<sup>+/+</sup> and FBXO41<sup>-/-</sup> mice over a period of 60 days. Four mice of each genotype (litter mates) from 4 independent litters from were included in the analysis (Student's t-test, \*\*\* $p < 0.001$ , \*\* $p < 0.01$ , mean + s.e.m.). (B-D) Graphs depict the performance of P30 FBXO41<sup>+/+</sup> and FBXO41<sup>-/-</sup> mice (littermates) when tested for hind limb clasping in B, gait analysis in C and ledge test in D. (B-D) Three mice of each genotype from three independent litters were included in the analysis (Student's t-test, \*\* $p < 0.01$ , \* $p < 0.05$  mean + s.e.m.). 0= normal phenotype, 3= worst manifestation of phenotype.

Owing to the persistent motor phenotype and the abnormal cerebellar morphology of the P30 FBXO41<sup>-/-</sup> mice, I wondered if impaired neuronal migration and possible faulty wiring in the P30 knockout mice cerebella could impact its cellular integrity. To investigate this possibility, I analyzed 5  $\mu\text{m}$  thick sagittal P30 FBXO41<sup>+/+</sup> and FBXO41<sup>-/-</sup> mice brain sections for indications of apoptosis using the TUNEL assay (Figure 3.17 A). While there was no increase in the number of TUNEL-positive cells in the cortex, I observed a significant increase in apoptotic cells/ $\text{mm}^2$  in the P30 knockout mouse hippocampus and cerebellum (Figure 3.17 B, C, D). Interestingly, most of the apoptotic cells in the P30 FBXO41<sup>-/-</sup> cerebellum seemed clustered at the intralobular outfolding and collapsed lobule VI. These results suggest that loss of FBXO41 not only affects morphology but also the cellular integrity of the cerebellum.

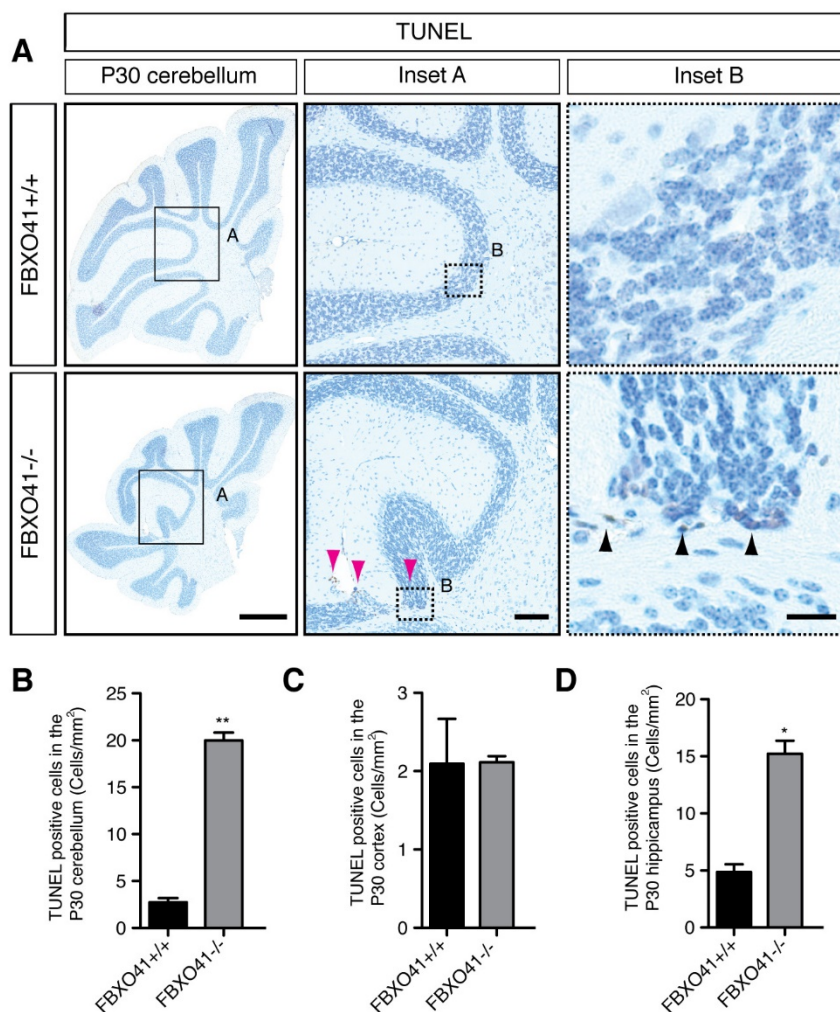


**Figure 3.17 P30 FBXO41<sup>-/-</sup> mice show increased apoptosis in the cerebellum:** (A) Representative images of the cerebellum from 5  $\mu$ m thick paraffin embedded sagittal brain sections of P30 FBXO41<sup>+/+</sup> and FBXO41<sup>-/-</sup> mice. These sections were processed immunohistochemically using a TUNEL detection kit, detecting apoptotic cells. Insets A and B depict higher magnifications, where pink arrowheads indicate clusters of apoptotic cells and black arrowheads indicate individual apoptotic cells. Scale bar equals 500  $\mu$ m for panel 1, 100  $\mu$ m for inset A and 20  $\mu$ m for inset B. (B, C, D) Quantification of TUNEL-positive cells (cells/mm<sup>2</sup>) within the cerebellar, cortical and hippocampal regions of P30 FBXO41<sup>+/+</sup> and FBXO41<sup>-/-</sup> mice from A. Quantifications were performed manually, in a blinded manner. Three different anatomically matched sections per animal from three independent littermates per genotype were included in the analyses. (Student's t-test, \*\*p<0.01, \*p<0.05, mean +s.e.m.).

To corroborate this finding, I performed a survival assay in cultured rat CGNs using shRNA to acutely knockdown FBXO41. Here, I transfected neurons at DIV2 with either control vector, the FBXO41 RNAi#5, or the non-functional FBXO41 RNAi#8 along with  $\beta$ -gal-expression plasmid, which served as a transfection marker. After analysis at DIV 6 for pyknotic nuclei and expression of cleaved caspase 3, both hallmarks of apoptosis, I

interestingly noticed that knockdown of FBXO41 resulted in increased cell death when compared to control (**Figure 3.18 A, B**). In order to establish the specificity of the FBXO41 knockdown, I additionally performed a rescue experiment, where I transfected either control U6 or FBXO41 RNAi#5 plasmid together with the control or the RNAi-resistant FBXO41-Res. The FBXO41-Res plasmid was previously generated in the lab. It is resistant to the knockdown by the FBXO41 RNAi#5 as it harbors silent mutations in the RNAi targeting region. While knockdown of FBXO41 lead to increased cell death, the FBXO41-Res plasmid was able to “rescue” the phenotype by restoring the number of dead cells observed to that of control levels (**Figure 3.18 C**). Collectively, these results support the notion that FBXO41 might be crucial for neuronal survival.

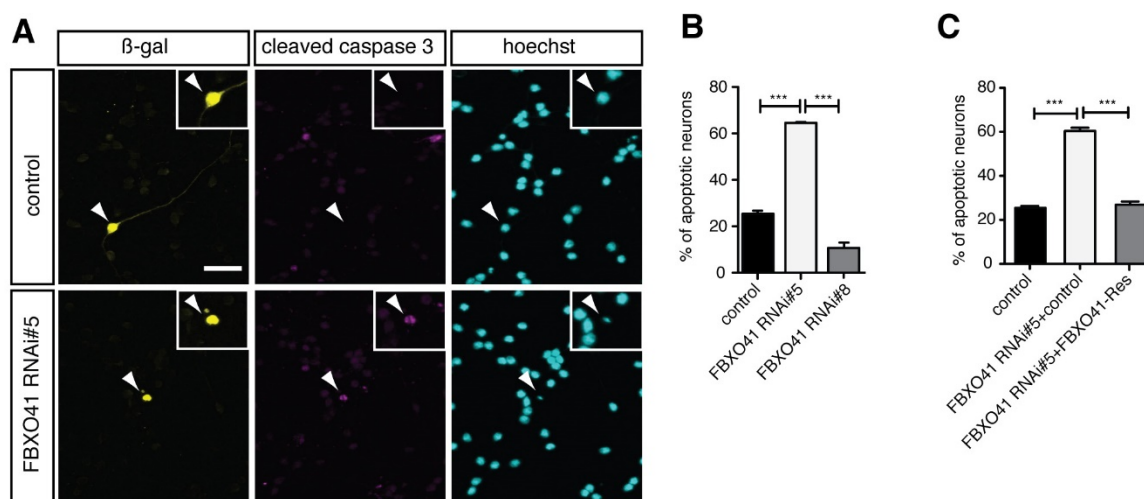


**Figure 3.18 FBXO41 is essential for neuronal survival:** (A) Representative images of cultured CGNs at DIV2 were transfected with either control U6 vector or the functional FBXO41 RNAi#5 together with a plasmid encoding  $\beta$ -gal that served as transfection marker. Four days after transfection at DIV6, the neurons were fixed and subjected to immunocytochemistry using the  $\beta$ -gal and cleaved caspase 3-specific antibodies as well as the DNA binding dye DAPI. Sale bar equals 50  $\mu$ m (B, C) Quantifications of percentage of cleaved caspase 3-positive apoptotic CGNs that were transfected at DIV2 with the indicated plasmids and processed as in A. Quantifications were done in a blinded manner. At least three independent experiments were included in the analyses (ANOVA, \*\*\* $p$ <0.001 + s.e.m).

### 3.1.9 FBXO41<sup>-/-</sup> mice show impaired axon growth:

Proteins found to influence neuronal migration are frequently also found to be implicated in regulation of neuronal morphology (Hossain and Morest, 2000; Tian et al., 2015; Vadhvani

*et al., 2013*). Recently, pathways regulating migration and neuronal morphology, mediated by E3 ligases have recently gained importance, for example the E3 ligases Cdh1 and Smurf1 that act in the same pathway of axon growth and neuronal migration (*Kannan et al., 2012b; Konishi et al., 2004*). Another study also identified the centrosomal E3 ligase FBXO31 also as a regulator of neurite morphology, polarity and neuronal migration (*Vadhvani et al., 2013*). Previous work from the lab demonstrated that loss of FBXO41 results in stunted axon growth. Interestingly, both acute knockdown of FBXO41 induced by RNAi in cultured rat CGNs as well as chronic loss of FBXO41, as observed in cultured CGNs from FBXO41<sup>+/+</sup>, <sup>+/-</sup> and <sup>-/-</sup> mice resulted in a specific reduction of axon length, with little or no effect on dendrite length or complexity (*Holubowska, 2013*). I used the previously generated FBXO41 knockout mice to recapitulate the *in vitro* findings of FBXO41 mediated axon growth regulation *in vivo*. Since the FBXO41<sup>-/-</sup> mice show most obvious gross morphological abnormality and neuronal migration in the cerebellum, I assessed the effect of loss of FBXO41 on axon length in the cerebellum by subjecting 30  $\mu$ m thick coronal cerebellar cryosections from P10 FBXO41<sup>+/+</sup> and FBXO41<sup>-/-</sup> animals to immunohistochemical analysis. Using the tau-specific antibody, I visualized the parallel fibers, which are the axonal tracts of the CGNs residing in the IGL within the cerebellum. I quantified the relative area occupied by tau positive parallel fiber tracts in the molecular layer. Interestingly, I observed a marked reduction in the percentage of relative area occupied by the parallel fiber tracts in the FBXO41<sup>-/-</sup> mice when compared to their healthy FBXO41<sup>+/+</sup> littermates (**Figure 3.19 A, B**).

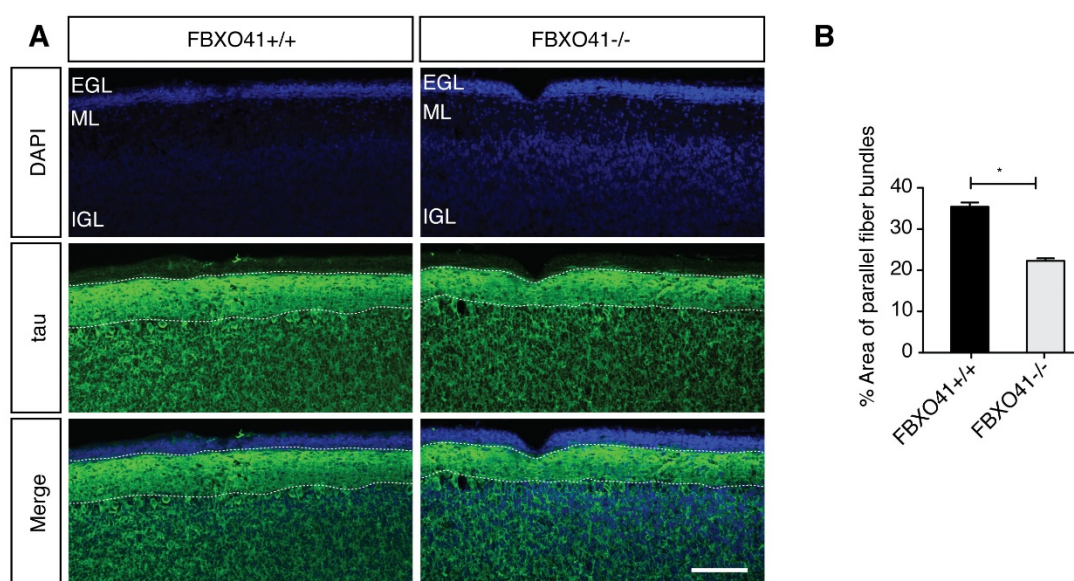


**Figure 3.19 FBXO41<sup>-/-</sup> mice display thinner parallel fiber bundles in the cerebellum:** (A) Representative confocal images of 30  $\mu\text{m}$  thick coronal cerebellar cryosections from P10 FBXO41<sup>+/+</sup> and FBXO41<sup>-/-</sup> mice, subjected to immunofluorescence staining using the tau antibody. Dotted lines indicate tau-positive parallel fiber bundles. EGL= external granule layer, ML= molecular layer, IGL= internal granule layer. Scale bar equals 100  $\mu\text{m}$ . (B) Graph represents the relative thickness of the parallel fibers from P10 FBXO41<sup>+/+</sup> and FBXO41<sup>-/-</sup> mice from A. Thickness is represented as percentage area occupied by the tau-positive axon bundles in the ML. Three different anatomically matched sections per animal were quantified. At least three FBXO41<sup>+/+</sup> and FBXO41<sup>-/-</sup> littermates were analyzed from three independent litters. All the analyses were carried out in a blinded manner (Student t-test, \* $p < 0.05$ , mean + s.e.m).

Other axonal tracts in the cerebellum include those of Purkinje cells, the climbing fiber and mossy fiber axon bundles. The Purkinje cell axon bundles run outwards from the cerebellum and synapse on the deep cerebellar nuclei. The climbing fibers, originating from the inferior olive, synapse on the dendrites of the Purkinje cell, while the mossy fiber axons send inward projections and synapse on the CGNs residing in the internal granule layer (*Sillitoe and Joyner, 2007; Sotelo, 2004*). Hence, I went on to evaluate the effects of loss of FBXO41 on the cerebellar white matter. Here, I subjected 5  $\mu\text{m}$  thick sagittal cerebellar sections obtained from FBXO41<sup>+/+</sup> and FBXO41<sup>-/-</sup> littermates to H&E staining and quantified the percentage of area occupied by the white matter tracts within the cerebellum of both FBXO41<sup>+/+</sup> and its FBXO41<sup>-/-</sup> littermates at 3 different ages, P12, P16 and P30. Interestingly, I observed reduced white matter tracts within the FBXO41<sup>-/-</sup> cerebella when compared to their healthy wild type littermates at all three ages, with a more pronounced reduction at P30 (**Figure 3.20 A, B**).

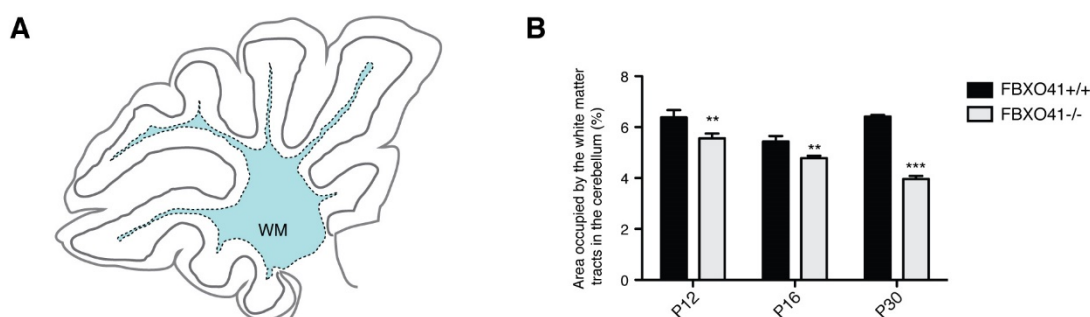


**Figure 3.20 FBXO41<sup>-/-</sup> mice show reduced white matter tracts within the cerebellum:** (A) Schematic diagram showing the sagittal view of the mouse cerebellum, with the area in blue representing the area occupied by the white matter tracts within the cerebellum. (B) The graph represents the area occupied by the white matter tracts relative to the total area of the cerebellum, in FBXO41<sup>+/+</sup> and FBXO41<sup>-/-</sup> cerebella at P12, P16 and P30. The relative area occupied by the white matter is represented as percentages. All the



quantifications were done in a blinded manner, with three different anatomically matched sections being quantified per animal. At least three FBXO41<sup>+/+</sup> and FBXO41<sup>-/-</sup> littermates from three independent litters were included in the analyses (Two-way ANOVA, \*\*\* $p < 0.001$ , \*\* $p < 0.01$ , mean + s.e.m).

These results, taken together with previous findings from the lab, bolster the notion that FBXO41 is a novel regulator of axon growth. Interestingly, similar to several previously mentioned proteins, FBXO41 also appears to regulate both neuronal migration and axon growth.

### 3.2 Molecular mechanism of FBXO41-mediated axon growth regulation:

Having described a role for FBXO41 in axon growth regulation, I wanted to understand the molecular mechanism of its function. FBXO41 belongs to the family of F-box proteins, which share the homologous F-box domain. Most F-box proteins form multi-subunit RING ligases, with various adaptor and scaffold proteins as well as the small RING finger proteins. While the RING finger protein is responsible for recruiting a specific E2 ubiquitin-conjugating enzyme to the complex, the F-box protein is an interchangeable part of the E3 ligase complex, conferring substrate specificity by recruiting individual substrates for ubiquitination (*Jin et al., 2004; Kipreos and Pagano, 2000; Zheng et al., 2002*). Based on the nature of ubiquitination, the ubiquitinated protein can have varying fates, ranging from proteolytic degradation to non-proteolytic events (*Komander and Rape, 2012*). Hence, to understand the nature of FBXO41-mediated events, I wanted to confirm whether it forms a functional E3 ligase, and if yes, identify putative substrates of this ligase, acting in the same pathway to exert their function. As a second aim of the study, I focused on identifying and characterizing the molecular players involved in FBXO41-mediated axon growth regulation.

#### 3.2.1 FBXO41 together with Skp1 and cullin7 forms an atypical SCF-like E3 ligase:

Most F-box proteins comprise the interchangeable component of the multi-subunit Skp1-cullin1-F-box (SCF) RING E3 ligase complex. They are thought to be responsible for substrate recruitment and thus conferring substrate specificity to the SCF E3 ligases (*Jin et al., 2004; Kipreos and Pagano, 2000*). Since the majority of F-box protein forming SCF complexes are known to bind to both Skp1 and cullin1, I went on to investigate if this was the case for FBXO41. In order to form a functional E3 ligase, F-box proteins interact with Skp1 and cullin1 via their F-box domain (*Deshaies, 1999; Deshaies and Joazeiro, 2009; Jin et al., 2004; Kipreos and Pagano, 2000*). Using HEK293T cells transfected with control, FBXO41 or FBXO41  $\Delta$ Fbox, a deletion mutant lacking the F-box domain (**Figure 3.21 A**), I performed immunoprecipitation analyses and confirmed that while FBXO41 associated with Skp1 in an F-box-dependent manner, it failed to interact with cullin1, irrespective of the presence or absence of its F-box domain (**Figure 3.21 B, C**). This, even though surprising, is not unheard of, as a previous study by Saiga and colleagues has previously identified

FBXO45 as an atypical F-box protein, which like FBXO41 associated with Skp1 but failed to do so with cullin1. Instead it interacted with Skp1 and Protein associated with Myc (PAM) to form a non-canonical E3 ligase (*Saiga et al., 2009*).

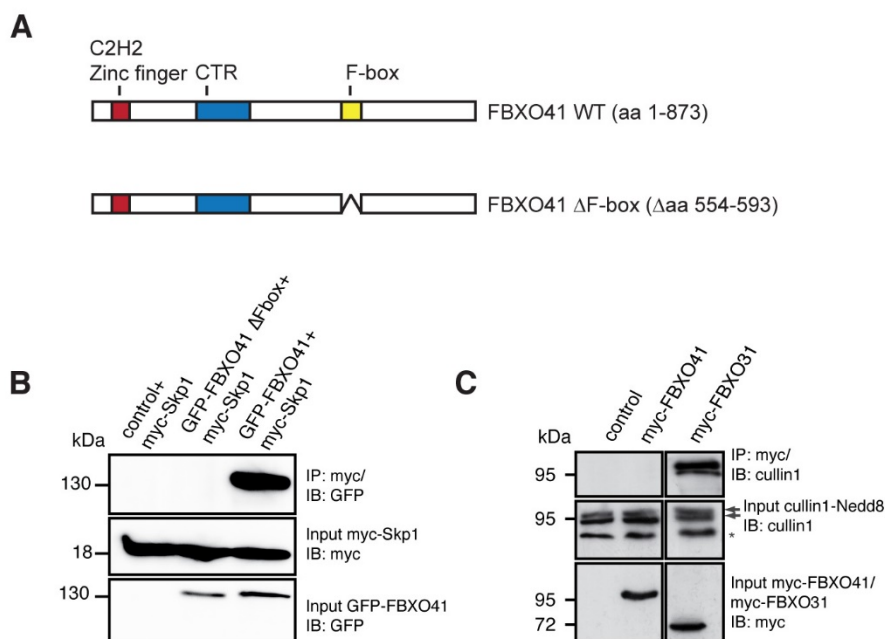


**Figure 3.21 FBXO41 interacts with Skp1 but not cullin1:** (A) Schematic representation of the FBXO41 full-length and the deletion mutant FBXO41 ΔFbox that lacks aa 554-593 (the F-box domain) (B) HEK293T cells were transfected with control vector, a plasmid encoding GFP-FBXO41 or GFP-FBXO41 ΔFbox together with the myc-Skp1 expression plasmid. 48 hours later, the cells were harvested and 1 mg lysate was subjected to co-immunoprecipitation (IP) using the myc antibody followed by immunoblotting (IB) with the GFP antibody. (C) HEK293T cells, transfected with control vector, a plasmid encoding myc-FBXO41 or myc-FBXO31 (which served as positive control) were harvested 48 hours post transfection. 1 mg of the procured lysates was then subjected to IP using the myc antibody followed by IB with the cullin1 antibody. Asterisk indicates non-specific band.

Till date apart from cullin1, the only other member of the cullin family known to form an SCF complex is cullin7. The F-box protein FBXW8 has been reported to form such a functional atypical SCF complex (*Sarikas et al., 2008*). Thus, I went on to investigate if FBXO41 too might interact with cullin7. I identified and confirmed the interaction of FBXO41 and cullin7 in HEK293T by straight and reciprocal co-immunoprecipitation analysis using myc-tagged FBXO41 and Flag-tagged cullin7 and respective controls (**Figure 3.22 A, B**). Additionally, I confirmed the interaction by performing a semi-endogenous co-immunoprecipitation analysis in HEK293T cells, immunoprecipitating for tagged FBXO41 and pulling down endogenous cullin7 (**Figure 3.22 C**). Finally, to bolster the notion that

FBXO41 interacts with cullin7, we first confirmed whether the FBXO41-specific antibody immunoprecipitates endogenous FBXO41 (**Figure 3.22 D**). Subsequently, I carried out an endogenous co-immunoprecipitation analysis using mouse brain tissue, immunoprecipitating for endogenous FBXO41 using the FBXO41-specific antibody and was able to pull down endogenous cullin7 (**Figure 3.22 E**). Further subcellular fractionation analyses by A. Gellerer confirmed that FBXO41 and cullin7 both localize to the cytoplasmic compartment in neurons (*A. Gellerer Master's, thesis*).

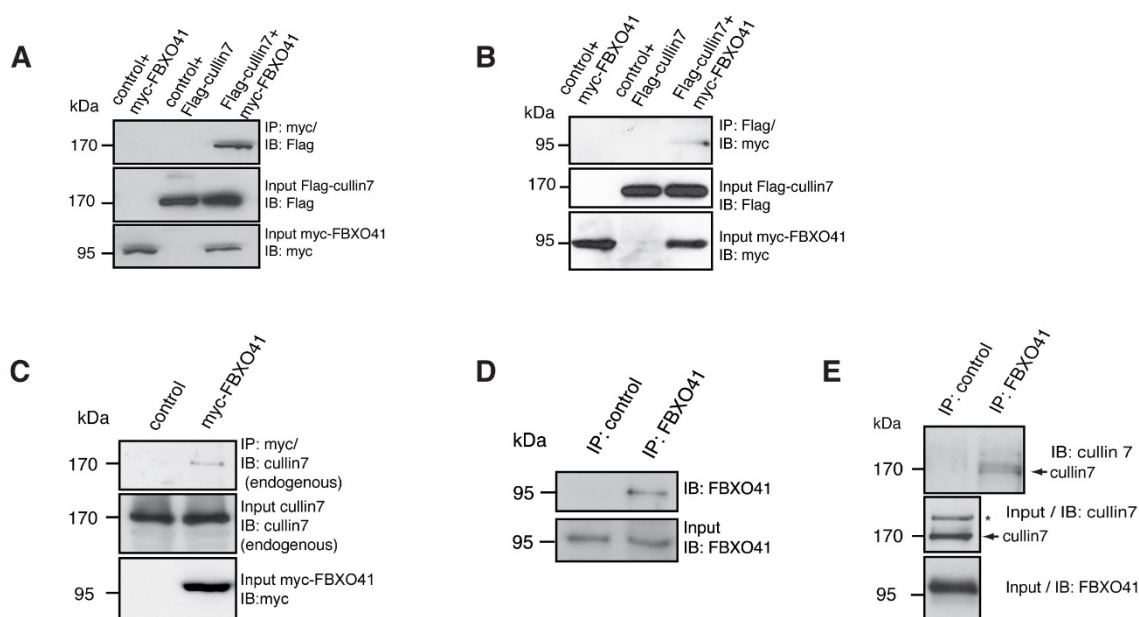


**Figure 3.22 FBXO41 interacts with cullin7:** (A, B) HEK293T cells were transfected with control vector and the myc-FBXO41 or the Flag-cullin7 expression plasmid or both expression plasmids together. Cells were lysed 48 hours after transfection and 1 mg of the harvested lysates were either subjected to IP with the myc antibody followed by IB with the Flag antibody as in A, or subjected to IP using the Flag antibody followed by IB using the myc antibody as in B. (C) 1 mg of lysates harvested from HEK293T cells, transfected with control or myc-FBXO41 expression plasmid, were subjected to IP with using the myc antibody followed by IB with the cullin7 antibody. (D) 1 mg of P14 mouse brain lysates were subjected to IP with either pre-immune serum (control) or the FBXO41 antibody, followed by IB with the custom made FBXO41 antibody. *This experiment was performed by Dr. A. Holubowska.* (E) 1 mg of P9 mouse cerebellar lysates were subjected to IP with either a control polyclonal antibody or the FBXO41-specific antibody with subsequent IB with the cullin7 antibody. Asterisk indicates non-specific band.

The only other F-box protein known to bind to cullin7, FBXW8 is also known to bind to cullin1 and although FBXW8 on one hand forms a canonical cullin1-SCF complex via its F-box domain, its interaction with cullin7 on the other hand was reported to be F-box-

independent (*Tsunematsu et al., 2006*). Hence, I investigated if the interaction between FBXO41 and cullin7 was F-box domain-dependent. Using the various deletion mutants of FBXO41 generated in the lab (**Figure 3.23 A, B**), I carried out a mapping analysis to identify the binding regions of cullin7 on FBXO41. Using co-immunoprecipitation analyses carried out in HEK293T cells, I identified the amino acids 1-35 at the N-terminus and the amino acids 593-873 at the C-terminus of FBXO41 to be responsible for its interaction with cullin7, as deletion mutants of FBXO41 lacking these amino acids failed to interact with cullin7 (**Figure 3.23 A, B**).

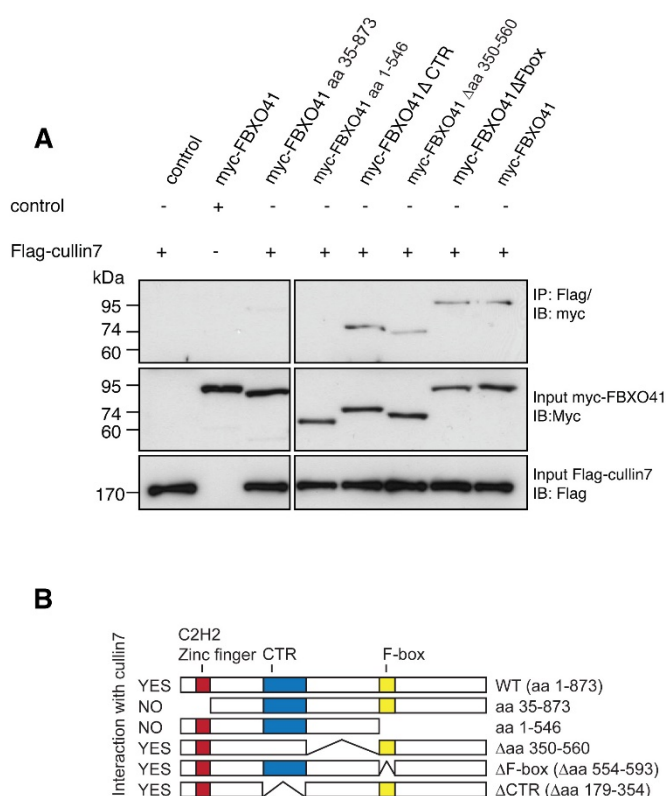


**Figure 3.23 FBXO41 interacts with cullin7 independent of its F-box domain:** (A) 1 mg lysates of HEK293T cells, transfected with the Flag-cullin7 plasmid together with the indicated FBXO41 deletion mutants, were subjected to IP using the Flag antibody followed by IB using the myc antibody. (B) Schematic summarizes the mapping analyses of FBXO41 and cullin7 shown in A.

Taken together, these results suggest that while FBXO41 interacts with Skp1 via its F-box domain, it interacts with cullin7 in an F-box-independent manner at its N- and C-terminus to form an atypical SCF-like complex.

In order to investigate if FBXO41-Cul7 forms a functional E3 ligase, an autoubiquitination assay was carried out by N. Schwedhelm-Domeyer. HEK293T cells were transfected with control, myc-FBXO41 or the ligase-dead deletion mutants myc-FBXO41 aa 35-873 or myc-FBXO41 ΔFbox, together with HA ubiquitin. After harvesting the cells, the lysates were denatured followed by immunoprecipitation using the myc antibody and subsequent

immunoblotting with the HA antibody to detect ubiquitin. A specific ubiquitin-positive smear representing functional ligase activity only appeared in the condition harboring myc-FBXO41. No smears were observed for control vector or for myc-FBXO41 aa 35-873 and myc-FBXO41  $\Delta$ Fbox, which cannot bind to cullin7 and Skp1, respectively and hence should not possess ligase activity (**Figure 3.24**).

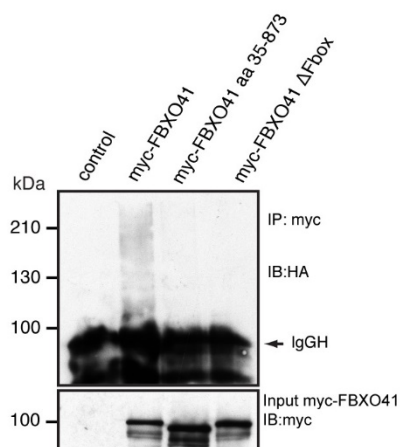


**Figure 3.24 FBXO41-Cul7 is a functional E3 ligase:**

48 hours after transfection, 1 mg of HEK293T lysates transfected with control vector or indicated myc-FBXO41 expression plasmids along with the HA-ubiquitin plasmid were processed following the “denaturing protocol” (Materials and methods section 2.17.6) and subsequently subjected to IP with the myc antibody followed by IB with the HA antibody. *This experiment was performed by N. Schwedhelm-Domeyer.*

This result not only demonstrates that FBXO41-Cul7 is a functional E3 ligase capable of ubiquitination, but also confirms that FBXO41’s interaction with both Skp1 and cullin7 are crucial for its ligase function.

### 3.2.2 Cytoplasmic FBXO41 promotes axon growth in an E3 ligase activity-dependent manner:

The previously established role of FBXO41 in the cerebellum along with prior results from the lab demonstrating on one hand that loss of FBXO41 resulted in shorter axons and excess FBXO41 resulted in longer axons (*Holubowska, 2013*) led me to investigate whether the integrity of the FBXO41-Skp1-Cul7 complex was crucial for its axon growth-promoting effect. In order to check if FBXO41’s association to the complex is essential for axon growth, I transfected the cultured rat CGNs at DIV1 with control, myc-FBXO41 or myc-FBXO41  $\Delta$ Fbox, which cannot bind to Skp1 or the myc-FBXO41 aa 35-873, that does not bind to cullin7. After 4 days in culture, I analyzed the axonal lengths of the transfected neurons. Interestingly, while FBXO41 full-length was able to exert its function resulting in longer axons, FBXO41  $\Delta$ F-box and FBXO41 aa 35-873 mutants could not stimulate axon growth

(Figure 3.25 A, B). This result suggests that the interaction of FBXO41 with both Skp1 and cullin7 are crucial for axon growth control.

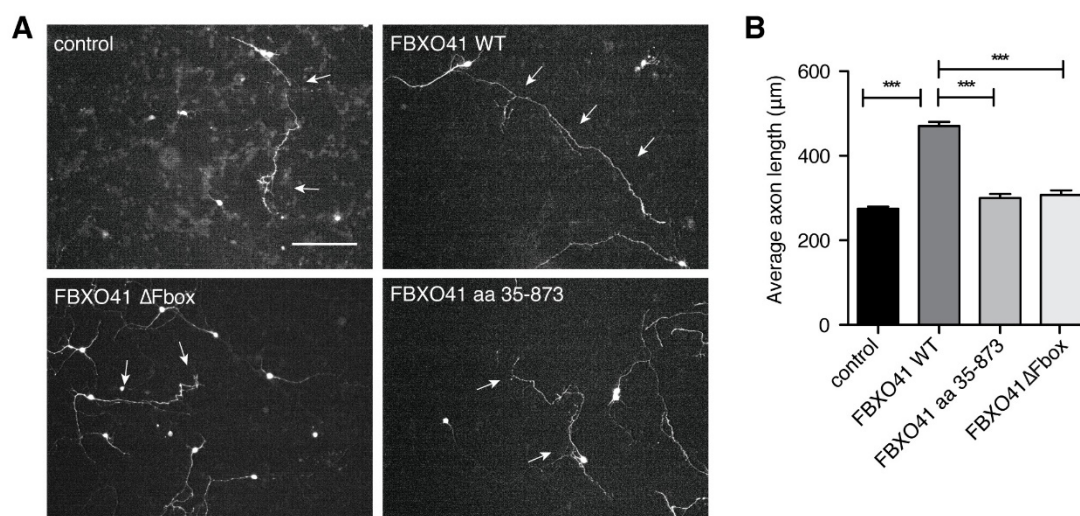


**Figure 3.25 FBXO41 regulates axon growth in a ligase activity-dependent manner:** (A) Representative images of rat CGNs transfected at DIV1 with control vector, FBXO41, FBXO41 aa 35-873 or FBXO41  $\Delta$ Fbox expression plasmid were fixed and subjected to immunocytochemistry at DIV5 using the GFP antibody. Subsequently, GFP-positive neurons were subjected to morphological analyses and their axonal lengths were measured (Materials and methods section 2.15). Arrows indicate axons. Scale bar equals 100  $\mu$ m. (B) Graph represents the quantification of axonal lengths from A. The average axonal lengths are represented in  $\mu$ m. All measurements and quantifications were done in a blinded manner. A total of 747 neurons from 3 independent experiments were measured (ANOVA, \*\*\* $p$ <0.001, mean + s.e.m.).

Additional results from the lab also illustrated that FBXO41 promotes axon growth independent of its localization to the centrosome, as deletion of its centrosomal targeting region had no effect on FBXO41's ability to promote axon length (Holubowska, 2013).

Collectively, these results indicate that FBXO41 together with Skp1 and cullin7 promotes axon growth in an E3 ligase activity-dependent manner, as the integrity of the FBXO41-Skp1-Cul7 complex in the cytoplasm is vital for its function in axon growth regulation.

### 3.2.3 The cytoskeletal protein neurofilament medium polypeptide (NFM) interacts with FBXO41:

In order to identify possible interaction partners of FBXO41 acting in the same pathway of axon growth regulation, the lab conducted yeast two-hybrid and identified the cyoskeletal component neurofilament medium polypeptide (NFM) among others as a putative interaction candidate. We confirmed the interaction of FBXO41 and NFM by co-immunoprecipitation analysis in HEK293T cells using tagged expression vectors of FBXO41 and NFM (**Figure 3.26 A**). Having validated the suitability of FBXO41 as well as NFM antibodies for co-immunoprecipitation analysis (**Figure 3.26 B**), I reconfirmed my Master's thesis findings, where I was able to validate the interaction between NFM and FBXO41 by means of endogenous co-immunoprecipitation analysis experiments, where I either immunoprecipitated FBXO41 or NFM from mouse P9 cortical lysates, followed by immunoblot analysis using NFM-or FBXO41-specific antibodies, respectively (**Figure 3.26 C, D**).

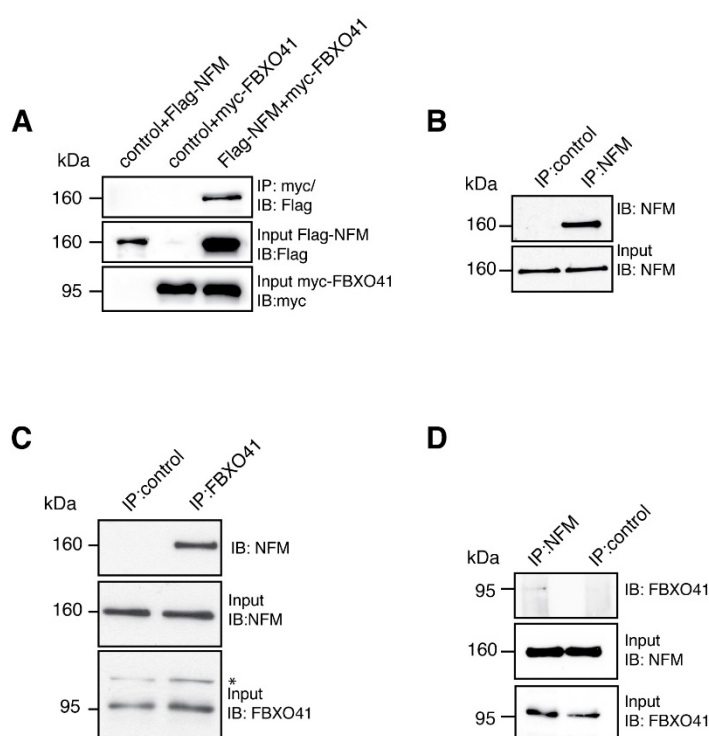


**Figure 3.26 FBXO41 interacts with NFM:** (A) 1 mg of HEK293T lysates transfected with either Flag-NFM, myc-FBXO41 together with appropriate control vectors, or both Flag-NFM and myc-FBXO41 were subjected to IP with the myc antibody followed by IB with the Flag antibody. (B) 1 mg of mouse P9 brain lysates were subjected to IP with either a control mouse monoclonal or the NFM antibody and subsequent IB with the NFM antibody. (C) 1 mg of mouse P9 brain lysates was subjected to IP with either pre-immune serum (control) or the FBXO41 antibody followed by IB with the NFM antibody. Asterisk indicates non-specific band. (D) 1 mg of mouse P9 brain lysates were subjected to IP with either a control



mouse monoclonal antibody or the NFM antibody, followed by IB with the FBXO41 antibody.

Additionally, further results from the lab indicate that FBXO41 and NFM colocalize in the cytoplasm, within the cell body and along the axon in CGNs (*Alina Gellerer, Master's thesis*). Taken together these results identify NFM as a novel interaction partner of FBXO41.

### 3.2.4 NFM is a substrate of FBXO41-Cul7:

Owing to the identification of NFM as an interaction partner of FBXO41, I reasoned that NFM could be an ubiquitination substrate of the FBXO41-Cul7 E3 ligase. I first determined whether NFM associates with other components of the FBXO41-Cul7 complex via FBXO41. Therefore, I subjected HEK293T cells transfected with plasmids expressing GFP-NFM, Flag-cullin7 and or myc-FBXO41 along with appropriate controls to co-immunoprecipitation with Flag antibody and subsequent immunoblot analysis with GFP antibody. Interestingly, I observed that NFM associates with cullin7 only in the presence of FBXO41, as absence of FBXO41 abolished this interaction (**Figure 3.27**). Other results from the lab identified DISC1 as another interactor of FBXO41. However, DISC1 was found to not interact with cullin7 irrespective of the presence and absence of FBXO41 (*Holubowska, 2013*). These results taken together indicate that NFM is specifically recruited to the FBXO41-Cul7 complex via FBXO41.

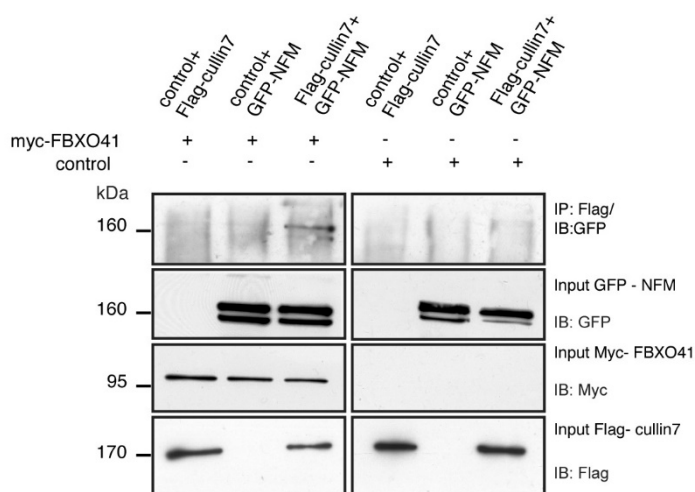


**Figure 3.27 NFM associates with cullin7 in the presence of FBXO41:**

1 mg of lysates harvested from HEK293T cells, transfected with the indicated plasmids, were subjected to IP with the Flag antibody, followed by IP with the Flag antibody, followed by IB with the GFP and myc antibodies.

Having established the association of NFM with FBXO41-Cul7, I went on to further investigate if NFM is ubiquitinated by FBXO41-Cul7. Therefore, I performed a cell-based ubiquitination assay, where Flag-NFM together with either myc-FBXO41 or the ligase-dead

myc-FBXO41  $\Delta$ Fbox and HA-tagged ubiquitin were expressed in HEK293T cells. In order to determine the ubiquitin chain type, the cells were additionally transfected with either HA-wild type ubiquitin, or the ubiquitin linkage mutants K48R or K63R, which are not able to form lysine (K)48- or K63-linked ubiquitin chains, respectively. The harvested cell lysates were subjected to the denaturing protocol (Materials and methods section 2.17.6), followed by immunoprecipitation using Flag-sepharose beads and immunoblotting using the HA antibody. I observed that full-length FBXO41 promoted ubiquitination of NFM, whereas the ligase-dead FBXO41  $\Delta$ Fbox failed to do so. Furthermore, the ubiquitin-smear was severely diminished in the condition with K63R ubiquitin, wherein K63-linked polyubiquitin chain formation was abolished (**Figure 3.28**). Collectively these findings indicate that FBXO41-Cul7 ubiquitinates NFM, mainly via K63-linked polyubiquitin chains.

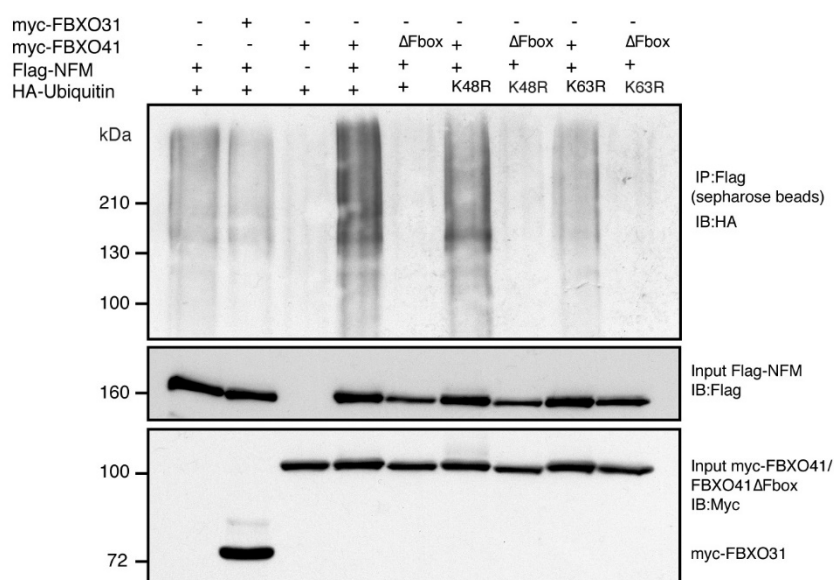


**Figure 3.28 FBXO41 ubiquitinates NFM via K63-linked polyubiquitination:** HEK293T cells were transfected with plasmids encoding Flag-NFM, either wild type or the indicated linkage mutants of HA-ubiquitin together with myc-FBXO41, myc-FBXO41  $\Delta$ Fbox or myc-FBXO31 (negative control) plasmids. 48 hours after transfection, 1 mg of the HEK293T cell lysates were processed according to the denaturing protocol (Materials and methods section 2.17.6), followed by IP with Flag-Sepharose beads and subsequent IB with the HA antibody.

### 3.2.5 Loss of FBXO41-Cul7 leads to destabilization of NFM:

Most K63-linked ubiquitin modifications are thought to lead to non-proteolytic consequences, resulting in varying outcomes of protein fate, such as functional modification,

stabilization etc (Bocquet *et al.*, 2009; Komander and Rape, 2012; Pickart and Eddins, 2004). Hence, I wondered if the K63-linked ubiquitination of NFM led to any change of NFM protein function. Since NFM is robustly expressed along the axons and together with NFL and NFH forms the predominant cytoskeleton of axons (Li *et al.*, 2012), I wondered if loss of FBXO41 affects the stability of NFM. To address this question, I evaluated the levels of NFM protein levels *in vivo* from the brain lysates of FBXO41<sup>+/+</sup> and FBXO41<sup>-/-</sup> animals at P5 and P16. Cerebellar lysates obtained from wild type and knockout littermates from three independent litters at P5 and P16 were subjected to immunoblot analyses using the NFM antibody. Interestingly, the levels of NFM were significantly reduced in the FBXO41<sup>-/-</sup> mice at both P5 and P16 when compared to their FBXO41<sup>+/+</sup> littermates (Figure 3.29 A, B, C, D).

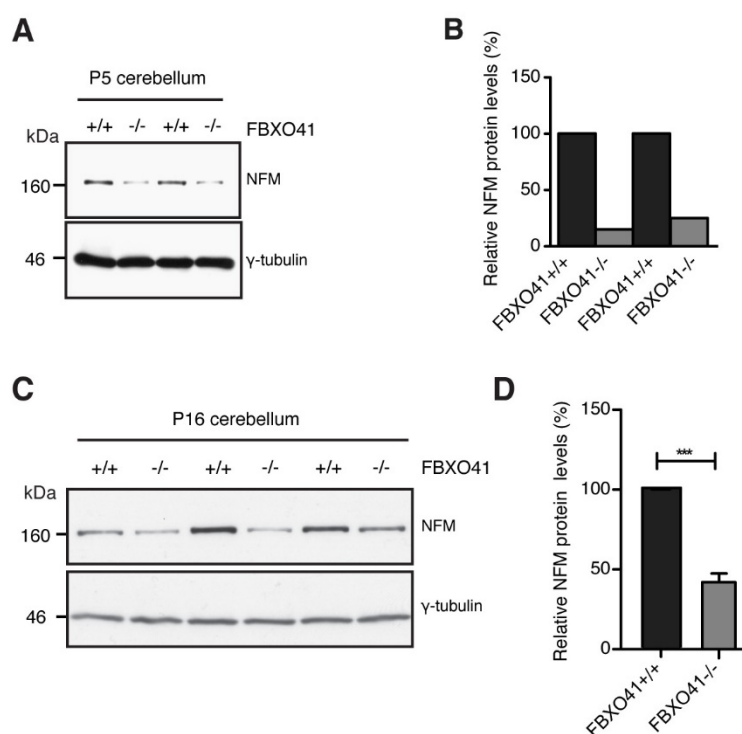


**Figure 3.29 FBXO41<sup>-/-</sup> mice show diminished NFM levels:** (A) 50  $\mu$ g of P5 cerebellar lysates isolated from FBXO41<sup>+/+</sup> and FBXO41<sup>-/-</sup> littermates were immunoblotted with the NFM and  $\gamma$ -tubulin antibodies. The latter served as loading control. Samples of lanes 1 and 2 and those of 3 and 4 are derived from littermates, respectively. *Sample collection and preparation was performed by Dr. A. Holubowska while the immunoblotting was done by N. Schwedhelm-Domeyer.* (B) Densitometric quantification of NFM protein levels in A NFM protein levels are normalized to that of FBXO41<sup>+/+</sup> NFM levels of each litter pair and then represented as percentage. (C) 50  $\mu$ g of P16 cerebellar lysates isolated from FBXO41<sup>+/+</sup> and FBXO41<sup>-/-</sup> littermates were immunoblotted with the NFM and  $\gamma$ -tubulin antibodies. The latter served as loading control. Samples in lanes 1 and 2, 3 and 4, and 5 and 6 are derived from representative littermates.

**(D)** Densitometric quantification of NFM protein levels in **C**. The NFM protein levels are normalized to the FBXO41+/+ levels of each litter pair. Normalized NFM protein levels are represented as percentage. At least 5 FBXO41+/+ and FBXO41-/- litter pairs were analyzed (Student's t-test, \*\*\*p<0.001, mean + s.e.m.).

Additional qRT-PCR analyses from the P16 cerebella of FBXO41+/+ and FBXO41-/- mice showed that NFM was not transcriptionally downregulated (**Figure 3.30**), suggesting that the downregulation of NFM in FBXO41-/- mice was not a consequence of transcriptional changes.

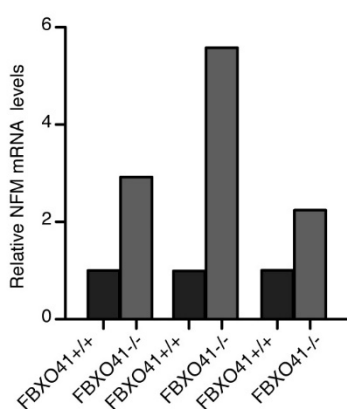


**Figure 3.30 NFM mRNA levels in the P16 FBXO41+/+ and FBXO41-/- mice:** Graph represents the relative fold change in NFM mRNA levels obtained from quantitative RT-PCR analyses using P16 FBXO41+/+ and FBXO41-/- cerebellar tissue. The obtained mRNA levels are relative to GAPDH, which served as a loading control, and are in turn normalized to the FBXO41+/+ of each litter. The graph shows fold change of NFM mRNA levels of 3 pairs of FBXO41+/+ and FBXO41-/- littermates. *Sample collection and analyses was performed by me, mRNA isolation and the qRT-PCR was performed by N.Schwedhelm-Domeyer.*

Additionally, I checked if the destabilization of NFM was purely a result of the lack of its ubiquitination by FBXO41-Cul7. I expressed control, myc-FBXO41, myc-FBXO41  $\Delta$ Fbox or myc-FBXO41 aa 35-873 together with Flag-NFM, followed by immunoblot analysis. Interestingly, I observed that NFM was destabilized in the conditions when expressed together with FBXO41 ligase-dead mutants as compared to FBXO41 full-length (**Figure 3.32 A, B**).

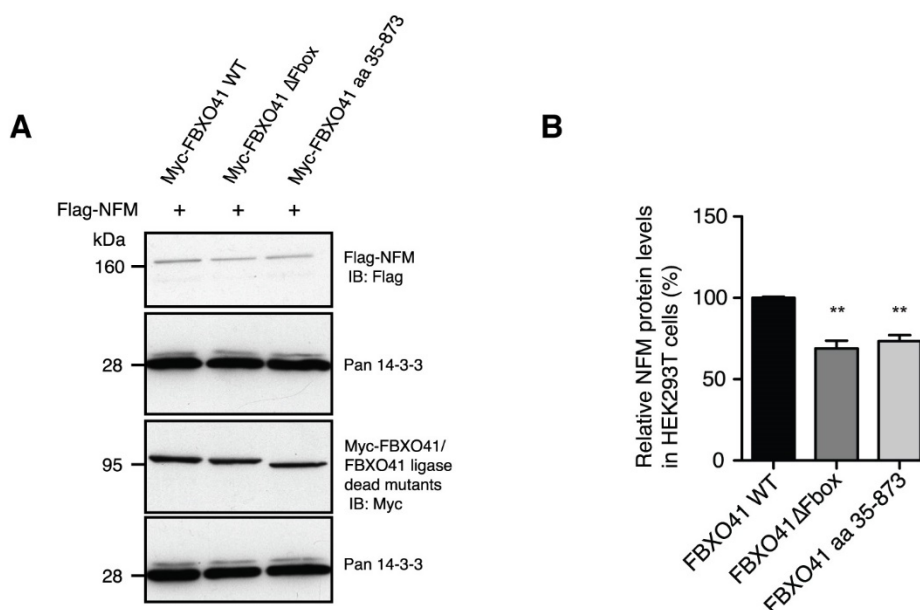


**Figure 3.31 Loss of FBXO41-Cul7 leads to destabilization of NFM:** (A) 50  $\mu$ g of lysates from HEK293T cells, transfected with plasmids encoding Flag-NFM, together with wild type FBXO41 or the ligase-dead mutants, FBXO41  $\Delta$ Fbox or FBXO41 aa 35-873, were subjected to immunoblotting with Flag, myc or pan 14-3-3 antibodies. Pan 14-3-3 served as loading control. (B) Graph represents the densitometric quantification of NFM protein levels of A. The NFM protein levels are relative to the loading in each lane and are further normalized to the wild type FBXO41 protein levels. The resulting difference in protein levels is represented as percentage. Quantifications were done from three independent experiments (Student's t-test, \*\* $p < 0.01$ , mean + s.e.m.).

Collectively, these results demonstrate loss of FBXO41-Cul7 leads to severe destabilization and downregulation of NFM *in vitro* as well as *in vivo* most likely due to a loss of ubiquitination modification.

### 3.2.6 Dysregulation of NFM levels leads to uncontrolled axon out growth:

NFM is a type IV neuronal intermediate filament, expressed abundantly in the cytosol and along the axons. It is thought to be responsible for regulating radial axon growth (Cleveland *et al.*, 1991; Li *et al.*, 2012). However, its role in regulation of longitudinal axon growth is understudied. In order to establish the role of NFM in axon growth regulation in CGNs, I first established the temporal expression of NFM in the cerebellum at various postnatal ages. I subjected cerebellar lysates from various postnatal ages to immunoblot analysis with an NFM-specific antibody. Surprisingly, I observed that NFM is upregulated and highly

expressed at developmental stages crucial for neurite outgrowth and lengthening of axons, rather than radial axonal growth (**Figure 3.32**).

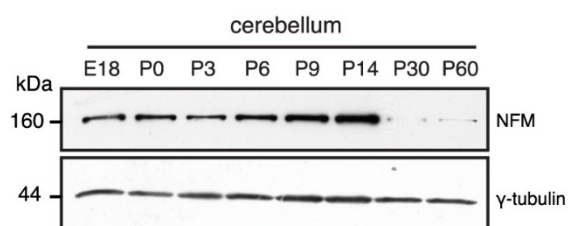


**Figure 3.32 NFM is expressed in the developing cerebellum of mice:** Cerebellar lysates from indicated ages were analyzed by immunoblotting with the NFM and  $\gamma$ -tubulin antibodies where the latter served as loading control.

Owing to its predominant axonal localization and robust expression during cerebellar development, I used cultured CGNs as a model system to investigate if NFM had any effects on axonal length. Taking a gain-of-function approach first, I transfected CGNs at DIV1 with either control or and NFM overexpression plasmids. Upon morphometric analysis of the axonal lengths of the transfected neurons at DIV 5, I observed that excess of NFM led to remarkably increased axonal length when compared to control neurons (**Figure 3.33 A, B**).

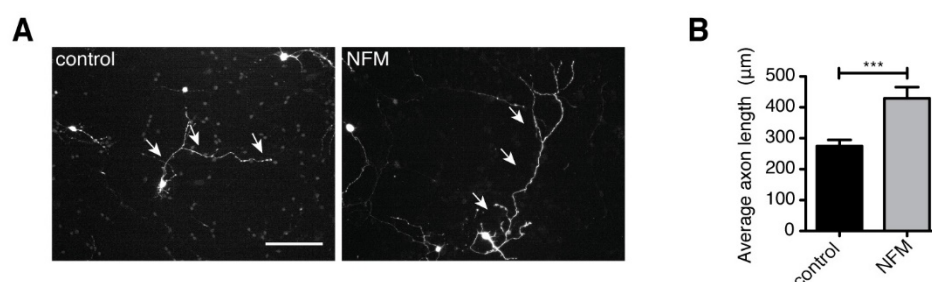


**Figure 3.33 NFM promotes axon growth: (A)** Representative images of rat CGNs that were transfected at DIV1 with either the control vector or the NFM expression plasmid, and subjected to axon growth assays (Materials and methods section 2.15) at DIV5. Arrows indicate axons. Scale bar equals 100  $\mu$ m. **(B)** Quantifications of the axonal lengths from **A**. The average axonal length is represented in  $\mu$ m. All measurements and quantifications were done in a blinded manner. A total of 254 neurons from 3 independent experiments were measured (Student's t-test, \*\*\* $p < 0.001$ , mean + s.e.m.).

Given that overexpression of NFM results in increased axon growth, I wondered if loss of NFM would have the opposite effect. Hence, I first generated a short hairpin RNAi that specifically targets and knocks down NFM (NFM RNAi#5). In addition to the functional RNAi (NFM RNAi#5), I also generated an NFM-specific non-functional shRNA (NFM RNAi#3), which was unable to knockdown NFM. I validated the shRNAs using HEK293T cells transiently transfected with myc-NFM expression plasmids (**Figure 3.34 A**). I further

confirmed the efficiency of the RNAi by knocking down endogenous NFM in cultured CGNs (**Figure 3.34 B**).

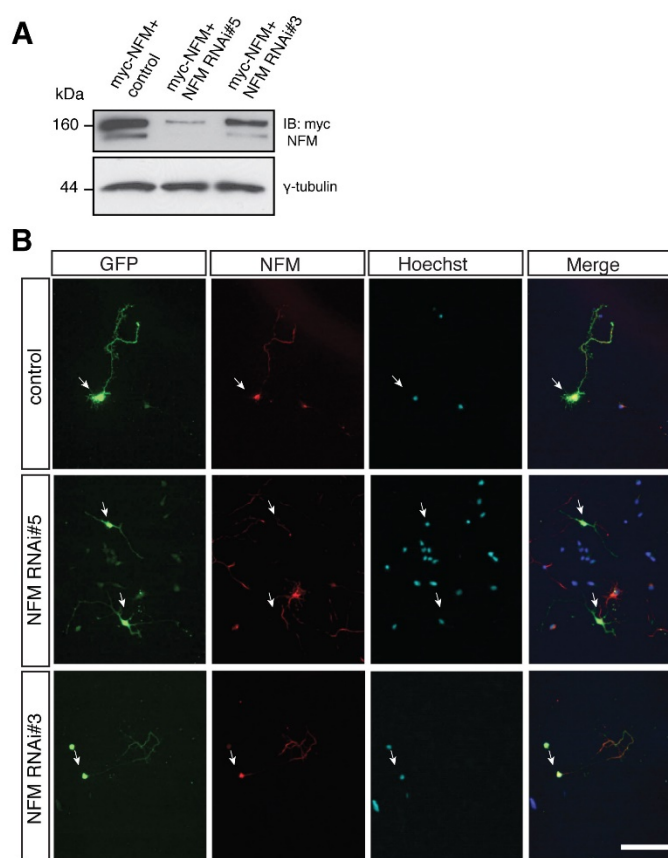


**Figure 3.34 Knockdown of NFM:** (A)

Lysates from HEK293T cells, transfected with the myc-NFM plasmid together with control, the functional NFM RNAi#5 or the non-functional NFM RNAi#3 plasmid, were lysed and immunoblotted using the myc and  $\gamma$ -tubulin antibodies. The latter served as loading control. (B) Representative images of rat CGNs at DIV1 transfected with control vector, the functional NFM RNAi#5 or the non-functional NFM RNAi#3 plasmid together with the transfection marker GFP. Neurons were subjected to immunocytochemistry at DIV5 using the GFP and NFM antibodies. Scale bar equals 100  $\mu$ m.

I observed that while the functional NFM RNAi#5 robustly knocked down NFM, the non-functional NFM RNAi#3 had no effect, both in HEK293T cells as well as in CGNs.

To determine the effect of loss of NFM on axonal length, I transfected cultured CGNs at DIV1 with either control U6, the functional NFM RNAi#5 or the non-functional NFM RNAi#3 plasmids and subjected the transfected cells to morphometric analyses four days later. Surprisingly, I observed that loss of NFM resulted in a pronounced increase of axon length when compared to the controls. The non-functional NFM RNAi#3 on the other hand had no effect on axon length and hence served as an additional negative control (**Figure 3.35 A, B**). While loss of NFM resulted in increased axonal length, it had no effect on primary axon branching and dendrite length (**Figure 3.35 C, D**).

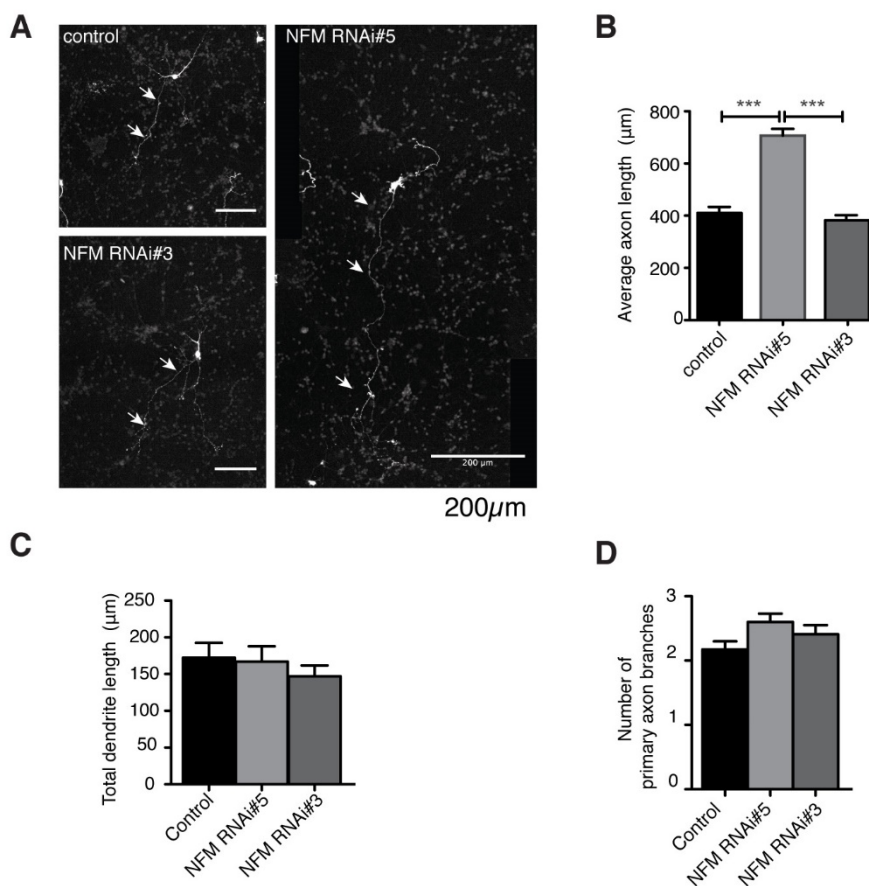


**Figure 3.35 Loss of NFM leads to uncontrolled axon growth:** (A) Representative images of rat CGNs that were transfected at DIV1 with either control vector, the functional NFM RNAi#5 or the non-functional NFM RNAi#3 plasmids together with the transfection marker GFP and subsequently subjected to axon growth measurements at DIV5. Arrows indicate axons. Scale bar equals 100 μm unless indicated otherwise. (B) Graph represents the quantifications of axon lengths from A. The average axonal lengths are represented in μm. (C) The total dendrite length of the neurons from A was measured, represented in μm. (D) Moreover, the primary axonal branches of the neurons from A were quantified. (B, C, D) All measurements and quantifications were done in a blinded manner. A total of 348 neurons from 3 independent experiments were measured (ANOVA, \*\*\*p<0.001, mean + s.e.m.).

In order to rule out possible off-target effects of the NFM RNAi, I performed a rescue experiment, wherein we first generated an RNAi-resistant myc-NFM expression vector (NFM-Res), which harbored four silent mutations in the region targeted by the functional NFM RNAi#5 (Figure 3.36 A). The efficiency of rescue or resistance to knockdown by the myc-NFM-Res expression plasmid was validated by co-transfecting myc-NFM expression plasmids or myc-NFM-Res plasmid together with the functional NFM RNAi#5 in HEK293T cells, followed by immunoblotting analysis. While the NFM RNAi#5 efficiently knocked down NFM, myc-NFM-Res was found to be resistant to RNAi (Figure 3.36 A). Following



generation and validation of the NFM-Res construct, I transfected CGNs at DIV1 with either control U6 vector or NFM RNAi#5 together with either control or NFM-Res plasmids. Four days later at DIV5, morphometric evaluation of the transfected neurons revealed that while loss of NFM resulted in increased axon length, co-expression of the NFM-Rescue plasmid together with the NFM RNAi#5 nullified this effect and restored axon lengths back to baseline levels (**Figure 3.36 B, C**).

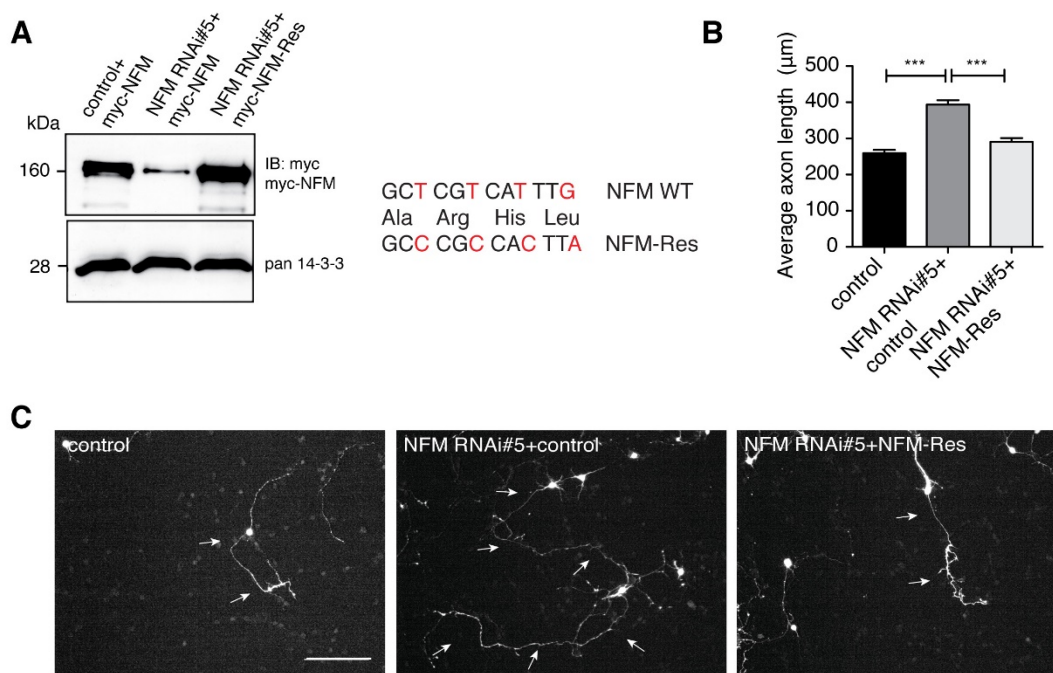
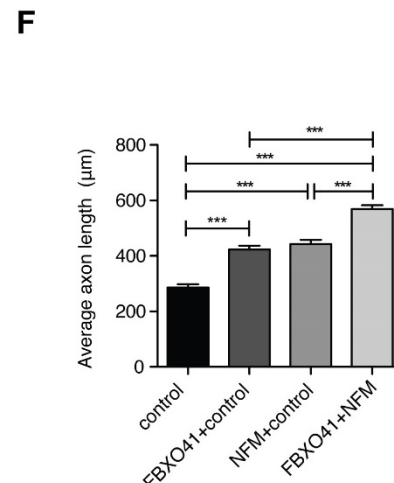
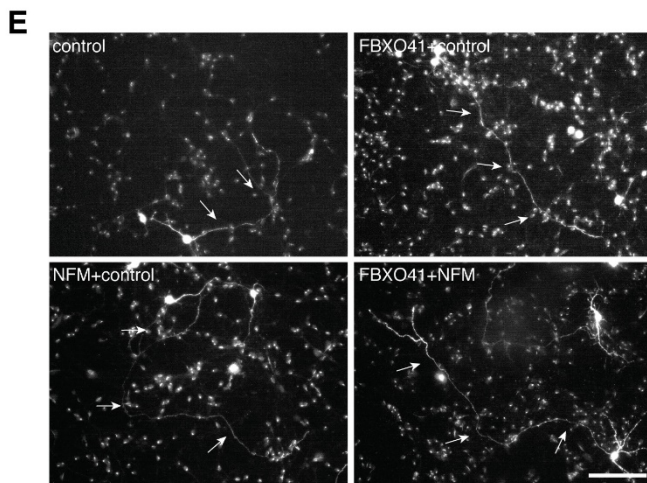
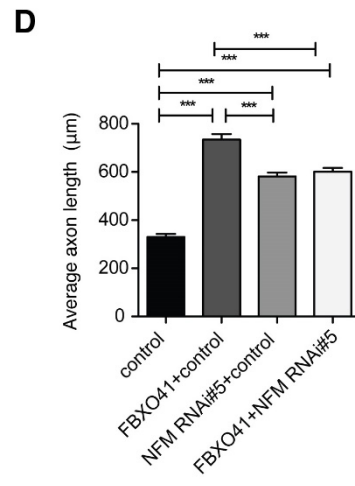
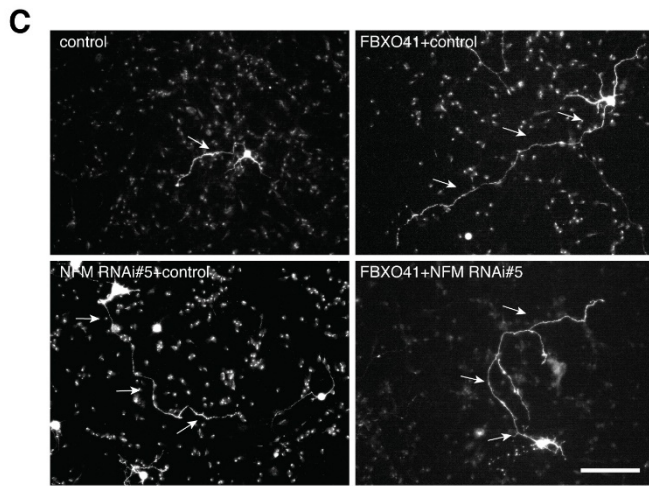
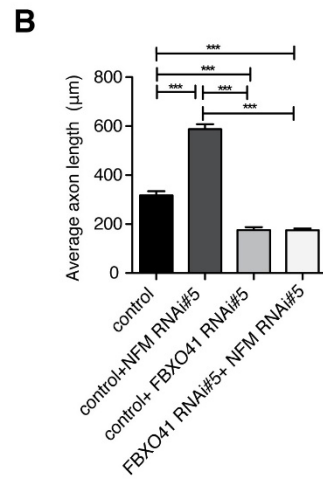
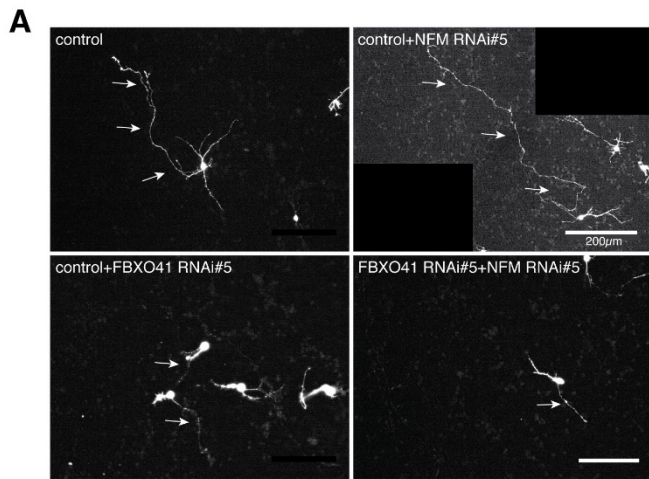


**Figure 3.36 NFM knockdown also promotes axon growth:** (A) 50 µg of lysates harvested from HEK293T cells, transfected with control, the myc-NFM or myc-NFM-Rescue (Res) plasmid together with control vector or the NFM RNAi#5 plasmid, were immunoblotted with the myc or pan 14-3-3 antibodies. The latter served as loading control. Schematic on the right shows the NFM RNAi#5 targeting region with the silent mutations indicated in red. (B) Quantifications of rat CGN axonal lengths, that were transfected at DIV1 with control, NFM RNAi#5 together with control or the NFM-Res plasmids, were subjected to axon growth assay at DIV5. All measurements and quantifications were done in a blinded manner. A total of 369 neurons from 3 independent experiments were measured. (ANOVA, \*\*\* $p < 0.001$ , mean + s.e.m.). (C) Representative images of transfected neurons from B. Arrows indicate axons. Scale bar equals 100 µm.

Collectively these results indicate that dysregulation of NFM protein levels leads to increased axonal lengths, as both excess and reduced NFM levels results in axon growth promotion.

### 3.2.7 NFM acts downstream of FBXO41 to promote axon growth:

Since both FBXO41 and its interaction partner NFM seem to regulate axonal length, I asked if they both act in the same pathway of axon growth regulation. In order to establish a functional relationship between the two proteins, I conducted a series of axonal morphometric analyses to deduce the epistatic nature between FBXO41 and NFM. I applied varying combinations of loss of function and gain-of-function approaches using FBXO41-specific RNAi and FBXO41 overexpression plasmids previously generated in the lab, together with NFM RNAi#5 and NFM overexpression plasmids. I first used the loss-of-function approach, where I transfected cultured CGNs at DIV1 with either control U6, FBXO41 RNAi#5, NFM RNAi#5 or both (FBXO41 RNAi#5 + NFM RNAi #5). As expected, loss of FBXO41 resulted in short axons and loss of NFM in longer axons, interestingly though loss of both FBXO41 and NFM mimicked the short axon phenotype observed for loss of FBXO41 alone (**Figure 3.37 A, B**). Additionally, I transfected cultured CGNs at DIV1 with either control, U6, FBXO41, NFM RNAi#5 or both (FBXO41 + NFM RNAi#5) (**Figure 3.37 C, D**). Predictably all 3 conditions of FBXO41 overexpression, NFM knockdown and FBXO41 overexpression together with NFM knockdown resulted in longer axons when compared to the control. However, it is interesting to note that the longer axons observed on knockdown of NFM alone are shorter than those observed in FBXO41 overexpression alone. Interestingly, in the fourth condition (FBXO41+NFM RNAi#5), the axonal lengths mimicked that of loss of NFM (NFM RNAi#5) and were significantly shorter than FBXO41 overexpression (**Figure 3.37 C, D**). I then took the gain-of-function epistasis analysis for FBXO41 and NFM by transfecting CGNs with control, FBXO41 and/or NFM expression plasmids. Expectedly, when compared to control, overexpression of FBXO41 or NFM and overexpression of both resulted in longer axons. Interestingly, overexpression of both FBXO41 together with NFM resulted in significant increase in axonal length when compared to the single overexpression conditions (**Figure 3.37 E, F**). Subsequently, on performing further axonal morphometric analyses, where I transfected CGNs with either control, FBXO41 RNAi#5, NFM or FBXO41 RNAi#5 and NFM plasmids together, I observed that overexpression of NFM could not rescue the short axon phenotype observed due to FBXO41 knockdown (**Figure 3.37 G, H**).



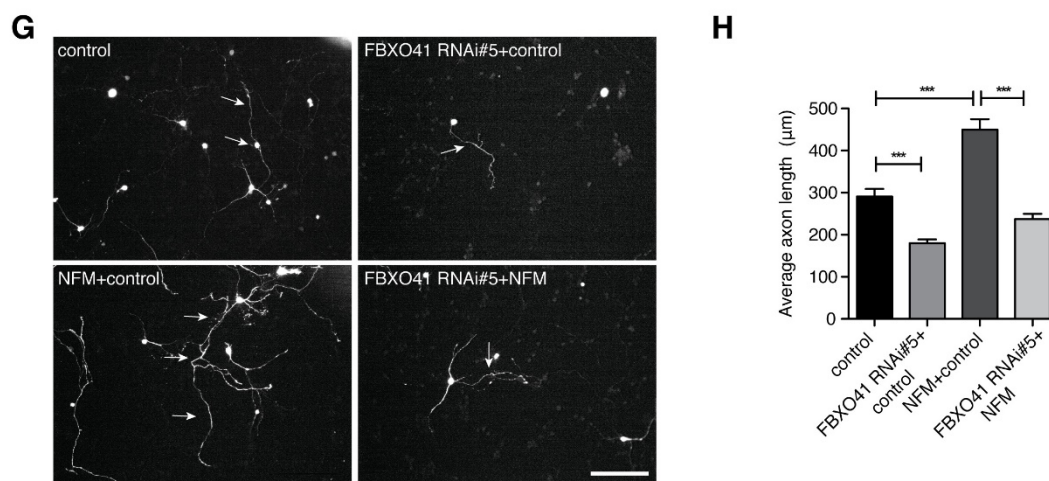


**Figure 3.37 The NFM / FBXO41 pathway of axon growth regulation:** (A) Representative images of rat CGNs that were transfected at DIV1 with control vector, NFM RNAi#5, FBXO41 RNAi#5, or both and were subjected to axon growth assay at DIV5. (B) Quantification of axonal lengths from A. The average axonal length is represented in  $\mu\text{m}$ . A total of 498 neurons from 3 independent experiments were measured (ANOVA,  $***p < 0.001$ , mean + s.e.m.). (C) Representative images of rat CGNs transfected at DIV1 with control vector, NFM RNAi#5, FBXO41 overexpression plasmid, or NFM RNAi together with FBXO41 overexpression plasmid that were processed and analysed for axon lengths as in A. (D) Quantification of axonal lengths from C. A total of 440 neurons from 3 independent experiments were measured (ANOVA,  $***p < 0.001$ , mean + s.e.m.). (E) Representative images of rat CGNs that were transfected at DIV1 with control vector, FBXO41 expression plasmid, the NFM expression plasmid or both plasmids were processed and their axonal lengths quantified as in A. (F) Quantification of axonal lengths from E. A total of 444 neurons from 3 independent experiments were measured (ANOVA,  $***p < 0.001$ , mean + s.e.m.). (G) Representative images of rat CGNs, which were transfected at DIV1 with either control vector, FBXO41 RNAi#5, the NFM expression plasmid or the FBXO41 RNAi together with the NFM plasmid, were processed and their axonal lengths measured quantified as in A. (H) Quantification of axonal lengths from G. A total of 519 neurons from 3 independent experiments were measured (ANOVA,  $***p < 0.001$ , mean + s.e.m.). (A, C, E, G) Arrows indicate axons and scale bars equal  $100 \mu\text{m}$ .

Collectively, these experiments offer two possibilities. Firstly, it suggests that FBXO41 is epistatic to NFM, which in the “conventional” sense would mean that NFM acts upstream of FBXO41. Secondly and more likely, considering their biochemical relationship of an E3 ligase (FBXO41-Cul7) and its non-proteolytic ubiquitination substrate (NFM), it is interesting to observe that NFM cannot exert its axon growth promoting effect in the absence of FBXO41 (Figure 3.37 G, H). Interestingly it also becomes clear that even though FBXO41 can still promote axon growth in the absence of NFM (Figure 3.37 C, D), the magnitude of its axon growth-promoting effect is reduced in the absence of NFM. Moreover, it becomes apparent that saturated amounts of both NFM and FBXO41 are crucial for

complete stimulation of axon growth. Additionally **Figure 3.37 C, D, E, F** hints at the existence of other NFM-independent FBXO41 axon growth regulation pathways, thus, indicating that FBXO41-Cul7 might act as a promiscuous ligase which interacts with several targets or substrates in control of axon growth regulation.

In order to rule out either of the two possibilities and to bring further clarity into the FBXO41-NFM hierarchy I additionally carried out a localization analysis experiment in cultured CGNs. Given that NFM is a cytoskeletal protein implicated in axonal transport (*Li et al., 2012; Rao et al., 2011*), together with the finding that FBXO41 is epistatic to NFM, it is plausible that NFM acts upstream of FBXO41 to localize or transport it along the axons. To test this, I transfected cultured CGNs with GFP-FBXO41 together with either control U6 or the functional NFM RNAi#5 plasmids. Four days following transfection the neurons were subjected to immunocytochemistry with GFP antibody to visualize the localization of FBXO41. Interestingly, FBXO41 localization and distribution remained unchanged irrespective of the presence or absence of NFM (**Figure 3.38**).

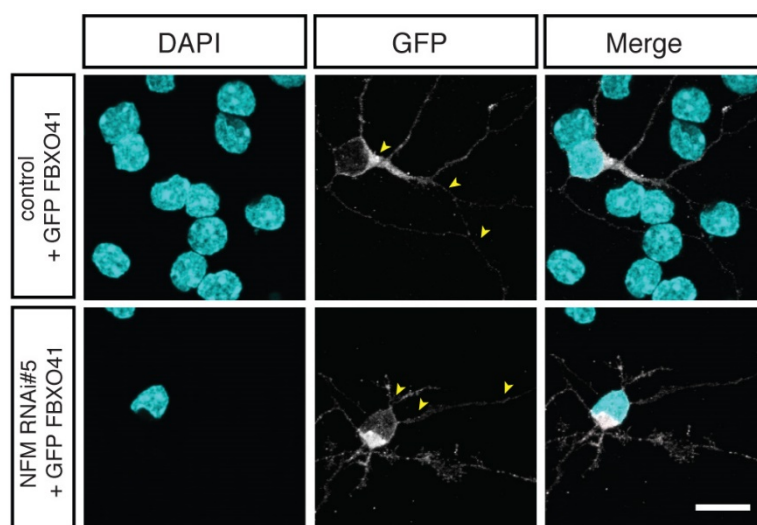


**Figure 3.38 Loss of NFM has no effect on FBXO41 localization:** Representative confocal images of cultured rat CGNs that were transfected with plasmids expressing GFP-FBXO41 together with control vector or NFM RNAi#5 at DIV1. The neurons were subjected to immunocytochemistry using the GFP antibody and the distribution of GFP-FBXO41 was assessed. Yellow arrows indicate cell body and axon of the transfected neuron. Scale bar equals 10  $\mu\text{m}$ .

Taking the reverse approach and testing whether NFM requires proper modification by FBXO41-Cul7, I additionally transfected cultured CGNs with GFP-NFM together with either control U6 or the functional FBXO41 RNAi#5 plasmids, followed by immunocytochemistry

at DIV5 with the GFP antibody to visualize NFM. Intriguingly, loss of FBXO41 led to defasciculated NFM within the axons of significantly more neurons when compared to control (**Figure 3.39 A, B**).

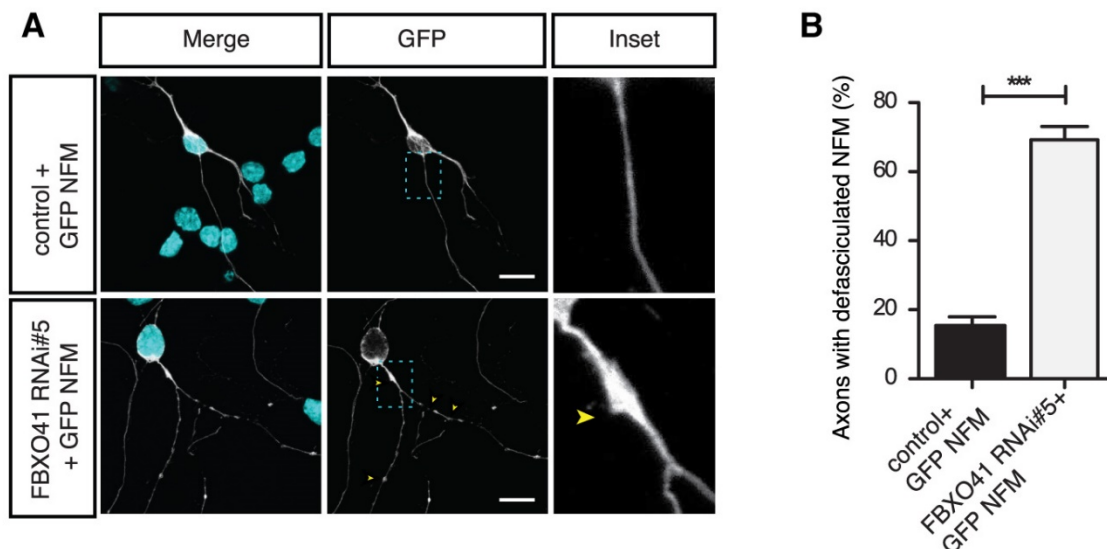


**Figure 3.39 Loss of FBXO41 leads to defasciculated NFM in axons: (A)** Representative confocal images of cultured CGNs, that were transfected at DIV1 with a plasmid expressing GFP-NFM together with control vector or FBXO41 RNAi#5. The cells were subjected to immunocytochemistry using the GFP antibody and the nature of distribution of GFP-NFM was assessed. Insets show higher magnification of the indicated region. Scale bar equals 10  $\mu$ m. Yellow arrowheads indicate defasciculated NFM along the axons **(B)** Quantification depicts the percentage of neurons having an abnormal distribution or localization of NFM along the cell body and axons as observed in **A** Results from least three independent experiments were included in the analyses (Student's t-test, \*\*\* $p < 0.001$ , mean + s.e.m).

These results taken together with the reduced NFM protein levels observed in the FBXO41<sup>-/-</sup> mouse cerebellum and in HEK293T cells in the presence of the ligase-dead versions of FBXO41, collectively establish FBXO41 as acting upstream of NFM to regulate its stability and axon growth in an ubiquitin dependent manner.

### 3.3 Behavioral analysis of the adult FBXO41<sup>+/-</sup> mice:

While FBXO41<sup>-/-</sup> displayed a severe behavioral phenotype at P16 and P30, FBXO41<sup>+/-</sup> mice were found to be indistinguishable from their FBXO41<sup>+/+</sup> littermates. To determine if only half the dosage of FBXO41 has any late onset motor phenotypes, which are not detectable at P16 and P30, I decided to behaviorally analyze adult FBXO41<sup>+/-</sup> mice and their FBXO41<sup>+/+</sup> littermates. In order to determine if the adult FBXO41<sup>+/-</sup> mice develop any abnormal phenotypes as a result of aging, I analyzed 17 FBXO41<sup>+/+</sup> and 23 FBXO41<sup>+/-</sup> male mice of two independent cohorts for a battery of motor and gait-tests at 10 months of age.

#### 3.3.1 FBXO41<sup>+/-</sup> mice show no abnormal appearance and body weight:

During the course of the experiment, the body weight of FBXO41<sup>+/+</sup> and FBXO41<sup>+/-</sup> mice was monitored. While the P16 FBXO41<sup>-/-</sup> mice showed drastically reduced body weight, FBXO41<sup>+/-</sup> mice were indistinguishable from their wild type littermates. I wondered if partial loss of FBXO41 would have an effect on body weight as a result of ageing. The FBXO41<sup>+/-</sup> mice showed no abnormal changes in body weights when compared to their wild type littermates (**Figure 3.40**).

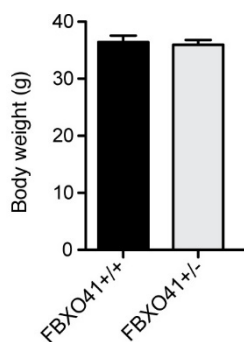


**Figure 3.40 FBXO41<sup>+/-</sup> do not show abnormal body weight at 10 months:** Average body weights of 17 FBXO41<sup>+/+</sup> and 23 FBXO41<sup>+/-</sup> mice at 10 months of age (ANOVA mean + s.e.m).

#### 3.3.2 Adult FBXO41<sup>+/-</sup> mice show no signs of abnormal locomotion and anxiety:

First, I tested the animals for both anxiety and general locomotor activity. Before the animals got used to the testing environment and the handler, I tested the anxiety of the FBXO41<sup>+/+</sup> and FBXO41<sup>+/-</sup> mice using the elevated plus maze. The elevated plus maze

typically consists of a elevated cross-shaped platform, having two open and two closed arms. Previously, several studies have established that while untreated mice tend to avoid open arms, mice that were treated with anxiogenic drugs spent longer time within the closed arms (*Pellow et al., 1985; Pellow and File, 1986; Treit and Fundytus, 1988*). These studies have collectively established the elevated plus maze as a valid test for measuring anxiety. During the test, the mice were placed at the center of the cross arms and allowed to freely explore the maze. The distance travelled by the mice and the time they spent in closed arms and the open arms was recorded. Upon analysis, I found no difference between the genotypes as both FBXO41<sup>+/+</sup> and FBXO41<sup>+/-</sup> mice displayed a natural avoidance for the open arms and spent maximum time within the closed arms. They also showed no difference in their locomotor activities, with both genotypes displaying increased activity levels in the closed arms compared to the open arms (**Figure 3.41 A, B**).

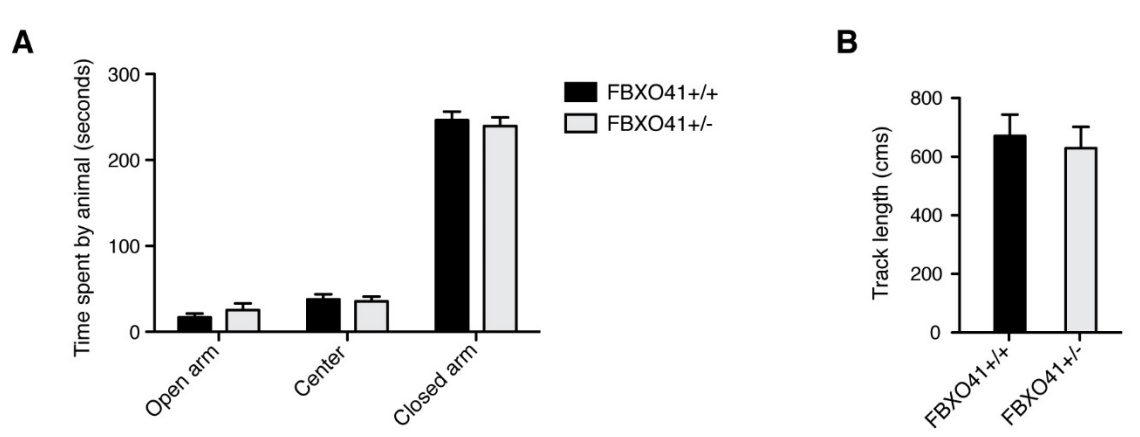


**Figure 3.41 FBXO41<sup>+/-</sup> mice do not show elevated anxiety levels in the elevated plus maze paradigm:**

(A) Graph represents the time spent by the animals in the open arm, center and the closed arm (Two-way ANOVA mean+s.e.m) (B) Graph represents the track lengths representing the distance travelled by the animals within the elevated plus maze (Student's t-test mean + s.e.m) (A, B) 17 FBXO41<sup>+/+</sup> and 23 FBXO41<sup>+/-</sup> animals (littermates) were analyzed.

Following the elevated plus maze, I subjected FBXO41<sup>+/+</sup> and FBXO41<sup>+/-</sup> mice to the open field test. In the open field test the mice are placed in a circular arena that is enclosed by walls at the periphery and has an open space in the center. The mice are allowed to explore the arena freely for a fixed period of time and the amount of locomotor activity and the time spent in the center verses the periphery is measured. Untreated healthy wild type mice much like in the elevated plus maze paradigm, avoid the open space in the center and tend to spend most time close to the wall (*Simon et al., 1994; Treit and Fundytus, 1988*). I measured the time spent by the mice in each of the quadrants of the open field namely the center,



intermediate and the periphery (**Figure 3.42 A**). In addition, I also quantified the distance travelled by them (**Figure 3.42 B**). FBXO41<sup>+/-</sup> mice were found to spend slightly more time in the intermediate zone than the periphery when compared to their FBXO41<sup>+/+</sup> littermates. Although the differences were not striking and no observable difference was present between the genotypes when comparing their track lengths.

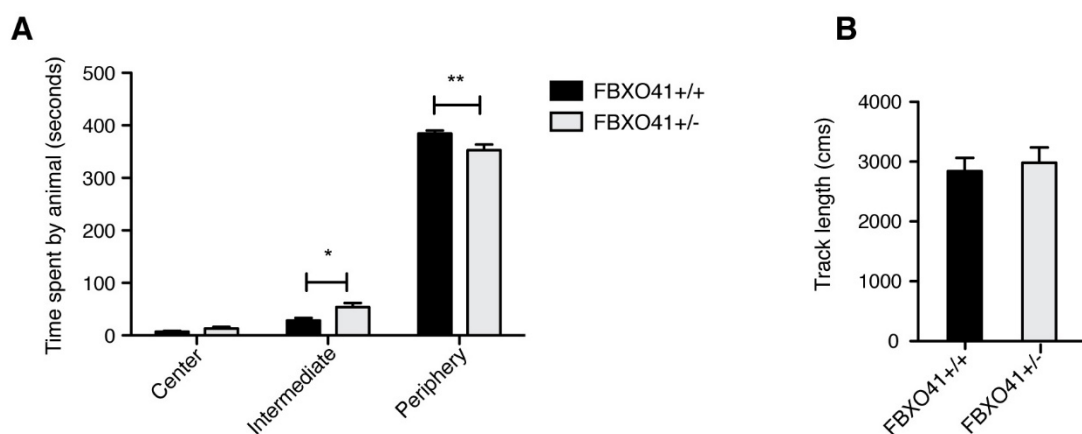


**Figure 3.42 FBXO41<sup>+/-</sup> mice display comparable locomotor activity in the open field arena: (A)** Graph represents the time spent by the animals in the center, intermediate and periphery of the open field arena (Two-way ANOVA mean + s.e.m) **(B)** Graph represents the track lengths representing the distance travelled by the animals within the open field arena (Student's t-test \*\*  $p < 0.01$ , \*  $p < 0.05$  mean + s.e.m) **(A, B)** 17 FBXO41<sup>+/+</sup> and 23 FBXO41<sup>+/-</sup> animals (littermates) were analyzed.

### 3.3.3 Absence of hind limb clasp in adult FBXO41<sup>+/-</sup> mice:

After testing for anxiety levels, the FBXO41<sup>+/+</sup> and FBXO41<sup>+/-</sup> mice were subjected to the “clasp test” as previously described in the Materials and Methods. Healthy mice when suspended by their tails tend to spread their fore and hind limbs away from the body, while mice suffering from neurological deficits tend to clasp their fore and hind limbs close to their body. The presence and increasing severity of clasp is often used as a hallmark for progressive neurodegeneration or neurological problems (*Guyenet et al., 2010*).

In order to determine if FBXO41<sup>+/-</sup> mice show age-related neurodegeneration or deficits, we evaluated the clasp behavior on the scale of 0-3. 0 represented absence of clasp and 3 represented severe clasp of both fore and hind limbs close to the animals body (**Figure 3.43**). No differences between genotypes were observed. This result suggests that most likely at the age analyzed (10 months) no acute neurodegeneration has taken place.

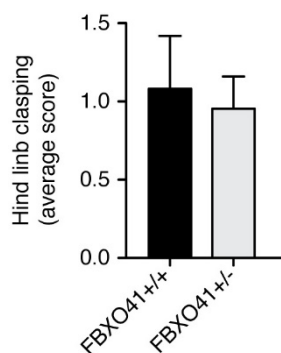


**Figure 3.43 FBXO41<sup>+/-</sup> mice display no hind limb clasping:** 10 month old FBXO41<sup>+/+</sup>, FBXO41<sup>+/-</sup> were tested for hind limb clasping. 0= normal phenotype, 3= worst manifestation of phenotype. A total of 17 FBXO41<sup>+/+</sup> and 23 FBXO41<sup>+/-</sup> animals were analyzed (Student's t-test mean + s.e.m)

### 3.3.4 Intact olfaction in adult FBXO41<sup>+/-</sup> mice:

Loss of olfactory sensation is one of the earliest signs of several neurodegenerative diseases such as Parkinson's or Alzheimer's. It often precedes motor dysfunction in neurodegenerative diseases (Kurtz *et al.*, 1989; Marras *et al.*, 2005; Tolosa *et al.*, 2007). I thus wanted to assess if the aged FBXO41<sup>+/-</sup> mice display any signs of diminished olfaction. I subjected the mice to the olfaction-testing paradigm. The time taken by each animal to find a hidden chocolate chip was measured. One chocolate chip was shallowly buried under the straw bedding in the cage (Materials and methods section 2.21.2.6). For the test, the mice were placed in the cage and allowed to search for the hidden chocolate chip. Each animal was subjected to three trials, with an interval of 50 minutes per trial. In the third trial, the chocolate chip was placed on the surface of the bedding, making sure that it was visible. This trial served as a control to ensure the animals preference for the chocolate chip. All animals performed better with each trial, which suggests olfactory learning and no differences between the genotypes were observed. (Figure 3.44)

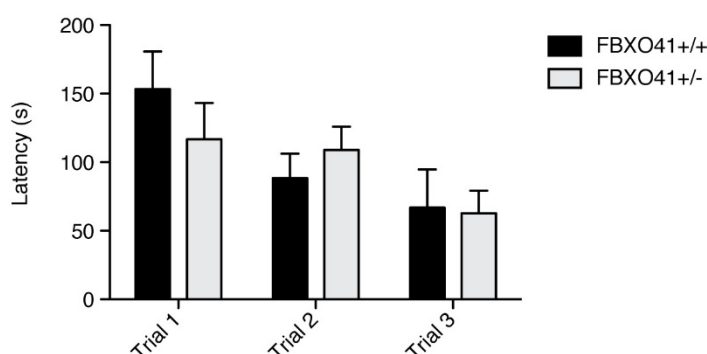


**Figure 3.44 FBXO41<sup>+/-</sup> mice do not show loss of olfaction:** 10 month old FBXO41<sup>+/+</sup>, FBXO41<sup>+/-</sup>

were tested for their olfactory acuity. The graph represents the time taken by the animals to find a hidden chocolate chip, relying on their sense of smell. A total of 17 FBXO41<sup>+/+</sup> and 23 FBXO41<sup>+/-</sup> animals were analyzed (Two-way ANOVA, mean + s.e.m)

### **3.3.5 Adult FBXO41 +/- display intact motor function and coordination:**

To test their motor coordination and function I subjected FBXO41<sup>+/+</sup> and FBXO41<sup>+/-</sup> mice to the rotarod test. On trial day 1, the mice were placed on the rotarod at accelerating speed for 2 minutes. The time spent on the rotarod and the acceleration was recorded. To assess their motor learning I additionally repeated the rotarod paradigm 3 hours and 24 hours after trial 1, respectively and analyzed their latency to fall and the acceleration at which they fall from the rotarod (**Figure 45 A, B**). At the first two trials both genotypes showed no signs of motor deficits and both performed equally well. After 24 hours in fact the FBXO41<sup>+/-</sup> mice seemed to perform even better in comparison to their FBXO41<sup>+/+</sup> littermates suggesting that their motor coordination and motor learning was not impaired.

I additionally subjected the mice to the balance beam test, where the mice were trained to reach from point A to B (home cage) on balance beams that were either 12mm or slightly more challenging, only 6 mm thick. On the test day, not only was the time taken by the animal to walk across the balance beam measured, but also their coordination quantified. I scored their coordination and extent of limb dragging on a scale of 0-7, with 7 representing normalcy and 0 being completely unable to cross the beam balance. Each animal was tested 3 times on the 12 mm and on the 6 mm wide beams. Expectedly, all animals performed worse on the narrower 6 mm beam when compared to the 12 mm beam. However, no differences were observed between the genotypes on neither the 12 mm nor the 6 mm thick beams for the time taken to cross as well as their scores for coordination (**Figure 45 C, D**).

Since FBXO41 is also expressed highly in the striatum and basal ganglia, I supplemented the previous experiments with the pole test, which is often used to assess basal ganglia-related motor dysfunction. Each animal was placed head-up on top of a pole whose base was placed in the home cage of the mice. Healthy mice, when placed on the pole head-up, orient themselves downward and descend down into the home cage. The animals were trained on the pole one day prior to the test day. On the test day the time taken by the animal to orient itself downward and descend down the pole was measured. Of the five trials, the best score

per animal was considered in the analyses. No significant differences were observed between the genotypes (**Figure 3.45 E**).

Taken together, these results indicate that FBXO41<sup>+/-</sup> mice show no obvious impairment in motor coordination or function even upon ageing.

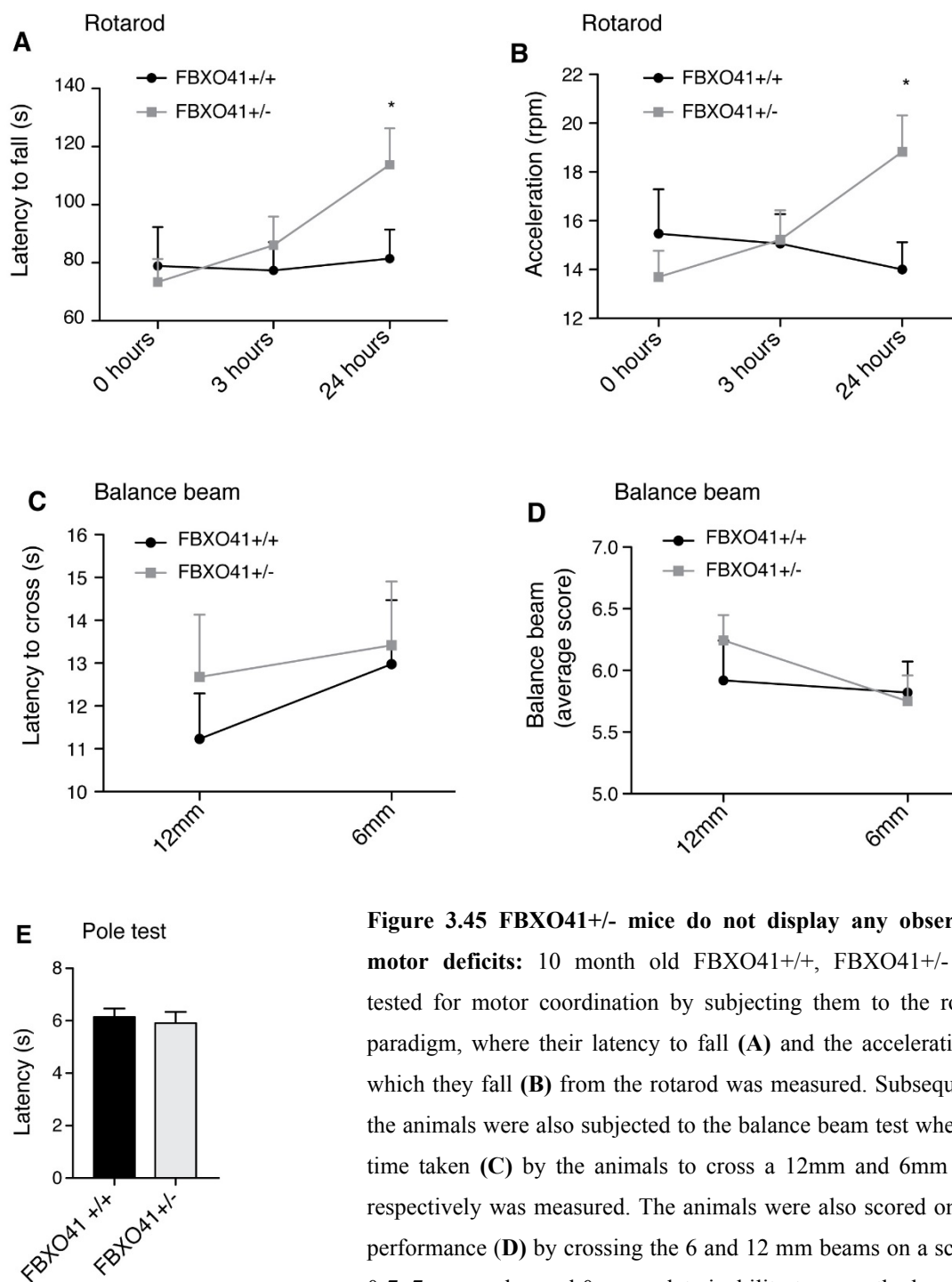


**Figure 3.45 FBXO41<sup>+/-</sup> mice do not display any observable motor deficits:** 10 month old FBXO41<sup>+/+</sup>, FBXO41<sup>+/-</sup> were tested for motor coordination by subjecting them to the rotarod paradigm, where their latency to fall (**A**) and the acceleration, at which they fall (**B**) from the rotarod was measured. Subsequently, the animals were also subjected to the balance beam test where the time taken (**C**) by the animals to cross a 12mm and 6mm beam respectively was measured. The animals were also scored on their performance (**D**) by crossing the 6 and 12 mm beams on a scale of 0-7. 7= normalcy and 0= complete inability to cross the beam. (**A-D**) A total of 17 FBXO41<sup>+/+</sup> and 23 FBXO41<sup>+/-</sup> animals were analyzed (Two-way ANOVA, \*  $p < 0.05$  mean + s.e.m). (**E**) The

time taken by the animals to reorient themselves downward and climb down a pole was measured. No differences in genotypes were observed (Student's t-test mean + s.e.m).

The aforementioned motor tests are usually used to identify obvious motor defects in rodents but often fail to point out subtle motor and gait abnormalities (*Camera et al., 2014; Sashindranath et al., 2015*). Since in the motor tests performed, FBXO41<sup>+/-</sup> mice showed no differences in comparison to their wild type littermates, I wondered if they may have minute gait abnormalities, which I may have missed. Thus to rule out this possibility, we additionally subjected the FBXO41<sup>+/-</sup> mice and their wild type littermates to Digigait analyses at 4,6 and 8 months of age (*These experiments were performed by C. Lancelin from the group of Dr. Till Marquardt at European Neuroscience Institute, Goettingen*). The Digigait analyses consists of a treadmill-like scenario for rodents, wherein the animals are made to walk along a conveyer belt moving at either constant or accelerating speeds. There is a camera placed below the conveyer belt, which records the animal walking on the conveyer belt. The software then uses the recorded movie of the animal walking to analyze various parameters such as stride lengths for each limb, paw area and so on. On analyses we found that in all the parameters analyzed the FBXO41<sup>+/-</sup> mice showed no difference when compared to their wild type littermates (*unpublished work from C. Lancelin*). These results not only corroborated previous findings that suggest that the FBXO41<sup>+/-</sup> mice show no age dependent motor deficits, but also ruled out possibilities of fine gait abnormalities.

---

## 4 Discussion

Neurodevelopmental events such as progenitor proliferation, differentiation, neuronal migration and neurite outgrowth need to be precisely timed in order to ensure the proper lamination and circuitry of the brain (*Ghashghaei et al., 2007; Hatten, 1999*). Apart from various cell-extrinsic factors, an array of cell-intrinsic regulators of neurodevelopment have been identified. The UPS and its components being one of the most recent additions to the list (*Kawabe and Brose, 2011*). E3 ligases are the most numerous of the UPS components and are critical for mediating spatial and temporal expression of proteins by recruiting specific protein substrates for ubiquitination (*Artinian et al., 2008; Hershko and Ciechanover, 1998; Hochstrasser, 1996*). Although previous studies have implicated several E3 ligases in the regulation of neurodevelopment, they still remain underexplored. A previous study from our lab identified the neuronal F-box protein FBXO41 as a potential regulator of axon growth and neuronal migration in the developing rat cerebellum (*Dr. A. Holubowska PhD thesis*). In this study, I explore the consequences of loss of FBXO41 function *in vivo*, using the FBXO41 conventional knockout mouse line. I report that FBXO41<sup>-/-</sup> mice display a severely ataxic gait together with accompanying defects in neuronal migration, axonal growth and early-onset neurodegeneration. Furthermore, I identify FBXO41-Cul7 as a novel CNS-specific E3 ligase that regulates axon growth in cerebellar granule neurons (CGNs), together with its non-proteolytic ubiquitination target NFM. Thus, providing new insights into the FBXO41-mediated pathway of axon growth control in CGNs. Taken together, this study establishes FBXO41 as a crucial regulator of cerebellar development.

### **4.1 Loss of the CNS-specific F-box protein FBXO41 results in an ataxia-like phenotype in mice along with impaired neuronal migration and neurodegeneration in the developing cerebellum:**

Neuronal migration is one of the key events that ensure proper layering and connectivity of the developing cerebellum (*Ghashghaei et al., 2007; Gleeson and Walsh, 2000*). The majority of the cerebellar development in rodents takes place postnatally, wherein the CGN precursors form a second germinal zone at the outer layer of the cerebellar anlage thereby forming the EGL. This event is followed by extensive proliferation and increase in CGN precursor numbers in the EGL and the proper migration of the newly differentiated CGNs

from the EGL, across the ML into the IGL (*Alder et al., 1996; Altman, 1972b; Marzban et al., 2014; Sillitoe and Joyner, 2007; Sotelo, 2004*). Various cell-extrinsic guidance and cell-intrinsic mechanisms that regulate the cytoskeletal dynamics also govern successful CGN migration in the cerebellum (*da Silva and Dotti, 2002; Kuijpers and Hoogenraad, 2011; Yacubova and Komuro, 2003*). A previous study from the lab identified the F-box protein FBXO41 as a cell-intrinsic regulator of neuronal migration in the developing cerebellum, showing a brain-dominant and neuronal expression that localizes to the centrosome as well as the cytoplasm (*Dr. A. Holubowska PhD thesis*). My results establish FBXO41 as a CNS-specific neuronal F-box protein with high levels of expression throughout the brain, including the cerebellum and some limited expression in the spinal cord. Using the FBXO41 knockout mouse line, I further investigated the role of FBXO41 *in vivo*.

Due to their high mortality in the first two postnatal weeks, FBXO41<sup>-/-</sup> mice were analyzed at P16. While the FBXO41<sup>+/-</sup> mice were indistinguishable from their wild type littermates, the FBXO41<sup>-/-</sup> mice displayed a severely ataxic gait characterized by uncoordinated movements, poor performance in the ledge test and rotarod and presence of severe hind limb claspings.

Upon histological analyses of the FBXO41<sup>-/-</sup> mouse brains, the most dramatic phenotype was observed in the cerebellum, which showed impaired neuronal migration. I analyzed the FBXO41<sup>-/-</sup> mice at three different ages, P12, P16 and P30 and found that all three ages showed more cells in the ML, most of which were CGNs. Interestingly, I also discovered that P12 FBXO41<sup>-/-</sup> cerebella displayed a thicker EGL as compared to wild type. Strikingly the P16 FBXO41<sup>-/-</sup> cerebella still possessed a residual EGL, while in FBXO41<sup>+/+</sup> cerebella neuronal migration was almost completed and the EGL had vanished. These findings are indicative of impaired neuronal migration. Intriguingly, the residual EGL of P16 FBXO41<sup>-/-</sup> cerebella harbored, in addition to postmitotic CGNs, mitotic precursor cells, suggesting that there could be a delay in progenitor differentiation that may also contribute to the delayed neuronal migration phenotype.

Further analysis revealed that impaired neuronal migration was CGN-specific and did not affect the Purkinje cell layer. This observation was consistent with the finding that FBXO41 is abundantly expressed in the IGL, but is completely absent from the Purkinje cells and ML. However, effects of impaired CGN migration on the synaptic connections between the Purkinje cell dendrites and parallel fibers (CGN axons) cannot be ruled out. By P30, the

residual EGL of FBXO41<sup>-/-</sup> mice had disappeared, but it still harbored more migrating CGNs when compared to the wild type. Collectively, these findings indicate that loss of FBXO41 decelerates migration of CGNs in the cerebellum, where they fail to migrate to the IGL within a developmentally appropriate time window. A similar developmental delay in CGN migration has also been reported in mouse models for the actin-binding protein profilin1 as well as the microtubule-binding protein adenomatous polyposis coli 2 (APC2) (*Kullmann et al., 2012; Shintani et al., 2012*). It is hence conceivable that FBXO41 might function as a cell-intrinsic regulator of the cytoskeleton either by directly influencing cytoskeletal dynamics or by intercepting extracellular, pro-migratory cues at the leading edge.

Previous results from the lab identified a dual localization of FBXO41 at the centrosome and the cytoplasm (*Dr. A. Holubowska PhD thesis*). The centrosome is known to serve as the major site of microtubule nucleation resulting in the formation of a microtubule cage thereby aiding in nucleokinesis and proper radial migration during neurodevelopment (*Higginbotham and Gleeson, 2007; Tsai and Gleeson, 2005*). Several centrosome-associated proteins including DISC1, NDEL1, Lis1, and the Par/aPKC complex have been previously reported to influence neuronal migration (*Kamiya et al., 2005; Sasaki et al., 2005; Solecki et al., 2004; Tanaka et al., 2004*). Interestingly, a previous study from the lab also reported that FBXO41 interacts with DISC1 and possibly NDEL1 to regulate neuronal migration (*Dr. A. Holubowska PhD thesis*). In order to establish if the centrosomal localization of FBXO41 was crucial for its neuronal migration regulating effect, we monitored the migration behavior of CGNs using *in vivo* experiments in the developing rat cerebellum. First and foremost the results showed that loss of FBXO41 is reproducible and confirms that the impaired neuronal migration phenotype observed in the FBXO41<sup>-/-</sup> mice is specifically due to loss of FBXO41. The results also suggest that the cytoplasmic FBXO41 is necessary and sufficient to stimulate neuronal migration, while the centrosomal FBXO41 has little or no influence highlighting FBXO41's centrosome-independent control of neuronal migration. This finding is both surprising and interesting. Since DISC1 for instance is also expressed extensively in the cytoplasm, nucleus and mitochondria (*James et al., 2004*), it is possible that FBXO41 interacts with DISC1 in the cytoplasm to exert its function on neuronal migration. Interestingly, FBXO41 was also previously reported to promote axon growth independent of its centrosomal localization (*Dr. A. Houlubowska, PhD Thesis*). These findings suggest that FBXO41 may have other important functions at the centrosome, e.g. regulation of progenitor proliferation and cell cycle exit, which need to be explored further.



Apart from impaired CGN migration, P30 FBXO41<sup>-/-</sup> mice also displayed abnormal foliation of the cerebellum, with reduced cerebellar size and intralobular outfoldings in folia IV and V. Since the most obvious histological phenotype observed in FBXO41<sup>-/-</sup> mice was in the cerebellum, the severely ataxic phenotype of the mice can be majorly attributed to the cerebellar defects. The absence inflammation and neurodegeneration in the P16 brain suggests that the motor phenotypes observed at P16 might be due to developmental abnormalities including impaired neuronal migration. Several studies have previously attributed ataxia-like phenotypes to dysfunction in cerebellar development, for instance a recent study reporting that deletion of the CNS-specific TGF- $\beta$  signaling protein Smad2 results in aberrant cerebellar morphology, impaired CGN migration, impaired Purkinje cell synaptic connections and early postnatal ataxia (*Wang et al., 2011*). Moreover, several human cerebellar ataxias have also been successfully modeled in mice including the Ahi1 knockout mouse, which displays abnormal cerebellar development and is viewed as a mouse model for Joubert's syndrome congenital ataxia (*Lancaster et al., 2011a*).

Interestingly, several forms of ataxias are also associated with neurodegenerative events in the cerebellum (*Assadi et al., 2008; Cummings et al., 1999*), for example the SCA1 transgenic mice modeling spinocerebellar ataxia type 1 displaying neurodegeneration of Purkinje cells as a result of nuclear localization and toxic accumulation of ataxin1 (*Klement et al., 1998*). Although the P30 FBXO41<sup>-/-</sup> cerebellum appears to catch up in neuronal migration, FBXO41<sup>-/-</sup> mice still show a persistent ataxic gait, uncoordinated movement and severe hind limb claspings. Moreover, P30 FBXO41<sup>-/-</sup> mice display a significantly smaller cerebellum together with pronounced foliation defects in folia IV, V and IV, which turned out to be a result of ongoing neurodegeneration as FBXO41<sup>-/-</sup> brains revealed a significant increase in apoptosis in the cerebella. Interestingly, the majority of the apoptotic cells appeared to be clustered in the abnormal folias. These results suggest that while the motor deficits observed at P16 are largely due to neurodevelopmental defects, the persistent motor phenotype in P30 FBXO41<sup>-/-</sup> mice as well as the reduced cerebellar size are a result of faulty wiring and compromised cerebellar architecture. Additionally, *in vitro* survival assays on cultured CGNs confirm that the observation of cell death in the FBXO41<sup>-/-</sup> brain can be attributed to loss of FBXO41. This further highlights the prosurvival nature of FBXO41, and its necessity in maintaining health and long-term integrity of neurons.

The delay in cerebellar development is accompanied by neurodegeneration and motor defects in the FBXO41<sup>-/-</sup> mice and thus accentuates the crucial function of FBXO41 in cerebellar development, cell health and proper motor coordination. The FBXO41<sup>-/-</sup> mice could hence be viewed as a model of cerebellar ataxia. Interestingly, several genes that are nowadays implicated in human cerebellar ataxias were first identified several decades ago in knockout mice models displaying cerebellar abnormalities and ataxia-like phenotypes. The staggerer mouse model, which is a knockout for the retinoic acid-related orphan nuclear receptor- $\alpha$  (ROR- $\alpha$ ), has been generated more than 50 years ago, but its interaction with ATAXIN1 and the link to spinocerebellar ataxia 1 (SCA1) has only recently been made (*Gold et al., 2003; Hamilton et al., 1996; Serra et al., 2004; Serra et al., 2006*). Similarly, human mutations in GIRD2 gene associated with cerebellar ataxia were identified 60 years after the GIRD2 gain of function mouse (lurcher) was generated (*Hills et al., 2013; Utine et al., 2013*). Most recently, mutations in the TRCP3 gene as observed in the Moonwalker mouse, have been implicated in human cerebellar ataxia (*Becker, 2014*). Since ~40% of cerebellar ataxias originate from unknown causes (*Sailer and Houlden, 2012*), it is conceivable that unidentified SNPs or mutations in the *Fbxo41* gene could be the underlying cause for some of them and hence genetic screens for mutations or variations in the *Fbxo41* gene are essential to establish the link from mouse to human cerebellar ataxias.

## **4.2 Molecular mechanisms guiding FBXO41-mediated axon growth:**

### **4.2.1 FBXO41-Cul7 is a CNS-specific neuronal E3 ligase:**

This study establishes FBXO41 as a neuronal and CNS-specific F-box protein that is highly expressed throughout the brain including the cerebellum. FBXO41 belongs to the F-box family of proteins that share a common F-box domain. Typically, most F-box proteins that form SCF complexes bind to Skp1 and cullin1 via their F-box domain (*Zheng et al., 2002*). However, unlike most F-box proteins, FBXO41 binds to Skp1 via its F-box domain, but fails to interact with cullin1. This is not surprising, as previously studies have unveiled the existence of F-box proteins that form non-canonical E3 ligase complexes that are cullin1 independent (*Skaar et al., 2013*). Previously, Saiga and colleagues identified another F-box protein FBXO45 that, similar to FBXO41, binds to Skp1 but not cullin1. Instead FBXO45 associates with the RING finger scaffold protein PAM to form a non-canonical E3 ligase,

which regulates neuronal migration and synapse formation (*Saiga et al., 2009*). Recent studies have also identified Fbxw8 as another F-box protein that, although capable of forming a standard SCF complex with cullin1, forms an alternate E3 ligase complex with Skp1 and cullin7 (*Sarikas et al., 2008*).

Cullin7 is the only other member of the cullin RING ligase family besides cullin1 that is known to bind to Skp1 and an F-box protein for substrate recognition. FBXW8 is the first identified F-box protein to assemble in an atypical SCF-like complex with cullin7 (*Sarikas et al., 2008*). My results introduce FBXO41 as the second F-box protein that assembles in an SCF-like complex with Skp1 and cullin7. While cullin1 binds to F-box proteins at their F-box domain, cullin7 on the other hand binds to Fbxw8 independent of its F-box domain (*Tsunematsu et al., 2006*). Correspondingly, through structure-function analysis using various FBXO41 deletion mutants, I observed that while FBXO41 binds to Skp1 via the F-box domain, its interaction with cullin7 is F-box-independent and is rather mediated by its N- and C- terminal domains. Further cell-based ubiquitination assays revealed that while the full-length FBXO41 harbored ligase activity and was capable of ubiquitination, deletion mutants of FBXO41 that could not bind to Skp1 (FBXO41  $\Delta$ Fbox) or cullin7 (FBXO41 aa 35-873), showed no ubiquitination activity, and were considered ligase-dead. These results establish FBXO41-Cul7 as a novel CNS-specific neuronal E3 ligase.

It is worthwhile to note that several studies have identified mutations in the *cullin7* gene, which lead to truncated cullin7 that lacks its cullin domain resulting in a non-functional protein. These mutations have been associated with the 3M syndrome and the Yakuts short stature syndrome. Both diseases are characterized by severe pre- and post-natal growth retardation, facial dysmorphism and skeletal abnormalities (*Huber et al., 2005; Maksimova et al., 2007*). The *cullin7*<sup>-/-</sup> mice have been reported to be embryonically lethal, showing intrauterine growth restrictions, placental abnormalities, and death due to respiratory distress (*Arai et al., 2003*). *Fbxw8*<sup>-/-</sup> mice, on the other hand show less severe phenotypes, but also display pre- and postnatal growth retardation and placental abnormalities. Only 30% of the *Fbxw8*<sup>-/-</sup> mice live past the first two postnatal weeks to survive until adulthood. Their body weights are only 75% of that of their wild type littermates. Apart from the growth retardation, *Fbxw8*<sup>-/-</sup> mice show no other prominent phenotypes (*Tsutsumi et al., 2008*). Interestingly, FBXO41<sup>-/-</sup> mice, similar to the *Fbxw8*<sup>-/-</sup> mice, show reduced life span, where >80% of the knockout mice die within the first two postnatal weeks. The remaining mice significantly

reduced body and brain size that already significantly differs at P5 and becomes progressively more pronounced by P16. Only few FBXO41<sup>-/-</sup> mice survive until adulthood with a lifespan of no more than 10 weeks. It is also worth noting that these knockout mice, even though gaining weight over time are always significantly smaller than their wild type littermates. In light of previous studies on cullin7<sup>-/-</sup> and Fbxw8<sup>-/-</sup> mice, the reduced lifespan as well as smaller body and brain sizes observed in the FBXO41<sup>-/-</sup> mice could be partially attributed to loss of FBXO41-Cul7 function.

#### **4.2.2 The FBXO41-Cul7–NFM pathway of axon growth control:**

Axon growth is one of the fundamental events during neurodevelopment that ensures the proper wiring and connectivity of the brain. Previous experiments in cultured rat CGNs identified FBXO41 as a cell-intrinsic regulator of axon growth. Furthermore, loss of FBXO41 resulted in shorter axons in cultured CGNs from FBXO41<sup>+/+</sup> and FBXO41<sup>-/-</sup> mice, with little or no effect on dendrites (Holubowska, 2013). Since FBXO41<sup>-/-</sup> mice display the most obvious phenotype in the cerebellum, I further analyzed the parallel fiber thickness and area occupied by white matter in the cerebella of the FBXO41<sup>-/-</sup> mice, wherein I observed significantly thinner, slightly defasciculated parallel fiber bundles in the P10 FBXO41<sup>-/-</sup> cerebella together with a progressive reduction in white matter area within the cerebellum of the FBXO41<sup>-/-</sup> mice at P12, P16 and P30. These findings support previous results from the lab and establish FBXO41 as an axon growth-promoting protein, wherein loss of FBXO41 leads to axon growth defects *in vivo*. Previously, Berglund and colleagues have demonstrated that ablation of the axon growth-regulating cell adhesion protein contactin results in severely ataxic mice, characterized by impaired CGN migration and similarly reduced thickness and defasciculation of parallel fibers along with dendritic defects in the CGNs (Berglund *et al.*, 1999). Thus, apart from being linked to impaired neuronal migration, the ataxia-like motor phenotypes in FBXO41<sup>-/-</sup> mice can also partially be attributed to defects in parallel fiber bundles *in vivo*.

Having established that FBXO41 associates with Skp1 and cullin7 to form a novel E3 ligase, I further went on to uncover the molecular mechanism governing FBXO41-mediated axon growth. Upon performing morphometric analysis of neurons, I observed that while full-length FBXO41 promoted axon growth in cultured CGNs, the ligase-dead versions of FBXO41 were unable to do so. This suggests that FBXO41 regulates axon growth in CGNs in a ligase activity-dependent manner by binding to both Skp1 and cullin7. These findings further

bolster the importance of FBXO41 in axon growth regulation and suggest that the axon growth deficits observed in FBXO41<sup>-/-</sup> mice could be due to loss of FBXO41-Cul7 E3 ligase function. A recent study from Litterman and colleagues demonstrated that Fbxw8-Cul7 regulates the morphology of Golgi apparatus and dendrites but interestingly not axon growth and patterning in rat CGNs (*Litterman et al., 2011*). Since E3 ligases are known to spatially and temporally regulate the expression of their substrates, it is conceivable that while Cul7-Fbxw8 specifically influences dendrite length, FBXO41-Cul7 is responsible for regulating axon growth in the developing cerebellum.

In order gain insight into the FBXO41-Cul7-mediated axon growth regulation, we conducted a Yeast Two-hybrid screen to identify potential interaction partners of FBXO41. From the list of candidates, I was able to identify NFM as a novel interaction partner of FBXO41. NFM is a neuron-specific, cytoskeletal protein that belongs to the family of type IV intermediate filaments. It binds and forms heteropolymers together with the three other neurofilaments NFL, NFH and  $\alpha$ -internexin (*Li et al., 2012*). NFL, NFH and NFM are structurally very similar containing a globular head, a  $\alpha$ -helical rod domain and a tail domain differing in amino acid composition. All neurofilaments contain a highly conserved rod domain, which is crucial for mediating their co-assembly and filament formation (*Bocquet et al., 2009*). The C-terminus of NFM and NFH is highly phosphorylated containing several KSP (Lys-Ser-Pro) repeats in their tail domains (*Rao et al., 2011*). NFM is predominantly expressed in the soma and in axons, where it has been implicated in regulation of radial axon growth, maintenance of axon caliber and as a result influencing its conduction velocity (*Eyer and Peterson, 1994; Garcia et al., 2003; Garcia et al., 2009; Rao et al., 2003*). My results indicate that NFM is expressed extensively in the developing cerebellum, observable from E18 onwards. This is surprising, as radial axon growth is regulated during myelination and occurs only after neurodevelopmental events including neuronal migration, axon growth and guidance have been completed (*Cleveland et al., 1991*). Several studies have previously reported internexin- $\alpha$ , NFL and NFM as one of the earliest intermediate filaments to be expressed during development much before radial axonal expansion, with NFM being expressed in conjunction with neurite formation (*Lariviere and Julien, 2004; Li et al., 2012; Pachter and Liem, 1984*). Interestingly, previous studies demonstrated that loss of NFM resulted in shorter axons and a slower axon elongation rate in *Xenopus* highlighting the potential role of NFM in axon outgrowth (*Akao et al., 1994; Walker et al., 2001*). In light of the previous studies and the high expression of NFM preceding radial axon growth, I reasoned that NFM could also play a

role in axon elongation in mammalian neurons. In this study, I explored the function of NFM in neurite extension by either using an shRNA approach that acutely knocks down NFM or using full-length NFM overexpression system. Surprisingly, both gain and loss of function of NFM resulted in an increase of axon length with no effect on dendrite length and axonal branching. Interestingly, a recent study implicated NFH, the sister-filament of NFM, and its phosphorylation in axon growth and stabilization (*Matz et al., 2015*). The study demonstrates that overexpression of NFH promotes axon growth in cultured neurons, that was similar to my observations of NFM gain of function. Owing to their similarity in structure and function, loss of either NFM or NFH has been previously reported to be compensated by increased phosphorylation of the other (*Shea and Chan, 2008*). Thus, the long axon phenotype of NFM knockdown could be in part due to compensational upregulation of NFH phosphorylation. Alternatively, it could also mean that NFM levels need to be tightly regulated for controlled axon growth. This observation, although surprising, is not unique to NFM as it is also observed in small GTPases such as Rac1, where a tight regulation of protein level is crucial for its function (*Kimberly et al., 2001*). In summary, my findings confirm the role of NFM in axon elongation and identify it as a novel regulator of axon growth in mammalian neurons.

Newly synthesized neurofilaments are transported as short heteromers along the axons via various microtubule motors, where they are highly phosphorylated by several kinases including JNK, Cdk5, MAPK and ERK1/2 (*Ackerley et al., 2003; Grant et al., 2001; Veeranna et al., 2004; Zhu et al., 2001*). The C-terminal phosphorylation of these neurofilament heteromers is crucial for integration and formation of the extremely stable internal cytoskeletal meshwork. The cytoskeletal infrastructure formed by these neurofilaments is extremely stable and is thought to be resistant to cell metabolic processes displaying a low turnover rate (*Yuan et al., 2009*). However, growing evidence suggests the presence of ubiquitinated neurofilament tangles in axons in several neurodegenerative diseases, suggesting ongoing ubiquitination and possible turnover of these cytoskeletal elements (*Gou and Leterrier, 1995; Lowe et al., 1988; Perrot et al., 2008*). The RING ligase TRIM22 was recently found to ubiquitinate and regulate the levels of NFL in several regions of the mouse brain, including the cerebellum. Loss of TRIM22 leads to an accumulation of NFL in axons, leading to neurodegeneration, and an ataxic phenotype in mice (*Balastik et al., 2008*). Having established NFM as an axon growth regulator and interactor of FBXO41, I reasoned whether NFM was an ubiquitination target of FBXO41-Cul7. After observing that NFM associates with the FBXO41-Cul7 complex, I went on to perform a cell-based

ubiquitination assay to determine if NFM was a substrate of FBXO41-Cul7. I observed that while FBXO41 full-length ubiquitinated NFM, the ligase-dead variant FBXO41 could not. Additionally, I also found that FBXO41-Cul7 ubiquitinated NFM via K63-linked polyubiquitin chains. Several studies have previously reported that K48-linked polyubiquitin chains target proteins for proteasomal degradation, while K63-linked polyubiquitination often leads to non-proteolytic events, such as DNA repair, regulation of signal transduction, kinase activation as well as lysosomal degradation (*Komander and Rape, 2012; Pickart and Eddins, 2004*). Hence, in order to understand the consequence of FBXO41-Cul7-mediated K63-linked polyubiquitination of NFM, I checked for the levels of NFM in FBXO41<sup>-/-</sup> mice, as well as in HEK293T cells transfected with either FBXO41 full-length or the ligase-dead deletion mutants FBXO41. Interestingly, I observed that loss of FBXO41 or loss of its the ligase activity resulted in decreased NFM levels, which is likely due to misregulated post-translational events rather than the transcriptional downregulation of NFM gene expression as NFM mRNA levels were unaltered. These results, when taken together identify NFM as a non-proteolytic substrate of FBXO41-Cul7, wherein it ubiquitinates and stabilizes NFM.

Gain- and loss-of function approaches to dissect the molecular relationship between NFM and FBXO41 suggest that the two interaction partners FBXO41 and NFM act in the same pathway of axon growth regulation. However, the results provide three possible interpretations or scenarios. 1) The observation that the short axon phenotype of FBXO41 knockdown was more dominant than both NFM over expression as well as NFM knockdown, suggests that FBXO41 is epistatic to NFM and thus acts downstream of NFM. This may be a possibility as NFM could influence the trafficking and distribution of FBXO41 along the axons. NFM as a cytoskeletal protein has been previously shown to bind to Myosin Va and influence the transport of organelles and distribution of axonal contents along the axon (*Rao et al., 2011*). 2) In light of the non-proteolytic substrate-ligase relationship of NFM and FBXO41-Cul7, it is also possible that lack of the FBXO41-Cul7-mediated ubiquitin modification on NFM hinders its ability to promote axon growth, thus making NFM the more downstream candidate. This is more likely, as K63-linked polyubiquitination modifications have been previously shown to influence protein function and stability (*Di Marcotullio et al., 2006*). Subsequent epistasis experiments also revealed that while FBXO41 could still promote axon growth in the absence of NFM, the full magnitude of its axon growth-promoting effect is significantly reduced without NFM. Additionally, it became apparent that only saturating amounts of both NFM and FBXO41 lead to complete stimulation of axon

growth. These results not only imply that FBXO41 and NFM act in the same pathway of axon growth, but also hint at other NFM-independent pathways of FBXO41-mediated axon growth regulation. The E3 ligase Cdh1/APC for example is known to ubiquitinate several targets such as FBXO31, Smurf1, p250GAP, SnoN and Id2, in parallel pathways to exert its function as an axon growth inhibitor (*Kannan et al., 2012a; Kannan et al., 2012b; Lasorella et al., 2006; Stegmuller et al., 2006; Vadhvani et al., 2013*). Taken together, my findings also offer a third interpretation where both scenario 1 and 2 are true. It could be that FBXO41 ubiquitinates NFM in order to stabilize, resulting in a stable cytoskeletal architecture. This could in turn could act as a feedback influencing the distribution and trafficking of FBXO41 along the axon for example to the growth cone, where it might exert its function on other downstream targets to influence axon growth. These findings highlight the complex relationship between FBXO41-Cul7 and its non-proteolytic substrate NFM.

In order to provide more clarity on the hierarchical relationship between the two, I further conducted a localization experiment to address the question whether loss of either NFM or FBXO41 influenced the cellular distribution of the other. While knockdown of NFM did not affect the localization of FBXO41, interestingly loss of FBXO41 resulted in abnormal appearance of GFP-NFM along the axons. While in control neurons, GFP-NFM was incorporated into the axonal architecture, FBXO41 RNAi neurons displayed apparent defasciculation of GFP-NFM. These results not only strengthen the notion that NFM indeed acts down stream of FBXO41, but also suggest that the interaction with FBXO41 might be crucial for the proper integration and stabilization of NFM along the axons. Recently, a study by Rao and colleagues demonstrated that the stability of the neurofilaments and their integration into the cytoskeletal network is phosphorylation-dependent. Interestingly, they demonstrate that loss of the phosphorylation tail of NFM or NFH resulted in destabilized neurofilaments that were readily turned over by the proteasome (*Rao et al., 2012*). Previously studies have also demonstrated K63-linked polyubiquitination mediated kinase activation in the NFk-B signaling pathway, where in the K63-linked polyubiquitin chains serve as scaffolds facilitating the signaling hub necessary for activation of the kinases TAK1 and IKK (*Kanayama et al., 2004*). Hence, it is plausible that the K63-linked polyubiquitin chain modification of NFM by FBXO41-Cul7, serves as a recognition or activation signal for various kinases leading to phosphorylation of NFM at its C-terminus by, thus regulating its stability and axon growth. This in part can explain the defasciculated appearance and decreased NFM levels in the absence of FBXO41. Interestingly, several studies have reported



that loss of NFM leads to severe downregulation of other neurofilaments including NFL and NFH in the axons, leading to a compromised axonal cytoskeleton (*Elder et al., 1998*). Consequently, diminished NFM levels in FBXO41<sup>-/-</sup> mice could also lead to reduced NFH and NFL.

The conventional “elongation and stabilization” model of axon growth states that axons achieve stable cytoskeletal architecture, supported by neurofilament scaffolds, only after reaching the target cell. A recent study by Lee and Shea demonstrates that NFH promoted axon growth and stabilization in differentiated NB2a/d1 cells, by means of its C-terminal phosphorylation (*Matz et al., 2015*). Owing to the structural similarity between NFM and NFH, it is plausible that NFM exerts its effect on axon growth in a similar manner. In their study, Lee and Shea propose an alternate axon growth model of “sequential stabilization”. They hypothesize, that the proximal regions of the growing axon undergoes sequential stabilization, achieved by a stable neurofilament-based cytoskeletal scaffold, which in turn provides further physical support for the distal part of the axon for continued growth and path finding. Based on their axon growth model and my experimental observations, I propose that the E3 ligase FBXO41-Cul7 regulates axon growth by ubiquitinating NFM via K63-linked polyubiquitin chains. This ubiquitin modification on NFM could directly lead to its stabilization, for example by preventing other ligases from ubiquitinating it, thus preventing its proteolytic turnover. Alternatively, the ubiquitination of NFM by FBXO41-Cul7 might serve as a signal recognition site for other posttranslational modifications, such as phosphorylation by specific kinases, ultimately leading to its stabilization. This could in turn provide the structural stability needed for further axon growth.

#### **4.3 FBXO41<sup>+/-</sup> mice do not show any signs of late onset motor phenotype:**

A previous study from the lab reported that FBXO41 is developmentally upregulated but is maintained at steady state levels in the postnatal brain including the cerebellum, suggesting post-developmental functions of FBXO41 (*Holubowska, 2013*). These might include maintenance of synapses, axonal transport and neuronal health. It is interesting to note that while FBXO41<sup>-/-</sup> mice display a striking motor phenotype characterized by an ataxic gait and uncoordinated movement at P16 as well as P30, the FBXO41<sup>+/-</sup> mice were indistinguishable from their wild type littermates. Since further analysis of the P30 FBXO41<sup>-/-</sup> mouse brains and *in vitro* cell culture experiments highlighted the role of FBXO41 in neuronal survival, I

speculated if loss of one of the FBXO41<sup>+/-</sup> gene alleles would result in an ageing-related onset behavioral phenotype, possibly as a consequence of late-onset neurodegenerative events. Hence, I subjected a 10 month-old cohort of male mice to a battery of behavioral tests to assess their general anxiety, locomotor activity, motor coordination and olfaction. At 10 months of age, I neither observed any differences in body weights nor did the genotypes show abnormal changes in anxiety when subjected to the elevated plus maze. Both genotypes had no differences in the amount of locomotor activity represented by track lengths. Interestingly, while FBXO41<sup>+/+</sup> mice preferred to spend time in the periphery of the open field close to the walls, FBXO41<sup>+/-</sup> mice showed a slight increase in the time spent in the intermediate quadrant compared to the periphery. This difference was very minute, however significant, which could be attributed to fewer numbers of wild types or be non-specific. On the other hand, it could suggest a mild decrease in anxiety levels in the FBXO41<sup>+/-</sup> mice. Some neurodegenerative disease patients as well as mouse models, for example those being affected by Parkinson's disease, display disinhibition in behavior as one of the early symptoms (*Paumier et al., 2013*). Interestingly, a recent study analyzing a Chinese Han population implicated specific SNPs in the *Fbxo41* gene as risk factors for Parkinson's Disease in females (*Liang et al., 2013*). Additionally, I analyzed the mice for signs of neurological defects by subjecting them to the hind limb clasp test. Both FBXO41<sup>+/+</sup> and FBXO41<sup>+/-</sup> mice were indistinguishable with no pronounced signs of hind limb clasp. I further subjected the animals to the balance beam test as well as rotarod to gauge their motor coordination. There was no difference between the genotypes in the balance beam test. In the rotarod test however, the FBXO41<sup>+/-</sup> mice seemed to outdo their wild type littermates, showing a steeper learning curve. This, however, should be considered as false-positive effect due to the fact that several wild type FBXO41<sup>+/+</sup> animals were unmotivated and gave up easily. Additional tests on olfaction as well as the pole test showed no difference within the two genotypes. The results of behavioral testing revealed that FBXO41<sup>+/-</sup> mice show neither signs of motor impairment nor olfactory and neurological defects, suggesting that half the dosage of *Fbxo41* is not enough to elicit obvious behavioral differences.

Even though there were no significant differences observed in motor coordination and gait between FBXO41<sup>+/+</sup> and FBXO41<sup>+/-</sup> mice, deficits in learning and memory, due to the high expression of FBXO41 in other areas of the brain, cannot be ruled out. On the other hand, the mice were only 10 months in age at the time of analysis, while most age dependent neurodegenerative models are usually studied at much older ages of 12 months or more.

Further analyses of the FBXO41<sup>+/-</sup> mice with a larger cohort should be hence performed at older ages, followed up by thorough histological analyses, in order to rule out any age dependent phenotypes.

#### **4.4 Open questions and scope for further research:**

Apart from the high expression in the cerebellum, FBXO41 is also abundantly expressed in other parts of the brain, for example the cortex, hippocampus and striatum. Hence, it is conceivable that the FBXO41<sup>-/-</sup> mice display impaired neuronal migration and deferred wiring in other regions of the brain. Analysis of the cortical and hippocampal regions at P12, P16 and P30 did not yield any obvious defects in these regions. These results suggest that either FBXO41 related impaired neuronal migration phenotype is cerebellum-specific, or that the migrational defects in the cortex or hippocampus have caught up over the course of development, which might be likely. Preliminary data from the lab for instance suggests that FBXO41<sup>-/-</sup> mice also show improper neuronal migration in the embryonic and neonatal cortex (*A.Gellerer, Master's thesis; Dr. M Vadhvani, unpublished data*). Thorough histological marker analysis of the developing cortex as well as the hippocampus would however be necessary in order to gain more clarity. Since FBXO41 is also very highly expressed in the postnatal adult brain, including the cortex, hippocampus and cerebellum, it could also serve in the formation and maintenance of synapses, which requires further investigation.

Owing to the increased apoptosis in the hippocampus it is also possible that along with the severe motor deficits the FBXO41<sup>-/-</sup> mice also suffer from impaired cognition. Interestingly, several studies have also associated the cerebellum to proper learning, memory, cognition and speech (*Boyden et al., 2004; Ferrucci et al., 2012; Marien et al., 2001; Stoodley, 2012; Strata et al., 2011; Strick et al., 2009*). For further analysis, generation of cortex and hippocampus specific conditional FBXO41<sup>-/-</sup> mice line might enable the study of the cognitive function in the FBXO41<sup>-/-</sup> mice and shed further light on FBXO41 function in other parts of the brain.

My results also indicate that FBXO41<sup>-/-</sup> mice display axon growth abnormalities in the cerebellum. Usage of cultured CGNs as a model system identified that the novel E3 ligase FBXO41-Cul7 regulates axon growth together with NFM via its non-proteolytic ubiquitnation, leading to NFM stabilization. Since FBXO41 as well as NFM are both

neuronal proteins expressed abundantly in the brain, it is likely their function in axon growth regulation is also conserved in other neuronal types. However, further experiments for example in cortical or hippocampal neurons will be important as a proof of principal. Since FBXO41 forms a cullin7 based E3 ligase it is very likely that, similar to axon growth, it also regulates neuronal migration and cell death in a ligase activity-dependent manner. Further experiments using the ligase-dead FBXO41 mutants would be necessary to confirm the same. Apart from impaired cerebellar development, defects in neuronal migration, deferred wiring of the other regions of the mouse brain could also greatly contribute to the motor symptoms observed in the FBXO41<sup>-/-</sup> mice. Further identification of FBXO41-Cul7 targets would greatly shed light on other FBXO41-mediated pathways and their implications.

#### 4.5 Conclusion:

The results from this study demonstrate that FBXO41 is indispensable for the timely migration of granule neurons during cerebellar development. Additionally, it also identifies a role for FBXO41 in neuronal survival and maintenance of proper cerebellar architecture and integrity. Behavioral analyses of the FBXO41<sup>-/-</sup> mice reveal a dramatic reduction in body size and severely ataxic gait. Since impaired cerebellar development is intimately linked to cerebellar ataxias, further research towards identifying possible mutations in the *Fbxo41* gene may perhaps contribute to resolving some of the unresolved causes of congenital ataxias. Although FBXO41 is neurodevelopmentally upregulated, it was also reported to have a high expression in the adult brain. The behavioral analyses of the adult FBXO41<sup>+/-</sup> mice however remained inconclusive in determining the role of FBXO41 in the adult brain.

At a molecular level FBXO41 has a dual localization, at the centrosome and the cytoplasm. My results identified the cytoplasmic FBXO41 to be responsible for regulating neuronal migration. Apart from regulating migration and neuronal survival, FBXO41 also promotes axon growth. In this study, I demonstrate that FBXO41 regulates axon growth in a ligase activity-dependent manner by forming the second known atypical SCF-like E3 ligase with Skp1 and cullin7. I additionally report that FBXO41-Cul7 interacts with the cytoskeletal protein NFM where FBXO41-Cul7 ubiquitinates NFM via non-proteolytic K63-linked polyubiquitination, leading to its stabilization. I further establish NFM as an axon growth-regulating protein that operates downstream of FBXO41 in axon growth control. Based on my findings in this study, I propose a working model as depicted in **Figure 4.1**. Identification

of other targets of FBXO41-Cul7 will be crucial in understanding the molecular mechanisms underlying neuronal migration, survival and identify other functions of this protein in the rest of the brain.

In conclusion, my work furthers our understanding of the F-box protein FBXO41 in the context of neurodevelopment. It provides a systematic overview of the role of FBXO41 *in vivo*, as well as gives new insights into the molecular mechanisms underlying its function, ultimately establishing FBXO41 as a key regulator of cerebellar development.

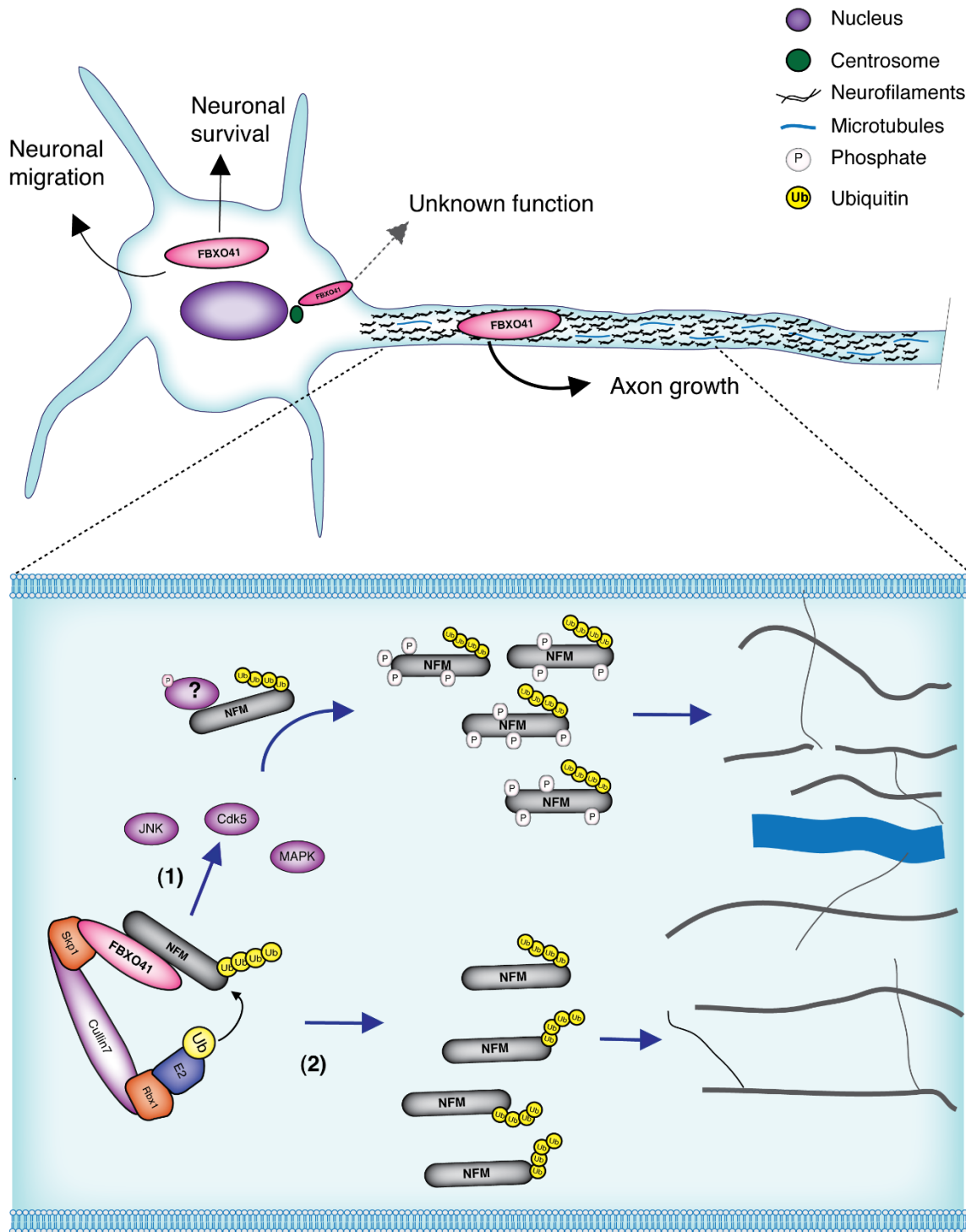


**Figure 4.1 Current working model of the F-box protein FBXO41 in cerebellar development:** the CNS-specific neuronal F-box protein FBXO41 localizes to the centrosome and the cytoplasm. While the cytoplasmic FBXO41 promotes neuronal migration and axon growth, the function of the centrosomal FBXO41 remains elusive. It additionally plays a role in neuronal survival, which appears to be crucial for the integrity of the cerebellum. FBXO41 interacts with Skp1 and cullin7 to form an atypical SCF-like E3 ligase, which promotes axon growth. The FBXO41-Cul7 ligase interacts with and ubiquitinates the neurofilament

protein NFM via non-proteolytic polyubiquitin chains, leading to its stabilization. **(1)** FBXO41-Cul7 mediated ubiquitination of NFM could directly lead to its stabilization, by preventing other types of ubiquitination from taking place that might otherwise lead to its proteolytic turnover. **(2)** NFM is a highly phosphorylated protein and, its phosphorylation is key for its stability (*Rao et al., 2012*). FBXO41-Cul7 mediated ubiquitin modification on NFM could also serve as a recognition signal for further phosphorylation of NFM leading to its stability. Both **(1)** and **(2)** would ultimately lead to stabilized NFM protein levels. NFM's integration into the growing axons might strengthen the cytoskeletal scaffold thus providing the necessary support for increased axonal elongation.

---

## 5 References

1. Ackerley, S., Thornhill, P., Grierson, A.J., Brownlees, J., Anderton, B.H., Leigh, P.N., Shaw, C.E., and Miller, C.C. (2003). Neurofilament heavy chain side arm phosphorylation regulates axonal transport of neurofilaments. *J Cell Biol* *161*, 489-495.
2. Akao, Y., Otsuki, Y., Kataoka, S., Ito, Y., and Tsujimoto, Y. (1994). Multiple Subcellular-Localization of Bcl-2 - Detection in Nuclear Outer-Membrane, Endoplasmic-Reticulum Membrane, and Mitochondrial-Membranes. *Cancer Res* *54*, 2468-2471.
3. Albus., J.S. (1989). Marr and Albus theories of the cerebellum two early models of associative memory. *Proc IEEE Comcon*.
4. Alcantara, S., Ruiz, M., De Castro, F., Soriano, E., and Sotelo, C. (2000). Netrin 1 acts as an attractive or as a repulsive cue for distinct migrating neurons during the development of the cerebellar system. *Development* *127*, 1359-1372.
5. Alder, J., Cho, N.K., and Hatten, M.E. (1996). Embryonic precursor cells from the rhombic lip are specified to a cerebellar granule neuron identity. *Neuron* *17*, 389-399.
6. Altman, J. (1972a). Postnatal development of the cerebellar cortex in the rat. 3. Maturation of the components of the granular layer. *J Comp Neurol* *145*, 465-513.
7. Altman, J. (1972b). Postnatal development of the cerebellar cortex in the rat. I. The external germinal layer and the transitional molecular layer. *J Comp Neurol* *145*, 353-397.
8. Altman, J., and Bayer, S.A. (1978). Prenatal development of the cerebellar system in the rat. I. Cytogenesis and histogenesis of the deep nuclei and the cortex of the cerebellum. *J Comp Neurol* *179*, 23-48.
9. Altman, J., and Bayer, S.A. (1985). Embryonic development of the rat cerebellum. I. Delineation of the cerebellar primordium and early cell movements. *J Comp Neurol* *231*, 1-26.
10. Arai, T., Kasper, J.S., Skaar, J.R., Ali, S.H., Takahashi, C., and DeCaprio, J.A. (2003). Targeted disruption of p185/Cul7 gene results in abnormal vascular morphogenesis. *Proc Natl Acad Sci U S A* *100*, 9855-9860.



11. Arimura, N., and Kaibuchi, K. (2007). Neuronal polarity: from extracellular signals to intracellular mechanisms. *Nat Rev Neurosci* 8, 194-205.
12. Artinian, J., McGauran, A.M., De Jaeger, X., Mouldous, L., Frances, B., and Rouillet, P. (2008). Protein degradation, as with protein synthesis, is required during not only long-term spatial memory consolidation but also reconsolidation. *Eur J Neurosci* 27, 3009-3019.
13. Aruga, J., Minowa, O., Yaginuma, H., Kuno, J., Nagai, T., Noda, T., and Mikoshiba, K. (1998). Mouse *Zic1* is involved in cerebellar development. *J Neurosci* 18, 284-293.
14. Assadi, M., Leone, P., Veloski, J.J., Schwartzman, R.J., Janson, C.G., and Campellone, J.V. (2008). Validating an Ataxia Functional Composite Scale in spinocerebellar ataxia. *J Neurol Sci* 268, 136-139.
15. Atkin, G., Hunt, J., Minakawa, E., Sharkey, L., Tipper, N., Tennant, W., and Paulson, H.L. (2014). F-box Only Protein 2 (Fbxo2) Regulates Amyloid Precursor Protein Levels and Processing. *Journal of Biological Chemistry* 289, 7038-7048.
16. Balastik, M., Ferraguti, F., Pires-da Silva, A., Lee, T.H., Alvarez-Bolado, G., Lu, K.P., and Gruss, P. (2008). Deficiency in ubiquitin ligase TRIM2 causes accumulation of neurofilament light chain and neurodegeneration. *Proc Natl Acad Sci U S A* 105, 12016-12021.
17. Becker, E.B. (2014). The Moonwalker mouse: new insights into TRPC3 function, cerebellar development, and ataxia. *Cerebellum* 13, 628-636.
18. Berglund, E.O., Murai, K.K., Fredette, B., Sekerkova, G., Marturano, B., Weber, L., Mugnaini, E., and Ranscht, B. (1999). Ataxia and abnormal cerebellar microorganization in mice with ablated contactin gene expression. *Neuron* 24, 739-750.
19. Bilimoria, P.M., and Bonni, A. (2008). Cultures of cerebellar granule neurons. *CSH Protoc* 2008, pdb prot5107.
20. Bixby, J.L., and Harris, W.A. (1991). Molecular mechanisms of axon growth and guidance. *Annu Rev Cell Biol* 7, 117-159.
21. Bocquet, A., Berges, R., Frank, R., Robert, P., Peterson, A.C., and Eyer, J. (2009). Neurofilaments bind tubulin and modulate its polymerization. *J Neurosci* 29, 11043-11054.

22. Borghesani, P.R., Peyrin, J.M., Klein, R., Rubin, J., Carter, A.R., Schwartz, P.M., Luster, A., Corfas, G., and Segal, R.A. (2002). BDNF stimulates migration of cerebellar granule cells. *Development* *129*, 1435-1442.
23. Bornstein, G., Bloom, J., Sitry-Shevah, D., Nakayama, K., Pagano, M., and Hershko, A. (2003). Role of the SCFSkp2 ubiquitin ligase in the degradation of p21Cip1 in S phase. *J Biol Chem* *278*, 25752-25757.
24. Boyden, E.S., Katoh, A., and Raymond, J.L. (2004). Cerebellum-dependent learning: the role of multiple plasticity mechanisms. *Annu Rev Neurosci* *27*, 581-609.
25. Camera, D., Boase, N.A., Kumar, S., Pow, D.V., and Poronnik, P. (2014). Subtle gait abnormalities in Nedd4 heterozygous mice. *Behav Brain Res* *260*, 15-24.
26. Carrano, A.C., Eytan, E., Hershko, A., and Pagano, M. (1999). SKP2 is required for ubiquitin-mediated degradation of the CDK inhibitor p27. *Nat Cell Biol* *1*, 193-199.
27. Casazza, A., Fazzari, P., and Tamagnone, L. (2007). Semaphorin signals in cell adhesion and cell migration: functional role and molecular mechanisms. *Adv Exp Med Biol* *600*, 90-108.
28. Cerminara, N.L., Lang, E.J., Sillitoe, R.V., and Apps, R. (2015). Redefining the cerebellar cortex as an assembly of non-uniform Purkinje cell microcircuits. *Nat Rev Neurosci* *16*, 79-93.
29. Chedotal, A. (2010). Should I stay or should I go? Becoming a granule cell. *Trends Neurosci* *33*, 163-172.
30. Chen, C.P., Chern, S.R., Shih, J.C., Wang, W., Yeh, L.F., Chang, T.Y., and Tzen, C.Y. (2001). Prenatal diagnosis and genetic analysis of type I and type II thanatophoric dysplasia. *Prenat Diagn* *21*, 89-95.
31. Chen, X., Wang, X., Sun, C., Chen, Q., O'Neill, F.A., Walsh, D., Fanous, A., and Kendler, K.S. (2008). FBXL21 association with schizophrenia in Irish family and case-control samples. *Am J Med Genet B Neuropsychiatr Genet* *147B*, 1231-1237.
32. Chizhikov, V., and Millen, K.J. (2003). Development and malformations of the cerebellum in mice. *Mol Genet Metab* *80*, 54-65.
33. Cleveland, D.W., Monteiro, M.J., Wong, P.C., Gill, S.R., Gearhart, J.D., and Hoffman, P.N. (1991). Involvement of neurofilaments in the radial growth of axons. *J Cell Sci Suppl* *15*, 85-95.

34. Connell-Crowley, L., Le Gall, M., Vo, D.J., and Giniger, E. (2000). The cyclin-dependent kinase Cdk5 controls multiple aspects of axon patterning in vivo. *Curr Biol* 10, 599-602.
35. Coskun, V., and Luskin, M.B. (2002). Intrinsic and extrinsic regulation of the proliferation and differentiation of cells in the rodent rostral migratory stream. *J Neurosci Res* 69, 795-802.
36. Cummings, C.J., Reinstein, E., Sun, Y., Antalffy, B., Jiang, Y., Ciechanover, A., Orr, H.T., Beaudet, A.L., and Zoghbi, H.Y. (1999). Mutation of the E6-AP ubiquitin ligase reduces nuclear inclusion frequency while accelerating polyglutamine-induced pathology in SCA1 mice. *Neuron* 24, 879-892.
37. D'Arca, D., Zhao, X., Xu, W., Ramirez-Martinez, N.C., Iavarone, A., and Lasorella, A. (2010). Huwe1 ubiquitin ligase is essential to synchronize neuronal and glial differentiation in the developing cerebellum. *Proc Natl Acad Sci U S A* 107, 5875-5880.
38. da Silva, J.S., and Dotti, C.G. (2002). Breaking the neuronal sphere: regulation of the actin cytoskeleton in neuritogenesis. *Nat Rev Neurosci* 3, 694-704.
39. Dent, E.W., and Gertler, F.B. (2003). Cytoskeletal dynamics and transport in growth cone motility and axon guidance. *Neuron* 40, 209-227.
40. Dent, E.W., Gupton, S.L., and Gertler, F.B. (2011). The growth cone cytoskeleton in axon outgrowth and guidance. *Cold Spring Harb Perspect Biol* 3.
41. Deshaies, R.J. (1999). SCF and Cullin/Ring H2-based ubiquitin ligases. *Annu Rev Cell Dev Biol* 15, 435-467.
42. Deshaies, R.J., and Joazeiro, C.A. (2009). RING domain E3 ubiquitin ligases. *Annu Rev Biochem* 78, 399-434.
43. Di Fonzo, A., Dekker, M.C., Montagna, P., Baruzzi, A., Yonova, E.H., Correia Guedes, L., Szczerbinska, A., Zhao, T., Dubbel-Hulsman, L.O., Wouters, C.H., *et al.* (2009). FBXO7 mutations cause autosomal recessive, early-onset parkinsonian-pyramidal syndrome. *Neurology* 72, 240-245.
44. Di Marcotullio, L., Ferretti, E., Greco, A., De Smaele, E., Po, A., Sico, M.A., Alimandi, M., Giannini, G., Maroder, M., Screpanti, I., *et al.* (2006). Numb is a suppressor of Hedgehog signalling and targets Gli1 for Itch-dependent ubiquitination. *Nat Cell Biol* 8, 1415-1423.

45. Dietrich, D.R. (1993). Toxicological and pathological applications of proliferating cell nuclear antigen (PCNA), a novel endogenous marker for cell proliferation. *Crit Rev Toxicol* 23, 77-109.
46. Eccles, J.C., Llinas, R., and Sasaki, K. (1966a). The excitatory synaptic action of climbing fibres on the Purkinje cells of the cerebellum. *J Physiol* 182, 268-296.
47. Eccles, J.C., Llinas, R., and Sasaki, K. (1966b). The mossy fibre-granule cell relay of the cerebellum and its inhibitory control by Golgi cells. *Exp Brain Res* 1, 82-101.
48. Eccles, J.C., Llinas, R., and Sasaki, K. (1966c). Parallel fibre stimulation and the responses induced thereby in the Purkinje cells of the cerebellum. *Exp Brain Res* 1, 17-39.
49. Edmondson, J.C., and Hatten, M.E. (1987). Glial-guided granule neuron migration in vitro: a high-resolution time-lapse video microscopic study. *J Neurosci* 7, 1928-1934.
50. Elder, G.A., Friedrich, V.L., Jr., Bosco, P., Kang, C., Gourov, A., Tu, P.H., Lee, V.M., and Lazzarini, R.A. (1998). Absence of the mid-sized neurofilament subunit decreases axonal calibers, levels of light neurofilament (NF-L), and neurofilament content. *J Cell Biol* 141, 727-739.
51. Eyer, J., and Peterson, A. (1994). Neurofilament-deficient axons and perikaryal aggregates in viable transgenic mice expressing a neurofilament-beta-galactosidase fusion protein. *Neuron* 12, 389-405.
52. Fang, W.K., Ko, F.Y., Wang, H.L., Kuo, C.H., Chen, L.M., Tsai, F.J., Tsai, C.H., Chen, Y.S., Kuo, W.W., and Huang, C.Y. (2009). The proliferation and migration effects of huangqi on RSC96 Schwann cells. *Am J Chin Med* 37, 945-959.
53. Feldman, R.M., Correll, C.C., Kaplan, K.B., and Deshaies, R.J. (1997). A complex of Cdc4p, Skp1p, and Cdc53p/cullin catalyzes ubiquitination of the phosphorylated CDK inhibitor Sic1p. *Cell* 91, 221-230.
54. Ferrucci, R., Giannicola, G., Rosa, M., Fumagalli, M., Boggio, P.S., Hallett, M., Zago, S., and Priori, A. (2012). Cerebellum and processing of negative facial emotions: cerebellar transcranial DC stimulation specifically enhances the emotional recognition of facial anger and sadness. *Cogn Emot* 26, 786-799.
55. Forget, A., Bihannic, L., Cigna, S.M., Lefevre, C., Remke, M., Barnat, M., Dodier, S., Shirvani, H., Mercier, A., Mensah, A., *et al.* (2014). Shh signaling protects Atoh1 from degradation mediated by the E3 ubiquitin ligase Huwe1 in neural precursors. *Dev Cell* 29, 649-661.

56. Frank, C.L., and Tsai, L.H. (2009). Alternative functions of core cell cycle regulators in neuronal migration, neuronal maturation, and synaptic plasticity. *Neuron* 62, 312-326.
57. Frescas, D., and Pagano, M. (2008). Deregulated proteolysis by the F-box proteins SKP2 and beta-TrCP: tipping the scales of cancer. *Nat Rev Cancer* 8, 438-449.
58. Garcia, M.L., Lobsiger, C.S., Shah, S.B., Deerinck, T.J., Crum, J., Young, D., Ward, C.M., Crawford, T.O., Gotow, T., Uchiyama, Y., *et al.* (2003). NF-M is an essential target for the myelin-directed "outside-in" signaling cascade that mediates radial axonal growth. *J Cell Biol* 163, 1011-1020.
59. Garcia, M.L., Rao, M.V., Fujimoto, J., Garcia, V.B., Shah, S.B., Crum, J., Gotow, T., Uchiyama, Y., Ellisman, M., Calcutt, N.A., *et al.* (2009). Phosphorylation of highly conserved neurofilament medium KSP repeats is not required for myelin-dependent radial axonal growth. *J Neurosci* 29, 1277-1284.
60. Ghashghaei, H.T., Lai, C., and Anton, E.S. (2007). Neuronal migration in the adult brain: are we there yet? *Nat Rev Neurosci* 8, 141-151.
61. Gleeson, J.G., and Walsh, C.A. (2000). Neuronal migration disorders: from genetic diseases to developmental mechanisms. *Trends Neurosci* 23, 352-359.
62. Glickstein, M., and Doron, K. (2008). Cerebellum: connections and functions. *Cerebellum* 7, 589-594.
63. Gold, D.A., Baek, S.H., Schork, N.J., Rose, D.W., Larsen, D.D., Sachs, B.D., Rosenfeld, M.G., and Hamilton, B.A. (2003). RORalpha coordinates reciprocal signaling in cerebellar development through sonic hedgehog and calcium-dependent pathways. *Neuron* 40, 1119-1131.
64. Goldowitz, D., and Hamre, K. (1998). The cells and molecules that make a cerebellum. *Trends Neurosci* 21, 375-382.
65. Goley, E.D., Ohkawa, T., Mancuso, J., Woodruff, J.B., D'Alessio, J.A., Cande, W.Z., Volkman, L.E., and Welch, M.D. (2006). Dynamic nuclear actin assembly by Arp2/3 complex and a baculovirus WASP-like protein. *Science* 314, 464-467.
66. Goley, E.D., and Welch, M.D. (2006). The ARP2/3 complex: an actin nucleator comes of age. *Nat Rev Mol Cell Biol* 7, 713-726.
67. Gong, B., Chen, F., Pan, Y., Arrieta-Cruz, I., Yoshida, Y., Haroutunian, V., and Pasinetti, G.M. (2010). SCFFbx2-E3-ligase-mediated degradation of BACE1

- attenuates Alzheimer's disease amyloidosis and improves synaptic function. *Aging Cell* 9, 1018-1031.
68. Gonzalez-Billault, C., Jimenez-Mateos, E.M., Caceres, A., Diaz-Nido, J., Wandosell, F., and Avila, J. (2004). Microtubule-associated protein 1B function during normal development, regeneration, and pathological conditions in the nervous system. *J Neurobiol* 58, 48-59.
69. Gou, J.P., and Leterrier, J.F. (1995). Possible involvement of ubiquitination in neurofilament degradation. *Biochem Biophys Res Commun* 217, 529-538.
70. Govek, E.E., Hatten, M.E., and Van Aelst, L. (2011). The role of Rho GTPase proteins in CNS neuronal migration. *Dev Neurobiol* 71, 528-553.
71. Grant, P., Sharma, P., and Pant, H.C. (2001). Cyclin-dependent protein kinase 5 (Cdk5) and the regulation of neurofilament metabolism. *Eur J Biochem* 268, 1534-1546.
72. Guyenet, S.J., Furrer, S.A., Damian, V.M., Baughan, T.D., La Spada, A.R., and Garden, G.A. (2010). A simple composite phenotype scoring system for evaluating mouse models of cerebellar ataxia. *J Vis Exp*.
73. Hamilton, B.A., Frankel, W.N., Kerrebrock, A.W., Hawkins, T.L., FitzHugh, W., Kusumi, K., Russell, L.B., Mueller, K.L., van Berkel, V., Birren, B.W., *et al.* (1996). Disruption of the nuclear hormone receptor RORalpha in staggerer mice. *Nature* 379, 736-739.
74. Hatten, M.E. (1985). Neuronal regulation of astroglial morphology and proliferation in vitro. *J Cell Biol* 100, 384-396.
75. Hatten, M.E. (1999). Central nervous system neuronal migration. *Annu Rev Neurosci* 22, 511-539.
76. Hatten, M.E., and Heintz, N. (1995). Mechanisms of neural patterning and specification in the developing cerebellum. *Annu Rev Neurosci* 18, 385-408.
77. Heintz, N., and Zoghbi, H.Y. (2000). Insights from mouse models into the molecular basis of neurodegeneration. *Annu Rev Physiol* 62, 779-802.
78. Hershko, A., and Ciechanover, A. (1998). The ubiquitin system. *Annu Rev Biochem* 67, 425-479.
79. Higginbotham, H.R., and Gleeson, J.G. (2007). The centrosome in neuronal development. *Trends Neurosci* 30, 276-283.

80. Hills, L.B., Masri, A., Konno, K., Kakegawa, W., Lam, A.T., Lim-Melia, E., Chandy, N., Hill, R.S., Partlow, J.N., Al-Saffar, M., *et al.* (2013). Deletions in GRID2 lead to a recessive syndrome of cerebellar ataxia and tonic upgaze in humans. *Neurology* *81*, 1378-1386.
81. Hirai, S., Cui de, F., Miyata, T., Ogawa, M., Kiyonari, H., Suda, Y., Aizawa, S., Banba, Y., and Ohno, S. (2006). The c-Jun N-terminal kinase activator dual leucine zipper kinase regulates axon growth and neuronal migration in the developing cerebral cortex. *J Neurosci* *26*, 11992-12002.
82. Hochstrasser, M. (1996). Ubiquitin-dependent protein degradation. *Annu Rev Genet* *30*, 405-439.
83. Holubowska, A., Mukherjee, C., Vadhvani, M., and Stegmuller, J. (2014). Genetic manipulation of cerebellar granule neurons in vitro and in vivo to study neuronal morphology and migration. *J Vis Exp*.
84. Holubowska, D.A. (2013). Characterization of the CNS-specific F-box protein in cerebellar development.
85. Hossain, W.A., and Morest, D.K. (2000). Fibroblast growth factors (FGF-1, FGF-2) promote migration and neurite growth of mouse cochlear ganglion cells in vitro: immunohistochemistry and antibody perturbation. *J Neurosci Res* *62*, 40-55.
86. Huard, J.M., Forster, C.C., Carter, M.L., Sicinski, P., and Ross, M.E. (1999). Cerebellar histogenesis is disturbed in mice lacking cyclin D2. *Development* *126*, 1927-1935.
87. Huber, C., Dias-Santagata, D., Glaser, A., O'Sullivan, J., Brauner, R., Wu, K., Xu, X., Pearce, K., Wang, R., Uzielli, M.L., *et al.* (2005). Identification of mutations in CUL7 in 3-M syndrome. *Nat Genet* *37*, 1119-1124.
88. Ito, M. (2002a). Historical review of the significance of the cerebellum and the role of Purkinje cells in motor learning. *Ann N Y Acad Sci* *978*, 273-288.
89. Ito, M. (2002b). The molecular organization of cerebellar long-term depression. *Nat Rev Neurosci* *3*, 896-902.
90. Ito, M. (2006). Cerebellar circuitry as a neuronal machine. *Prog Neurobiol* *78*, 272-303.
91. Itoh, M., Li, S., Ohta, K., Yamada, A., Hayakawa-Yano, Y., Ueda, M., Hida, Y., Suzuki, Y., Ohta, E., Mizuno, A., *et al.* (2011). Cayman ataxia-related protein is a presynapse-specific caspase-3 substrate. *Neurochem Res* *36*, 1304-1313.

92. James, R., Adams, R.R., Christie, S., Buchanan, S.R., Porteous, D.J., and Millar, J.K. (2004). Disrupted in Schizophrenia 1 (DISC1) is a multicompartimentalized protein that predominantly localizes to mitochondria. *Mol Cell Neurosci* 26, 112-122.
93. Jandke, A., Da Costa, C., Sancho, R., Nye, E., Spencer-Dene, B., and Behrens, A. (2011). The F-box protein Fbw7 is required for cerebellar development. *Dev Biol* 358, 201-212.
94. Jin, J., Cardozo, T., Lovering, R.C., Elledge, S.J., Pagano, M., and Harper, J.W. (2004). Systematic analysis and nomenclature of mammalian F-box proteins. *Genes Dev* 18, 2573-2580.
95. Kalil, K., and Dent, E.W. (2005). Touch and go: guidance cues signal to the growth cone cytoskeleton. *Curr Opin Neurobiol* 15, 521-526.
96. Kamiya, A., Kubo, K., Tomoda, T., Takaki, M., Youn, R., Ozeki, Y., Sawamura, N., Park, U., Kudo, C., Okawa, M., *et al.* (2005). A schizophrenia-associated mutation of DISC1 perturbs cerebral cortex development. *Nat Cell Biol* 7, 1167-1178.
97. Kanayama, A., Seth, R.B., Sun, L., Ea, C.K., Hong, M., Shaito, A., Chiu, Y.H., Deng, L., and Chen, Z.J. (2004). TAB2 and TAB3 activate the NF-kappaB pathway through binding to polyubiquitin chains. *Mol Cell* 15, 535-548.
98. Kannan, M., Lee, S.J., Schwedhelm-Domeyer, N., Nakazawa, T., and Stegmuller, J. (2012a). p250GAP is a novel player in the Cdh1-APC/Smurf1 pathway of axon growth regulation. *PLoS One* 7, e50735.
99. Kannan, M., Lee, S.J., Schwedhelm-Domeyer, N., and Stegmuller, J. (2012b). The E3 ligase Cdh1-anaphase promoting complex operates upstream of the E3 ligase Smurf1 in the control of axon growth. *Development* 139, 3600-3612.
100. Kawabe, H., and Brose, N. (2011). The role of ubiquitylation in nerve cell development. *Nat Rev Neurosci* 12, 251-268.
101. Kawaji, K., Umeshima, H., Eiraku, M., Hirano, T., and Kengaku, M. (2004). Dual phases of migration of cerebellar granule cells guided by axonal and dendritic leading processes. *Mol Cell Neurosci* 25, 228-240.
102. Kennedy, T.E. (2000). Cellular mechanisms of netrin function: long-range and short-range actions. *Biochem Cell Biol* 78, 569-575.
103. Kerjan, G., Dolan, J., Haumaitre, C., Schneider-Maunoury, S., Fujisawa, H., Mitchell, K.J., and Chedotal, A. (2005). The transmembrane semaphorin Sema6A controls cerebellar granule cell migration. *Nat Neurosci* 8, 1516-1524.



104. Kim, A.H., Puram, S.V., Bilimoria, P.M., Ikeuchi, Y., Keough, S., Wong, M., Rowitch, D., and Bonni, A. (2009). A centrosomal Cdc20-APC pathway controls dendrite morphogenesis in postmitotic neurons. *Cell* *136*, 322-336.
105. Kimberly, W.T., Zheng, J.B., Guenette, S.Y., and Selkoe, D.J. (2001). The intracellular domain of the beta-amyloid precursor protein is stabilized by Fe65 and translocates to the nucleus in a Notch-like manner. *Journal of Biological Chemistry* *276*, 40288-40292.
106. Kipreos, E.T., and Pagano, M. (2000). The F-box protein family. *Genome Biol* *1*, REVIEWS3002.
107. Klement, I.A., Skinner, P.J., Kaytor, M.D., Yi, H., Hersch, S.M., Clark, H.B., Zoghbi, H.Y., and Orr, H.T. (1998). Ataxin-1 nuclear localization and aggregation: role in polyglutamine-induced disease in SCA1 transgenic mice. *Cell* *95*, 41-53.
108. Knoepfler, P.S., Cheng, P.F., and Eisenman, R.N. (2002). N-myc is essential during neurogenesis for the rapid expansion of progenitor cell populations and the inhibition of neuronal differentiation. *Genes Dev* *16*, 2699-2712.
109. Komander, D., and Rape, M. (2012). The Ubiquitin Code. *Annu Rev Biochem* *81*, 203-229.
110. Komuro, H., and Yacubova, E. (2003). Recent advances in cerebellar granule cell migration. *Cell Mol Life Sci* *60*, 1084-1098.
111. Komuro, H., Yacubova, E., and Rakic, P. (2001). Mode and tempo of tangential cell migration in the cerebellar external granular layer. *J Neurosci* *21*, 527-540.
112. Konishi, Y., Stegmuller, J., Matsuda, T., Bonni, S., and Bonni, A. (2004). Cdh1-APC controls axonal growth and patterning in the mammalian brain. *Science* *303*, 1026-1030.
113. Kuijpers, M., and Hoogenraad, C.C. (2011). Centrosomes, microtubules and neuronal development. *Mol Cell Neurosci* *48*, 349-358.
114. Kullander, K., and Klein, R. (2002). Mechanisms and functions of Eph and ephrin signalling. *Nat Rev Mol Cell Biol* *3*, 475-486.
115. Kullmann, J.A., Neumeier, A., Gurniak, C.B., Friauf, E., Witke, W., and Rust, M.B. (2012). Profilin1 is required for glial cell adhesion and radial migration of cerebellar granule neurons. *EMBO Rep* *13*, 75-82.

116. Kurtz, P., Schuurman, T., and Prinz, H. (1989). Loss of smell leads to dementia in mice: is Alzheimer's disease a degenerative disorder of the olfactory system? *J Protein Chem* 8, 448-451.
117. Lai Wing Sun, K., Correia, J.P., and Kennedy, T.E. (2011). Netrins: versatile extracellular cues with diverse functions. *Development* 138, 2153-2169.
118. Lalonde, R., and Strazielle, C. (2001). Motor performance and regional brain metabolism of spontaneous murine mutations with cerebellar atrophy. *Behav Brain Res* 125, 103-108.
119. Lancaster, M.A., Gopal, D.J., Kim, J., Saleem, S.N., Silhavy, J.L., Louie, C.M., Thacker, B.E., Williams, Y., Zaki, M.S., and Gleeson, J.G. (2011a). Defective Wnt-dependent cerebellar midline fusion in a mouse model of Joubert syndrome. *Nat Med* 17, 726-731.
120. Lancaster, M.A., Schroth, J., and Gleeson, J.G. (2011b). Subcellular spatial regulation of canonical Wnt signalling at the primary cilium. *Nat Cell Biol* 13, 700-707.
121. Langerveld, A.J., Mihalko, D., DeLong, C., Walburn, J., and Ide, C.F. (2007). Gene expression changes in postmortem tissue from the rostral pons of multiple system atrophy patients. *Mov Disord* 22, 766-777.
122. Lappe-Siefke, C., Goebbels, S., Gravel, M., Nicksch, E., Lee, J., Braun, P.E., Griffiths, I.R., and Nave, K.A. (2003). Disruption of *Cnp1* uncouples oligodendroglial functions in axonal support and myelination. *Nat Genet* 33, 366-374.
123. Lariviere, R.C., and Julien, J.P. (2004). Functions of intermediate filaments in neuronal development and disease. *J Neurobiol* 58, 131-148.
124. Lasorella, A., Stegmuller, J., Guardavaccaro, D., Liu, G., Carro, M.S., Rothschild, G., de la Torre-Ubieta, L., Pagano, M., Bonni, A., and Iavarone, A. (2006). Degradation of Id2 by the anaphase-promoting complex couples cell cycle exit and axonal growth. *Nature* 442, 471-474.
125. Leggio, M.G., Molinari, M., Neri, P., Graziano, A., Mandolesi, L., and Petrosini, L. (2000). Representation of actions in rats: the role of cerebellum in learning spatial performances by observation. *Proc Natl Acad Sci U S A* 97, 2320-2325.

126. Lewis, T.L., Jr., Courchet, J., and Polleux, F. (2013). Cell biology in neuroscience: Cellular and molecular mechanisms underlying axon formation, growth, and branching. *J Cell Biol* 202, 837-848.
127. Li, F., Liu, S., Ouyang, Y., Fan, C., Wang, T., Zhang, C., Zeng, B., Chai, Y., and Wang, X. (2012). Effect of celecoxib on proliferation, collagen expression, ERK1/2 and SMAD2/3 phosphorylation in NIH/3T3 fibroblasts. *Eur J Pharmacol* 678, 1-5.
128. Liang, H., Song, Z., Lei, J., Tang, J., Xu, H., Deng, X., Qi, Y., Zheng, W., and Deng, H. (2013). Genetic analysis of the F-box only protein 41 gene in Chinese Han patients with Parkinson's disease. *Parkinsonism Relat Disord* 19, 918-920.
129. Litterman, N., Ikeuchi, Y., Gallardo, G., O'Connell, B.C., Sowa, M.E., Gygi, S.P., Harper, J.W., and Bonni, A. (2011). An OBSL1-Cul7Fbxw8 ubiquitin ligase signaling mechanism regulates Golgi morphology and dendrite patterning. *Plos Biol* 9, e1001060.
130. Liu, Z., Lin, X., Cai, Z., Zhang, Z., Han, C., Jia, S., Meng, A., and Wang, Q. (2011). Global identification of SMAD2 target genes reveals a role for multiple co-regulatory factors in zebrafish early gastrulas. *J Biol Chem* 286, 28520-28532.
131. Lowe, J., Blanchard, A., Morrell, K., Lennox, G., Reynolds, L., Billett, M., Landon, M., and Mayer, R.J. (1988). Ubiquitin is a common factor in intermediate filament inclusion bodies of diverse type in man, including those of Parkinson's disease, Pick's disease, and Alzheimer's disease, as well as Rosenthal fibres in cerebellar astrocytomas, cytoplasmic bodies in muscle, and mallory bodies in alcoholic liver disease. *J Pathol* 155, 9-15.
132. Lowery, L.A., and Van Vactor, D. (2009). The trip of the tip: understanding the growth cone machinery. *Nat Rev Mol Cell Biol* 10, 332-343.
133. Luong, T.N., Carlisle, H.J., Southwell, A., and Patterson, P.H. (2011). Assessment of motor balance and coordination in mice using the balance beam. *J Vis Exp*.
134. Maksimova, N., Hara, K., Miyashia, A., Nikolaeva, I., Shiga, A., Nogovicina, A., Sukhomyasova, A., Argunov, V., Shvedova, A., Ikeuchi, T., *et al.* (2007). Clinical, molecular and histopathological features of short stature syndrome with novel CUL7 mutation in Yakuts: new population isolate in Asia. *J Med Genet* 44, 772-778.

135. Marien, P., Engelborghs, S., Fabbro, F., and De Deyn, P.P. (2001). The lateralized linguistic cerebellum: a review and a new hypothesis. *Brain Lang* 79, 580-600.
136. Marin, O., Plump, A.S., Flames, N., Sanchez-Camacho, C., Tessier-Lavigne, M., and Rubenstein, J.L. (2003). Directional guidance of interneuron migration to the cerebral cortex relies on subcortical Slit1/2-independent repulsion and cortical attraction. *Development* 130, 1889-1901.
137. Marin, O., and Rubenstein, J.L. (2001). A long, remarkable journey: tangential migration in the telencephalon. *Nat Rev Neurosci* 2, 780-790.
138. Mark F Bear, M.A.P., Barry. W Connors (2006). *Exploring the brain*. Lippincott Williams & Wilkins.
139. Marras, C., Goldman, S., Smith, A., Barney, P., Aston, D., Comyns, K., Korell, M., Langston, J.W., Ross, G.W., and Tanner, C.M. (2005). Smell identification ability in twin pairs discordant for Parkinson's disease. *Mov Disord* 20, 687-693.
140. Marzban, H., Del Bigio, M.R., Alizadeh, J., Ghavami, S., Zachariah, R.M., and Rastegar, M. (2014). Cellular commitment in the developing cerebellum. *Front Cell Neurosci* 8, 450.
141. Matsuura, K., Kabuto, H., Makino, H., and Ogawa, N. (1997). Pole test is a useful method for evaluating the mouse movement disorder caused by striatal dopamine depletion. *J Neurosci Methods* 73, 45-48.
142. Matz, A., Lee, S.J., Schwedhelm-Domeyer, N., Zanini, D., Holubowska, A., Kannan, M., Farnworth, M., Jahn, O., Gopfert, M.C., and Stegmuller, J. (2015). Regulation of neuronal survival and morphology by the E3 ubiquitin ligase RNF157. *Cell Death Differ* 22, 626-642.
143. Mauk, M.D., Medina, J.F., Nores, W.L., and Ohyama, T. (2000). Cerebellar function: coordination, learning or timing? *Curr Biol* 10, R522-525.
144. Maupin-Furlow, J. (2012). Proteasomes and protein conjugation across domains of life. *Nat Rev Microbiol* 10, 100-111.
145. Middleton, F.A., and Strick, P.L. (1998). The cerebellum: an overview. *Trends Neurosci* 21, 367-369.
146. Millen, K.J., and Gleeson, J.G. (2008). Cerebellar development and disease. *Curr Opin Neurobiol* 18, 12-19.

147. Mir, A., Sritharan, K., Mittal, K., Vasli, N., Araujo, C., Jamil, T., Rafiq, M.A., Anwar, Z., Mikhailov, A., Rauf, S., *et al.* (2014). Truncation of the E3 ubiquitin ligase component FBXO31 causes non-syndromic autosomal recessive intellectual disability in a Pakistani family. *Hum Genet* *133*, 975-984.
148. Miyata, T., Maeda, T., and Lee, J.E. (1999). NeuroD is required for differentiation of the granule cells in the cerebellum and hippocampus. *Genes Dev* *13*, 1647-1652.
149. Miyazawa, K., Himi, T., Garcia, V., Yamagishi, H., Sato, S., and Ishizaki, Y. (2000). A role for p27/Kip1 in the control of cerebellar granule cell precursor proliferation. *J Neurosci* *20*, 5756-5763.
150. Moore, D.L., and Goldberg, J.L. (2011). Multiple transcription factor families regulate axon growth and regeneration. *Dev Neurobiol* *71*, 1186-1211.
151. Nadarajah, B., and Parnavelas, J.G. (2002). Modes of neuronal migration in the developing cerebral cortex. *Nat Rev Neurosci* *3*, 423-432.
152. Nakayama, K., Nagahama, H., Minamishima, Y.A., Miyake, S., Ishida, N., Hatakeyama, S., Kitagawa, M., Iemura, S., Natsume, T., and Nakayama, K.I. (2004). Skp2-mediated degradation of p27 regulates progression into mitosis. *Dev Cell* *6*, 661-672.
153. Narayan, S., Tang, B., Head, S.R., Gilmartin, T.J., Sutcliffe, J.G., Dean, B., and Thomas, E.A. (2008). Molecular profiles of schizophrenia in the CNS at different stages of illness. *Brain Res* *1239*, 235-248.
154. Ohshima, T., Gilmore, E.C., Longenecker, G., Jacobowitz, D.M., Brady, R.O., Herrup, K., and Kulkarni, A.B. (1999). Migration defects of cdk5(-/-) neurons in the developing cerebellum is cell autonomous. *J Neurosci* *19*, 6017-6026.
155. Pachter, J.S., and Liem, R.K. (1984). The differential appearance of neurofilament triplet polypeptides in the developing rat optic nerve. *Dev Biol* *103*, 200-210.
156. Paisan-Ruiz, C., Guevara, R., Federoff, M., Hanagasi, H., Sina, F., Elahi, E., Schneider, S.A., Schwingenschuh, P., Bajaj, N., Emre, M., *et al.* (2010). Early-onset L-dopa-responsive parkinsonism with pyramidal signs due to ATP13A2, PLA2G6, FBXO7 and spatacsin mutations. *Mov Disord* *25*, 1791-1800.
157. Pak, C.W., Flynn, K.C., and Bamburg, J.R. (2008). Actin-binding proteins take the reins in growth cones. *Nat Rev Neurosci* *9*, 136-147.

158. Pasterkamp, R.J., and Kolodkin, A.L. (2003). Semaphorin junction: making tracks toward neural connectivity. *Curr Opin Neurobiol* *13*, 79-89.
159. Pateras, I.S., Apostolopoulou, K., Koutsami, M., Evangelou, K., Tsantoulis, P., Liloglou, T., Nikolaidis, G., Sigala, F., Kittas, C., Field, J.K., *et al.* (2006). Downregulation of the KIP family members p27(KIP1) and p57(KIP2) by SKP2 and the role of methylation in p57(KIP2) inactivation in nonsmall cell lung cancer. *Int J Cancer* *119*, 2546-2556.
160. Paumier, K.L., Sukoff Rizzo, S.J., Berger, Z., Chen, Y., Gonzales, C., Kaftan, E., Li, L., Lotarski, S., Monaghan, M., Shen, W., *et al.* (2013). Behavioral characterization of A53T mice reveals early and late stage deficits related to Parkinson's disease. *PLoS One* *8*, e70274.
161. Pellow, S., Chopin, P., File, S.E., and Briley, M. (1985). Validation of Open - Closed Arm Entries in an Elevated Plus-Maze as a Measure of Anxiety in the Rat. *J Neurosci Meth* *14*, 149-167.
162. Pellow, S., and File, S.E. (1986). Anxiolytic and Anxiogenic Drug Effects on Exploratory Activity in an Elevated Plus-Maze - a Novel Test of Anxiety in the Rat. *Pharmacol Biochem Be* *24*, 525-529.
163. Perrot, R., Berges, R., Bocquet, A., and Eyer, J. (2008). Review of the multiple aspects of neurofilament functions, and their possible contribution to neurodegeneration. *Mol Neurobiol* *38*, 27-65.
164. Peters, J.M. (1998). SCF and APC: the Yin and Yang of cell cycle regulated proteolysis. *Curr Opin Cell Biol* *10*, 759-768.
165. Peters, J.M. (2006). The anaphase promoting complex/cyclosome: a machine designed to destroy. *Nat Rev Mol Cell Biol* *7*, 644-656.
166. Pickart, C.M. (2001). Mechanisms underlying ubiquitination. *Annu Rev Biochem* *70*, 503-533.
167. Pickart, C.M., and Eddins, M.J. (2004). Ubiquitin: structures, functions, mechanisms. *Biochim Biophys Acta* *1695*, 55-72.
168. Polleux, F., and Snider, W. (2010). Initiating and growing an axon. *Cold Spring Harb Perspect Biol* *2*, a001925.
169. R R Llinas, K.D.W., E J Lang (2004). Ch.7 Cerebellum. In Shepard GM *The synaptic organization of the brain*.

170. Radyushkin, K., Hammerschmidt, K., Boretius, S., Varoqueaux, F., El-Kordi, A., Ronnenberg, A., Winter, D., Frahm, J., Fischer, J., Brose, N., *et al.* (2009). Neuroligin-3-deficient mice: model of a monogenic heritable form of autism with an olfactory deficit. *Genes Brain Behav* 8, 416-425.
171. Rakic, P. (1971). Guidance of neurons migrating to the fetal monkey neocortex. *Brain Res* 33, 471-476.
172. Rakic, P. (1972). Mode of cell migration to the superficial layers of fetal monkey neocortex. *J Comp Neurol* 145, 61-83.
173. Rao, M.V., Campbell, J., Yuan, A., Kumar, A., Gotow, T., Uchiyama, Y., and Nixon, R.A. (2003). The neurofilament middle molecular mass subunit carboxyl-terminal tail domains is essential for the radial growth and cytoskeletal architecture of axons but not for regulating neurofilament transport rate. *J Cell Biol* 163, 1021-1031.
174. Rao, M.V., Mohan, P.S., Kumar, A., Yuan, A., Montagna, L., Campbell, J., Veeranna, Espreafico, E.M., Julien, J.P., and Nixon, R.A. (2011). The myosin Va head domain binds to the neurofilament-L rod and modulates endoplasmic reticulum (ER) content and distribution within axons. *PLoS One* 6, e17087.
175. Rao, M.V., Yuan, A., Campbell, J., Kumar, A., and Nixon, R.A. (2012). The C-terminal domains of NF-H and NF-M subunits maintain axonal neurofilament content by blocking turnover of the stationary neurofilament network. *PLoS One* 7, e44320.
176. Rapoport, M., van Reekum, R., and Mayberg, H. (2000). The role of the cerebellum in cognition and behavior: a selective review. *J Neuropsychiatry Clin Neurosci* 12, 193-198.
177. Rio, C., Rieff, H.I., Qi, P., Khurana, T.S., and Corfas, G. (1997). Neuregulin and erbB receptors play a critical role in neuronal migration. *Neuron* 19, 39-50.
178. Rotin, D., and Kumar, S. (2009). Physiological functions of the HECT family of ubiquitin ligases. *Nat Rev Mol Cell Biol* 10, 398-409.
179. Saiga, T., Fukuda, T., Matsumoto, M., Tada, H., Okano, H.J., Okano, H., and Nakayama, K.I. (2009). Fbxo45 forms a novel ubiquitin ligase complex and is required for neuronal development. *Mol Cell Biol* 29, 3529-3543.
180. Sailer, A., and Houlden, H. (2012). Recent advances in the genetics of cerebellar ataxias. *Curr Neurol Neurosci Rep* 12, 227-236.

181. Sarikas, A., Xu, X., Field, L.J., and Pan, Z.Q. (2008). The cullin7 E3 ubiquitin ligase: a novel player in growth control. *Cell Cycle* 7, 3154-3161.
182. Sasaki, S., Mori, D., Toyo-oka, K., Chen, A., Garrett-Beal, L., Muramatsu, M., Miyagawa, S., Hiraiwa, N., Yoshiki, A., Wynshaw-Boris, A., *et al.* (2005). Complete loss of Ndel1 results in neuronal migration defects and early embryonic lethality. *Mol Cell Biol* 25, 7812-7827.
183. Sashindranath, M., Daglas, M., and Medcalf, R.L. (2015). Evaluation of gait impairment in mice subjected to craniotomy and traumatic brain injury. *Behav Brain Res* 286, 33-38.
184. Segal, R.A., Pomeroy, S.L., and Stiles, C.D. (1995). Axonal growth and fasciculation linked to differential expression of BDNF and NT3 receptors in developing cerebellar granule cells. *J Neurosci* 15, 4970-4981.
185. Serra, H.G., Byam, C.E., Lande, J.D., Tousey, S.K., Zoghbi, H.Y., and Orr, H.T. (2004). Gene profiling links SCA1 pathophysiology to glutamate signaling in Purkinje cells of transgenic mice. *Hum Mol Genet* 13, 2535-2543.
186. Serra, H.G., Duvick, L., Zu, T., Carlson, K., Stevens, S., Jorgensen, N., Lysholm, A., Burrig, E., Zoghbi, H.Y., Clark, H.B., *et al.* (2006). RORalpha-mediated Purkinje cell development determines disease severity in adult SCA1 mice. *Cell* 127, 697-708.
187. Sgaier, S.K., Millet, S., Villanueva, M.P., Berenshteyn, F., Song, C., and Joyner, A.L. (2005). Morphogenetic and cellular movements that shape the mouse cerebellum; insights from genetic fate mapping. *Neuron* 45, 27-40.
188. Shea, T.B., and Chan, W.K. (2008). Regulation of neurofilament dynamics by phosphorylation. *Eur J Neurosci* 27, 1893-1901.
189. Shintani, T., Takeuchi, Y., Fujikawa, A., and Noda, M. (2012). Directional neuronal migration is impaired in mice lacking adenomatous polyposis coli 2. *J Neurosci* 32, 6468-6484.
190. Shoukimas, G.M., and Hinds, J.W. (1978). The development of the cerebral cortex in the embryonic mouse: an electron microscopic serial section analysis. *J Comp Neurol* 179, 795-830.
191. Sillitoe, R.V., and Joyner, A.L. (2007). Morphology, molecular codes, and circuitry produce the three-dimensional complexity of the cerebellum. *Annu Rev Cell Dev Biol* 23, 549-577.



192. Simon, P., Dupuis, R., and Costentin, J. (1994). Thigmotaxis as an Index of Anxiety in Mice - Influence of Dopaminergic Transmissions. *Behav Brain Res* *61*, 59-64.
193. Skaar, J.R., Pagan, J.K., and Pagano, M. (2013). Mechanisms and function of substrate recruitment by F-box proteins. *Nat Rev Mol Cell Biol* *14*, 369-381.
194. Skowyra, D., Craig, K.L., Tyers, M., Elledge, S.J., and Harper, J.W. (1997). F-box proteins are receptors that recruit phosphorylated substrates to the SCF ubiquitin-ligase complex. *Cell* *91*, 209-219.
195. Solecki, D.J., Liu, X.L., Tomoda, T., Fang, Y., and Hatten, M.E. (2001). Activated Notch2 signaling inhibits differentiation of cerebellar granule neuron precursors by maintaining proliferation. *Neuron* *31*, 557-568.
196. Solecki, D.J., Model, L., Gaetz, J., Kapoor, T.M., and Hatten, M.E. (2004). Par6alpha signaling controls glial-guided neuronal migration. *Nat Neurosci* *7*, 1195-1203.
197. Sotelo, C. (2004). Cellular and genetic regulation of the development of the cerebellar system. *Prog Neurobiol* *72*, 295-339.
198. Stegmuller, J., Konishi, Y., Huynh, M.A., Yuan, Z., Dibacco, S., and Bonni, A. (2006). Cell-intrinsic regulation of axonal morphogenesis by the Cdh1-APC target SnoN. *Neuron* *50*, 389-400.
199. Stoodley, C.J. (2012). The cerebellum and cognition: evidence from functional imaging studies. *Cerebellum* *11*, 352-365.
200. Strata, P., Scelfo, B., and Sacchetti, B. (2011). Involvement of cerebellum in emotional behavior. *Physiol Res* *60 Suppl 1*, S39-48.
201. Strick, P.L., Dum, R.P., and Fiez, J.A. (2009). Cerebellum and nonmotor function. *Annu Rev Neurosci* *32*, 413-434.
202. Tanaka, T., Serneo, F.F., Higgins, C., Gambello, M.J., Wynshaw-Boris, A., and Gleeson, J.G. (2004). Lis1 and doublecortin function with dynein to mediate coupling of the nucleus to the centrosome in neuronal migration. *J Cell Biol* *165*, 709-721.
203. Tian, D., Diao, M., Jiang, Y., Sun, L., Zhang, Y., Chen, Z., Huang, S., and Ou, G. (2015). Anillin Regulates Neuronal Migration and Neurite Growth by Linking RhoG to the Actin Cytoskeleton. *Curr Biol*.

204. Tolosa, E., Compta, Y., and Gaig, C. (2007). The premotor phase of Parkinson's disease. *Parkinsonism Relat Disord* *13 Suppl*, S2-7.
205. Trakhtenberg, E.F., and Goldberg, J.L. (2012). Epigenetic regulation of axon and dendrite growth. *Front Mol Neurosci* *5*, 24.
206. Treit, D., and Fundytus, M. (1988). Thigmotaxis as a Test for Anxiolytic Activity in Rats. *Pharmacol Biochem Be* *31*, 959-962.
207. Trouillas, P., Takayanagi, T., Hallett, M., Currier, R.D., Subramony, S.H., Wessel, K., Bryer, A., Diener, H.C., Massaquoi, S., Gomez, C.M., *et al.* (1997). International Cooperative Ataxia Rating Scale for pharmacological assessment of the cerebellar syndrome. The Ataxia Neuropharmacology Committee of the World Federation of Neurology. *J Neurol Sci* *145*, 205-211.
208. Tsai, L.H., and Gleeson, J.G. (2005). Nucleokinesis in neuronal migration. *Neuron* *46*, 383-388.
209. Tsunematsu, R., Nishiyama, M., Kotoshiba, S., Saiga, T., Kamura, T., and Nakayama, K.I. (2006). Fbxw8 is essential for Cull1-Cul7 complex formation and for placental development. *Mol Cell Biol* *26*, 6157-6169.
210. Tsutsumi, T., Kuwabara, H., Arai, T., Xiao, Y., and Decaprio, J.A. (2008). Disruption of the Fbxw8 gene results in pre- and postnatal growth retardation in mice. *Mol Cell Biol* *28*, 743-751.
211. Utine, G.E., Haliloglu, G., Salanci, B., Cetinkaya, A., Kiper, P.O., Alanay, Y., Aktas, D., Boduroglu, K., and Alikasifoglu, M. (2013). A homozygous deletion in GRID2 causes a human phenotype with cerebellar ataxia and atrophy. *J Child Neurol* *28*, 926-932.
212. Vadhvani, M., Schwedhelm-Domeyer, N., Mukherjee, C., and Stegmuller, J. (2013). The centrosomal E3 ubiquitin ligase FBXO31-SCF regulates neuronal morphogenesis and migration. *PLoS One* *8*, e57530.
213. Veeranna, Kaji, T., Boland, B., Odrlic, T., Mohan, P., Basavarajappa, B.S., Peterhoff, C., Cataldo, A., Rudnicki, A., Amin, N., *et al.* (2004). Calpain mediates calcium-induced activation of the erk1,2 MAPK pathway and cytoskeletal phosphorylation in neurons: relevance to Alzheimer's disease. *Am J Pathol* *165*, 795-805.
214. Voogd, J., and Glickstein, M. (1998a). The anatomy of the cerebellum. *Trends Cogn Sci* *2*, 307-313.

215. Voogd, J., and Glickstein, M. (1998b). The anatomy of the cerebellum. *Trends Neurosci* 21, 370-375.
216. Walker, K.L., Yoo, H.K., Undamatla, J., and Szaro, B.G. (2001). Loss of neurofilaments alters axonal growth dynamics. *J Neurosci* 21, 9655-9666.
217. Wang, L., Nomura, M., Goto, Y., Tanaka, K., Sakamoto, R., Abe, I., Sakamoto, S., Shibata, A., Enciso, P.L., Adachi, M., *et al.* (2011). Smad2 protein disruption in the central nervous system leads to aberrant cerebellar development and early postnatal ataxia in mice. *J Biol Chem* 286, 18766-18774.
218. Wang, V.Y., and Zoghbi, H.Y. (2001). Genetic regulation of cerebellar development. *Nat Rev Neurosci* 2, 484-491.
219. Welchman, R.L., Gordon, C., and Mayer, R.J. (2005). Ubiquitin and ubiquitin-like proteins as multifunctional signals. *Nat Rev Mol Cell Biol* 6, 599-609.
220. Westbrook, T.F., Hu, G., Ang, X.L., Mulligan, P., Pavlova, N.N., Liang, A., Leng, Y., Maehr, R., Shi, Y., Harper, J.W., *et al.* (2008). SCFbeta-TRCP controls oncogenic transformation and neural differentiation through REST degradation. *Nature* 452, 370-374.
221. White, J.J., and Sillitoe, R.V. (2013). Development of the cerebellum: from gene expression patterns to circuit maps. *Wiley Interdiscip Rev Dev Biol* 2, 149-164.
222. Wingate, R.J. (2001). The rhombic lip and early cerebellar development. *Curr Opin Neurobiol* 11, 82-88.
223. Yacubova, E., and Komuro, H. (2003). Cellular and molecular mechanisms of cerebellar granule cell migration. *Cell Biochem Biophys* 37, 213-234.
224. Yang, X.W., Wynder, C., Doughty, M.L., and Heintz, N. (1999). BAC-mediated gene-dosage analysis reveals a role for Zipro1 (Ru49/Zfp38) in progenitor cell proliferation in cerebellum and skin. *Nat Genet* 22, 327-335.
225. Yang, Y., and Bonni, A. (2010). Releasing the brake on presynaptic development: Cdc20-APC triggers NeuroD2 degradation to drive presynaptic differentiation. *Cell Cycle* 9, 2255-2256.
226. Yoshimura, T., Kawano, Y., Arimura, N., Kawabata, S., Kikuchi, A., and Kaibuchi, K. (2005). GSK-3beta regulates phosphorylation of CRMP-2 and neuronal polarity. *Cell* 120, 137-149.

227. Yuan, A., Sasaki, T., Rao, M.V., Kumar, A., Kanumuri, V., Dunlop, D.S., Liem, R.K., and Nixon, R.A. (2009). Neurofilaments form a highly stable stationary cytoskeleton after reaching a critical level in axons. *J Neurosci* *29*, 11316-11329.
228. Zhao, X., Heng, J.I., Guardavaccaro, D., Jiang, R., Pagano, M., Guillemot, F., Iavarone, A., and Lasorella, A. (2008). The HECT-domain ubiquitin ligase Huwe1 controls neural differentiation and proliferation by destabilizing the N-Myc oncoprotein. *Nat Cell Biol* *10*, 643-653.
229. Zheng, N., Schulman, B.A., Song, L., Miller, J.J., Jeffrey, P.D., Wang, P., Chu, C., Koepp, D.M., Elledge, S.J., Pagano, M., *et al.* (2002). Structure of the Cull1-Rbx1-Skp1-F boxSkp2 SCF ubiquitin ligase complex. *Nature* *416*, 703-709.
230. Zhou, F.Q., and Snider, W.D. (2006). Intracellular control of developmental and regenerative axon growth. *Philos Trans R Soc Lond B Biol Sci* *361*, 1575-1592.
231. Zhu, X., Raina, A.K., Rottkamp, C.A., Aliev, G., Perry, G., Boux, H., and Smith, M.A. (2001). Activation and redistribution of c-jun N-terminal kinase/stress activated protein kinase in degenerating neurons in Alzheimer's disease. *J Neurochem* *76*, 435-441.

## Appendix 1

List of plasmid constructs that were generated in the lab and used in this study along with their respective primer numbers:

Vector plasmid	Cloned by	Primers
pCMV-myc-FBXO41	N. Schwedhelm-Domeyer	18556/18552
pCMV-myc-FBXO41-Res	A. Holubowska	19036/19037
pCMV-myc-FBXO41-Res $\Delta$ CTR	A. Holubowska	19036/19037
pCMV-myc-FBXO41 $\Delta$ Fbox	C. Mukherjee	18556/19426/19427/18552
pCMV-myc-FBXO41 $\Delta$ CTR	N. Schwedhelm-Domeyer	18556/18031/18032/18552
pCMV-myc-FBXO41 aa 35-873	N. Schwedhelm-Domeyer	18551/18552
pCMV-myc-FBXO41 aa 1-546	N. Schwedhelm-Domeyer	18556/18557
pCMV-myc-FBXO41 $\Delta$ aa 350-560	N. Schwedhelm-Domeyer	18556/28477/28478/18552
pEGFP-C2-FBXO41	J. Stegmüller	
pc3XFlag-CMV-10.dna-NFM	C. Mukherjee	29301/29302
pCMV-myc-NFM	C. Mukherjee	29218/29219-2
pCMV-myc-NFM-Res	N. Schwedhelm-Domeyer	27508/27509
pCMV-myc-Skp1	J. Stegmüller	15454/15455
pBluescript-U6-FBXO41 RNAi#5	J. Stegmüller	16104/16105
pBluescript-U6-FBXO41 RNAi#8	J. Stegmüller	20268/20269
pBluescript-U6-NFM RNAi#5	C. Mukherjee	24562/24563
pBluescript-U6-NFM RNAi#3	C. Mukherjee	24560/24561

Plasmids obtained from other sources:

<b>Plasmid</b>	<b>Obtained from</b>
pEGFP-C2-NFM	A. Brown (Ohio State University, USA)
pcDNA 3.1-Flag-Cullin7	Z.Q. Pan (Mount Sinai School of Medicine, New York)

## Appendix 2

Sequence and primer numbers of primers used for Genotyping and qRT-PCR

<b>Primers</b>	<b>Purpose</b>	<b>Primer number</b>	<b>Sequence 5'-3'</b>
FBXO41 WT/KO Forward	Genotyping	23322	ATCCACCTAGACCTAGTAATCTTA
FBXO41 WT Reverse	Genotyping	23323	CTTCTCCAGGGCGCGGAT
FBXO41 KO Reverse	Genotyping	23560	AATGCGCTCAGGTCAAATTCAG
NFM primer Forward	qRT-PCR	32180	GACACCATCCAGCAGTTGG
NFM primer Reverse	qRT-PCR	32181-2	ACTTTGGTCTTCTGAATCTTACTGGA
GAPDH Forward	qRT-PCR	4876	
GAPDAH Reverse	qRT-PCR	4877-2	

Sequence of primers used for cloning the various constructs used in this study

<b>Primer number</b>	<b>Sequence 5'-3'</b>

15654	ATTACTCGAGTAATGCCTACGATAAAGTTGCAGAGTTC
15455	TTAAGCGGCCGCTCACTTCTCTTCACACCACTGGTT
16104	AAGATTCTGCACATCAAGGTAAGTTAACGACCTTGATGTGCA GAAT
16105	AATTCAAAAAGAAGATTCTGCACATCAAGGTCGTTAACTTACCT TGA
18031	ATCGAATTCATGGCCTCGCTGGACCTACCGTACCG
18032	ATCGGATCCTTAGCAGCCACCTTCTACCTTGATGTGCAGAATC TTC
18551	ATCGAATCCTTTACGAGACGCTCTACATCC
18552	ATCCTCGAGTTAGCAACCACCTTCTACCTT
18556	ATCGAATTCTTATGGCCTCGCTGGACC
18557	ATCCTCGAGTTATGGGCTGATGACCTCATT
19036	GAGGCCTGGCTTCTCGAAAATCCTCCATATCAAGGTAGAAGG TGG
19037	CCACCTTCTACCTTGATATGGAGGATTTTCGAGAAGCCAGGCC TC
19426	TATTTGGAACAGACTCGGGCATTAGCTCGCATCTTGAGGATTT
19427	TATAAATCCTCAAGATGCGAGCTAATGCCCGAGTCTGTTCCA
20268	AGCTGCTACTGCCGTCCCCTAAGTTAACGAGGGCAGGCAGT AGC
20269	AATTCAAAAAGAGCTGCTACTGCCGTGCCCTCGTTAACTTAGGG CAC
24560	AAGAGTGGTTCAAATGCCGCAAGTTAACGGCGGCATTTGAAC CACTCTTCTTTTG



24561	AATTCAAAAGAAGAGTGGTTCAAATGCCGCCGTTAACTTGCG GCATTTGAACCACTCTT
24562	GGAAATGGCTCGTCATTTGCAAGTTAACGGCAAATGACGAGC CATTTCCCTTTTG
24563	AATTCAAAAGGGAAATGGCTCGTCATTTGCCGTTAACTTGCA AATGACGAGCCATTTCC
27508	GGGGAACCAAGTGGGAAATGGCCCGGCACTTACGAGAATACC AGG
27509	CCTGGTATTCTCGTAAGTGCCGGGCCATTTCCCACTTGGTTCC CC
28477	CAGCACACCCAGTGCCGCCCTTTCCTGTATCTTCAC
28478	GTGAAGATACAGAAGAGGGCGGCACTGGGTGTGCTG
29218	ATAGAATTCGGATGAGCTACACGCTGGACTCG
29219-2	TATGGTACCTTAGTCACCCTGGGTGACTTCCTT
29301	ATAGAATTCGATGAGCTACACGCTGGACTCG
29302	TATGGTACCAATTAGTCACCCTGGGTGACTTCCTT

---

---

## Curriculum Vitae

---

---

### Chaitali Mukherjee

#### Personal details:

Address: Annastrasse 66, App. 81  
37075 Göttingen

Date of birth: 04.04.1989

Place of birth: Patna, India

Nationality: Indian

Email: [mukherjee@em.mpg.de](mailto:mukherjee@em.mpg.de)

#### Education:

**04/2011 - 04/2015 :** **Georg-August University Göttingen., IMPRS**  
Neuroscience program,  
Dr.rer.nat

**10/ 2009 - 04/2011:** **Georg-August University Göttingen., IMPRS**  
Neuroscience program,  
Master of Science

**06/2006 - 04/2009** **Mount Carmel College, Bangalore university, India**  
Chemistry, Zoology, Microbiology (CZM)  
Bachelor of Science

#### Stipends and honors:

**2009-2010** Stipend of the Excellence Foundation for the promotion of the Max

Planck Society.

**2008-2009** Awarded certificate for outstanding student in Zoology

**2008-2009** Awarded certificate for outstanding student in Chemistry

**Publications:**

**Mukherjee, C**<sup>\*</sup>, Holubowska, A<sup>\*</sup>, Schwedhelm-Domeyer, N., Mitkovski, M., Lee, S-J., Kannan, M., Matz, A., Vadhvani, M., and Stegmuller, J. (2015). Loss of neuron-specific F-box protein FBXO41 models an ataxia-like phenotype in mice with neuronal migration defects and degeneration in the cerebellum. *Jouranl of Neuroscience. In press*

*\* Equal contribution*

**Mukherjee, C**<sup>\*</sup>, Holubowska, A<sup>\*</sup>, Schwedhelm-Domeyer, N., Gellerer, A., Kannan, M and Stegmuller, J. (2015). The E3 ubiquitin ligase FBXO41-Cul7 regulates axon growth in cerebellar granule neurons. *Jouranl of Neuroscience. In revision*

*\* Equal contribution*

Holubowska, A., **Mukherjee, C.**, Vadhvani, M., and Stegmuller, J. (2014). Genetic manipulation of cerebellar granule neurons in vitro and in vivo to study neuronal morphology and migration. *J Vis Exp.*

Vadhvani, M., Schwedhelm-Domeyer, N., **Mukherjee, C.**, and Stegmuller, J. (2013). The centrosomal E3 ubiquitin ligase FBXO31-SCF regulates neuronal morphogenesis and migration. *PLoS One 8*, e57530.